

DYNAMIC RESPONSE OF BRIDGES TO NEAR-FAULT,
FORWARD DIRECTIVITY GROUND MOTIONS

By

ELIOT BONVALOT

A thesis submitted in partial fulfillment of
the requirements of the degree of

MASTER OF SCIENCE IN CIVIL ENGINEERING

WASHINGTON STATE UNIVERSITY
Department of Civil and Environmental Engineering

AUGUST 2006

To the faculty of Washington State University:

The members of the Committee appointed to examine the thesis of ELIOT BONVALOT
find it satisfactory and recommend that it be accepted.

Chair

ACKNOWLEDGEMENTS

This research was performed in the Department of Civil and Environmental Engineering at Washington State University, Pullman, Washington. Funding was provided by the Federal Highway Administration. The Washington State Department of Transportation provided technical support throughout the project. Their support is greatly appreciated.

I am grateful to Dr. William Cofer, the chairman of my committee, for his patience and guidance through this project. I would also like to thank Dr. Adrian Rodriguez-Marek and Dr. Cole C. McDaniel for their participation and assistance on my committee. A special thanks for Mr. Adel Al-Assaf and Mr. Reza Sehhati. You have not only been a help with research, but sincere friends to me. I would also like to thank my family for the encouragement they have been.

DYNAMIC RESPONSE OF BRIDGES TO NEAR-FAULT, FORWARD DIRECTIVITY GROUND MOTIONS

Abstract

By Eliot Bonvalot, M.S.
Washington State University
August 2006

Chair: William F. Cofer

Research over the last decade has shown that pulse-type earthquake ground motions that result from forward-directivity effects can result in significant damage to structures. The objective of this research is to use recent ground motion data to improve the understanding of the response of typical reinforced concrete and precast concrete bridges to pulse-type ground motions that result from forward directivity effects.

Nonlinear, dynamic finite element analysis was applied to three bridges, and they generally survived forward directivity ground motions without significant damage to the columns. However, column flexural failure was predicted for one of them when subjected to two of the forward directivity ground motions. The bridge models often indicated distress at the abutments, including pounding, and exceedance of abutment strength limits.

The response of bridges to forward directivity ground motions was found to be highly dependent upon the coincidence of the bridge fundamental period and the ground motion velocity pulse period. The severity of the demand is controlled by the ratio of the pulse period to bridge fundamental period.

Analysis results showed that most of the damage in the bridge columns during forward directivity ground motions occurred at the beginning of the record in response to the velocity pulse. Therefore, a ground motion consisting of a sinusoidal single pulse may be sufficient to evaluate bridge performance for forward directivity ground motions.

A study of the effect of foundation flexibility showed that not including Soil-Structure-Interaction might lead to over-conservatism, especially for the FDGMs.

Nonlinear SDOF analyses were performed, but they are not recommended in the case of forward directivity ground motions since the results were not consistent. However, the use of the acceleration response spectra to compute the expected response of the bridges was found to be quite successful for both non-forward directivity and forward directivity ground motions. A response modification factor must be used to include the inelasticity effect on the maximum base shear in the columns.

Due to the variation in the acceleration response spectra with period caused by forward directivity ground motions, to amplify the spectra for design does not provide a reliable basis for representing near-fault, forward directivity ground motions. Depending on the importance of the bridge being designed or assessed, the appropriate approach taken with forward directivity ground motions should be carefully considered by the designer.

TABLE OF CONTENTS

	Page
ACKNOWLEDGEMENTS.....	iii
ABSTRACT.....	iv
TABLE OF FIGURES.....	xi
TABLE OF TABLES.....	xxiii
CHAPTER 1: Introduction.....	1
1.1) Introduction and Background	1
1.2) Research objectives.....	2
1.3) Seismic Activity in Western Washington State	3
1.4) Bridge Modeling.....	4
CHAPTER 2: Literature Review	5
2.1) Near-Fault (NF), Forward Directivity Ground Motions (FDGMs)	5
2.1.1) Strike-slip and dip-slip fault.....	5
2.1.2) Fault Normal/Fault Parallel.....	6
2.1.3) Near-Fault, Forward Directivity effects.....	8
2.2) The Seattle fault	13
2.3) Structural response to FDGM.....	17
2.3.1) Effects on Buildings.....	17
2.3.2) Effects on Bridges.....	20
2.4) Current near-fault seismic design provisions for bridges	22
2.5) Soil-Structure Interaction.....	24

2.5.1)	Foundation models.....	24
2.5.1.1)	Spread footings	25
2.5.1.2)	Pile foundations	26
2.5.2)	Damping.....	28
2.5.3)	Previous Research Papers	29
CHAPTER 3: Column Modeling and ABAQUS		32
3.1)	The Orozco columns.....	32
3.1.1)	Geometry and reinforcement	32
3.1.2)	Loading and test setup	33
3.1.3)	Recorded responses from testing	35
3.1.4)	Finite Element Modeling of the Columns.....	36
3.1.4.1)	Global geometric modeling.....	36
3.1.4.2)	Material models	40
3.1.4.2.1)	Concrete.....	40
3.1.4.2.2)	Longitudinal Steel.....	47
3.1.5)	ABAQUS Results	48
3.2)	Lehman column	49
3.2.1)	Geometry and reinforcement	49
3.2.2)	Loading and test setup	51
3.2.3)	Recorded responses from testing	52
3.2.4)	Finite Element modeling of the column.....	54
3.2.5)	ABAQUS Results	55
3.3)	Conclusion	56

CHAPTER 4: Seismic Analysis of Bridges.....58

4.1) Seismic Excitations..... 58

 4.1.1) Ground Motion Selection..... 58

 4.1.2) Ground Motion Characteristics..... 59

4.2) Coordinate Axes..... 61

4.3) WSDOT Bridge Selection..... 62

4.4) WSDOT Bridge 405/46N-E..... 63

 4.4.1) Geometry and reinforcement 63

 4.4.2) Structural Model 70

 4.4.2.1) Boundary and Connectivity Conditions..... 75

 4.4.2.2) Damping..... 79

 4.4.2.3) Loading and Ground Motions..... 79

 4.4.2.4) Bridge Frequency Content 80

4.5) WSDOT Bridge 520/19E-N..... 82

 4.5.1) Geometry and reinforcement 82

 4.5.2) Structural Model 89

 4.5.2.1) Bridge Frequency Content 90

4.6) WSDOT Bridge 90/26A 91

 4.6.1) Geometry and reinforcement 91

 4.6.2) Structural Model 97

 4.6.2.1) Boundary and Connectivity Conditions..... 99

 4.6.2.2) Loading and Ground Motions..... 103

 4.6.2.3) Bridge Frequency Content 103

CHAPTER 5: WSDOT Bridge Results	106
5.1) General Bridge Behavior	106
5.1.1) Bridge 405 and Bridge 520	106
5.1.2) Bridge 90.....	111
5.2) Forward Directivity Effect – Frequency Content	116
5.1.2.1) Longitudinal Response.....	124
5.1.2.2) Transverse Response.....	133
5.3) Velocity Pulse Period Effect.....	135
5.4) Soil-Structure Interaction Effect.....	139
5.5) Comparison with a SDOF system.....	140
5.6) AASHTO prediction comparison	143
5.7) Acceleration Spectra prediction comparison	150
CHAPTER 6: Conclusion	152
REFERENCE.....	157
APPENDIX A.....	169
A.1 Shear Capacity Degradation Model.....	169
A.2 Foundation Stiffnesses – FEMA 356 (2000).....	170
A.3 Longitudinal Abutment Response – Caltrans (2004).....	172
A.4 AASHTO (2004) procedure.....	175
APPENDIX B	177
B.1 Ground Motions Characteristics	177
B.2 Bridge 405 Input Data.....	190
B.2.1 Material Properties	190

B.3 Bridge Output Data	191
B.4 Bridges Finite Element Input Files	195

TABLE OF FIGURES

Figure 1.1.1: Typical cross-section of northwestern Washington State showing hypocenters of earthquakes since 1970. After Ludwin et al. (1991).	4
Figure 2.1.1: Schematic Diagrams of surface fault displacement (Slemmons, 1977).....	6
Figure 2.1.2: The large velocity pulse occurs in the fault-normal direction (Somerville, 1993).....	7
Figure 2.1.3: Rupture-directivity effects in the recorded displacement time histories of the 1989 Loma Prieta earthquake, for the fault-normal (top) and fault-parallel (bottom) components. (EERI, 1995).....	8
Figure 2.1.4: Zones of directivity	9
Figure 2.1.5: Map of the Landers region showing the location of the rupture of the 1992 Landers earthquake (which occurred on three segments), the epicenter, and the recording stations at Lucerne and Joshua Tree. The strike normal velocity time histories at Lucerne and Joshua Tree exhibit forward and backward directivity effects, respectively. (From Somerville, 1997).....	10
Figure 2.1.6: An example of forward directivity effect on Site A (Abrahamson, 1998).....	11
Figure 2.1.7: Schematic diagrams showing the orientations of fling step and directivity pulse for strike-slip and dip-slip faulting. (Somerville et al., 1997).....	12
Figure 2.2.1: Map showing tracklines of USGS high-resolution, multichannel, seismic-reflection profiles near the Seattle fault zone. (USGS; http://earthquake.usgs.gov/)	14
Figure 2.2.2: The Seattle Area Map showing the Seattle fault zone (Brocher et al. 2004) .	16
Figure 2.5.1: Schematic of discrete foundation models for the spread footing foundation: (a) bent structure; (b) foundation models. (McGuire et al., 1994).....	26

Figure 2.5.2: Schematic of models for the pile foundation: (a) bent structure; (b) foundation models. (Cofer, 1994).....	28
Figure 2.5.3: Collapsed of an 18-span viaduct section of Hanshin Expressway (from Ghasemi, 1996).....	30
Figure 3.1.1: Column elevation (Orozco, 2002).....	33
Figure 3.1.2: Input time history (Orozco, 2002).....	34
Figure 3.1.3: test setup (Orozco, 2002).....	35
Figure 3.1.4: Overall view after pulse loading (Orozco, 2002).....	35
Figure 3.1.5: Recorded response: hysteretic force-displacement curve and dashed Ruaumoko (Carr, 1996) prediction (Orozco, 2002).....	36
Figure 3.1.6: Response of columns with different sized elements (Légeron, 2005)	37
Figure 3.1.7: Column with 6 elements (13 points)	38
Figure 3.1.8: Default 3 radially, 8 circumferentially integration points, through the beam cross section and two integration point locations (in red) along the length of the 3-node element.....	38
Figure 3.1.9: Column model in ABAQUS.....	39
Figure 3.1.10: Input time history during the ABAQUS analysis.....	39
Figure 3.1.11: Stress-Strain Model Proposed for Monotonic Loading of Confined and Unconfined Concrete (Mander & Priestley, 1988).....	43
Figure 3.1.12: Stress–Strain Relationship for the Concrete in Compression	44
Figure 3.1.13: Experimental Behavior of Concrete under Tension (Mazars, 1989).....	44
Figure 3.1.14: Tensile Stress-Strain Curve of the Concrete	45
Figure 3.1.15: Behavior of concrete (Légeron, 2005)	46

Figure 3.1.16: Steel Stress-Strain Curve.....	48
Figure 3.1.17: Comparison of Orozco (light gray) and ABAQUS results (solid red)	49
Figure 3.2.1: Specimen Geometry and Reinforcement of the Lehman column. (Lehman, 2000).....	50
Figure 3.2.2: Experimental configuration (Lehman, 2000)	51
Figure 3.2.3: Imposed displacement during the test (Lehman, 2000)	52
Figure 3.2.4: Final damage state (Lehman, 2000)	53
Figure 3.2.5: Force – Displacement Response (Lehman, 2000).....	54
Figure 3.2.6: Imposed displacement during the ABAQUS analysis	55
Figure 3.2.7: Comparison of Lehman and ABAQUS results	56
Figure 4.1.1: Non FDGMs Acceleration Spectra (Log. scale)	59
Figure 4.1.2: Non FDGMs Acceleration Spectra.....	60
Figure 4.2.1: Bridge Coordinate Axes	61
Figure 4.3.1: Bridge location	62
Figure 4.3.2: The Seattle Area Map showing the Seattle fault zone and bridge location (Brocher et al. 2004)	63
Figure 4.4.1: Bridge 405 Aerial View	64
Figure 4.4.2: Bridge 405 Elevation.....	65
Figure 4.4.3: Bridge 405 Plan.....	65
Figure 4.4.4 Bridge 405 Deck cross-section.....	65
Figure 4.4.5: Bridge 405 Column Sections (Crossbeam & Circular column).....	66
Figure 4.4.6: Crossbeam plan view.....	66
Figure 4.4.7: Bridge 405 Hinge Elevation (between crossbeam and deck).....	67

Figure 4.4.8: Bearing Pad	67
Figure 4.4.9: Bridge 405 Girder Stop	67
Figure 4.4.10: Bridge 405 Bent Elevation	68
Figure 4.4.11: Bridge Foundation Spread Footing for Bents.....	69
Figure 4.4.12: Bridge 405 Abutment and Deck Elevation View	69
Figure 4.4.13: Bridge 405 East and West Abutments.....	70
Figure 4.4.14: Bridge 405 Spine Model.....	71
Figure 4.4.15: Bridge 405 deck cross-section.....	71
Figure 4.4.16: Bridge 405 deck solid and spine models.....	72
Figure 4.4.17: Bridge 405 deck in torsion	72
Figure 4.4.18: Bridge 405 cross-sections.....	74
Figure 4.4.19: FE model of the soil, abutment and deck interaction in the transverse direction	75
Figure 4.4.20: FE model of the soil, abutment and deck interaction, in the longitudinal direction	76
Figure 4.4.21: Force-Displacement Curve of the abutment gap spring and connector in series	76
Figure 4.4.22: Bridge Model Boundary Conditions	78
Figure 4.4.23: Applied earthquake at the foundation nodes.....	80
Figure 4.4.24: Longitudinal mode of vibration.....	81
Figure 4.4.25: Transverse mode of vibration.....	82
Figure 4.5.1: Bridge 520 Aerial View	83
Figure 4.5.2: Bridge 520 Elevation.....	83

Figure 4.5.3: Bridge 520 Plan	84
Figure 4.5.4: Bridge 520 Deck cross-section.....	84
Figure 4.5.6: Bridge 520 Column Sections (Crossbeam & Circular column).....	85
Figure 4.5.7: Crossbeam plan view.....	85
Figure 4.5.8: Bridge 520 Hinge Elevation (between crossbeam and deck).....	86
Figure 4.5.9: Bearing Pad	86
Figure 4.5.10: Bridge 520 Girder Stop	86
Figure 4.5.11: Bridge 520 Bent Elevation	87
Figure 4.5.12: Bridge Foundation Spread Footing for Bents.....	88
Figure 4.5.13: Bridge 520 West Abutment and Deck Elevation View.....	88
Figure 4.5.14: Bridge 520 East and West Abutments.....	89
Figure 4.5.15: Bridge 520 East and West Abutments.....	89
Figure 4.6.1: Bridge 90 Aerial View	91
Figure 4.6.2: Bridge 90 Aerial Views.....	92
Figure 4.6.3: Bridge 90 Elevation.....	92
Figure 4.6.4: Bridge 90 Plan.....	93
Figure 4.6.5: Bridge 90 Concrete box girder cross-section	93
Figure 4.6.6: Guided Bearing Pad.....	94
Figure 4.6.7: Fixed Bearing Pad	94
Figure 4.6.8: Bridge 90 columns.....	95
Figure 4.6.9: Wing Wall	96
Figure 4.6.10: Bridge 90 Abutment and Deck Elevation View	96
Figure 4.6.11: Bridge 90 East and West Abutments.....	96

Figure 4.6.12: Bridge 90 Spine Model.....	97
Figure 4.6.13: Bridge 405 deck meshed cross-section	98
Figure 4.6.14: Bridge 90 Deck FEMs.....	98
Figure 4.6.15: Output Results of Bridge 90 Deck FEM – Torsion Model	98
Figure 4.6.16: Rebar locations in the column cross-section	99
Figure 4.6.17: FE model of the soil, abutments, and deck interaction in the longitudinal direction	100
Figure 4.6.18: Abutment Force-Displacement Curves	100
Figure 4.6.19: P-Y curve comparison example	101
Figure 4.6.20: Bridge 90 Model Boundary Conditions	102
Figure 4.6.21: Applied earthquake at the foundation nodes.	103
Figure 4.6.22: Bridge 90 Longitudinal mode of vibration.....	104
Figure 4.6.23: Bridge 90 Transverse mode of vibration.....	105
Figure 5.1.1: Moquegua GM Time History	107
Figure 5.1.2: Cathedral in Moquegua, a stone structure with stone walls and stone vaults, sustained damage and lost one of its vaults (Photo by E. Fierro).....	107
Figure 5.1.3: Moment-Curvature hysteresis curves in the transverse (red) and longitudinal (black) column direction.....	108
Figure 5.1.4: Force-Displacement hysteresis curves in the transverse (left) and longitudinal (right) direction.....	108
Figure 5.1.5: Transverse (red) and longitudinal (black) column displacement time history	109
Figure 5.1.6: Transverse (red) and longitudinal (black) column base shear time history .	109

Figure 5.1.7: Bridge 405 Force – Displacement hysteresis curve, in the longitudinal direction, including the column shear capacity in dashed green	110
Figure 5.1.8: Total Strain Energy in the system	110
Figure 5.1.9: Abutment Hysteresis Force-Displacement (left) and Force Time History curve (right)	111
Figure 5.1.10: Izmit GM Time History.....	112
Figure 5.1.11: A mosque stood with a few other structures amid the rubble of collapsed buildings in the town of Golcuk, 60 miles east of Istanbul (Associated Press Photo, Enric Marti, 1999).	112
Figure 5.1.12: Moment-Curvature hysteresis curves at the column top (blue) and at the pile (red) in the longitudinal direction	113
Figure 5.1.13: Column Force-Displacement hysteresis curves in the longitudinal (left) and transverse (right) direction	114
Figure 5.1.14: Force-Displacement hysteresis curves in the longitudinal (left) and transverse (right) direction.....	114
Figure 5.1.15: Total Strain Energy in the system	115
Figure 5.1.16: Abutment Hysteresis Force-Displacement (left) and Force Time History curve (right)	115
Figure 5.2.1: Bridge 405 ARS of the FN components of the Ground Motions.....	117
Figure 5.2.2: Bridge 405 ARS of the FP components of the Ground Motions.....	117
Figure 5.2.3: Bridge 520 ARS of the FN components of the Ground Motions.....	118
Figure 5.2.4: Bridge 520 ARS of the FP components of the Ground Motions.....	118
Figure 5.2.5: Bridge 90 ARS of the FN components of the Ground Motions.....	119

Figure 5.2.6: Bridge 90 ARS of the FP components of the Ground Motions.....	119
Figure 5.2.7: Bridge 405 Max Longitudinal Base Shear, S_a 's at $T_l = 0.65s$	125
Figure 5.2.8: Bridge 520 Max Longitudinal Base Shear, S_a 's at $T_l = 0.80s$	125
Figure 5.2.9: Bridge 90 Max Longitudinal Column Shear, S_a 's at $T_l = 0.82s$	125
Figure 5.2.10: Bridge 405 Max Longitudinal relative Displacement, S_a 's at $T_l = 0.65s$...	125
Figure 5.2.11: Bridge 520 Max Longitudinal relative Displacement, S_a 's at $T_l = 0.80s$...	126
Figure 5.2.12: Bridge 90 Max Longitudinal relative Displacement, S_a 's at $T_l = 0.82s$	126
Figure 5.2.13: Bridge 405 Energy dissipated by plastic deformation in the system through time for the non-FD (dashed) and FDGMs (solid)	127
Figure 5.2.14: Bridge 520 Energy dissipated by plastic deformation in the system through time for the non-FD (dashed) and FDGMs (solid)	128
Figure 5.2.15: Bridge 90 Energy dissipated by plastic deformation in the system through time for the non-FD (dashed) and FDGMs (solid). Column failure noted for KJM Inv and RRS Inv records.....	128
Figure 5.2.16: Bridge 405 Force-Displacement and Moment-Curvature hysteresis curve from the FD KJM GM, in the longitudinal direction.....	129
Figure 5.2.17: Bridge 90 Moment-Curvature hysteresis curve of column C_4 from the FD KJM ground motion, in the longitudinal direction, including the USC prediction curve in dashed red	130
Figure 5.2.18: Bridge 90 Force – Displacement hysteresis curve of column C_4 from the FD KJM GM, in the longitudinal direction, including the column shear capacity in dashed green.....	130
Figure 5.2.19: Bridge 405 Max Transverse Base Shear, S_a 's at $T_l = 0.18 s$	133

Figure 5.2.20: Bridge 520 Max Transverse Base Shear, S_a 's at $T_t = 0.17$ s	134
Figure 5.2.21: Bridge 90 Max Transverse Column (C_4) Shear, S_a 's at $T_t = 0.47$ s.....	134
Figure 5.2.22: Bridge 405 Max Transverse relative Displacement, S_a 's at $T_t = 0.18$ s	134
Figure 5.2.23: Bridge 520 Max Transverse relative Displacement, S_a 's at $T_t = 0.17$ s	134
Figure 5.2.24: Bridge 90 Max Transverse Column (C_4) relative Displacement, S_a 's at $T_t =$ 0.47 s.....	135
Figure 5.3.1: Bridge 405 (left), Bridge 520 (right), and Bridge 90 (down) Max Displacement Vs. Velocity Pulse Period	136
Figure 5.3.2: Bridge 405 (left), Bridge 520 (right), and Bridge 90 (down) Max Displacement Vs. Peak Ground Acceleration (PGA).....	137
Figure 5.3.3: Bridge 405 (left), Bridge 520 (right), and Bridge 90 (down) Max Displacement Vs. Peak Ground Velocity (PGV) of the FDGMs	137
Figure 5.3.4: Velocity Pulse Period Models Vs. Moment Magnitude (from Rodriguez- Marek, 2000).....	139
Figure 5.4.1: Bridge 520 longitudinal (left) and transverse (right) Max Base Shear, with or without SSI	140
Figure 5.4.2: Bridge 520 longitudinal (left) and transverse (right) Max Column Displacement, with or without SSI.....	140
Figure 5.5.1: (Bridge 405) Maximum SDOF displacement compared to the longitudinal ABAQUS model response	142
Figure 5.5.2: (Bridge 520) Maximum SDOF displacement compared to the longitudinal ABAQUS model response	143

Figure 5.6.1: Uniform hazard response spectra for 2% and 10% probability of exceedance in 50 years for San Francisco, California.....	144
Figure 5.6.2: Bridge 405 ARS of the FN components of the ground motions, and the one used for the AASHTO design procedure	145
Figure 5.6.3: Bridge 405 ARS of the FP components of the GMs, and the one used for the AASHTO design procedure	145
Figure 5.6.4: Bridge 520 ARS of the FN component of the GMs, and the one used for the AASHTO design procedure	146
Figure 5.6.5: Bridge 520 ARS of the FP component of the GMs, and the one used for the AASHTO design procedure	146
Figure 5.6.6: Bridge 90 ARS of the FN component of the GMs, and the one used for the AASHTO design procedure	147
Figure 5.6.7: Bridge 90 ARS of the FP component of the GMs, and the one used for the AASHTO design procedure	147
Figure 5.6.8: Bridge 405 Maximum longitudinal (left) and transverse (right) governing column base shears compared to the AASHTO (2004) design prediction	148
Figure 5.6.9: Bridge 520 Maximum longitudinal (left) and transverse (right) governing column base shears compared to the AASHTO (2004) design prediction	148
Figure 5.6.10: Bridge 90 Maximum longitudinal (left) and transverse (right) column shears (column C_4) compared to the AASHTO (2004) design prediction.....	149
Figure 5.6.11: Bridge 405 (left), Bridge 520 (right) and Bridge 90 (down) maximum governing column displacements compared to the AASHTO (2004) design prediction ..	149

Figure 5.7.1: Bridge 405 (left), Bridge 520 (right) and Bridge 90 (down) maximum governing column shears compared to the ARS.....	151
Figure 5.7.2: Bridge 405 (left) and Bridge 520 (right) maximum governing column displacement compared to the ARS.....	151
Figure A.1-1: k curve.....	170
Figure A.2-1: Elastic Solutions for Rigid Footing Spring Constraints (FEMA 356, 2000)	171
Figure A.3-1: Effective Abutment Stiffness.....	173
Figure A.3-2: Effective Abutment Area.....	174
Figure A.3-3 Bridge 405 Abutments force-displacement curve.....	174
Figure A.3-4 Bridge 90 Abutments force-displacement curve.....	175
Figure A.3-1: AASHTO bridge seismic design procedure chart.....	175
Figure B.1-1: Characteristics of SYL - Sylmar - Olive View Med FF.....	178
Figure B.1-2: Characteristics of BAM - Bam Station.....	179
Figure B.1-3: Characteristics of RRS - 5968 (77) Rinaldi Receiving Sta.....	180
Figure B.1-4: Characteristics of F14 - Fault Zone14.....	181
Figure B.1-5: Characteristics of T75 - TCU075-W (g).....	182
Figure B.1-6: Characteristics of KJM - Kobe.....	183
Figure B.1-7: Characteristics of LCN – 24 Lucerne.....	184
Figure B.1-8: Characteristics of IZT - Izmit, Kocaeli 1999.....	185
Figure B.1-9: Characteristics of 702 - Fire Station #28, Nisqually 2001.....	186
Figure B.1-10: Characteristics of MOQ – Moquegua, Peru 2001.....	187
Figure B.1-11: Characteristics of SSU - Santa Susana, Northridge 1994.....	188
Figure B.1-12: Characteristics of T71 - TCU-071, Chi Chi 1999.....	189

Figure B.2-1: Compressive stress-strain concrete curve.....	190
Figure B.2-2: Tensile stress-strain concrete curve.....	190
Figure B.2-3: Compressive stress-strain steel 60 curve.....	191

TABLE OF TABLES

Table 2.2.1: Seattle fault dip.....	15
Table 3.2.1: Steel properties	51
Table 4.1.1: FDGM characteristics.....	60
Table 4.2.1: Local and Global Coordinate Systems	61
Table 4.4.1: Torsional results and comparison.....	73
Table 4.4.2 Frequency content of Bridge 405.....	81
Table 4.5.1: Frequency content of Bridge 520	90
Table 4.6.1: Frequency content of Bridge 90	104
Table 5.2.1: Summary of the GM characteristics and the Bridge 405 column response parameters.....	121
Table 5.2.2: Summary of the GM characteristics and the Bridge 520 column response parameters.....	122
Table 5.2.3: Summary of the GM characteristics and the Bridge 90 column response parameters.....	123
Table 5.2.4: fundamental bridge periods and FDGM's velocity pulse periods (T_v).....	127
Table 5.2.5: Bridge 405 Abutment pounding	131
Table 5.2.6: Bridge 520 Abutment pounding	132
Table 5.2.7: Bridge 90 Abutment pounding	132
Table A.2 -1 Bridge 405 Footing Spring stiffnesses.....	171
Table A.2 -2 Bridge 520 Footing Spring stiffnesses.....	171
Table A.2 -3 Bridge 90 Footing Spring stiffnesses.....	172
Table B.2-1: Material densities.....	191

Table B.3-1: Bridge 405 results for the northwest column.....	192
Table B.3-2: Bridge 520 results for the northwest column.....	193
Table B.3-3: Bridge 90 results for the northern column (C4).....	194

CHAPTER 1: Introduction

1.1) Introduction and Background

Ground motion recordings have provided increasing proof that ground shaking near a fault rupture may be characterized by a large, long-period pulse, capable of causing severe structural damage. This occurs for sites located in the direction of rupture propagation, where the fault rupture propagates towards the site at a speed close to the shear wave velocity. This phenomenon is known as Forward Directivity (FD). As a result, most of the seismic energy from the rupture arrives within a short time window at the beginning of the record. The radiation pattern of shear dislocation around the fault causes the fault-normal component to be typically more severe than the fault-parallel component. This phenomenon affects the response of structures located in the near-fault region, which is assumed to extend approximately 20 to 30 km (13 to 19 miles) from the seismic source, and therefore requires consideration in the design process.

Recent structural design codes, e.g. the 1997 Uniform Building Code, partially account for near-fault effects by introducing source type and distance dependent near-fault factors to the traditional design spectrum. However, these factors are inadequate to provide consistent protection because they pay little attention to the physical structure response characteristics to near-fault ground motions. Moreover, emerging concepts of performance-based seismic design require a quantitative understanding of response covering the range from nearly elastic behavior to highly inelastic behavior. Much work is needed to identify and quantify the site dependent characteristics of near-fault ground

motions and to address issues concerning the response of different types of structures to these ground motions.

The objective of this research is to use the wealth of recent ground motion data to improve the understanding of the response of typical reinforced concrete and precast concrete bridges to pulse-type ground motions that result from forward-directivity effects.

1.2) *Research objectives*

The specific objectives of this research include:

- Determine the influence of Forward Directivity Ground Motions (FDGMs) on structural response.
- Determine the influence of Soil-Structure-Interaction (SSI) on the seismic demand to structures subject to FDGMs.
- Provide design and assessment recommendations for bridges likely to be affected by near-fault FDGMs.

This research will benefit the profession by reducing the uncertainty associated with near-fault ground motions and the resulting structural response. Many structures are founded in close proximity to faults and must account for this hazard. However, current methods do not properly consider FDGMs. This is partly due to the lack of recorded near-fault ground motions and the difficulty in characterizing the near-fault ground motions for sites without recorded time histories.

The tasks that were performed include:

- Bridges were selected for analysis and development of bridge models
- Three-dimensional nonlinear finite element models of the bridges were developed to study the response of the structures to FDGMs. In addition, the influence of soil-structure interaction on the response of bridges subject to FDGMs was investigated.
- The bridge models were analyzed for a suite of both Forward Directivity and non-Forward Directivity earthquake records created by Gillie (2005) specifically for this research. Key performance parameters included member flexural and shear force demands, member inelastic rotation demands, bridge deck connection demands, bridge abutment demands, and overall system drift demands (Priestley, 2003). Since site response can play an important role in both the FDGM pulse period and the pulse amplitude, the influence of site response was incorporated into the ground motions and modeled with springs simulating the soil conditions expected at the bridge sites.

1.3) *Seismic Activity in Western Washington State*

The Seattle area is located near the Cascadia Subduction Zone (CSZ) where the Juan de Fuca plate is being subducted beneath the North American plate. Subduction zones typically exhibit two types of earthquakes: interplate, and intraplate. These events typically occur at depths of 30-70 km. In addition, a subduction zone will also show shallow crustal events at depths 0-30 km as shown in Figure 1.3.1.

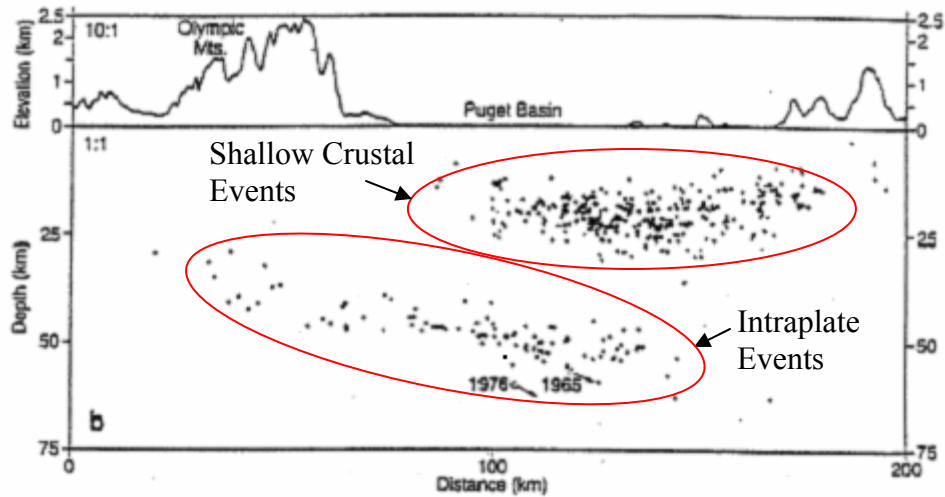


Figure 1.1.1: Typical cross-section of northwestern Washington State showing hypocenters of earthquakes since 1970. After Ludwin et al. (1991).

1.4) Bridge Modeling

Three WSDOT bridges, designated as 405/46N-E, 520/19E-N, and 90/26A were selected for study in this research. The bridges were selected by the WSDOT based on their proximity to a fault. Being constructed during the 1990's, they are characteristic of the actual design practice.

Each bridge was modeled with a 3D nonlinear dynamic implicit Finite Element Model (FEM). Soil-structure-interaction was included in the models as well. ABAQUS V6.5 was used to model each bridge. ABAQUS is a robust finite element software with the capability for modeling the nonlinear response of structures when subjected to earthquakes. The modeling of the bridges is described in more detail in Chapter 4. The results are shown in Chapter 5, with conclusions and recommendations in Chapter 6.

CHAPTER 2: Literature Review

In this chapter, a review of the near-fault, forward directivity origins and effects is presented. After a brief description of the Seattle fault, the structural response to FDGM, the current near-fault design code provisions for bridges, and the effects of soil-structure interaction are also discussed.

2.1) Near-Fault (NF), Forward Directivity Ground Motions (FDGMs)

These paragraphs attempt to clarify the basic geotechnical and seismological notions involved in this research. Depending on the site location and the fault rupture type, ground motions can develop Forward Directivity (FD) or non-forward directivity behavior.

2.1.1) Strike-slip and dip-slip fault

There are three different kinds of faults (Figure 2.1.1):

- Normal, dip-slip fault. The fault plane of a normal fault dips away from the uplifted crustal block. Faulting occurs in response to extension.
- Reverse, dip-slip fault. The fault plane of a reverse fault dips beneath the uplifted crustal block. Faulting occurs in response to compression.
- Strike-slip fault. Crustal blocks slide past each other. The slip may be left lateral or right lateral.

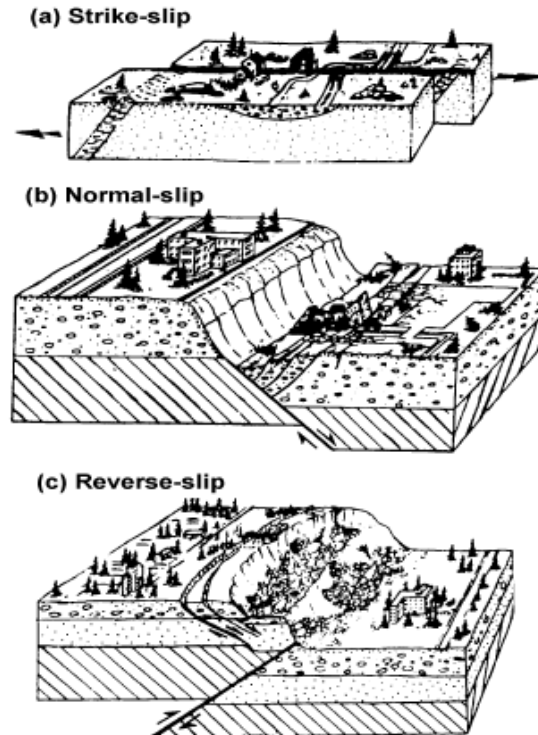


Figure 2.1.1: Schematic Diagrams of surface fault displacement (Slemmons, 1977)

2.1.2) Fault Normal/Fault Parallel

Somerville pointed out two types of radiation patterns. The SH (tangential motion) radiation pattern contains a maximum coincident with the direction of rupture propagation (see Figure 2.1.2). On the contrary, the SV (radial motion) radiation pattern demonstrates a minimum in the rupture direction. This results, counter-intuitively, in the large velocity pulse being visible only in the fault-normal direction, with no noticeable pulse in the fault-parallel direction (Abrahamson, 1998; and Somerville and Graves, 1993). In fact, the peak velocity in the fault-normal direction under these conditions is often twice the value of that in the fault parallel direction (Mayes and Shaw, 1997). For sites within 10 km of the rupture surface, one would expect to see a pulse in the same direction as the ground slippage, that is, in the fault-parallel direction in the case of a

Strike-slip event. Indeed, a static residual displacement is visible; however, this static displacement does not correspond to a significant pulse in the velocity time history. There is a pulse due to static displacement, but it is a long period pulse and typically is not damaging to structures. One can appreciate the difference between fault-normal and fault-parallel in Figure 2.1.3.

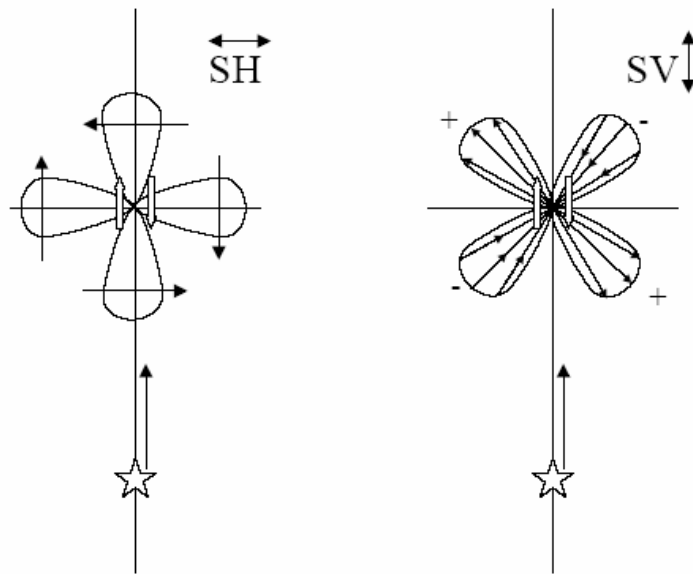


Figure 2.1.2: The large velocity pulse occurs in the fault-normal direction (Somerville, 1993)

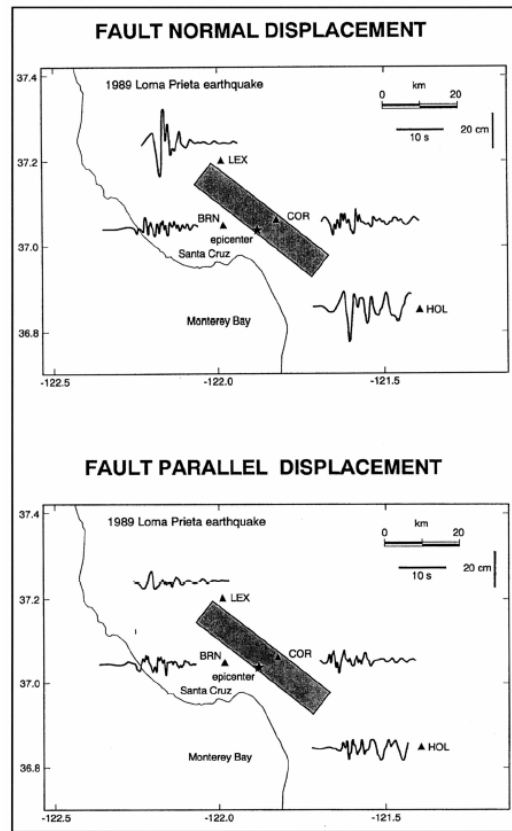


Figure 2.1.3: Rupture-directivity effects in the recorded displacement time histories of the 1989 Loma Prieta earthquake, for the fault-normal (top) and fault-parallel (bottom) components. (EERI, 1995)

2.1.3) Near-Fault, Forward Directivity effects

Directivity effects can be classified as forward, reverse (or backward), and neutral. Forward directivity occurs when the rupture propagates toward a site and the direction of slip on the fault is also toward the site, while reverse directivity is when the rupture progresses away from the site. Within the research community, the term “directivity effects” has come to mean “forward directivity effects” because forward directivity is more likely to be responsible for the ground motions that cause damage.

Figure 2.1.4 portrays the three zones of directivity, with the star representing the epicenter and the black line indicating the fault.

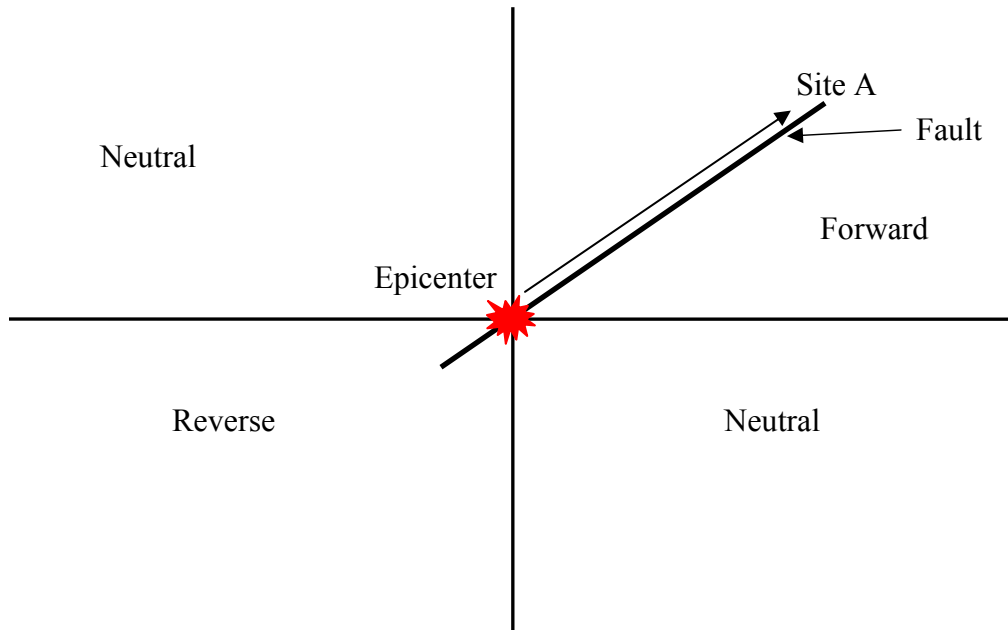


Figure 2.1.4: Zones of directivity

Somerville et al. (1997), illustrate the directivity effect in strike-slip faulting using the strike-normal components of ground velocity from two near-fault recordings of the magnitude 7.3 Landers earthquake (Figure 2.1.5).

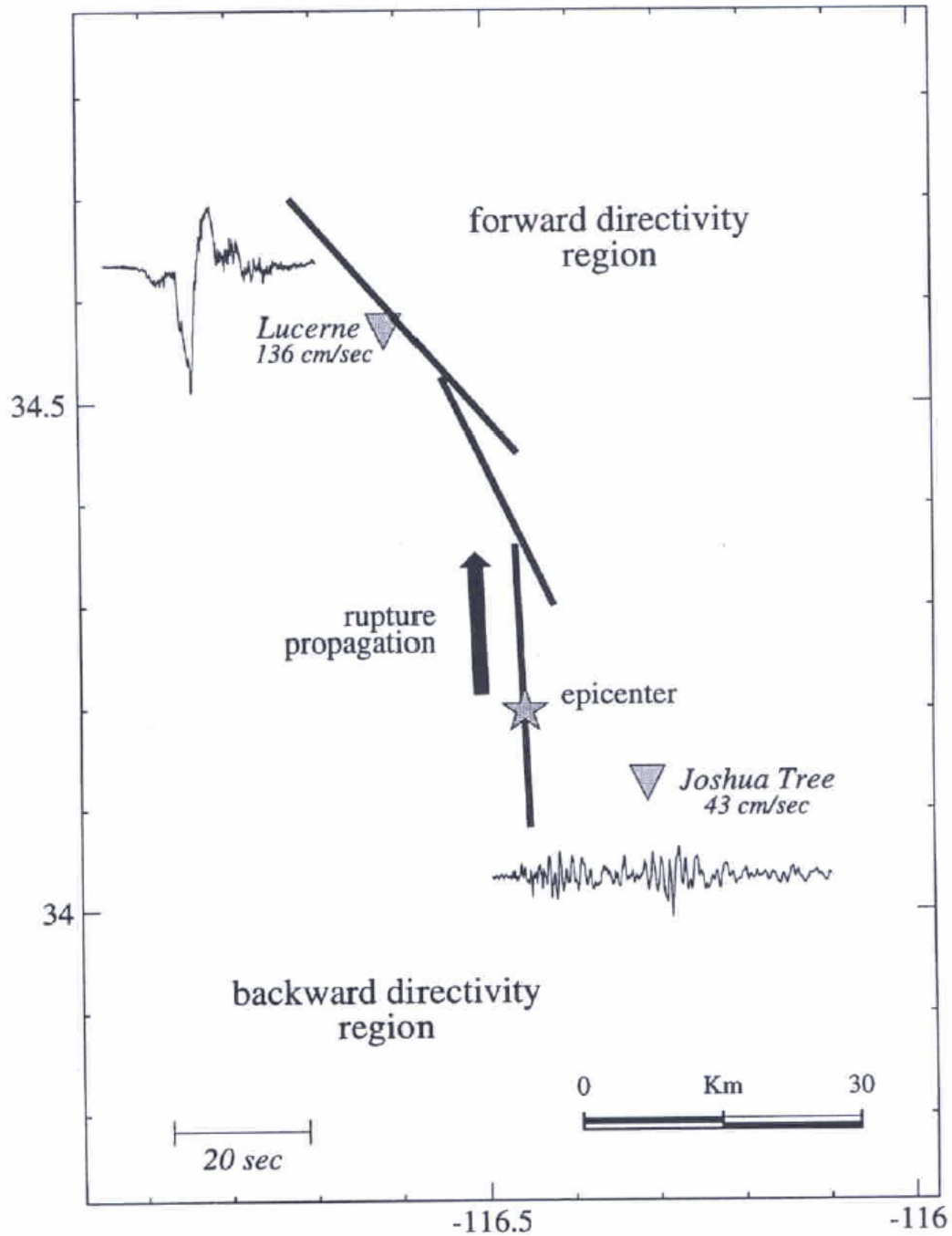


Figure 2.1.5: Map of the Landers region showing the location of the rupture of the 1992 Landers earthquake (which occurred on three segments), the epicenter, and the recording stations at Lucerne and Joshua Tree. The strike normal velocity time histories at Lucerne and Joshua Tree exhibit forward and backward directivity effects, respectively. (From Somerville, 1997)

The rupture often propagates at a velocity close to the velocity of shear wave radiation (Abrahamson 1998; Somerville et al. 1997). The energy is accumulated in front of the propagating rupture and is expressed as a large velocity pulse. This energy propagation is similar to a sonic boom because the energy is concentrated immediately ahead at the rupture front as is shown for Site A in Figure 2.1.6.

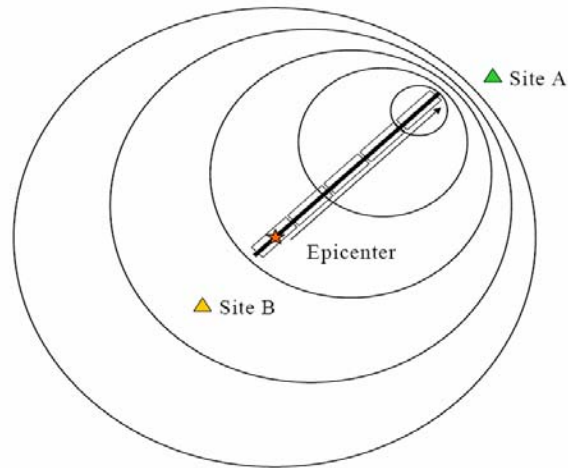


Figure 2.1.6: An example of forward directivity effect on Site A (Abrahamson, 1998)

In strike-slip faulting, the directivity pulse occurs on the strike-normal component while the fling step occurs on the strike parallel component. In dip-slip faulting, both the fling step and the directivity pulse occur on the strike-normal component. The orientations of fling step and directivity pulse for strike-slip and dip-slip faulting are shown schematically in Figure 2.1.7.

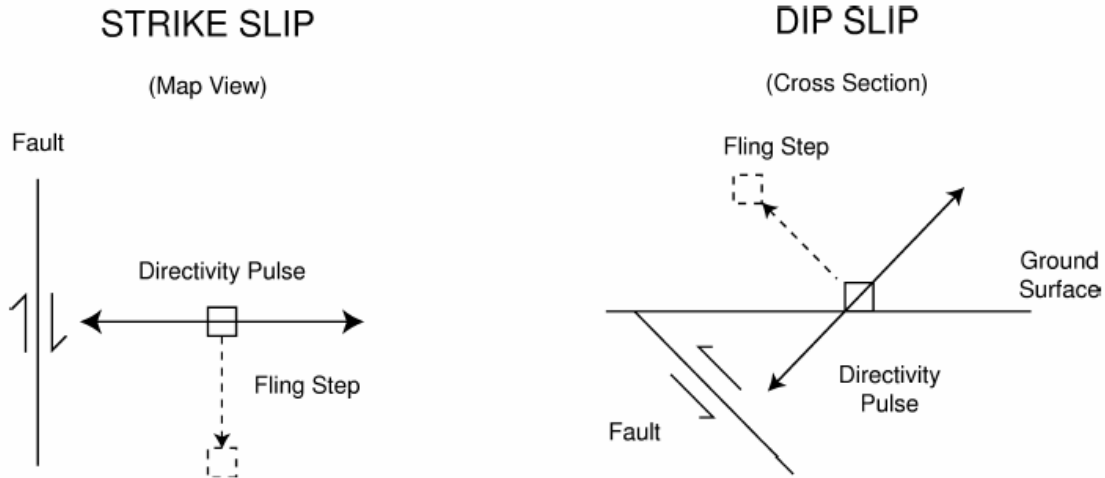


Figure 2.1.7: Schematic diagrams showing the orientations of fling step and directivity pulse for strike-slip and dip-slip faulting. (Somerville et al., 1997)

Although Forward Directivity Ground Motions (FDGMs) pose a significant threat to structures, this threat is not equal for all structures. For example, coincidence of the structure and pulse period intuitively leads to a large structural response for a given earthquake. The FDGM pulse period is proportional to the earthquake magnitude, lengthening as the earthquake magnitude increases. As a result, damage due to smaller magnitude earthquakes can be more significant for short period structures than damage due to larger magnitude earthquakes, since the near-fault pulse period is closer to the fundamental period of the structure in the smaller magnitude earthquake. This contradicts conventional engineering intuition that directly correlates damage potential with earthquake magnitude, thus highlighting the need for a unique way to accurately assess the potential for structural damage due to FDGMs. Although consisting only of a few cycles, the pulses can impose large inelastic drift on structures, resulting in significant permanent deformations.

Stewart et al. (2001) stated that ground motions close to a ruptured fault can be significantly different than those further away from the seismic source. The near-fault

zone is typically assumed to be within a distance of about 20-30 km (12-19 miles) from a ruptured fault. Within this near-fault zone, ground motions are significantly influenced by the rupture mechanism, the direction of rupture propagation relative to the site, and possible permanent ground displacements resulting from the fault slip.

The study of the near-source large velocity pulse is a fairly new topic in earthquake engineering. It has been studied by Attalla et al. (1998), Hall and Aagaard (1998), Hall et al. (1995), and Somerville and Graves (1993). Somerville and al. (1997) described the effects of rupture directivity with an empirical model and provided guidelines for the specification of response spectra and time histories. Chopra and Chintanapakdee (2001) compared the response of SDOF systems to fault-normal and fault-parallel ground motions. The fault-normal component of many, but not all, near-fault ground motions imposes much larger deformation and strength demands compared to the fault-parallel component over a wide range of vibration periods. In contrast, the two components of most far-fault records are quite similar in their demands.

2.2) *The Seattle fault*

Scientists discovered the Seattle Fault in 1965 when studying gravity data for the Puget Sound region (USGS). In 1987, scientists began finding evidence of great earthquakes of magnitude 8 to magnitude 9 in the Cascadia Subduction Zone off the Washington Coast; these earthquakes occur about every 500 to 600 years. Five years later, a team of scientists discovered the first evidence that the Seattle Fault was active with a magnitude 7.3 earthquake that also generated a tsunami in Puget Sound about 1,100 years ago. In the mid to late 1990s, using high-resolution imaging, scientists found evidence of other surface faults. Field evidence shows that large earthquakes with

magnitude 6.5 or greater have occurred on six major fault systems in the Puget Sound region. Scientists estimate that these earthquakes have a recurrence interval of 333 years. The Seattle Fault is a geologic fault in the North American Plate that runs from the Issaquah Alps to Hood Canal in Washington state. It passes through Seattle, Washington just south of Downtown and is believed to be capable of generating an earthquake of at least $M_w = 7.0$. The Seattle Fault therefore has the potential to cause extensive damage to the city.

The Seattle Fault has not been responsible for an earthquake since the city's settlement in the 1850's. The Seattle fault is the best-studied fault within the tectonically active Puget Lowland in western Washington.

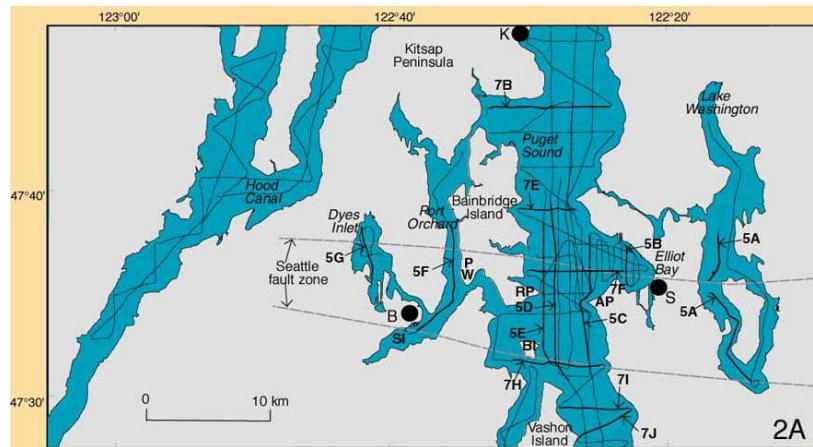


Figure 2.2.1: Map showing tracklines of USGS high-resolution, multichannel, seismic-reflection profiles near the Seattle fault zone. (USGS; <http://earthquake.usgs.gov/>)

Opinions diverge regarding the Seattle fault geometry, the style of upper crustal deformation, and the driving force for motion on the fault. These impact the ability to assess the seismic hazard of the fault. The Seattle fault geometry can be roughly defined as reverse, dip-slip, 4-7 km wide and 60-65 km long. The dip direction is south. Various

dips have been proposed for the Seattle fault zone as shown in Table 2.2.1. Both Johnson et al. (1994, 1999) and Calvert and Fisher (2001) identified four sub-parallel, south-dipping fault strands in the Seattle fault zone. Figure 2.2.2 shows the estimated location of the fault trace and, consequently, the Seattle fault zone.

Table 2.2.1: Seattle fault dip

Author	Dip evaluation	Based on
Johnson et al. (1994, 1999)	45°–60° for the top 6 km of the fault and 45°–65° for the top 1 km	high-resolution seismic reflection
Calvert and Fisher (2001)	60° for the top 1 km of the fault	P-wave velocities from seismic-reflection data
Pratt et al. (1997)	45° for the top 6 km, shallowing to 20°–25° at depths of 6–16 km	Industry data
Brocher et al. (2001)	Unspecified steep dip (>65° in their Figures) extending to a depth of 28 km.	
Van Wagoner et al. (2002)	Projected epicenters from the earthquake catalog delineate a diffuse zone of seismicity with an even higher dip, 70°–80°, extending from the surface location of the Seattle fault zone to a depth of 25 km	
U. S. ten Brink, P. C. Molzer	Dip range of 35°–45° down to a depth of 7 km	The seismic reflection and refraction data

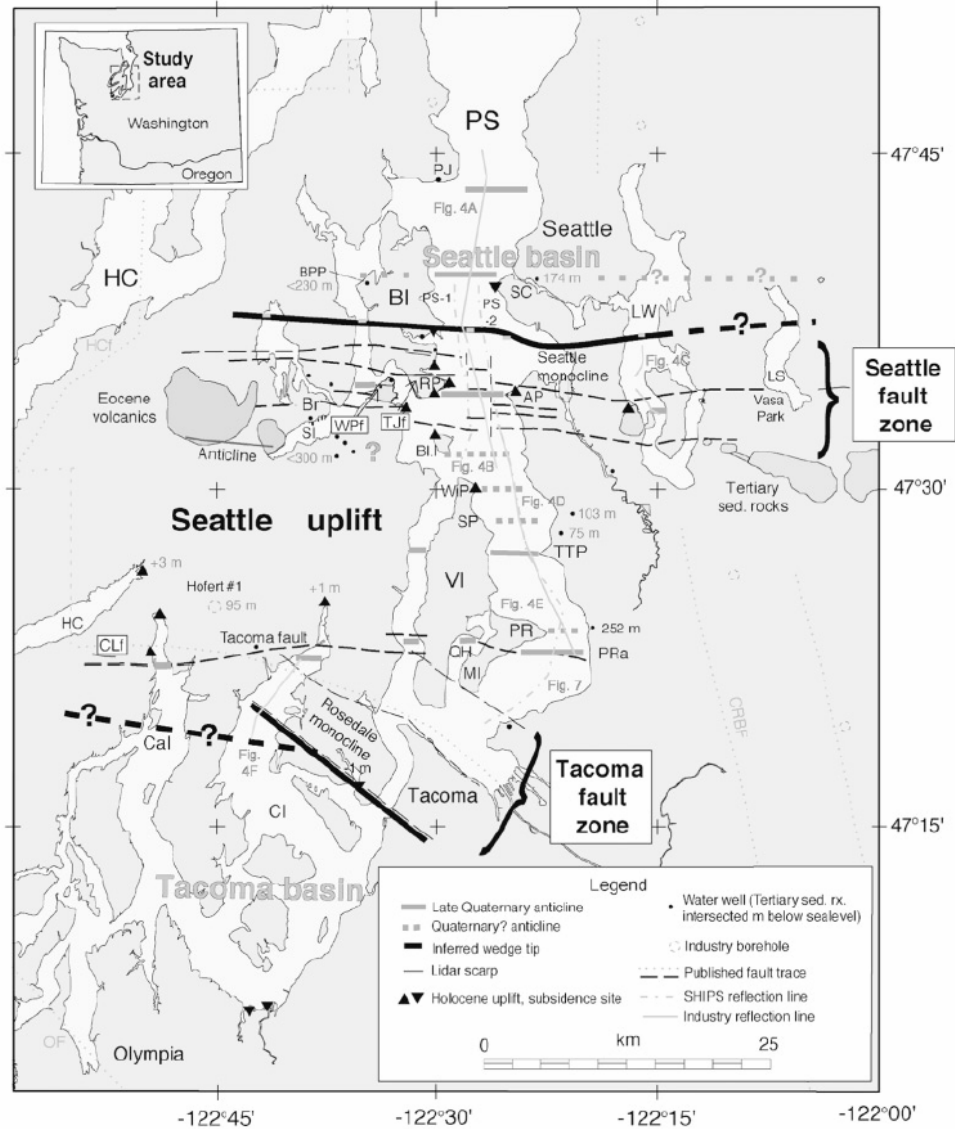


Figure 2.2.2: The Seattle Area Map showing the Seattle fault zone (Brocher et al. 2004)

Even with a well-known geometry of the fault, the direction of rupture is unpredictable. Therefore, it is recommended that all structures that fall within the near field of an active fault be designed for a possible velocity pulse.

2.3) Structural response to FDGM

This section features reviews of articles involving descriptions of near-fault ground motions, and the effects of near-source large velocity pulses on structures.

The effects of FDGMs on structures were first recognized in the 1970's (Bertero, 1976). However, engineers largely ignored FDGMs in structural design until after the 1994 Northridge earthquake. Since then, a number of studies have been directed at the effect of near-fault ground motions on structural response, prompting revision of design codes. In current practice, rupture directivity effects are generally taken into account by modifications to the elastic acceleration response spectrum at 5% damping (Somerville et al. 1997, Somerville 2003).

2.3.1) Effects on Buildings

The study of the effects of near-source ground motions on structures has generally been limited to the effects on buildings. Bertero et al. (1978) studied buildings that were severely damaged during the 1971 San Fernando earthquake and the implications of pulses on pre-1971 aseismic design methods. Their result showed that the near-fault ground motions with pulses can induce strong structural responses. In the same way, Anderson and Naeim (1984) showed that near-field ground motions with pulses could induce dramatically high response in fixed-base buildings. Hall et al. (1995) performed an analytical study on a 20-story steel moment frame structure and a three-story base-isolated building in the Greater Los Angeles area. They simulated a magnitude 7.25 earthquake on a blind-thrust fault. They indicated that the demands made by the near-fault ground motions could far exceed the capacity of flexible high-rise and base-isolated buildings. Iwan (1996), Attalla et al. (1998), and Hall and Aagaard (1998) completed

further analytical studies on near-source effects on buildings. Iwan (1997) stated that the pulses in the near-field ground motions travel through the height of the buildings as waves, and that the conventional techniques using the modal superposition method and the response spectrum analysis may not capture the effect of these pulses. Iwan also proposed the use of a drift spectrum for near-field ground motions. But Chopra and Chintanapakdee (1998), in their preliminary investigation, concluded that the response spectrum analysis is accurate for engineering applications and should be preferred over the drift spectrum. Malhotra (1999) studied the response characteristics of near-fault pulse-like ground motions and showed that ground motions with high peak ground velocity (PGV) to peak ground acceleration (PGA) ratios have wide acceleration-sensitive regions in their response spectra. This phenomenon will increase the base shear, inter-story drift, and ductility demand of high-rise buildings. Chai and Loh (1999) used three types of velocity pulse to determine the strength reduction factor of structures. They found that the strength demand depends on the pulse duration and the ratio of pulse duration to the natural period of the structure.

Nakashima et al. (2000) examined the response behavior of steel moment frames subjected to near-fault ground motions recorded in recent earthquakes in Japan, Taiwan and the US, and found that the largest story drifts are all similar among Japanese, Taiwanese and the American near-fault records.

By investigating the response of single degree of freedom (SDOF) systems under near-fault and far-field earthquake motions in the context of spectral regions, Chopra and Chintanapakdee (2001) found that for the same ductility factor, the near-fault ground motions impose a larger strength demand than the far-field motions do. Loh et al. (2002)

carried out a series of experimental studies to develop a regression-based hysteretic model. They used this hysteretic model to study the basin effect and the near-fault effect of ground motion subjected to Chi-Chi earthquakes. Alavi and Krawinkler (2004) studied the behavior of moment-resisting frame structures subjected to near-fault ground motions. The results demonstrate that structures with a period longer than the pulse period respond very differently from structures with a shorter period. For the former, early yielding occurs in higher stories but the high ductility demands migrate to the bottom stories as the ground motion becomes more severe. For the latter, the maximum demand always occurs in the bottom stories.

Recent near-fault ground motion research with respect to structures includes work by Makris and Black (2004) on dimensional analysis of structures subjected to near-fault ground motions, Iwan (1995) on specification of near-fault ground motions, Yang and Agrawal (2002) on the use of passive and semi-active control systems for near fault applications, Filiatrault and Trembley (1998) on the use of passive dampers in near field applications, Symans et al. (2003) on the use of passive dampers in wood structures subject to near-fault ground motions, and Krawinkler and Alavi (1998) on improving design procedures for near-fault ground motions.

The papers of Sucuogly et al. (1999) and Makris and Black (2004) examined the influence of peak ground velocity on the failure probability of structures. Sucuogly et al. (1999) make a clear distinction between acceleration pulses and velocity pulses and indicate correctly that “structural damage caused by ground excitation is closely related with the dominant acceleration pulse. If the peak ground velocity is reached immediately following the dominant acceleration pulse, then the peak velocity reflects the impulsive

character or strength in the acceleration records.” Makris and Black (2004) investigated the “goodness” of peak ground velocity as a dependable intensity measure for the earthquake shaking of civil structures. The paper identifies two classes of near-fault ground motions: those where the peak ground velocity is the integral of a distinguishable acceleration pulse and those where the peak ground velocity is the result of a succession of high-frequency acceleration spikes. It is shown that the shaking induced by the former class is in general much more violent than the shaking induced by the latter class.

2.3.2) Effects on Bridges

Bridges less than about 10 km from a fault rupture may be subjected to very large accelerations, velocities, and displacements that challenge traditional methods of seismic design. Not only is it difficult to design bridges that will be built at these locations, but also many of the assumptions used in determining the demands on these bridges may no longer hold true. For instance, engineers perform an elastic analysis to derive the demands on a bridge, under the assumption that the maximum linear and nonlinear displacements are about equal (Newmark 1971). This assumption may not be valid close to the fault rupture.

Recently, many simulations and analyses have been performed for specific bridges. Mayes and Shaw (1997) evaluated the response of 16 columns designed using the Caltrans Bridge Design Specifications to several seismic events involving near-fault ground motions. Liao et al. (2000) studied the dynamic behavior of a five-span concrete pier bridge subjected to both near-fault and far-field ground motions. Their results also support the conclusion that higher ductility demands and base shear are caused by near-fault earthquake ground motions than by far-field earthquake ground motions.

Orozco and Ashford (2002) investigated three flexural columns subjected to a large pulse and subsequent cyclic loading at increasing multiples of yield ductility. These columns were compared to columns tested at UC Irvine (Hamilton 2000) under a non-pulse cyclic loading. It was found that the flexural columns performed well. During the pulse they exhibited increased strength and smaller plastic hinge lengths when compared to the non-pulse loading, but the ultimate strengths and ductilities were similar.

Ghasemi and Park (2004) subjected the Bolu Viaduct, struck by the 1999 Duzce earthquake in Turkey, to near-fault ground motions. They took into account a static ground dislocation in the fault-parallel direction. This analysis showed that the displacement of the superstructure relative to the piers exceeded the capacity of the bearings at an early stage of the earthquake, causing damage to the bearings as well as to the energy dissipation units. The analysis also indicated that shear keys, both longitudinal and transverse, played a critical role in preventing collapse of the deck spans.

Shen and Tsai (2004) evaluated the performance of a seismically isolated bridge under a Near-Fault Earthquake. The near-fault effect amplifies the seismic response of the isolated bridge when the pulse period is close to the effective period of the isolation system. In the same way, Wen-I Liao et al. (2004) performed a comparison of the dynamic response of isolated and non-isolated continuous girder bridges subjected to near-fault ground motions. Only the longitudinal response was considered. The effects on base shear reduction of a seismically isolated bridge with the far-field ground motion input is more significant than those with the near-fault ground motion input. The PGV/PGA value is identified as the key parameter that controls the response

characteristics of bridges under near-fault ground motion. The base shear and displacement demand of isolated bridges are significantly influenced by this parameter.

Despite the number of recent research projects on near-fault ground motions, significant work is still needed to provide an improved understanding of the response of structures to FDGMs and to develop appropriate design provisions (Alavi and Krawinkler 2000; Milonakis and Reinhorn 2001; Zhang and Iwan 2002). There is still significant uncertainty in how to properly account for FDGMs, as illustrated by the latest changes to the design for FDGMs in building codes (e.g. AASHTO) and the current lack of recognition of the effect of the near-fault pulse period on the response of structures. Research is needed in the area of soil-structure interaction in near-fault ground motions as well to determine the influence of soil type on the FDGMs and the corresponding structural response.

2.4) Current near-fault seismic design provisions for bridges

This paragraph should give a better understanding of the basis in the current provisions for both the ground motion demand and the bridge capacity under FDGM's.

As a consequence of recent earthquakes, including the 1989 Loma Prieta, 1994 Northridge and 1995 Hyogo-ken Nanbu earthquakes, seismic design codes for highway bridges have been revised. Design Specifications of Highway Bridges were fully revised in 1996 in Japan. In 1994, Part 2 Bridges in Eurocode 8 Design Provisions for Earthquake Resistance of Structures was proposed as the European Pre-standard (Pinto 1995). In New Zealand, the Transit New Zealand Bridge Manual was revised in 1995 (TNZ 1995, Chapman 1995). In the United States, the American Association of Highway and Transportation Officials (AASHTO) published two codes for the design of highway

bridges: Standard Specifications for Highway Bridges and LRFD Bridge Design Specifications. The Department of Transportation of the State of California (Caltrans) has developed independent seismic design specifications, which are similar to, but not the same as, the AASHTO provisions. The ATC-32 recommendation was published to improve Caltrans seismic design practice (ATC 1996). Caltrans recently developed the Seismic Design Methodology (Caltrans 1999a) and the Seismic Design Criteria (Caltrans 1999b).

Concerning bridges, AASHTO LRFD Bridge Design Specification (Section 3.10.2) states that “special studies to determine site- and structure-specific acceleration coefficients shall be performed by a qualified professional if the site is located close to an active fault.” Caltrans (Feb. 2004) states that a “site-specific response spectrum is required when a bridge is located in the vicinity of a major fault.” (*Section 6.1.2.2 and 2.1 Caltrans Seismic Design Criteria, February 2004 Version 1.3*)

The 1997 edition of the UBC for the first time introduced two near-source factors: acceleration-related N_a and velocity-related N_v , the purpose of which is to increase the soil-modified ground motion parameters C_a and C_v when there are active faults capable of generating large-magnitude earthquakes within 15 km or 9 miles of a Seismic Zone 4 site. These factors became necessary in view of the artificial truncation of Z-values to 0.4 in UBC Seismic Zone 4. These near-source factors are not found in the 2000 IBC because the artificial truncation of ground motion is not a feature of that code.

2.5) Soil-Structure Interaction

Soil-structure interaction refers to the effect that the foundation soil has on the dynamic response of a structure and, conversely, the effect of the structure on the soil motion.

Modak (1995) stated that ground conditions at the site affect the earthquake response of structures. Two aspects of this influence are important:(1) *site effect* – the amplifying (or attenuating) effect of local geology on the intensity as well as its filtering effect on the frequency characteristics of the transmitted seismic waves, and (2) *soil-structure-interaction* – the effect of the surrounding soil properties of a structure on the structural response.

From the analytical standpoint, one may view soil-structure-interaction as consisting of two distinct effects: (a) *inertial interaction*, which arises from the motion of the foundation relative to the surrounding soil associated with the transmission of inertial forces from the structure to the adjoining soil; and (b) *kinematic interaction*, which can occur in the absence of inertial forces, that arise when a relatively stiff structural foundation can not conform to the distortion of the soil generated by the passage of seismic waves. (Derecho and Huckelbridge 1991)

2.5.1) Foundation models

Many researchers have developed foundation models. The following paragraphs describe those models.

2.5.1.1) Spread footings

Spread footings are typically built in competent material. In such cases, the foundation is so stiff that a fixed connection is adequate for describing its behavior. When the soil is marginal, the foundations should be modeled by spring elements or other methods. A simple method is to represent the foundation by a 6x6 stiffness matrix that can be determined from the foundation dimensions and the average elastic properties of the supporting soil. A general formulation of the elastic stiffness terms in the matrix has been developed for a rigid footing on a semi-infinite elastic half-space by closed-form solutions. The stiffness in the three translational and three rotational directions is provided, along with four off-diagonal terms. The embedment effects of the foundation may be included to modify the stiffness coefficient (Lam and Martin, 1986).

McGuire et al. (1994) tested many discrete foundation elements to model the behavior of the spread footing foundation. Five foundation models were considered, as shown in Figure 2.5.1. One model consisted of fixed supports, one consisted of elastic supports, and three had damped elastic supports that required three, five, and eleven parameters per degree-of-freedom, respectively. Results showed that it is not necessary to use a complex damped model. Employing simple spring-only foundation models (at least to account for soil far-field effects) is enough to represent the bridge foundation. The spring stiffness values are based on the static stiffness of an elastic half-space. Damped models can be used for soft soil (Veletsos and Verbic 1973, and Wolf 1988).

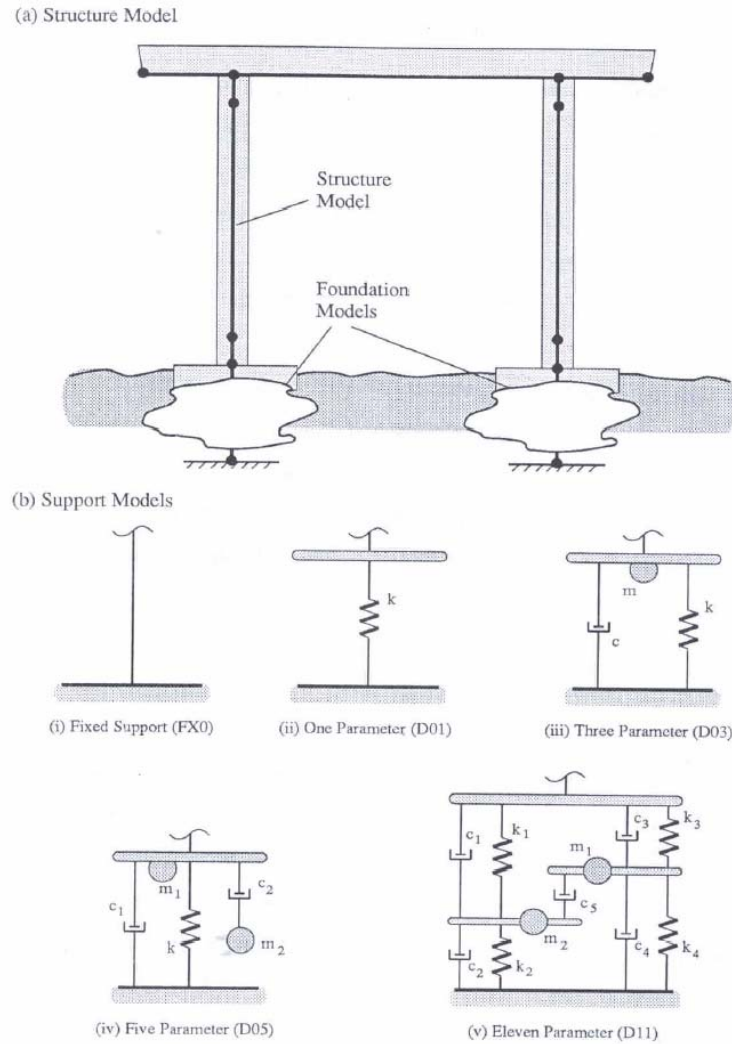


Figure 2.5.1: Schematic of discrete foundation models for the spread footing foundation: (a) bent structure; (b) foundation models. (McGuire et al., 1994)

2.5.1.2) Pile foundations

Bridge foundations are supported on piles because of weak soil, potential scour, or other factors. The pile foundations may include a single shaft or a group of piles integrated by a pile cap that supports a bent or abutment. There are various methods for modeling piles and pile foundations. A common nonlinear procedure is the p - y method that produces a family of nonlinear lateral force-displacement relations at various depths

along an individual pile (Reese 1977, Matlock et al. 1981). These relationships can be used to develop a 6x6 stiffness matrix at the top of each pile. The pile stiffnesses are combined to develop a 6x6 stiffness matrix for the foundation. Computer software, such as *L-Pile* and *Group* (Reese 2000), has been developed for applying this procedure to model piles and pile foundations.

Dameron and Sobash (1997) used a spring/damper to model the interactions between structure and foundation, and foundation and soil (or water). Comparison between linear and nonlinear foundation models shows that a linear foundation model does a poor job of predicting the response after the initial ground motion pulse.

McGuire et al. (1994, and Cofer et al., 1994) also studied pile foundations. Four foundation models were compared, as well as fixed-base supports. Three of the four foundation models were discrete springs or spring/damper systems, which modeled the pile cap behavior “seen” by the column bases. The fourth foundation model was a Winkler-type pile foundation. These five support conditions are shown in Figure 2.5.2.

The Winkler-pile was modeled with standard linear elastic beam elements and the soil was represented as a distributed elastic stiffness, which depended upon soil properties and the radius of the pile. For pile foundations, either the Winkler pile or pile head models may be used, but the pile head models are recommended because far fewer elements are required for the analysis.

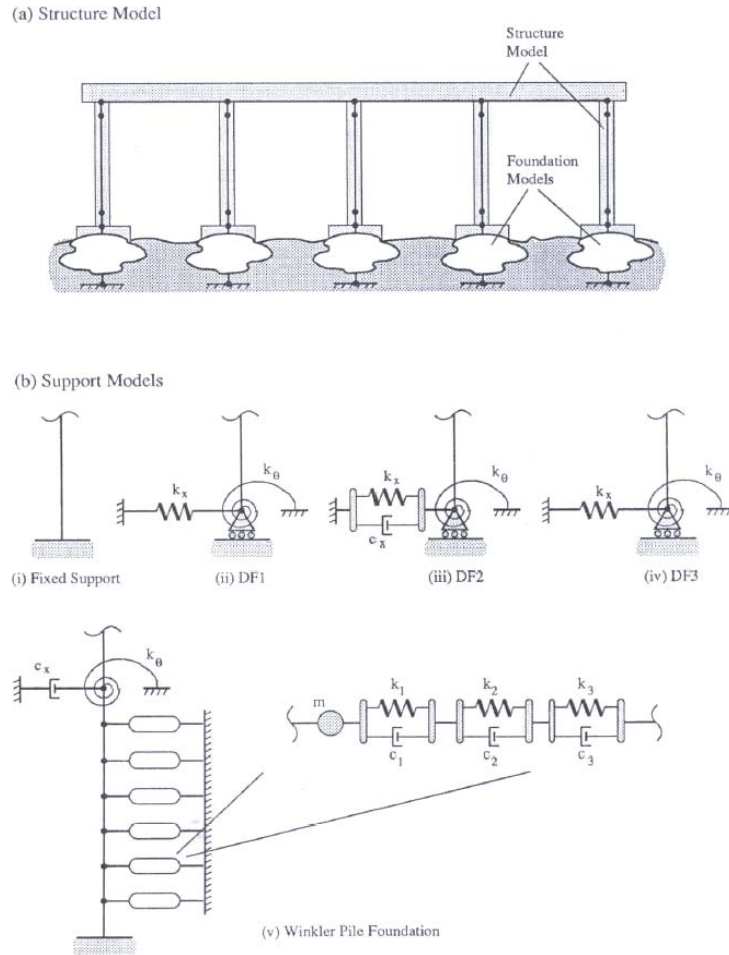


Figure 2.5.2: Schematic of models for the pile foundation: (a) bent structure; (b) foundation models. (Cofer, 1994)

2.5.2) Damping

Radiation damping is an important factor that can influence foundation–soil–structure interaction. Since radiation damping is a result of the stiffness differences between the piles (including pile cap) and the surrounding soil, it manifests primarily at higher frequencies and low soil damping. If gaps open between the foundation and soil, there can be no radiation damping. Hence, the accurate modeling of radiation damping, particularly if the top soil layers are cohesive, can be complex. A simple approach that

has been adopted by many researchers (e.g. Maragakis and Jennings 1987, Spyrakos 1992, Zhang and Makris 2002) is to use frequency independent springs and dashpots to represent the soil–foundation system. Such models, however, do not consider possible gaps during seismic excitation. Given the uncertainties in modeling the overall soil–foundation behavior and the fact that frequency independent dashpots generally deamplify the structural system response, it is not uncommon to neglect radiation damping altogether. In their investigation of the observed behavior of a two span overcrossing, Makris et al. (1995) were able to simulate the response of the bridge without the need for radiation damping. The simulations by Ciampoli and Pinto (1995) of a bridge also did not incorporate radiation damping. Additionally, recent investigations by Bielak and al. (2003) and Tongaonkar and Jangid (2003) indicate that in some cases radiation damping can be ignored with only minor effects on the system behavior.

2.5.3) Previous Research Papers

A number of papers in recent years have described investigations on the influence of the SSI on the behavior of bridges. In particular, Sweet (1993), and McCallen and Romstadt (1994) performed finite element analyses of bridge structures subjected to earthquake loads. However, Sweet did not approximate the geometry of pile groups, as he was unable to analyze a full model with available computer hardware. On the other hand, McCallen and Romstadt (1994) performed a remarkable full-scale analysis of the soil–foundation–bridge system. The soil material (cohesionless soil) was modeled using an equivalent elastic approach (using the Ramberg–Osgood material model through standard modulus reduction and damping curves developed by Seed et al., 1984). In studies by Chen and Penzien (1977) and Dendrou et al. (1985), the bridge

system was analyzed including the soil, but the models used very coarse finite element meshes.

Tongaonkar and Jangid (2002) showed that SSI affects the bearing displacements at the abutment and that ignoring these effects will cause the analysis to underestimate the design displacement at abutments, which may be crucial from the design point of view.

The effects of Soil-Structure-Interaction (SSI) are considered to be beneficial to the structure under the following conditions: (1) There are no significant permanent deformations in the structure resulting from yielding of the pier, or (2) the energy dissipation (hysteretic loops) of the system with SSI is smaller than that with a fixed foundation, leading to the conclusion that there is less damage to the structure.

The most dramatic failure during the Kobe earthquake was the collapse of an elevated section of the pile-supported Hanshin Expressway (see Figure 2.5.3). Gazetas and Mylonakis (1998) presented an analysis suggesting that period lengthening due to foundation flexibility may have resulted in increased structural forces during the earthquake due to forward directivity effects.



Figure 2.5.3: Collapsed of an 18-span viaduct section of Hanshin Expressway (from Ghasemi, 1996)

Jeremic and Kunnath (2004) studied the SSI of the I-880 viaduct. Foundation springs were obtained from a detailed 3D finite element model of the pile group foundation system using elastic soil properties. The site is located within 10 km of the Hayward Fault and is also in the immediate vicinity of the San Andreas Fault. The spectra contain rupture directivity effects. They were generated for both fault-parallel (FP) and fault-normal (FN) directions.

The SSI can either be beneficial or detrimental to the structure depending on the ground motion. Their analysis demonstrated the difficulty associated with developing guidelines for design since SSI effects are not only a function of the structural system and the soil–foundation behavior but also dependent on the ground motion. In general, this suggests that SSI effects should be evaluated on a case-by-case basis without generalizing the findings of a particular study.

McGuire's results (1994) indicate that the effect of incorporating foundation models on the predicted response is very dependent on the natural frequencies of the structure and the frequency content of the earthquake.

Mylonakis and Papastamatiou (2001), who studied bridge response on soft soil to nonuniform seismic excitation, observed that foundation rotations due to kinematic and inertial soil structure interaction tend to increase the response of the piers at low frequencies, but reduce response at high frequencies.

Dicleli (2006) concluded that, in the near-fault zones, linear elastic analysis may generally be used for the preliminary design of bridges. However, for the final design of bridges located in the near-fault zones, three dimensional nonlinear time history analysis seems more appropriate.

CHAPTER 3: Column Modeling and ABAQUS

Determining the appropriate force-displacement characterization for the columns in the modeled bridges is a key aspect in obtaining accurate results since the bridge stiffness is primarily influenced by the column elastic and inelastic response. Using ABAQUS, columns that had been tested previously were modeled.

The bridge columns that were considered were well-confined since they were chosen to represent bridges that were recently designed (1989-1993). Under design guidelines that specify appropriate column confinement, two tests were chosen to be modeled. Orozco (2002) tested well-confined columns under a large velocity pulse. Lehman (2000) studied well-confined columns (in accordance to the Applied Technology Council, ATC 32) with different longitudinal reinforcement ratios and aspect ratios to characterize the response of modern bridge columns to lateral loads.

3.1) *The Orozco columns*

3.1.1) Geometry and reinforcement

The test specimen had a diameter of 410 mm (16 in) that corresponds to a 1.83 m (72 in) prototype bridge column diameter. In addition, the test specimen had a height of 1.83 m (72 in) that corresponds to the prototype bridge column height of 8.23 m (324 in). The height of the bridge column was measured from the top of the footing to the center of the load stub. An elevation view of the column is seen in Figure 3.1.1.

The longitudinal reinforcing steel consisted of twelve 13 mm (0.5 in) diameter (#4) bars that were spaced equally, which produced a steel/concrete ratio of 1.2%. The

longitudinal steel had a yield strength of 416 MPa (Grade 60), conforming to ASTM 706 or equivalent, with a yield stress that should not exceed 520 MPa (75 ksi). The transverse reinforcement was 16 mm² (W2.5) ASTM with a yield strength of 555 MPa (Grade 80). The spiral was spaced at 32 mm (1.25 in) on center continuous from the base of the footing to the top of the load stub.

The concrete cover from the face of the bridge column to the face of the spiral was 13 mm (0.5 in). The concrete compressive strength of the column measured on the day of the test was 32.1 MPa (see section 3.2.2 for a description of the tests).

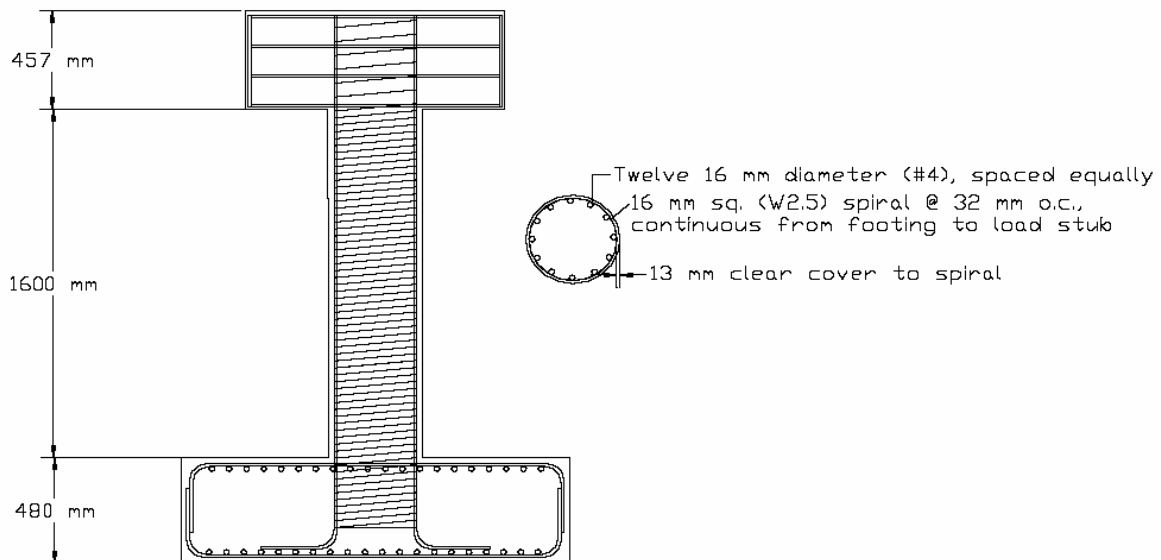


Figure 3.1.1: Column elevation (Orozco, 2002)

3.1.2) Loading and test setup

To study the effects of the large velocity pulse, two 22% scale bridge columns were tested. The bridge columns were subjected to a velocity pulse followed by a cyclic loading history. The specimen was loaded dynamically.

The test was completed with an actuator at a rate of 1 m/s (39 in/s). The input displacement time history was designed to model a near-fault displacement history. The loading history was composed of a cyclic loading history based on drift ratios of 0.5%, 1.0%, 1.5%, 2.0%, 3.0%, 4.0%, 5.0%, and 6.0%. Each drift ratio had three peaks in both the positive and negative directions. The input time histories were a combination of the pulse and the cyclic loading history. The saw-toothed displacement time history of the test is plotted in Figure 3.1.2.

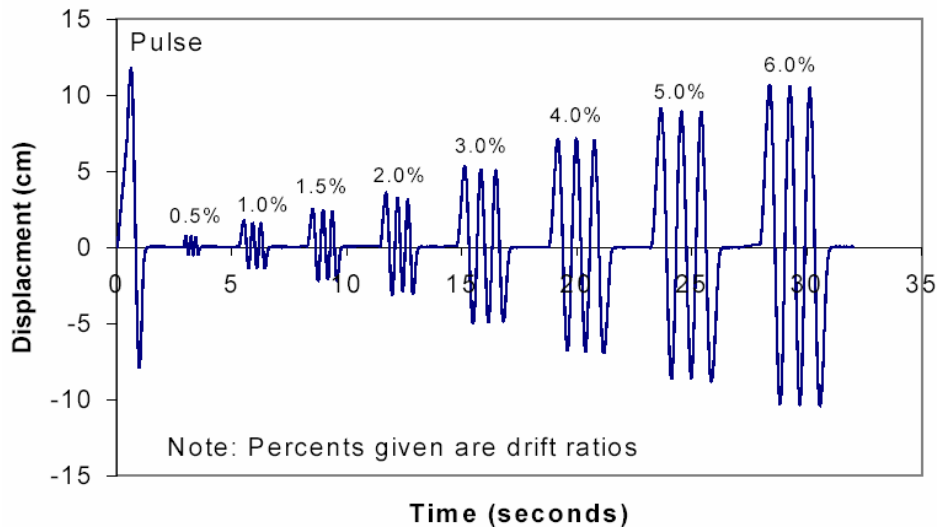


Figure 3.1.2: Input time history (Orozco, 2002)

The test setup is shown in Figure 3.1.3. The test specimen was secured to the strong floor by eight 35 mm (1-3/8 in), yield strength 1040 MPa (Grade 150) high strength bars stressed to 667 kN (150 kips). A 979 kN (220 kip) capacity actuator, with a \pm 610 mm (24 in) stroke, was attached in between the strong wall and load stub. No axial force was imposed to the column during the test.

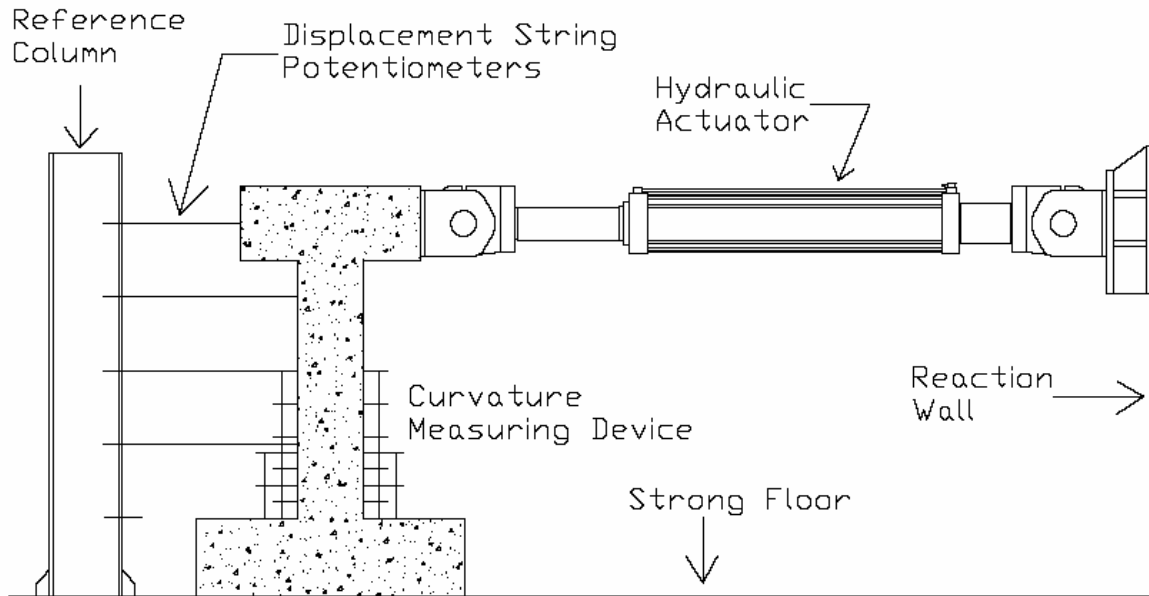


Figure 3.1.3: test setup (Orozco, 2002)

3.1.3) Recorded responses from testing

Test results are shown in Figures 3.1.4 and 3.1.5. What is most relevant to this research is the force-displacement hysteretic curve which characterizes the column behavior. One can see the Force-Displacement prediction given by the software Ruaumoko (Carr, 1996) in Figure 3.1.5.

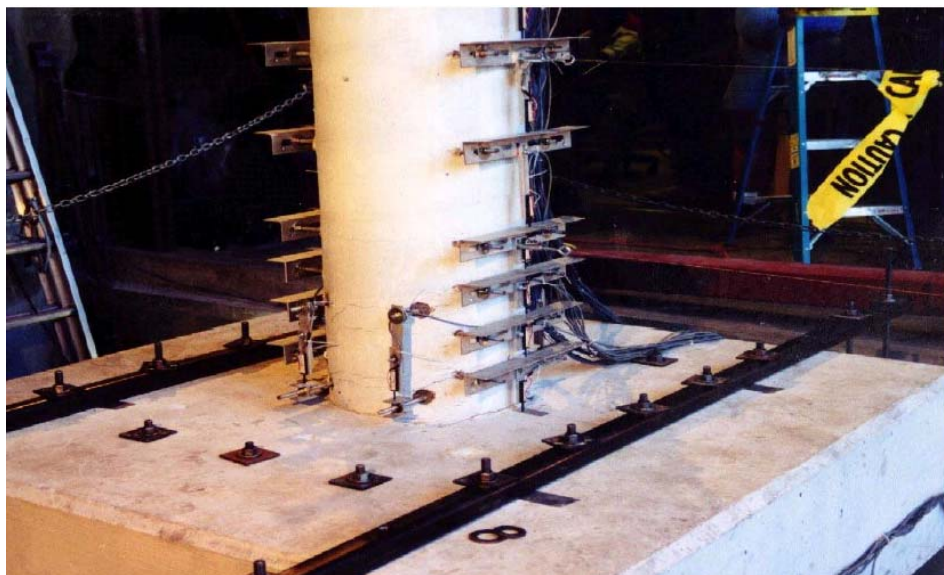


Figure 3.1.4: Overall view after pulse loading (Orozco, 2002)

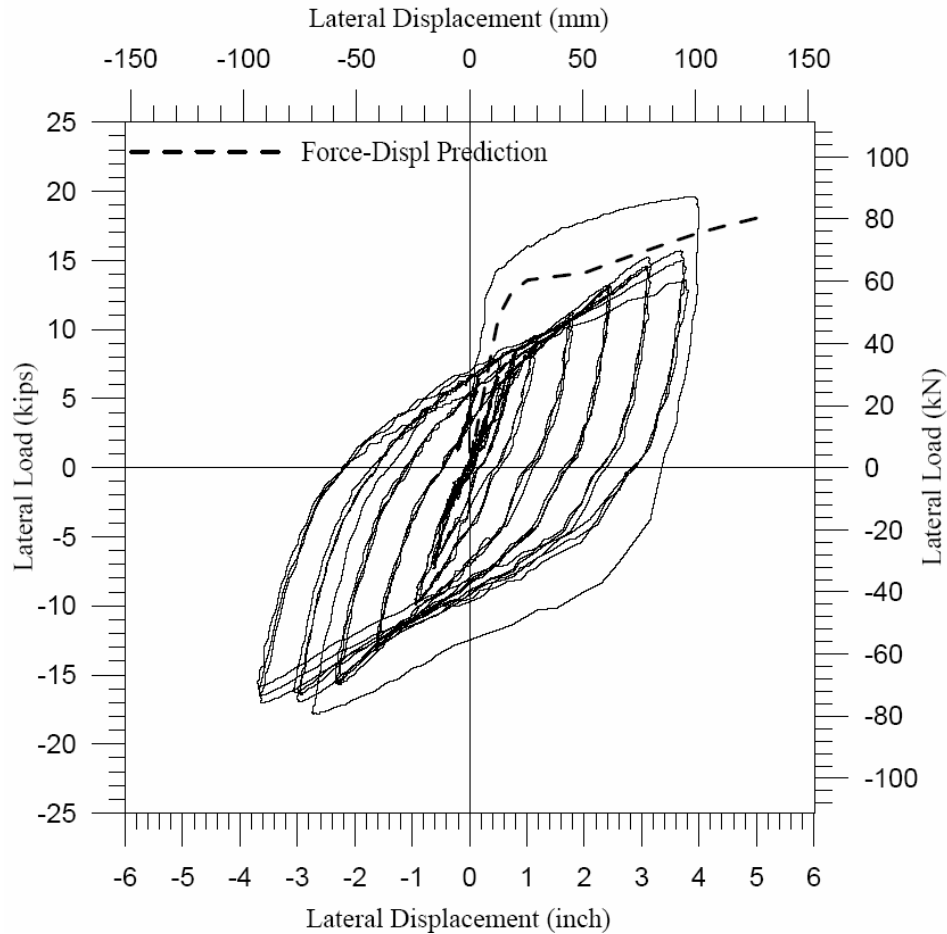


Figure 3.1.5: Recorded response: hysteretic force-displacement curve and dashed Ruaumoko (Carr, 1996) prediction (Orozco, 2002)

3.1.4) Finite Element Modeling of the Columns

3.1.4.1) Global geometric modeling

The Finite Element nonlinear static analysis was performed on ABAQUS/Standard with a 3D model. The columns were discretized by 3-node quadratic Timoshenko (shear flexible) beam elements. The length of the elements was made equal to (or a bit higher than) the plastic hinge length, L_p , given by Priestley (1996), as follows:

The plastic hinge length is approximated as

$$L_p = 0.08L + 0.022f_{ye}d_{bl} \geq 0.044f_{ye}d_{bl} \quad (f_{ye} \text{ in MPa}) \quad (3.1)$$

$$L_p = 0.08L + 0.15f_{ye}d_{bl} \geq 0.3f_{ye}d_{bl} \quad (f_{ye} \text{ in ksi}) \quad (3.2)$$

Where L is the length from the plastic hinge to the point of contraflexure. For a column in double bending, L is at the column mid-height. f_{ye} is the effective yield strength of the steel and d_{bl} is the diameter of the longitudinal reinforcing steel. The second portion in the equation accounts for the strain penetration of the longitudinal steel in the footing. The plastic hinge length is important because it directly affects the post-yield displacements. The choice in the size of the element is important since behavior results for a column are functions of the element length (Figure 3.1.6).

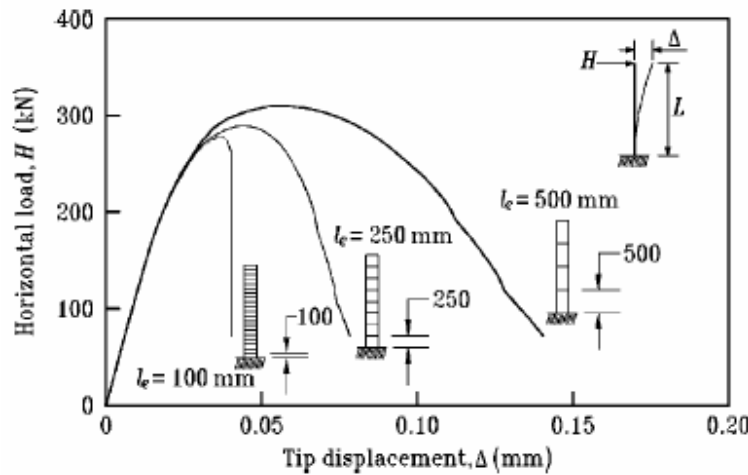


Figure 3.1.6: Response of columns with different sized elements (Légeron, 2005)

The columns were all made of 6 elements (Figure 3.1.7), each integrated at the top and bottom. For the four top elements, the default integration points were used through the thickness for economy, as shown in Figure 3.1.8. More integration points (5 radially, 12 circumferentially) were imposed to the two bottom elements of the column because more accuracy in the results is required there due to the occurrence of damage.

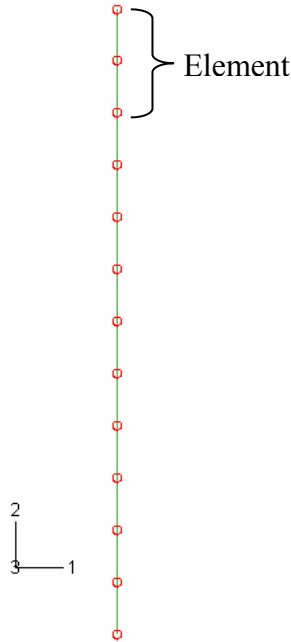


Figure 3.1.7: Column with 6 elements (13 points)

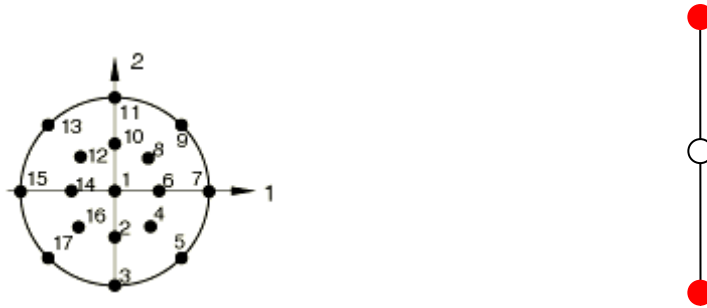


Figure 3.1.8: Default 3 radially, 8 circumferentially integration points, through the beam cross section and two integration point locations (in red) along the length of the 3-node element

The column was fixed at the bottom. An imposed displacement Δu was applied at the top of the column as shown in Figure 3.1.9.

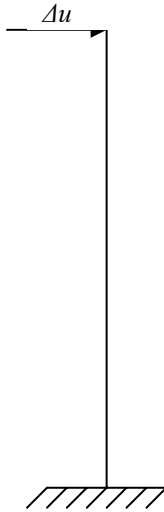


Figure 3.1.9: Column model in ABAQUS

During the finite element analysis, there was no need to include three cycles at each displacement level as was done in the tests, since ABAQUS will give the exact same results for each cycle. The damage occurring in the column can be modeled only when the demand (loading) increases. Figure 3.1.10 shows the imposed displacement history used during the finite element analysis.

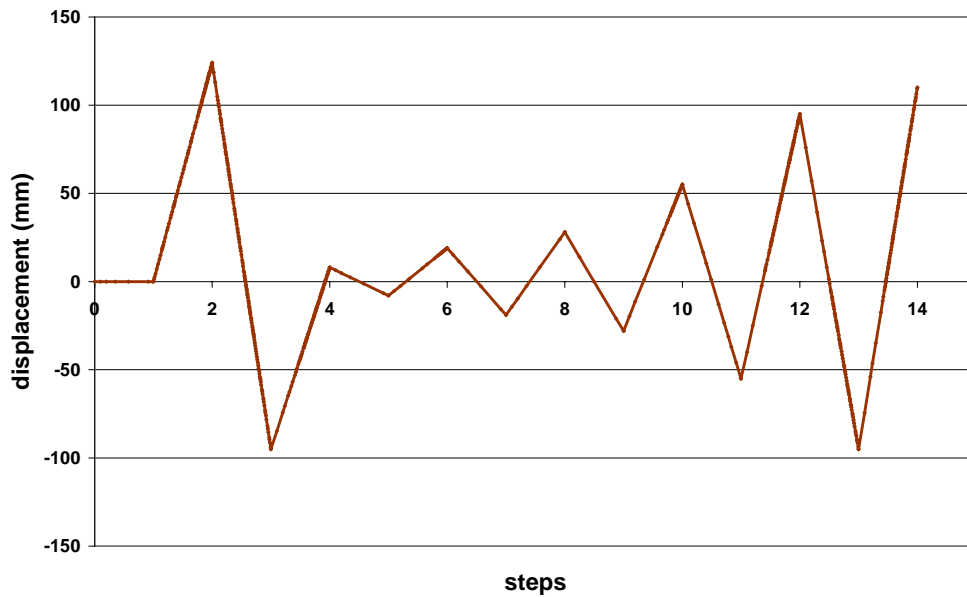


Figure 3.1.10: Input time history during the ABAQUS analysis

3.1.4.2) Material models

The material models used in ABAQUS are well established in practice. The material models used in this study were the smeared crack concrete model, and the metal plasticity model that includes both kinematic and isotropic hardening. This section describes them and gives the final input material properties.

3.1.4.2.1) Concrete

The ABAQUS User Manual (2004) gives a description of the smeared crack concrete model which:

- “provides a general capability for modeling concrete in all types of structures, including beams, trusses, shells, and solids;
- can be used for plain concrete, even though it is intended primarily for the analysis of reinforced concrete structures;
- can be used with rebar to model concrete reinforcement;
- consists of an isotropically hardening yield surface that is active when the stress is dominantly compressive and an independent ‘crack detection surface’ that determines if a point fails by cracking;
- uses oriented damaged elasticity concepts (smeared cracking) to describe the reversible part of the material's response after cracking failure;
- requires that the linear elastic material model be used to define elastic properties.”

The input parameters for the smeared crack concrete model are the modulus of elasticity, and the compressive and tensile stress-strain curves. These parameters are described below.

Modulus of elasticity:

It has been determined by Priestley (2003) that the moment of inertia of reinforced concrete columns should be reduced to account for initial cracking. In ABAQUS, because beam properties result from integration over the cross section, the modulus of elasticity E_c had to be changed to take into account the effect of the moment of inertia reduction. A new value of $E_{cc} = E_c/2$ was tested. The initial slope of the force-displacement curve was found to be approximately equal to that of the experimental one. Note that the actual predicted value of the concrete modulus of elasticity is given by Priestley (1996):

$$E_c = 4780 \sqrt{f'_c} \quad (\text{MPa}) \quad (3.3)$$

In this way, the effective bending stiffness of the element is properly modified.

Compressive stress – strain relationship:

The properties for confined concrete differ from those for unconfined concrete. Mander and Priestley (1988) developed a stress-strain model for concrete subjected to uniaxial compressive loading and confined by transverse reinforcement. Since ABAQUS cannot model the transverse reinforcement for the 3D beam element, the confined concrete properties have to be computed from empirical data. The peak compressive stress (f'_{cc}) that can be developed in the confined concrete is (Mander and Priestley, 1988):

$$f'_{cc} = f'_c \left(2.254 \sqrt{1 + \frac{7.94 f'_l}{f'_c}} - \frac{2 f'_l}{f'_c} - 1.254 \right) \quad (3.4)$$

Where:

$$f'_l = K_e f_l \quad (3.5)$$

$$f_l = \frac{2f_{yh}A_{sp}}{D's} \quad (3.6)$$

$$\varepsilon_{cc} = 0.002 \left[1 + 5 \left(\frac{f'_{cc}}{f'_c} - 1 \right) \right] \quad (3.7)$$

$$K_e = A_e/A_{cc} \quad (3.8)$$

$$A_{cc} = A_c (1 - \rho_{cc}) \quad (3.9)$$

In the above equations, f_l is the maximum lateral confining stress at yield in the transverse reinforcing steel. f'_l is the effective confining stress, and K_e is the confinement effectiveness coefficient. f'_c is the compressive strength of unconfined concrete; f_{yh} is the yield strength in the transverse reinforcement; A_{sp} is the area of the transverse reinforcing bar; D' is the diameter of the confined column core; s is the vertical spacing of transverse reinforcement; ρ_{cc} is the ratio of the area of longitudinal reinforcement to the area of core of the section; A_c is the area of the core of the section enclosed by the center lines of the perimeter spiral; A_e is the area of the effectively confined concrete core; and ε_{cc} is the strain when f'_{cc} is reached.

The ultimate strain reached in the confined concrete is based upon a relationship proposed by Priestley et al. (1996).

$$\varepsilon_{cu} = 0.004 + \frac{1.4\rho_s f_{yh} \varepsilon_{su}}{f'_{cc}} \quad (3.10)$$

According to Priestley et al., Equation 3.10 is intended to be used for design, typically being conservative by 50%. However, this equation was used unchanged. Figure 3.1.11 summarizes the difference in behavior between unconfined and confined concrete. The entire concrete section was assigned these confined concrete properties, including the concrete cover. The behavior of the column is assumed to be governed by the confined concrete section, because the concrete cover thickness is relatively small compared to the diameter of the entire section. Figure 3.1.12 shows the typical compressive stress-strain curve input into ABAQUS.

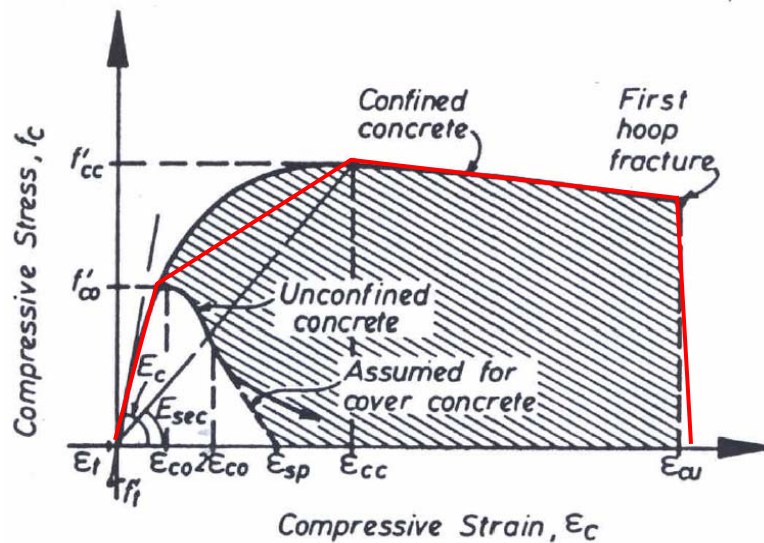


Figure 3.1.11: Stress-Strain Model Proposed for Monotonic Loading of Confined and Unconfined Concrete (Mander & Priestley, 1988)

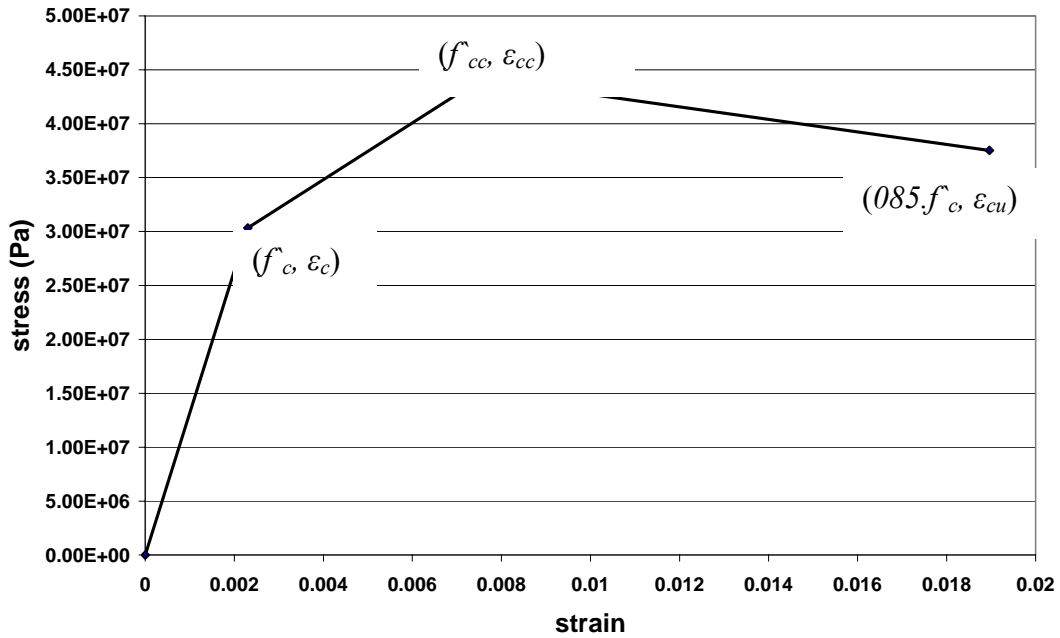


Figure 3.1.12: Stress–Strain Relationship for the Concrete in Compression

Tension stress – strain relationship:

Very little research has been performed to specify the full stress-strain behavior for tension in concrete. However, Mazars (1989) reports the relationship, shown in Figure 3.1.13.

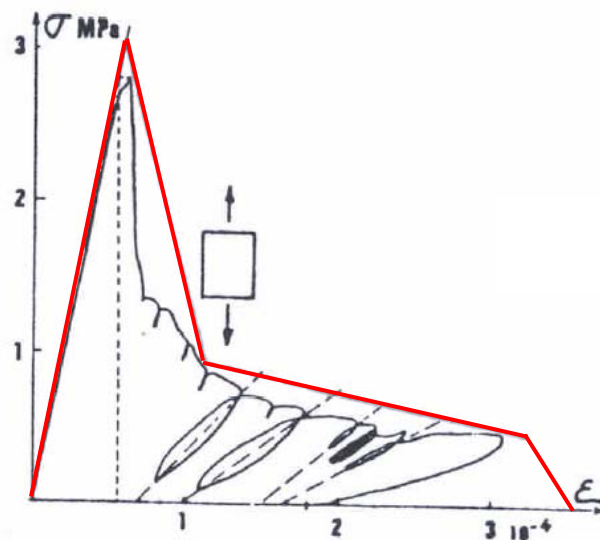


Figure 3.1.13: Experimental Behavior of Concrete under Tension (Mazars, 1989)

Effects associated with the rebar and the concrete interface, such as bond slip and dowel action, are modeled approximately by introducing some “tension stiffening” into the concrete modeling to simulate load transfer across cracks through the rebar.

The ABAQUS Manual states that “the interaction between the rebars and the concrete tends to reduce the mesh sensitivity, provided that a reasonable amount of tension stiffening is introduced in the concrete model to simulate this interaction. This requires an estimate of the tension stiffening effect, which depends on such factors as the density of reinforcement, the quality of the bond between the rebar and the concrete, the relative size of the concrete aggregate compared to the rebar diameter, and the mesh.”

“The choice of tension stiffening parameters is important since, generally, more tension stiffening makes it easier to obtain numerical solutions. Too little tension stiffening will cause the local cracking failure in the concrete to introduce temporarily unstable behavior in the overall response of the model.” (ABAQUS manual 2004)

The tensile concrete cracking stress is given by Priestley (1996):

$$f'_t = 0.75 \sqrt{f'_c} \quad (\text{MPa, concrete in flexural tension}) \quad (3.10)$$

The typical tensile stress – strain curve used during ABAQUS analysis is shown in Figure 3.1.14.

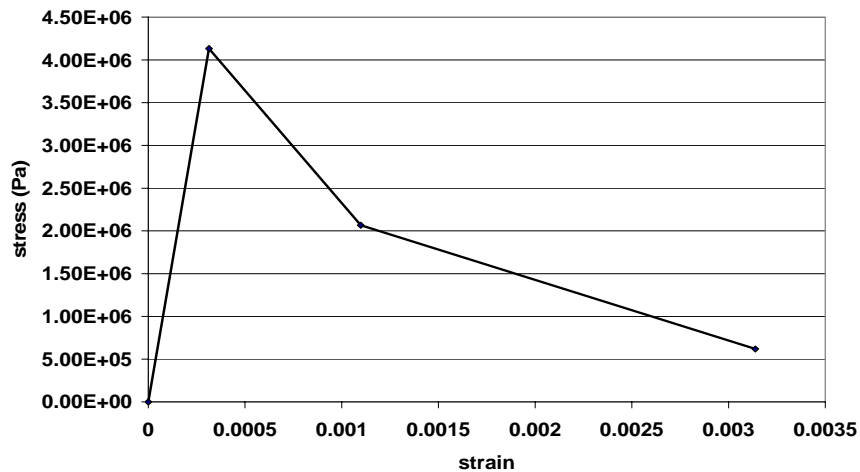


Figure 3.1.14: Tensile Stress-Strain Curve of the Concrete

Damage in the concrete:

ABAQUS gives many possible ways to model the damage occurring in the concrete. Reinforced concrete columns exhibit many damage mechanisms including pinching, spalling, bond failure, rebar buckling, and cracking. Figure 3.1.15 describes the main behavior of the concrete during the damaging process. Because of the many interacting effects, it is difficult to specify a structural model. The concrete smeared cracking model was used to capture the overall damage behavior of the column.

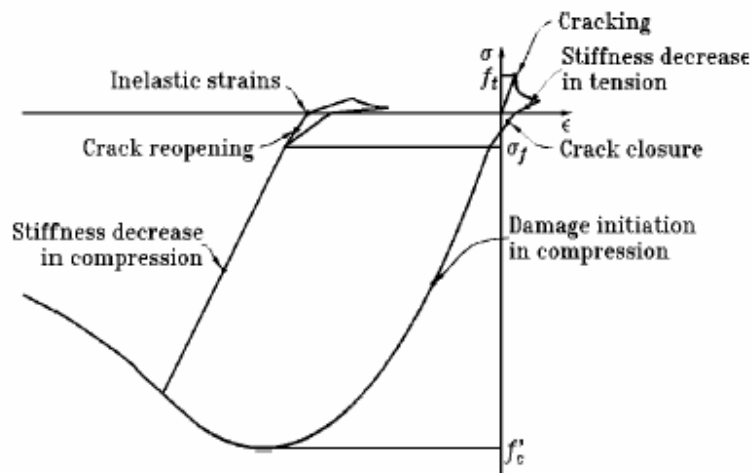


Figure 3.1.15: Behavior of concrete (Légeron, 2005)

The model is a smeared crack model, in the sense that it does not track individual “macro” cracks. Rather, constitutive calculations are performed independently at each integration point of the finite element model, and the presence of cracks enters into these calculations through the effect of the cracks on the stress and material stiffness associated with the integration point.

When concrete is loaded in compression, it initially exhibits elastic response. As the stress is increased, some nonrecoverable (inelastic) straining occurs, and the response of the material softens. An ultimate stress is reached, after which the material loses

strength until it can no longer carry any stress. If the load is removed at some point after inelastic straining has occurred, the unloading response is softer than the initial elastic response. However, this effect is ignored in the model. When a uniaxial specimen is loaded into tension, it responds elastically until, at a stress that is typically 7-10% of the ultimate compressive stress, cracks form so quickly that - even on the stiffest testing machines available - it is very difficult to observe the actual behavior. For the purpose of developing the model, the material is assumed to lose strength through a softening mechanism that is dominantly a damage effect, in the sense that open cracks can be represented by a loss of elastic stiffness (as distinct from the nonrecoverable straining that is associated with classical plasticity effects, such as that used for the compressive behavior model). The model neglects any permanent strain associated with cracking; that is, cracks are assumed to close completely when the stress across them becomes compressive

3.1.4.2.2) Longitudinal Steel

In ABAQUS, reinforcement in concrete structures is typically provided by means of rebars, which are one-dimensional rods. Rebars are typically used with metal plasticity models to describe the behavior of the rebar material and are superposed on a mesh of standard element types used to model the concrete. Figure 3.1.16 shows the steel stress-strain relation of the longitudinal rebars. This is based on the Caltrans 1999 grade 60 steel values. Special models have been developed in ABAQUS for metals subject to cyclic loading. The model chosen is one that includes both kinematic and isotropic hardening.

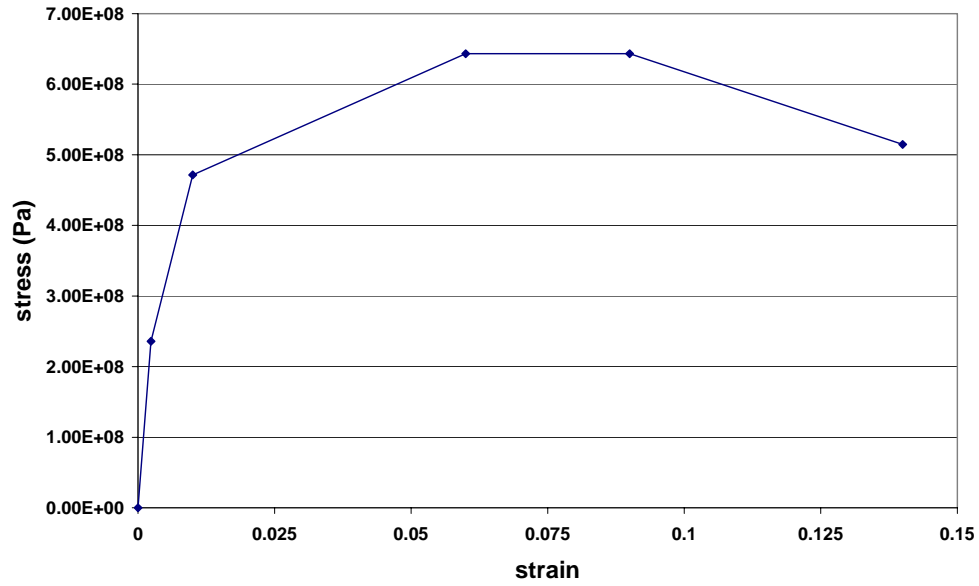


Figure 3.1.16: Steel Stress-Strain Curve

3.1.5) ABAQUS Results

Once the finite element computations were done, the shear force at the bottom of the column was plotted as a function of the imposed displacement to give the hysteretic curves shown in the following figures.

Figure 3.1.17 shows the force-displacement curves, compared with experimental results. The solid red lines are from the finite element analyses.

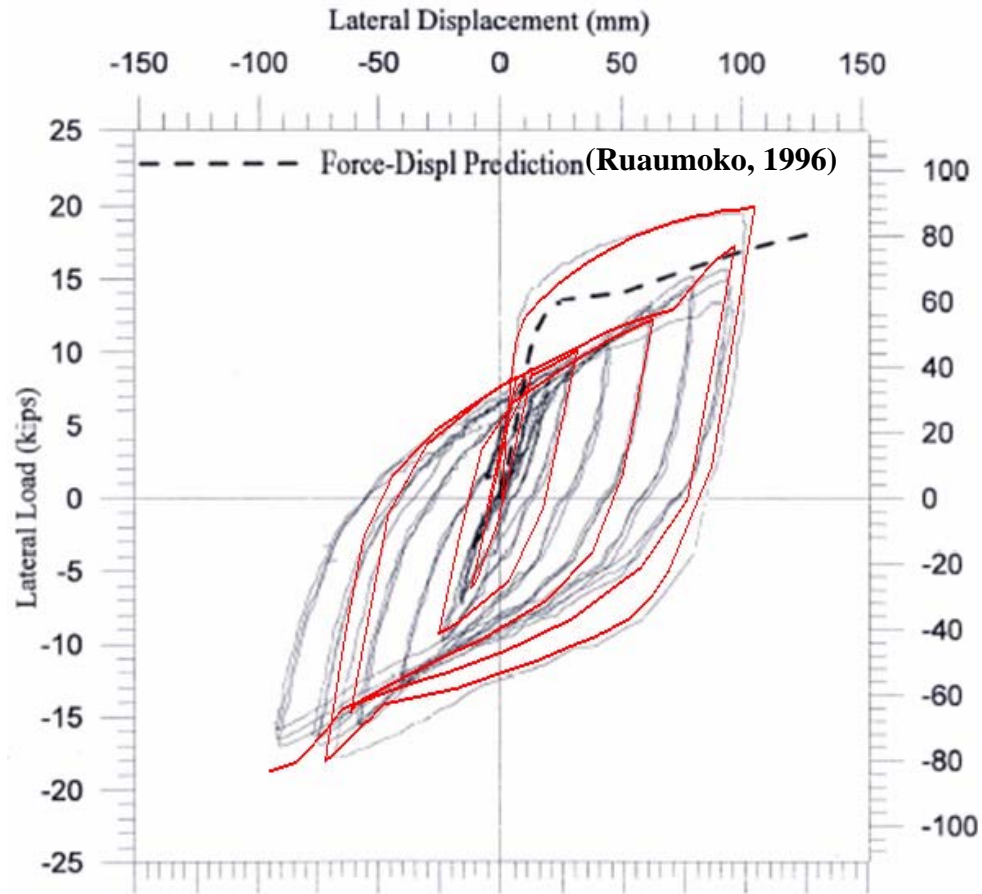


Figure 3.1.17: Comparison of Orozco (light gray) and ABAQUS results (solid red)

3.2) Lehman column

The ABAQUS results were quite accurate when compared to those of Orozco's tests. To provide further validation of the modeling technique, a different set of test results were obtained and analyzed (Lehman, 2000).

3.2.1) Geometry and reinforcement

The column diameter was selected to be 61 cm (2 feet) to model a 1.83 m (6 feet) diameter prototype column (one-third full scale). The column was 2.44m (8 feet) tall. The

concrete cover was 1.9 cm ($\frac{3}{4}$ inch) thick. Column and joint details of the test specimen are shown in Figure 3.2.1.

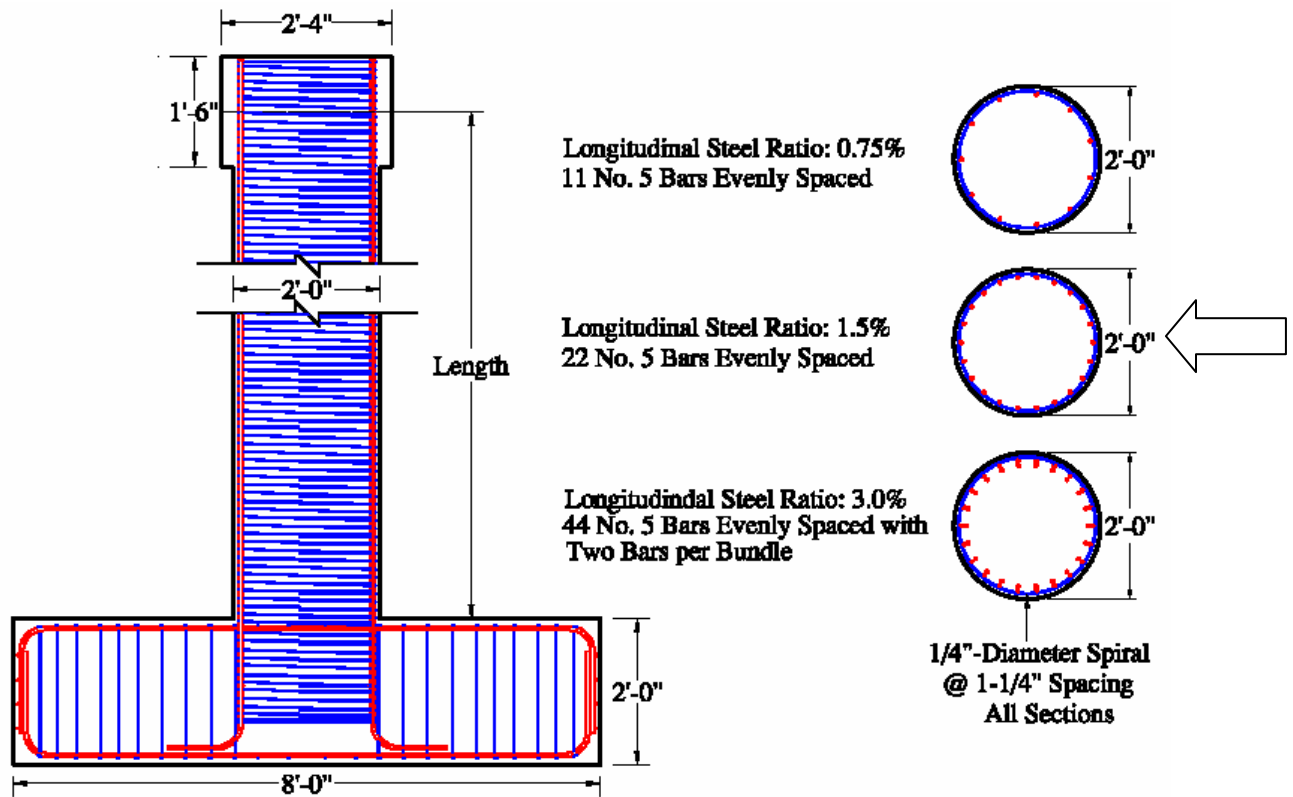


Figure 3.2.1: Specimen Geometry and Reinforcement of the Lehman column. (Lehman, 2000)

The column was reinforced with 1.5% longitudinal steel (22 No.5 bars) and had an aspect ratio of 4. The longitudinal reinforcement was spaced evenly around the column circumference. The longitudinal reinforcement was embedded into the joint to a depth of 54.61 cm (21.5 inches), approximately equivalent to 34 bar diameters. The column spiral reinforcement ratio was 0.7%. The spiral was 0.64 cm ($\frac{1}{4}$ inches) in diameter smooth wire spaced at 3.17 cm ($1\frac{1}{4}$ inches). The spiral reinforcement was continuous throughout the column height and joint depth. Table 3.2.1 gives the steel

properties. The compressive strength of the concrete used on the day of the test was 30 MPa (4.4 ksi).

Table 3.2.1: Steel properties

Bar	Yield (ksi)	Ultimate (ksi)
Longitudinal rebars	68.4	93.3
Spiral	96.9	98.9

3.2.2) Loading and test setup

Axial and lateral loads were applied to the top of the column. Figure 3.2.2 depicts the experimental configuration. The applied axial load of 667 kN (150 kips) was approximately equivalent to $0.07f_c A_g$, where f_c = actual concrete compressive strength and A_g is the column gross section area. The axial load ratio chosen corresponded to average axial load ratios found in single-column bent bridge construction. The axial load was applied through a spreader beam using post-tensioned rods placed on either side of the column. The lateral load was applied using a servo-controlled hydraulic actuator that was attached to the top of the column.

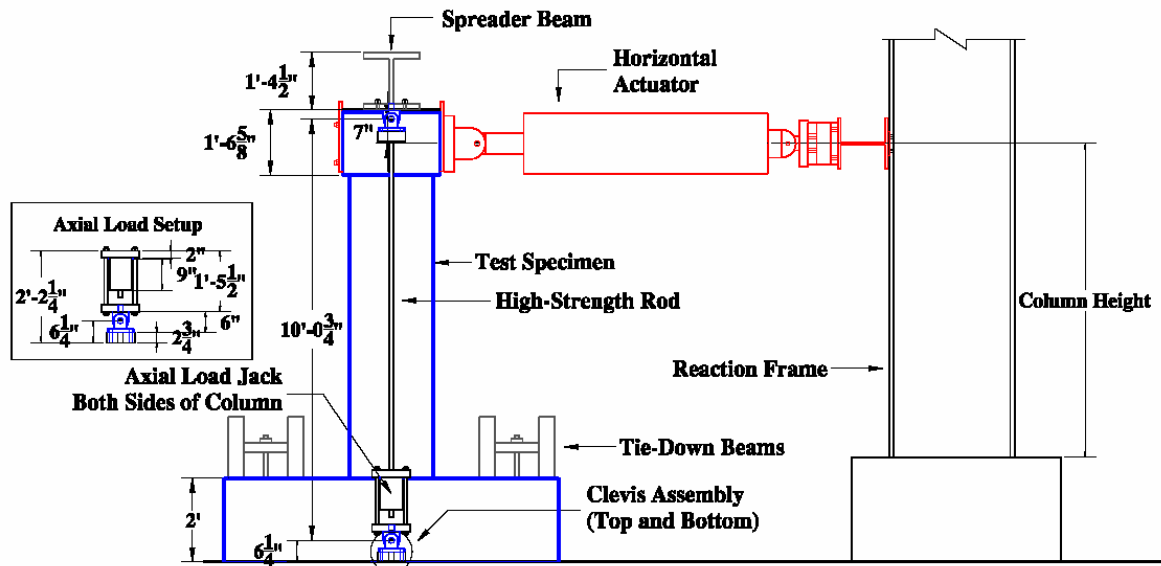


Figure 3.2.2: Experimental configuration (Lehman, 2000)

The imposed displacement history included three cycles at each displacement level (Figure 3.2.3). Note that no initial pulse was applied and that the rate of loading was very slow. The imposed displacement history depends upon the effective yield displacement given by the following equation:

$$\Delta_y' = \frac{M_n}{M_y} \Delta_y \quad (3.11)$$

The computed effective yield displacement was 2.34 cm (0.92 inches).

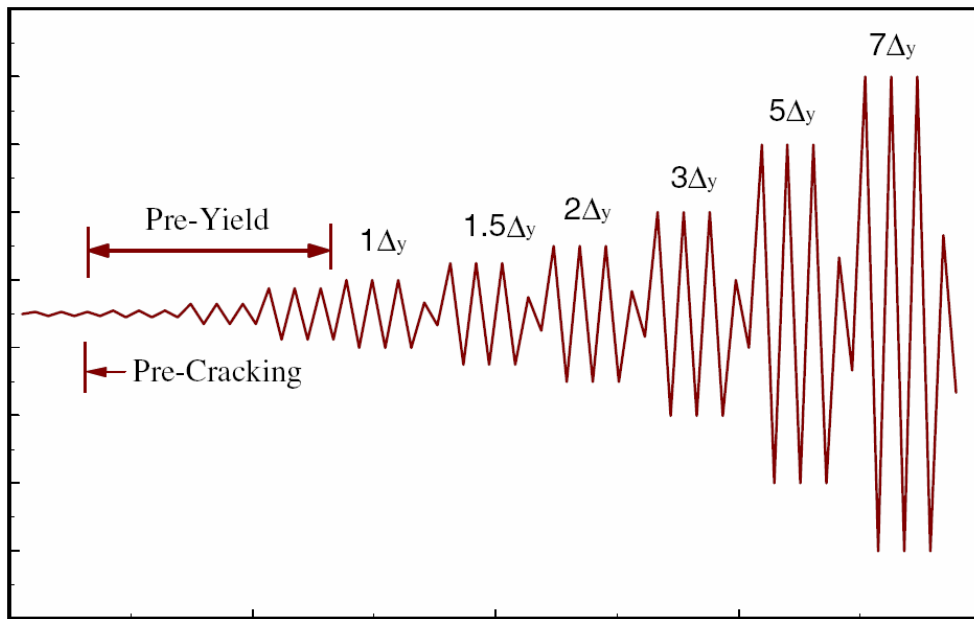


Figure 3.2.3: Imposed displacement during the test (Lehman, 2000)

3.2.3) Recorded responses from testing

Bending and slip were observed to dominate the column response.

A brief chronological description of the visual indications was provided:

1. Cracking of the concrete
2. First yield of longitudinal steel
3. Spalling above the column-footing interface
4. Spirals and longitudinal steel exposed; complete loss of the concrete cover

5. Extension of spiral and longitudinal bar buckling
6. Spiral fracture
7. Longitudinal bar fracture
8. Failure of the column

Figure 3.2.4 shows the final damage state at the bottom of the column, where all visible bars on both faces buckled. Figure 3.2.5 shows the force-displacement hysteretic curve recorded during the test.



Figure 3.2.4: Final damage state (Lehman, 2000)

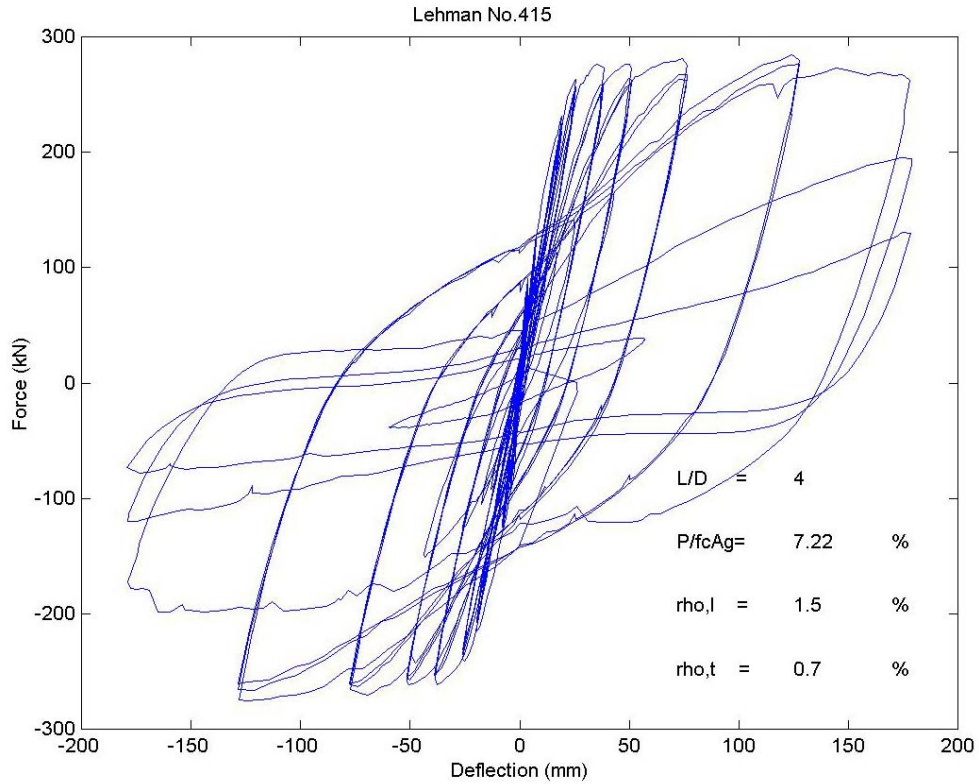


Figure 3.2.5: Force – Displacement Response (Lehman, 2000)

One observes pinching behavior due to the cracks starting from an imposed displacement of 7.6 cm (3 in). Compared to the specimens from Orozco’s tests, this column developed a lot more pinching.

3.2.4) Finite Element modeling of the column

The methods used to compute the geometry and the material parameters were the same as described earlier (section 3.1.4). Figure 3.2.6 shows the imposed displacement used during the finite element analysis.



Figure 3.2.6: Imposed displacement during the ABAQUS analysis

3.2.5) ABAQUS Results

Once the finite element computations were complete, the shear force at the bottom of the column was plotted as a function of the imposed displacement to give the hysteretic curves shown in Figure 3.2.7. Figure 3.2.7 also shows the force-displacement curves, compared with experimental results. The ABAQUS model was shown to generate an accurate backbone curve. The values of peak force and both initial and subsequent stiffness were predicted quite accurately. The increased pinching observed with Lehman’s tests was underestimated. Pinching likely results from damage between the concrete and the rebars and it may be affected by the rate of loading. As a consequence, the ABAQUS finite element model will have a tendency to overestimate the energy dissipated from the column hysteretic behavior.

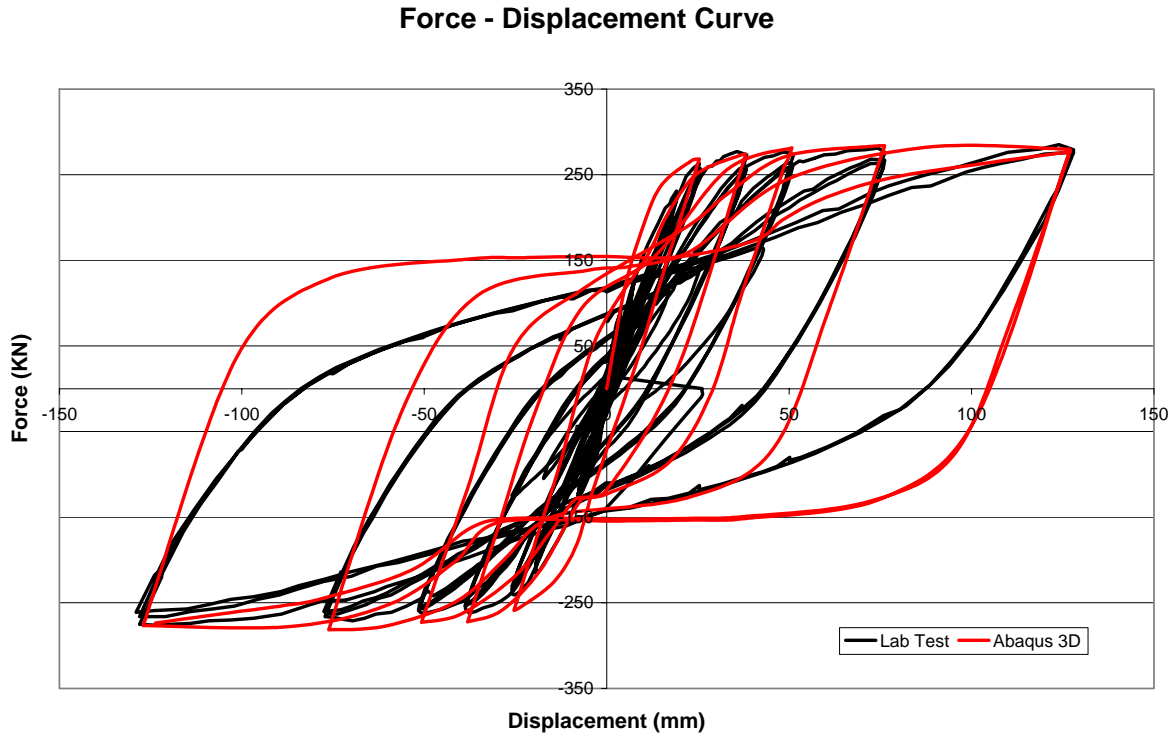


Figure 3.2.7: Comparison of Lehman and ABAQUS results

3.3) Conclusion

In order to verify that a model using the ABAQUS finite element software can accurately simulate the cyclic behavior of well-confined reinforced concrete columns when subjected to FDGM's, two test specimens were modeled. While many material properties for the concrete and steel reinforcing were defined using accepted practice, a number of parameters are numerical in nature, rather than being based on known physical properties. The latter were defined by matching the overall test results of Orozco, for which pulse-type loading was used to simulate FDGM ground motion. Then, with essentially the same values, the tests of Lehman were modeled. The following conclusions may be drawn.

Both finite element models were shown to generate accurate backbone curves. The values of peak force and both initial and subsequent stiffness were predicted quite

accurately. While the cyclic behavior was simulated relatively well for the dynamic test of Orozco, the increased pinching observed with Lehman's tests was underestimated. Pinching likely results from damage between the concrete and the rebars and it may be affected by the rate of loading. The loading rate during an earthquake more nearly matches that of Orozco's dynamic test than those of the others.

By modifying the geometry and the physical material properties of Orozco's test specimen to match those of Lehman's test specimen, a reasonably accurate model was conveniently obtained. All numerical material parameters were unchanged except for the tensile damage variable, which was decreased to better match the strength behavior when the loading did not include an initial pulse.

The ABAQUS model that was developed was shown to provide accurate simulations for a test specimen that was designed and loaded specifically for FDGM. For a similar specimen with a more traditional test sequence, the same model gave reasonably accurate results, the only significant difference being that the hysteresis curve did not fully represent the level of pinching. With the favorable results, the ABAQUS model can be used with confidence to evaluate the seismic performance of bridges subjected to forward directivity ground motions.

CHAPTER 4: Seismic Analysis of Bridges

4.1) *Seismic Excitations*

This section describes the ground motion selection process, in addition to the main characteristics of the selected ground motions.

4.1.1) Ground Motion Selection

To obtain a set of non-Forward Directivity (FD) Ground Motions (GMs), a probabilistic seismic hazard analysis (PSHA) for each bridge site, including deaggregation, was performed by Gillie (2005), leading to a target design spectrum for each bridge. Deaggregation helps determine which pairs of M_w and R to use when choosing ground motions for site specific evaluations. Once the ranges of magnitude and distance were determined, all ground motions that satisfied these requirements were selected for further analysis from the PEER database (PEER 2000). In some cases the distance and magnitudes were expanded to obtain motions that best satisfied the following criteria: similar faulting type, recorded on rock, response spectra matching the shape of the target spectra, and no FD characteristics. Spectral matching was applied to the non-FDGMs to fit the target spectra. Finally, a one dimensional site response analysis was performed on the ground motions to take into account the nature of the surrounding soil at the foundation of each bridge. The non-FDGMs were composed of 3 sets, one for each bridge, of 5 ground motions with both the fault normal and fault parallel components. The FDGMs were selected based on the expected ground motions from the Seattle Fault Zone. They did not have spectral matching and site response either to preserve their period content integrity. For more details, see the thesis of Gillie (2005).

4.1.2) Ground Motion Characteristics

The non-FDGM spectral accelerations are showed in Figures 4.1.1 and 4.1.2. The bridge acceleration spectra, in colors, were derived from the target spectrum (the Equal Hazard Spectrum from the PSHA), to include site response. The spectral accelerations for Bridge 405 and Bridge 520 were very similar because their soil properties were similar.

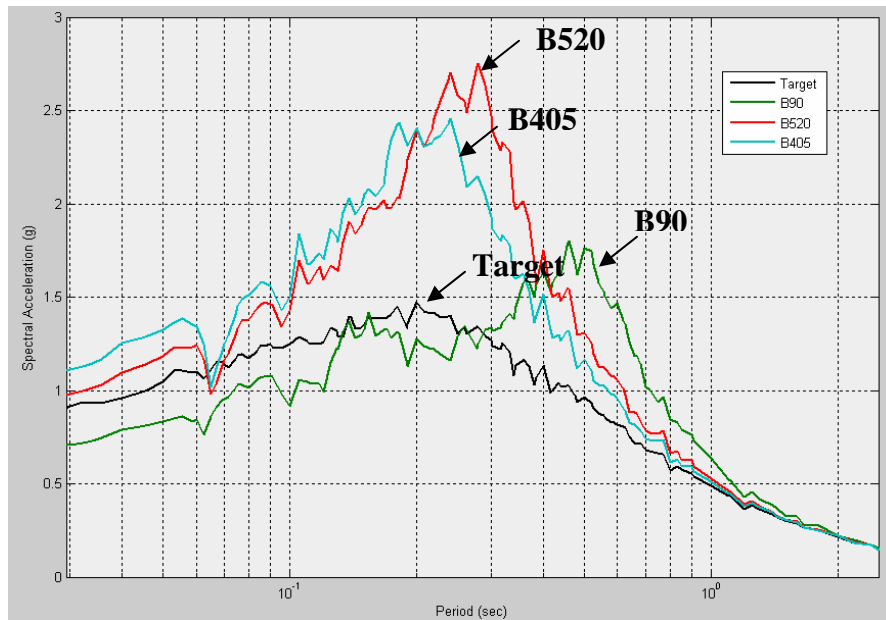


Figure 4.1.1: Non FDGMs Acceleration Spectra (Log. scale)

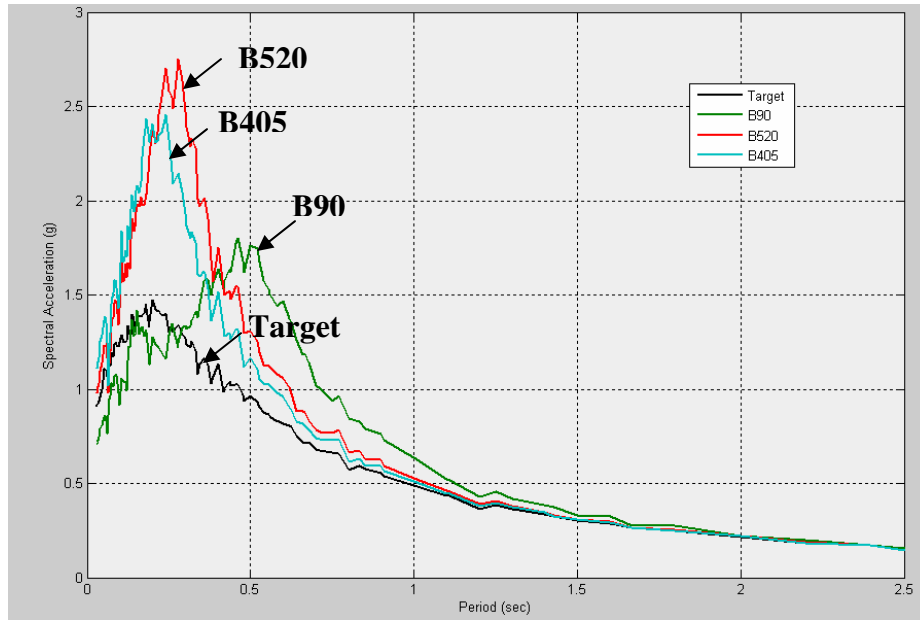


Figure 4.1.2: Non FDGMs Acceleration Spectra

The selected FDGMs and their characteristics are listed in Table 4.1.1. For each ground motion component, the record length and the Peak Ground Acceleration (*PGA*) are indicated. The ground motion acceleration, velocity and displacement time histories, spectral acceleration, and velocity are in Appendix B.1.

Table 4.1.1: FDGM characteristics

GM	Magnitude	Time (s)	GM Component	<i>PGA</i> (g)
Sylmar	6.7	20	FN	0.733
			FP	0.595
T75	7.6	50	FN	0.314
			FP	0.278
KJM	6.9	26	FN	0.854
			FP	0.548
BAM	6.5	15	FN	0.880
			FP	0.647
F14	6.0	21	FN	1.015
			FP	0.857
RRS	6.7	15	FN	0.887
			FP	0.390

4.2) Coordinate Axes

The longitudinal axis of each bridge was oriented along the global X axis following the positive right hand rule sign convention for the global Y and Z axes. Local and global coordinate systems are defined in Table 4.2.1 below. Figure 4.2.1 shows the different coordinate axes.

Table 4.2.1: Local and Global Coordinate Systems

Global Coordinate Axes		Local Coordinate Axes		
Bridge Direction	Global Axes	Trans. Elements	Long. Elements	Vert. Elements
Transverse	Y	X	Y	Y
Longitudinal	X	Y	X	Z
Vertical	Z	Z	Z	X

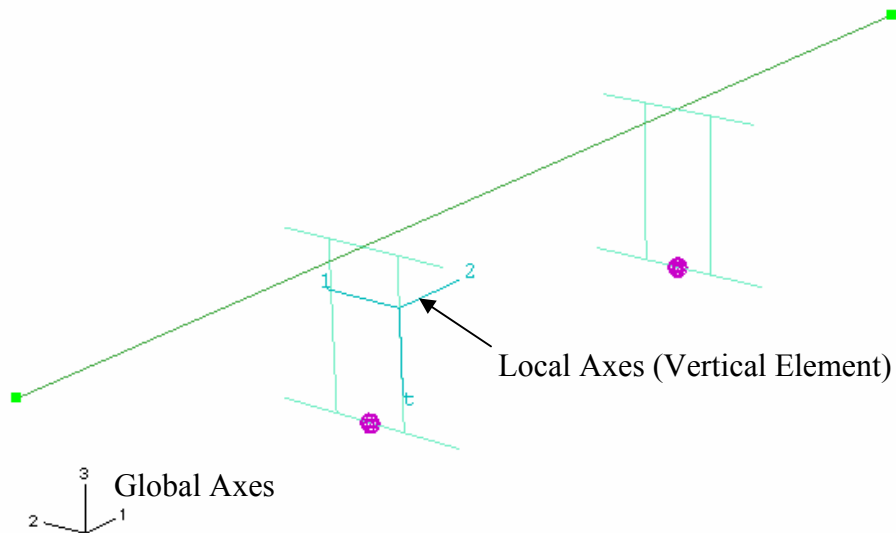


Figure 4.2.1: Bridge Coordinate Axes

4.3) WSDOT Bridge Selection

The bridges were selected based on their geographical location, close to the Seattle fault region. Figures 4.3.1 and 4.3.2 show the locations of the bridges and the fault region, respectively.

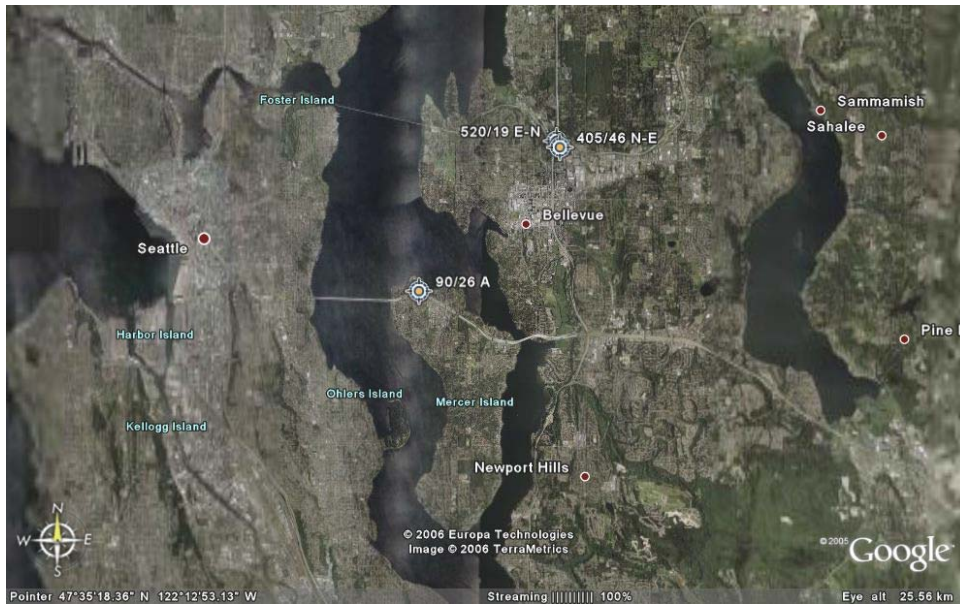


Figure 4.3.1: Bridge location

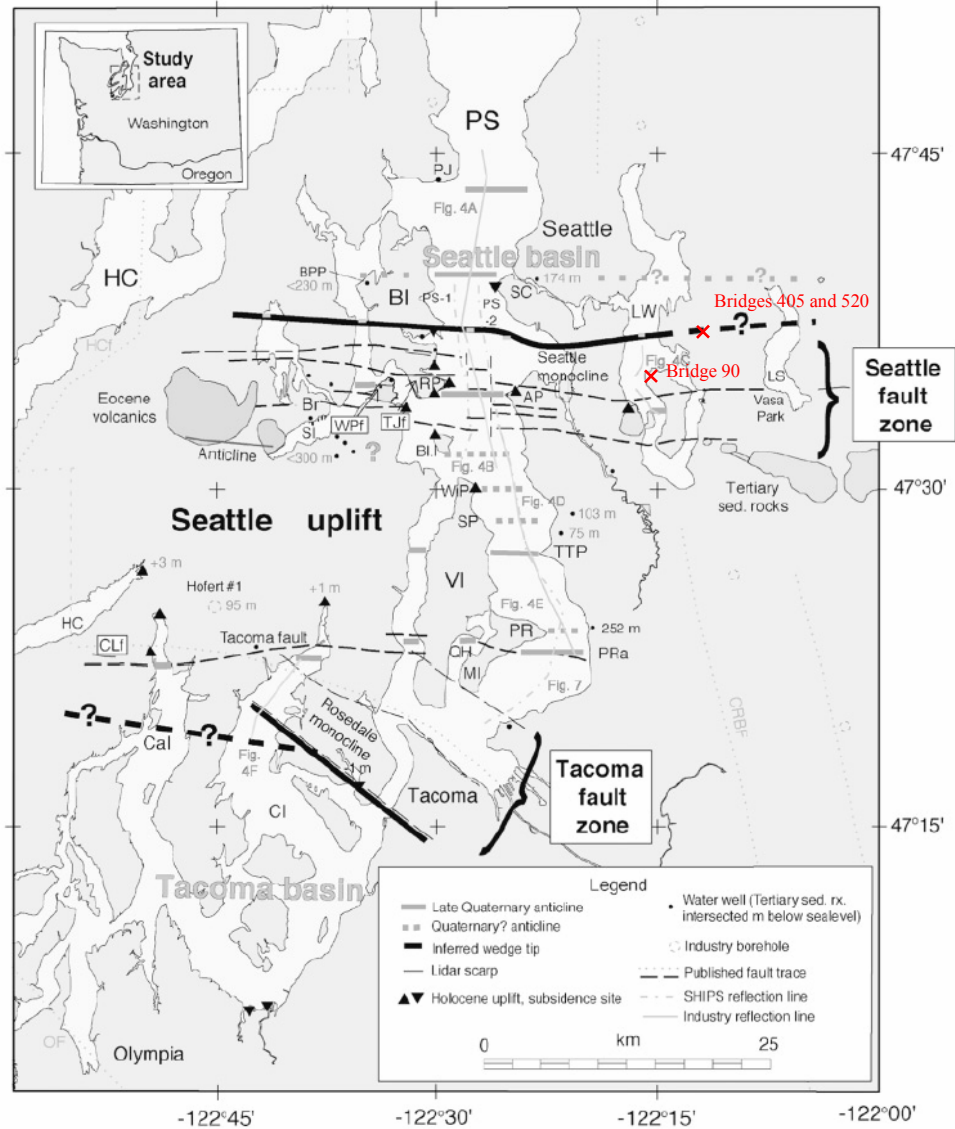


Figure 4.3.2: The Seattle Area Map showing the Seattle fault zone and bridge location (Brocher et al. 2004)

4.4) WSDOT Bridge 405/46N-E

4.4.1) Geometry and reinforcement

Bridge 405/46N-E is an overpass located at 116th Avenue N. E. in Bellevue, Washington. In 1993, the bridge was built to service traffic on SR 405 at the junction

with SR 520. By today's standards, the columns are considered well-reinforced, well-confined and adequately lap-spliced.



Figure 4.4.1: Bridge 405 Aerial View

The bridge length is 50.3 m (165 ft) back to back of pavement seats and consists of three spans. The western and eastern ramps are 15.85 m (52 ft) long with the center ramp measuring 18.6 m (61 ft) in length. The bridge has no skew to it. Plan and elevation views are shown below in Figures 4.4.2 and 4.4.3.

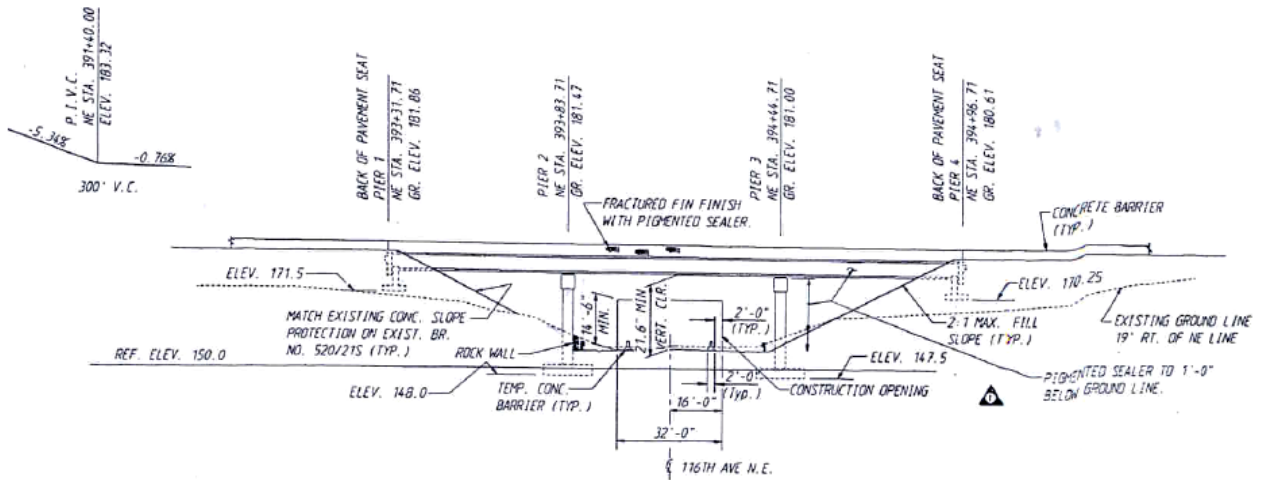


Figure 4.4.2: Bridge 405 Elevation

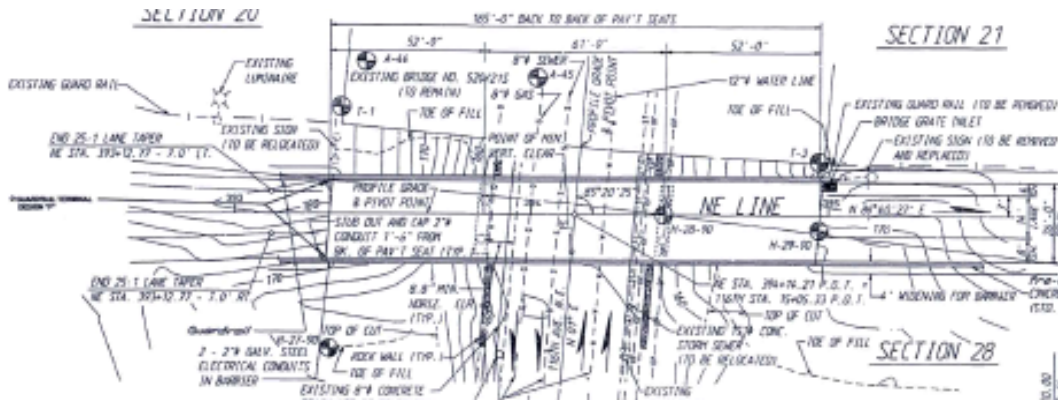


Figure 4.4.3: Bridge 405 Plan

The deck, shown in Figure 4.4.4, is composed of pre-tensioned concrete beams. Each span includes three girders spaced 2.90 m (114.4 in) on center. Overlaid on top of the girders is a 17.8 cm (7 in) thick, 8.46 m (27.75 ft) wide reinforced concrete deck slab.

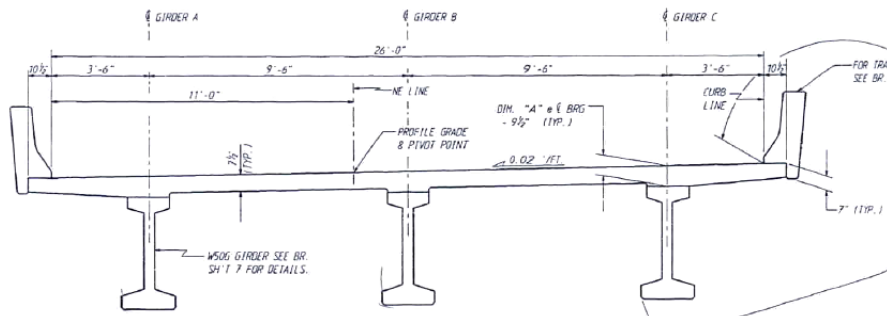


Figure 4.4.4 Bridge 405 Deck cross-section

At each of the two bents, a 1.22x1.22 m (4x4 ft) crossbeam transversely connects the two columns. Figure 4.4.5 below shows the geometry and steel reinforcement. Each crossbeam extends 7 m (23 ft) in length (Figures 4.4.6 and 4.4.7). The steel reinforcement consists of five No. 9 bars located at the top and five No. 8 bars at the bottom of each crossbeam. Four No. 6 bars are located at the side edges and run longitudinally along the crossbeam. For shear reinforcement, No. 5 stirrups are spaced evenly along each member. The columns and crossbeam were cast monolithically adding considerable rigidity to each bent.

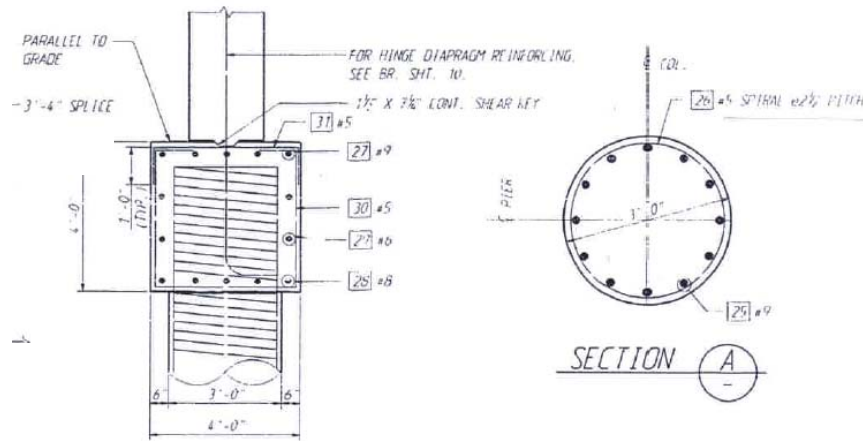


Figure 4.4.5: Bridge 405 Column Sections (Crossbeam & Circular column)

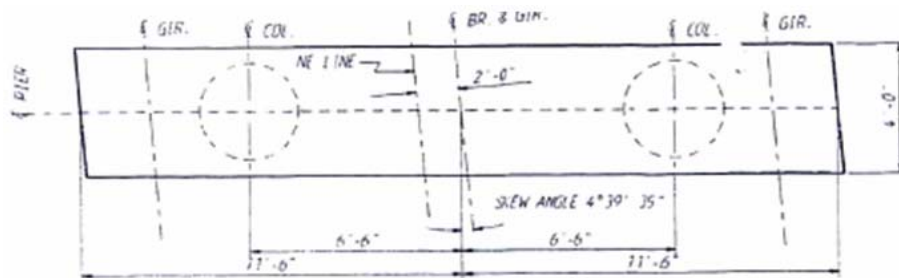


Figure 4.4.6: Crossbeam plan view

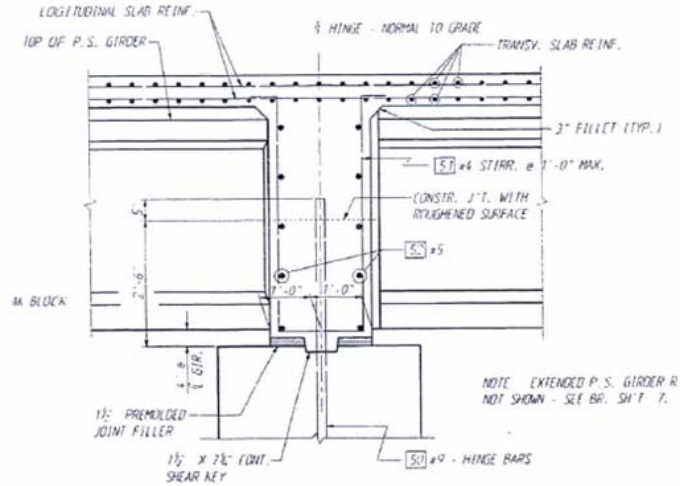


Figure 4.4.7: Bridge 405 Hinge Elevation (between crossbeam and deck)

The I-girders rest upon laminated elastomeric bearing pads located on top of the abutment seats. They are restrained in the transverse direction by girder stops. Figures 4.4.8 and 4.4.9 show the elastomeric bearing pad and the girder stops.

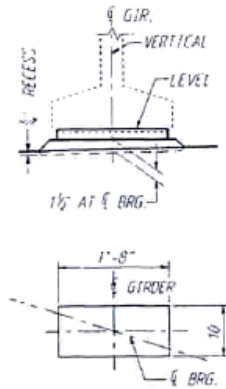


Figure 4.4.8: Bearing Pad

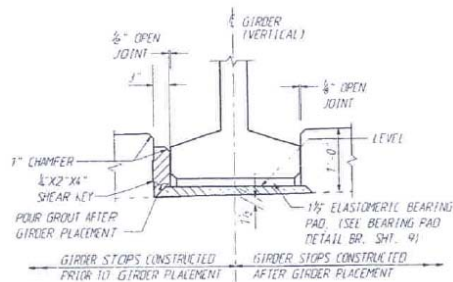


Figure 4.4.9: Bridge 405 Girder Stop

At each bent, the bridge deck is monolithically constructed. The height of the columns at both bents is approximately 8.53 m (28 ft). The clear column height is about 6.7 m (22 ft). The columns are spaced at 3.96 m (13 ft) centerline to centerline. Each column has a cross-sectional diameter of 0.91 m (3 ft). Twelve evenly spaced No. 9 bars provide the longitudinal reinforcement within each column. This provides a longitudinal

reinforcing ratio of 1.18%. The clear cover measures 3.8 cm (1.5 in.). Transverse reinforcement is provided by No. 5 bars spaced at 6.35 cm (2.5 in.) on center resulting in a transverse reinforcement ratio of 1.50%. Figure 4.4.10 shows the elevation view of the columns. Supporting each column is a spread footing. Supporting each column is a spread footing.

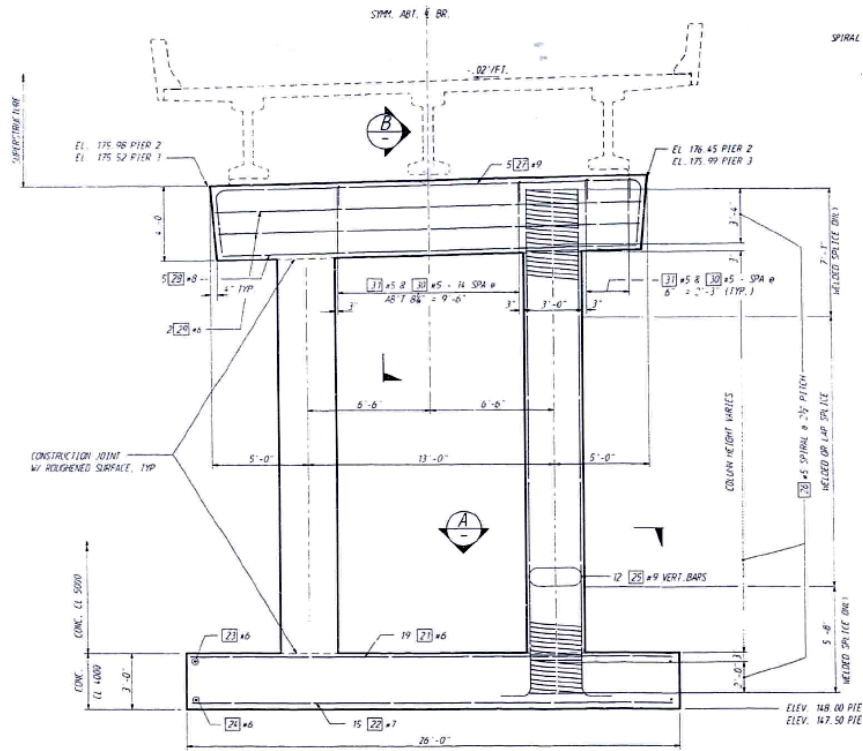


Figure 4.4.10: Bridge 405 Bent Elevation

The length, width and depth of the spread footings are 7.92 m (26 ft), 4.27 m (14 ft), and 0.91 m (3 ft), respectively.

The footings are reinforced at the bottom with fourteen No. 7 bars and at the top with eighteen No. 6 bars in the direction of the width. In the length direction, it is reinforced with twenty five No. 6 bars at the top and thirty eight No. 6 bars at the bottom. A plan view of a spread footing is shown in Figure 4.4.11.

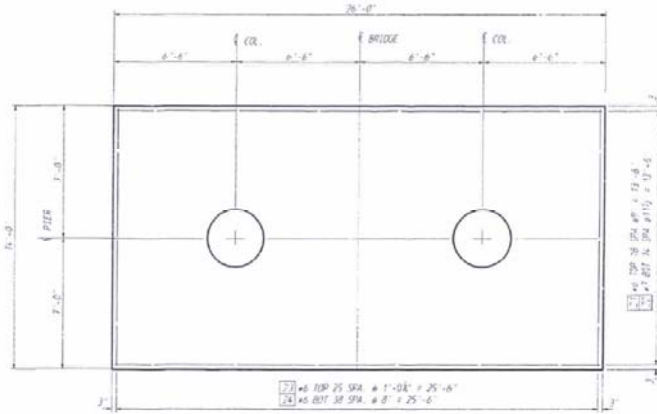


Figure 4.4.11: Bridge Foundation Spread Footing for Bents

Both abutments are about 3 m (10 ft) deep. Due to no endwall being on the abutments, there is no transverse resistance in the event of an earthquake. A footing measuring 8.6 m (28.1 ft) in length, 1.92 m (6.3 ft) in width, and 0.46 m (1.5 ft) in depth is located directly underneath the abutment-deck seating block. The elevation view of the west and east abutments is shown in Figure 4.4.13.

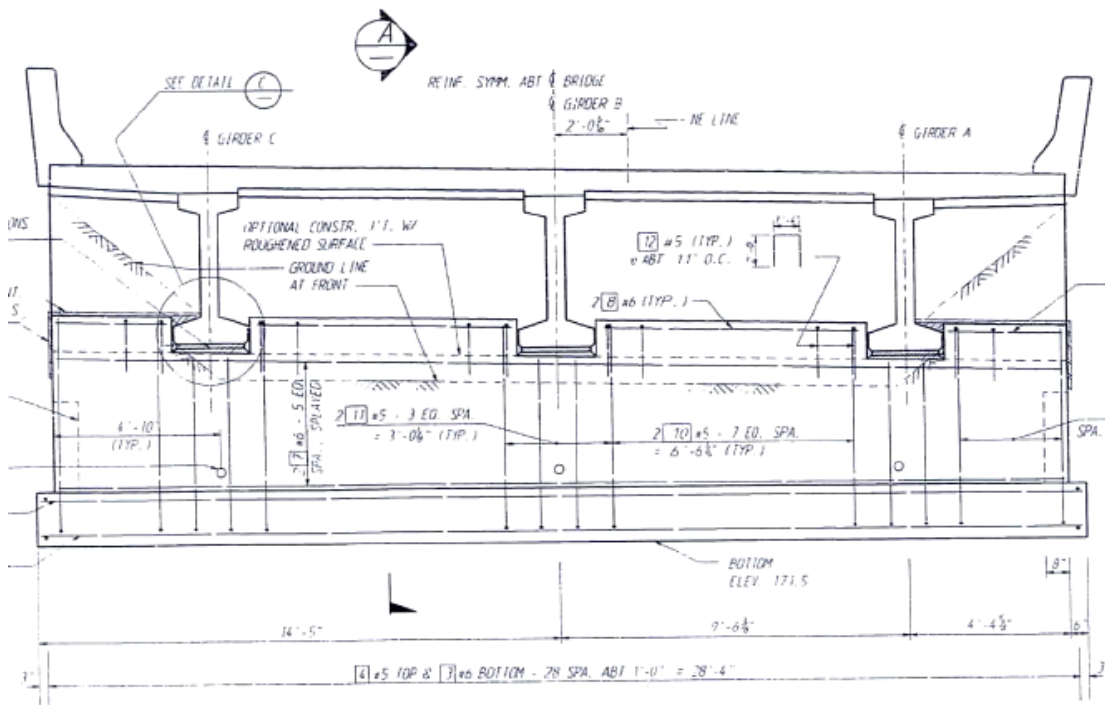


Figure 4.4.12: Bridge 405 Abutment and Deck Elevation View

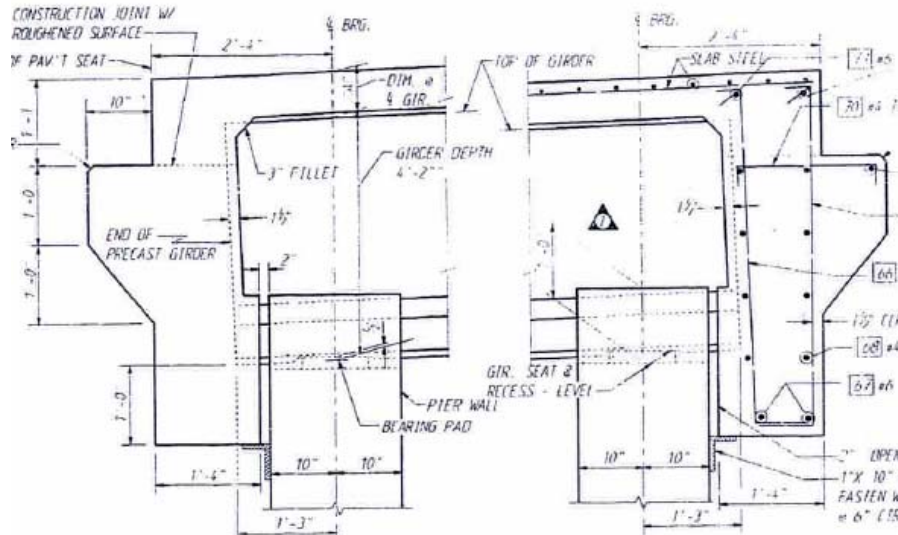


Figure 4.4.13: Bridge 405 East and West Abutments

The footings and abutment walls were constructed with WSDOT Class 4000 mix concrete providing a compressive strength of $f'_c = 27.6$ MPa (4 ksi). The concrete in the prestressed girders was specified to be class 6000. The concrete in the columns, crossbeam, diaphragms, and slabs was specified to be class 5000. The reinforcing steel conforms to AASHTO M31 Grade 60 with a yield strength of $f_y = 413.6$ MPa (60 ksi).

4.4.2) Structural Model

The Finite Element nonlinear dynamic implicit analysis was performed on ABAQUS/Standard with a 3D model. The bridge was discretized by 3-node quadratic Timoshenko (shear flexible) beam elements, resulting in a so-called spine model, as shown in Figure 4.4.14.

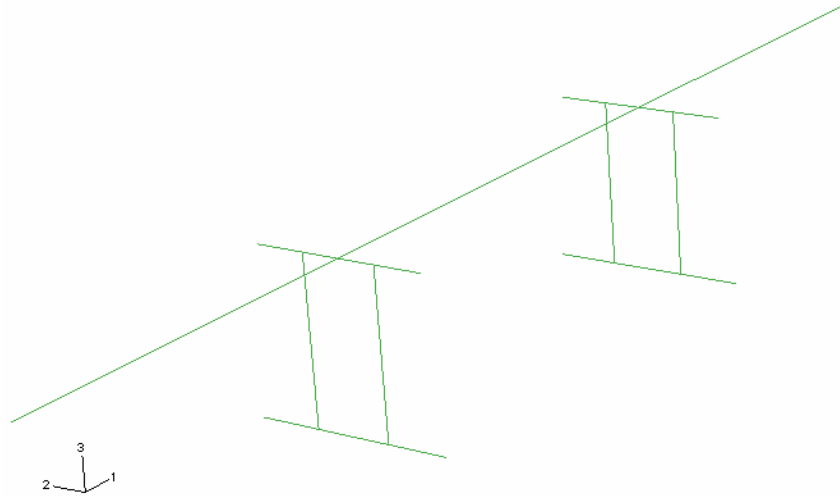


Figure 4.4.14: Bridge 405 Spine Model

For the deck, ABAQUS can generate from a meshed region with 2D warping elements beam cross-section properties that can be used in a subsequent beam element analysis. Figure 4.4.15 shows the assigned deck cross-section.

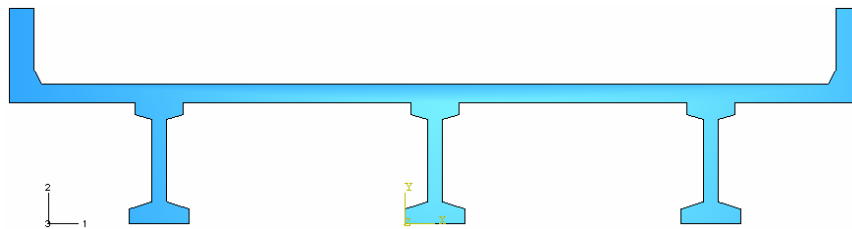


Figure 4.4.15: Bridge 405 deck cross-section

The torsional rigidity is calculated over the two-dimensional region meshed with warping elements. In the elastic range, warping is small and ABAQUS assumes that warping prevention at the ends can be neglected. The axial warping stresses are therefore assumed to be negligible, but the torsional shear stresses are assumed to be of the same order of magnitude as the stresses due to axial forces and bending moments.

A solid Finite Element Model (FEM) of the Bridge 405 deck was created to investigate the effect of these assumptions. A simple model, based on a cantilever beam under flexure or torsion, was also modeled with a single beam element.

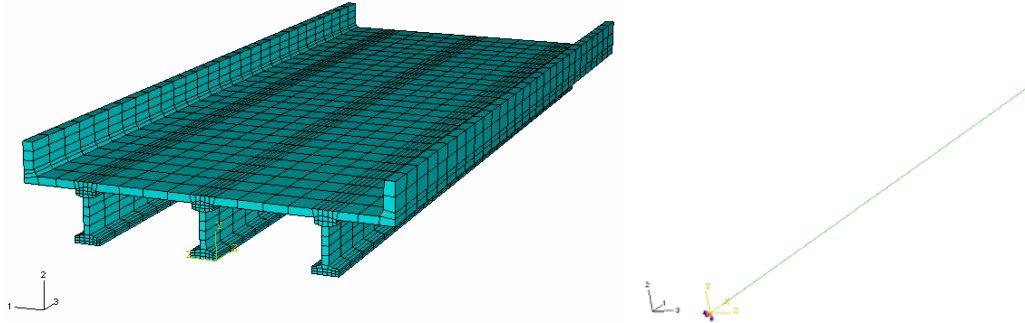


Figure 4.4.16: Bridge 405 deck solid and spine models

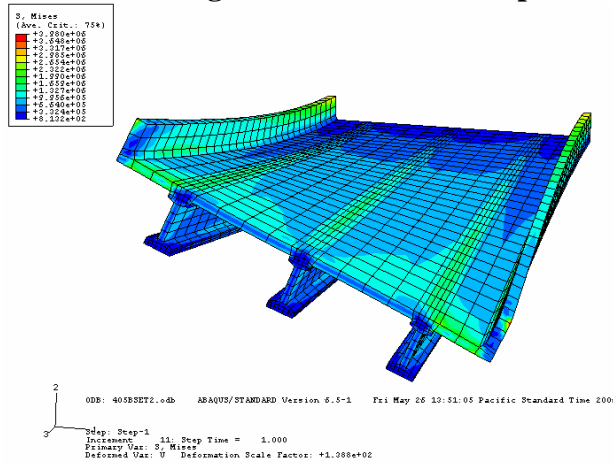


Figure 4.4.17: Bridge 405 deck in torsion

An axial torque of 360 kN.m was applied at the end of both cantilever beam models and the end rotation values were compared. The rotation of the spine cantilever model with the original torsional stiffness was over three times that of the detailed finite element model (Table 4.4.1). This result indicates that the restriction of warping has a significant effect on torsional stiffness. Because of the rigid connection of the deck to the cap beams, the restriction of warping is justified for the deck, and the torsional stiffness, GJ , was increased accordingly for the bridge model.

Table 4.4.1: Torsional results and comparison

	Solid FEM	Spine model				
<i>GJ</i> (Torsional Stiffness)		6.31E+08	1.58E+09	1.89E+09	2.21E+09	2.52E+09
Multiplication factor		x 1	x 2.5	x 3	x 3.5	x 4
End Rotation (rad)	0.00336	0.01134	0.00454	0.00378	0.00324	0.00284

The bending characteristics in both directions were also compared. The results (horizontal and vertical displacements) for both models were in close agreement, matching within 6% error.

In conclusion, the torsional stiffness that was used for the spine FEM of Bridge 405 was the original torsional stiffness value computed by ABAQUS multiplied by 3.5. Figure 4.4.18 shows the applied cross-section profiles to the different bridge elements. The modeling of the bridge columns was based on that of Orozco's and Lehman's column specimens, described in Chapter 3.

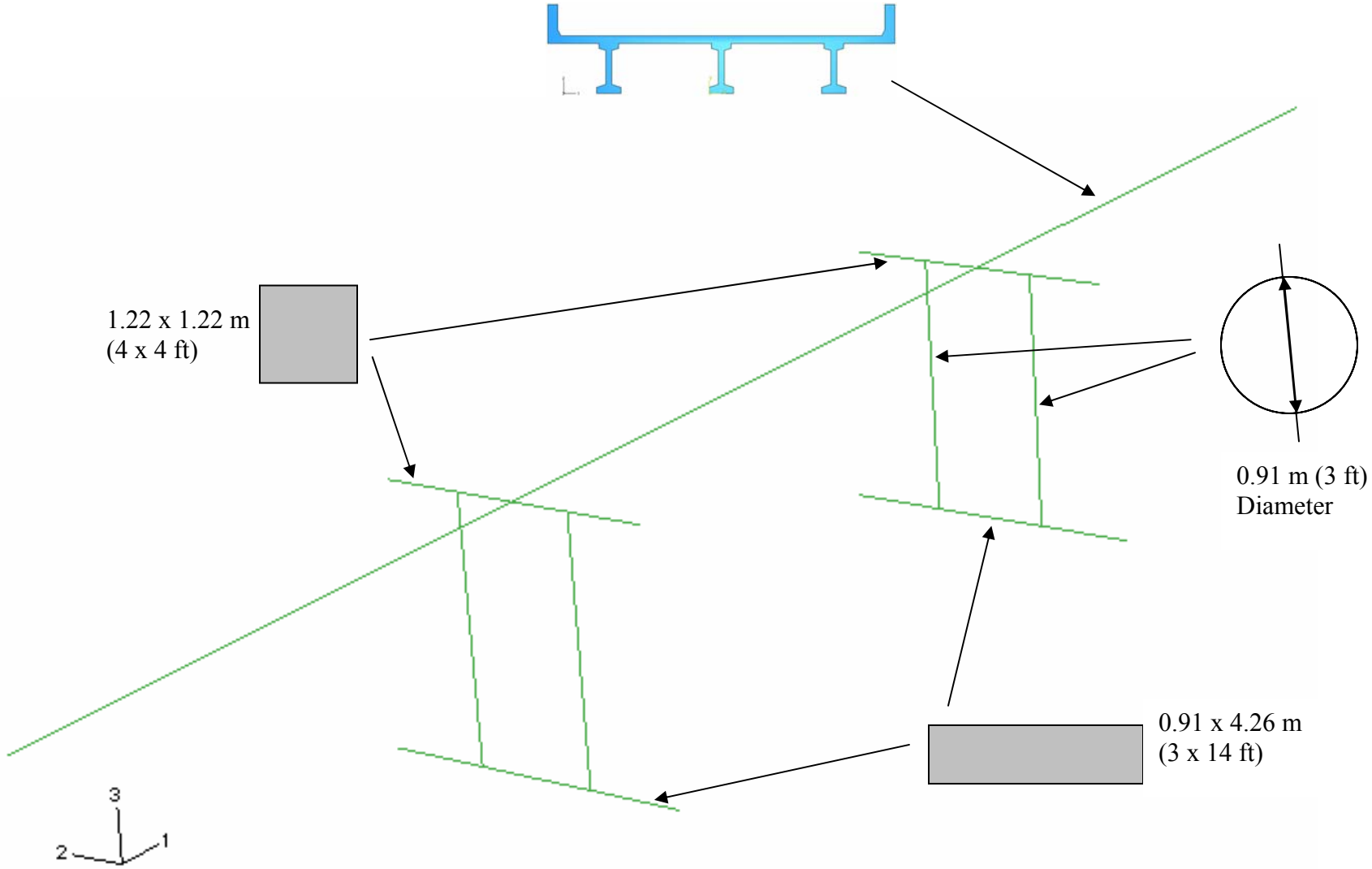


Figure 4.4.18: Bridge 405 cross-sections

4.4.2.1) Boundary and Connectivity Conditions

Where the deck meets each bent, there is no fixity between the girders and the cap beam. Therefore, the internal transverse moment was released at the crossbeam to model a hinge boundary condition.

Linear springs were used to connect the deck to the abutments. These springs represent the bearing pads. There was one bearing pad spring at each abutment. The abutments were modeled as a single node with a lumped mass. Linear springs connected the soil to the abutments to represent the Soil-Structure Interaction (SSI). The SSI was determined following the FEMA 356 (2000) procedure (See Appendix A.2), based on the geometric characteristics of the abutment footing.

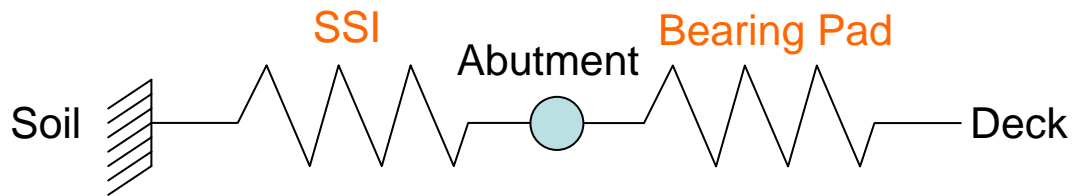


Figure 4.4.19: FE model of the soil, abutment and deck interaction in the transverse direction

The longitudinal stiffness of the bearing pads was based on equation 4.1. The other stiffnesses of the bearing pads were set relatively high to model the resistance of the girder stops in the transverse and rotational degrees of freedom of the bridge.

$$k = \frac{GA}{h} \quad (4.1)$$

Where G is the shear modulus, A is the cross-sectional area, and h is the height. In the longitudinal direction, a nonlinear gap spring and a connector element were added in parallel to the bearing pad spring to model the 5 cm (2 in) gap between the abutment and

the deck (see Figure 4.4.20). The connector was defined as a nonlinear spring including the plasticity effect to model the damage of the abutment resulting from pounding. The connector force-displacement curve was determined following the Caltrans – Seismic Design Criteria – procedure (see Appendix A.3).

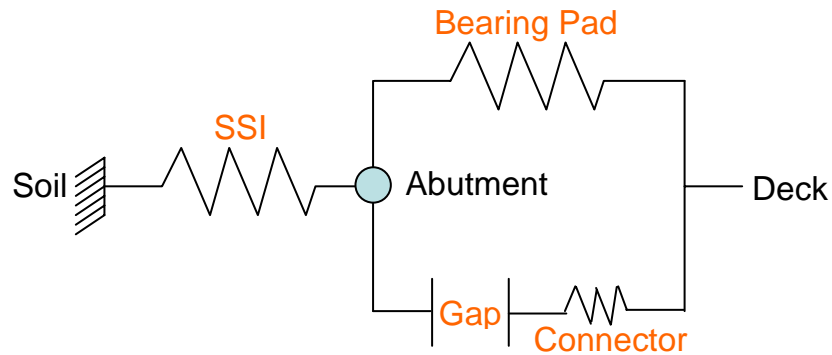


Figure 4.4.20: FE model of the soil, abutment and deck interaction, in the longitudinal direction

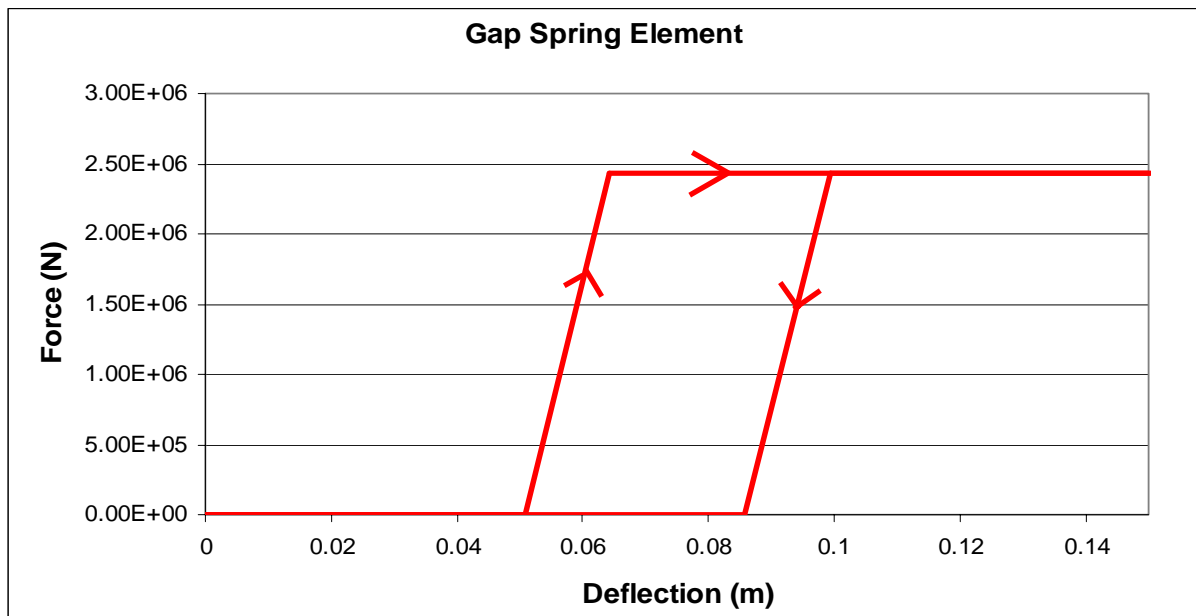
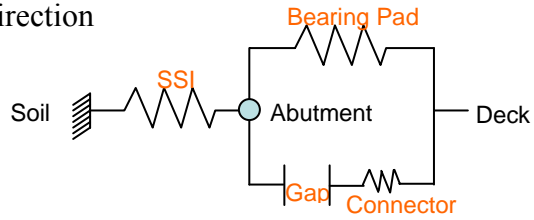


Figure 4.4.21: Force-Displacement Curve of the abutment gap spring and connector in series

At the bottom and top of the columns, rigid connections were used to replicate the stiff foundation footing and crossbeam, respectively. The abutment and column footing soil springs were applied at the abutment and column footing nodes. Figure 4.4.22 shows a summary of the different applied boundary and connection conditions.

In the longitudinal direction



and

For the 5 other DOF

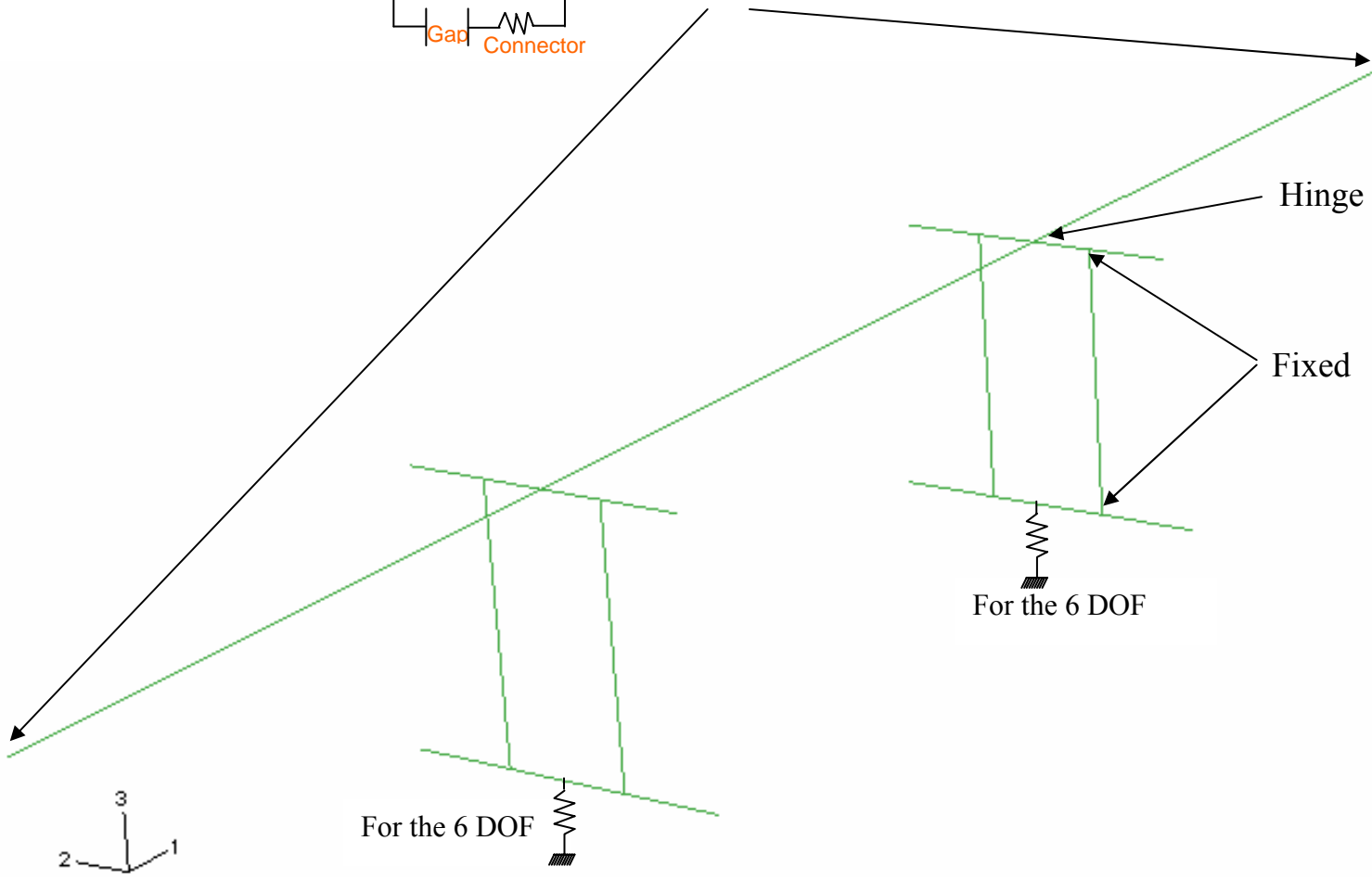


Figure 4.4.22: Bridge Model Boundary Conditions

4.4.2.2) Damping

Rayleigh damping was specified for all bridge models. Equation 4.2 defines the damping relationship in the equation of motion:

$$[C] = \alpha[M] + \beta[k] \quad (4.2)$$

where α and β are damping factors. Generally, detailed damping ratio information is not known about a structure, which results in the control frequencies having the same damping ratio. Under this condition, α and β are found by:

$$\begin{Bmatrix} \alpha \\ \beta \end{Bmatrix} = \frac{2\xi}{\omega_i + \omega_j} \begin{Bmatrix} \omega_j \omega_i \\ 1 \end{Bmatrix} \quad (4.3)$$

Where ω_i and ω_j are two control natural frequencies and ξ is the damping ratio. For all analyses, the damping ratio was specified as 5%.

4.4.2.3) Loading and Ground Motions

The ground motions were applied at the foundation nodes in the transverse, vertical and longitudinal directions. If not known, the vertical components of the ground motions were taken as 66% of the respective fault normal components. Figure 4.4.23 shows the nodes at which the earthquake was applied. Gravity load was applied to the whole model.

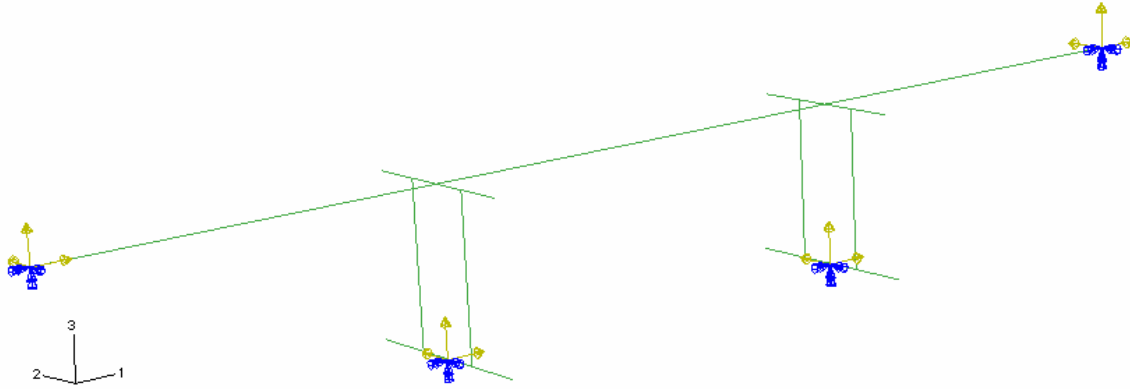


Figure 4.4.23: Applied earthquake at the foundation nodes

4.4.2.4) Bridge Frequency Content

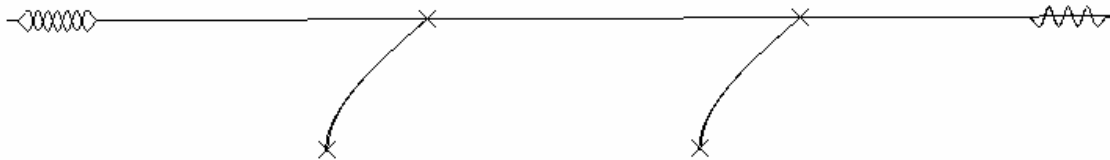
ABAQUS, through a frequency extraction procedure, performs eigenvalue extraction to calculate the natural frequencies and the corresponding mode shapes of the bridge model. It includes initial stress and load stiffness effects due to preloads and initial conditions. The eigenvalue Equation 4.4 to solve for the natural frequencies of an undamped finite element model is

$$(-\omega^2 M^{MN} + K^{MN})\Phi^N = 0 \quad (4.4)$$

Where M^{MN} is the mass matrix which is symmetric and positive definite, K^{MN} is the stiffness matrix, Φ^N is the eigenvector, and M and N are degrees of freedom. Table 4.4.2 summarizes the frequency content of Bridge 405. The first mode of vibration of Bridge 405 is in its longitudinal direction with a frequency of 1.5 Hz (period, $T = 0.65$ sec). The bridge transverse direction is excited by its third mode of vibration with a frequency of 5.5 Hz ($T = 0.18$ sec). Figures 4.4.24 and 4.4.25 show the two modes of deformation.

Table 4.4.2 Frequency content of Bridge 405

Eigenvalue Output						
Mode No	Eigenvalue	Frequency		Generalized Mass	Governing DOF	
		(Rad/Time)	(Cycles/Time)			
1	91.619	9.5718	1.5234	4.40E+05	X-Component	
2	869.5	29.487	4.6931	1.10E+07	X-Rotation	
3	1224.3	34.989	5.5687	2.65E+05	Y-Component	
4	1236.7	35.166	5.5969	1.68E+07		
5	1278.8	35.76	5.6913	2.91E+06		
Participation Factors						
Mode No	X-Component	Y-Component	Z-Component	X-Rotation	Y-Rotation	Z-Rotation
1	1.0133	-1.62E-16	-3.71E-15	4.93E-16	-5.77E-02	4.43E-15
2	2.19E-16	-1.51E-04	3.62E-06	-0.41261	-9.11E-05	-3.79E-03
3	8.01E-14	1.1277	-1.08E-07	-0.66719	2.71E-06	28.357
4	3.69E-15	6.46E-07	-7.84E-12	4.48E-07	6.04E-05	0.129
5	-7.33E-15	0.13137	-5.98E-06	0.57259	1.50E-04	3.3032
Effective Mass						
Mode No	X-Component	Y-Component	Z-Component	X-Rotation	Y-Rotation	Z-Rotation
1	4.52E+05	1.15E-26	6.05E-24	1.07E-25	1467.3	8.63E-24
2	5.23E-25	0.24894	1.44E-04	1.86E+06	9.10E-02	157.4
3	1.70E-21	3.37E+05	3.08E-09	1.18E+05	1.94E-06	2.13E+08
4	2.29E-22	7.00E-06	1.03E-15	3.37E-06	6.12E-02	2.79E+05
5	1.56E-22	50217	1.04E-04	9.54E+05	6.58E-02	3.18E+07



```

3
|
| ODB: 405bridge.odb  ABAQUS/STANDARD Version 5.5-1  Thu Jun 22 14:43:42 Pacific Standard Time 2006
|
1
|
| Step: Step-3
| Mode 1: Value = 94.889  Freq = 1.5503  (cycles/time)
| Deformed Var: U  Deformation Scale Factor: +5.039e+00

```

Figure 4.4.24: Longitudinal mode of vibration

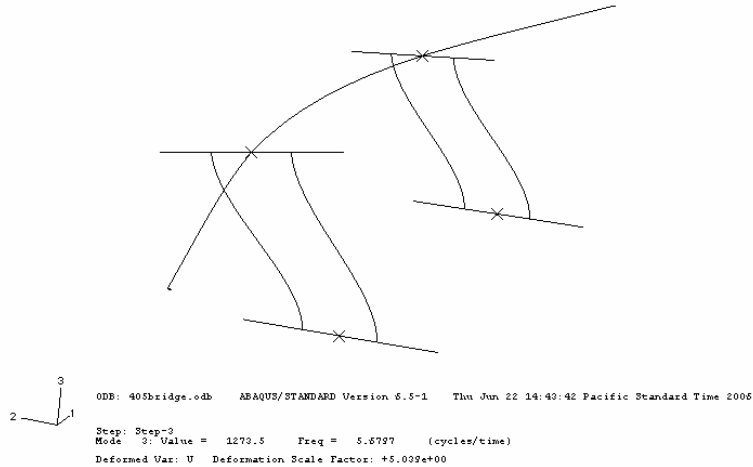


Figure 4.4.25: Transverse mode of vibration

4.5) WSDOT Bridge 520/19E-N

4.5.1) Geometry and reinforcement

Bridge 520/19E-N is an overpass located at Northup way in Bellevue, Washington. In 1993, the bridge was built to service traffic on SR 405 at the junction with SR 520. By today's standards, the columns are considered well-reinforced, well-confined and adequately lap-spliced.

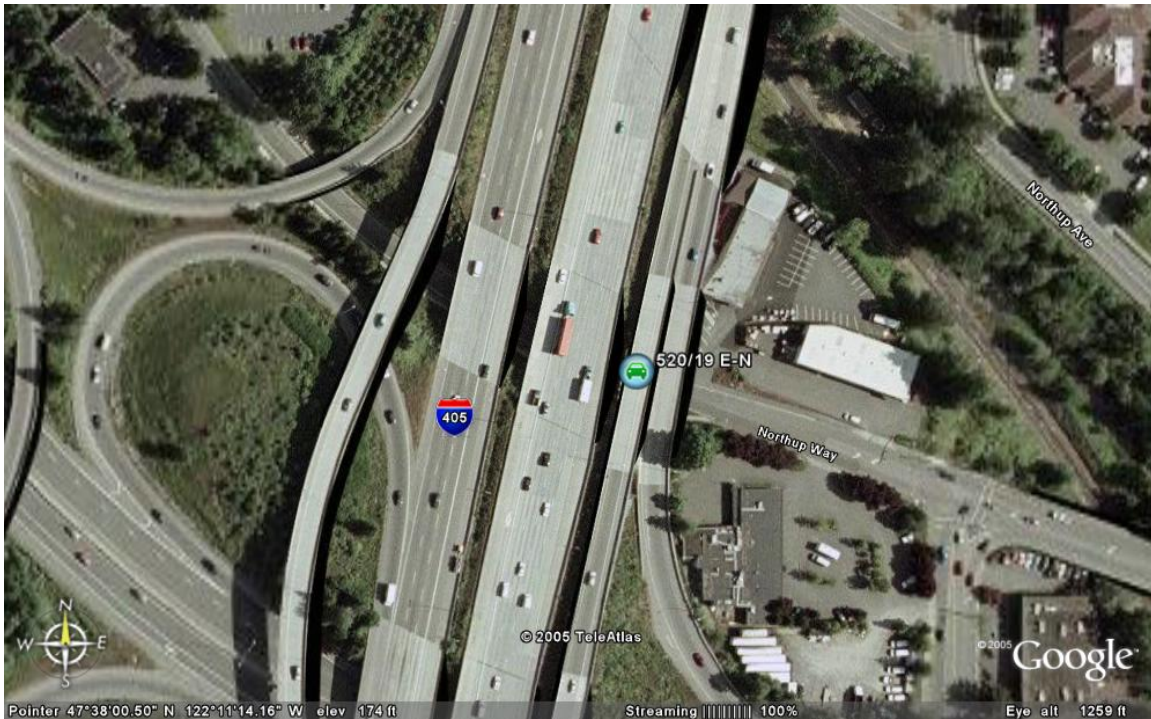


Figure 4.5.1: Bridge 520 Aerial View

The bridge length is 50 m (162 ft) back to back of pavement seats and consists of three spans. The southern and northern ramps are 13.4 m and 16.5 m (44 ft and 54 ft) long with the center ramp measuring 19.5 m (64 ft) in length. The bridge has no skew to it. Plan and elevation views are shown below in Figures 4.5.2 and 4.5.3.

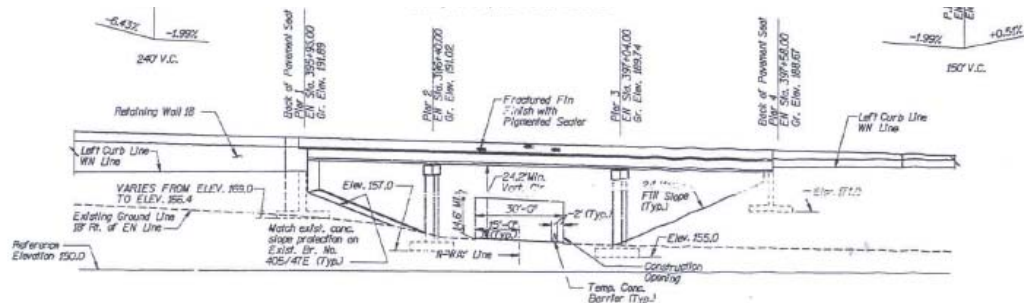


Figure 4.5.2: Bridge 520 Elevation

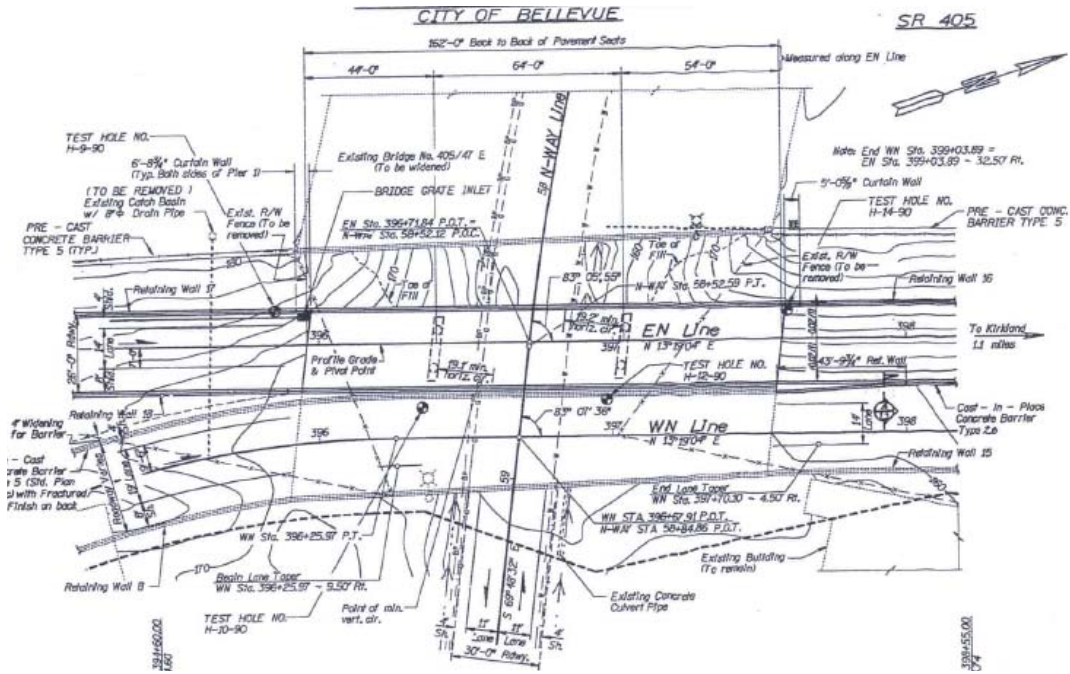


Figure 4.5.3: Bridge 520 Plan

The deck is composed of pre-tensioned concrete beams as showed on Figure 4.5.4. Each span includes three girders spaced 2.90 m (114.4 in) on center. Overlaid on top of the girders is a 17.8 cm (7 in) thick, 8.46 m (27.75 ft) wide reinforced concrete deck slab.

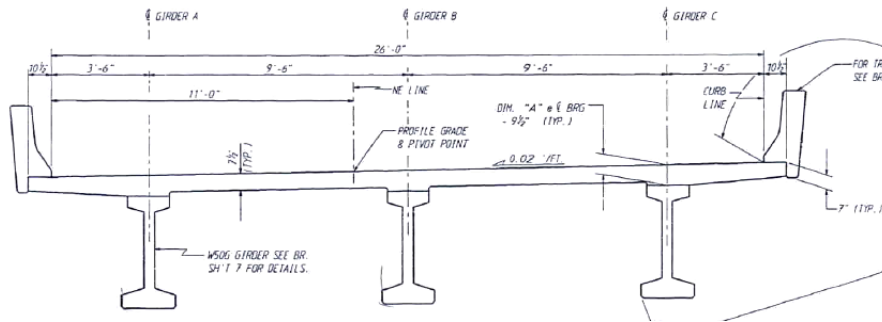


Figure 4.5.4: Bridge 520 Deck cross-section

At each of the two bents, a 1.22x1.22 m (4x4 ft) crossbeam transversely connects the two columns. Figure 4.5.6 below shows the geometry and steel reinforcement. Each crossbeam extends 7 m (23 ft) in length (Figures 4.5.7 and 4.5.8). The steel reinforcement

consists of six No. 9 bars located at the top and four No. 9 bars at the bottom of each crossbeam. For shear reinforcement, No. 5 stirrups are spaced evenly along each member. The columns and crossbeam were cast monolithically, adding considerable rigidity to each bent.

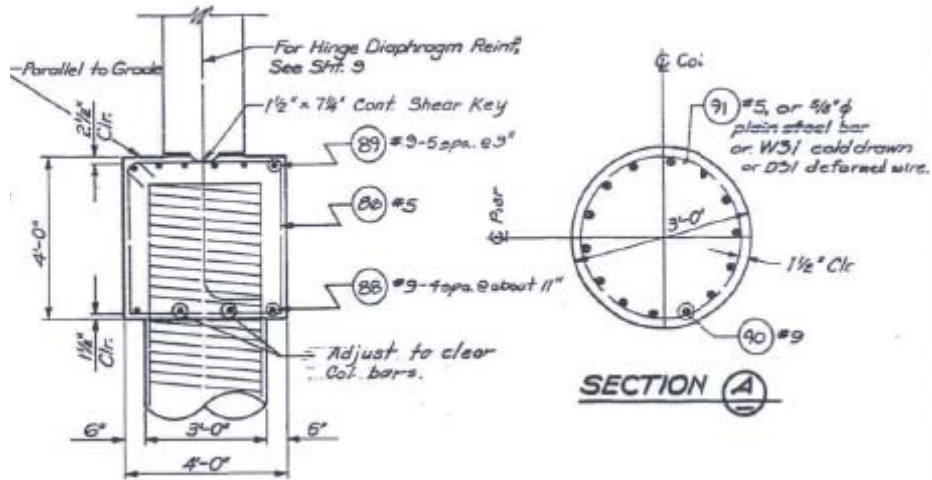


Figure 4.5.6: Bridge 520 Column Sections (Crossbeam & Circular column)

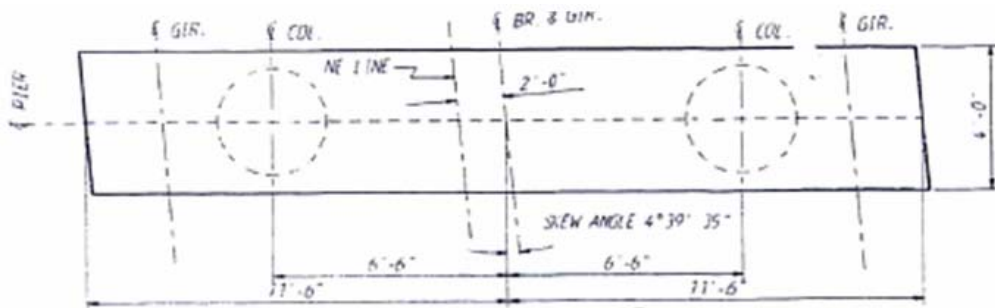


Figure 4.5.7: Crossbeam plan view

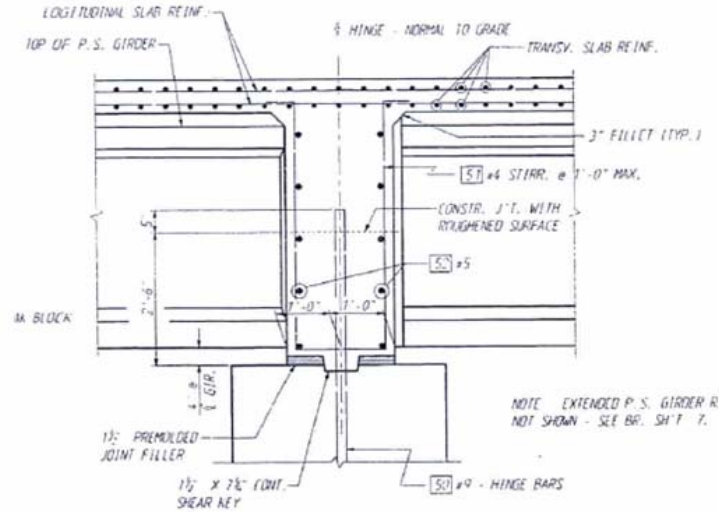


Figure 4.5.8: Bridge 520 Hinge Elevation (between crossbeam and deck)

The I-girders rest upon laminated elastomeric bearing pads located on top of the abutment seats. They are restrained in the transverse direction by girder stops. Figures 4.5.9 and 4.5.10 show the elastomeric bearing pad and the girder stops.

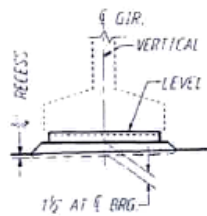


Figure 4.5.9: Bearing Pad

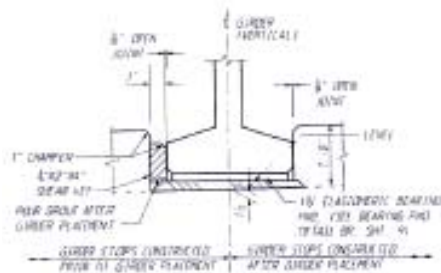


Figure 4.5.10: Bridge 520 Girder Stop

At each bent, the bridge deck is monolithically constructed. The height of the columns at both bents is approximately 10.6 m (34.7 ft). The clear column height is about 8.58 m (28.14 ft). The columns are spaced at 3.96 m (13 ft) centerline to centerline. Each column has a cross-sectional diameter of 0.91 m (3 ft). Fourteen evenly spaced No. 9 bars provide the longitudinal reinforcement within each column. This provides a longitudinal reinforcing ratio of 1.37%. The clear cover measures 3.8 cm (1.5 in.).

Transverse reinforcement is provided by No. 5 bars spaced at 6.35 cm (2.5 in.) on center resulting in a transverse reinforcement ratio of 1.50%. Figure 4.5.11 shows the elevation view of the columns. Supporting each column is a spread footing.

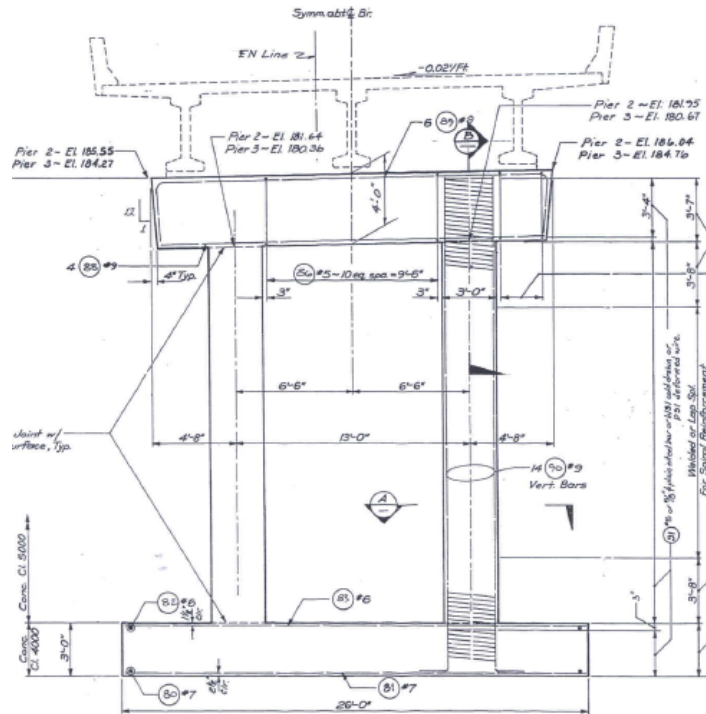


Figure 4.5.11: Bridge 520 Bent Elevation

The length, width and depth of the spread footings are 7.92 m (26 ft), 4.57 m (15 ft), and 0.91 m (3 ft), respectively.

The footings are reinforced at the bottom with twenty one No. 7 bars and at the top with fifteen No. 6 bars in the direction of the width. In the length direction, they are reinforced with twenty five No. 6 bars at the top and thirty four No. 7 bars at the bottom. A plan view of a spread footing is shown in Figure 4.5.12.

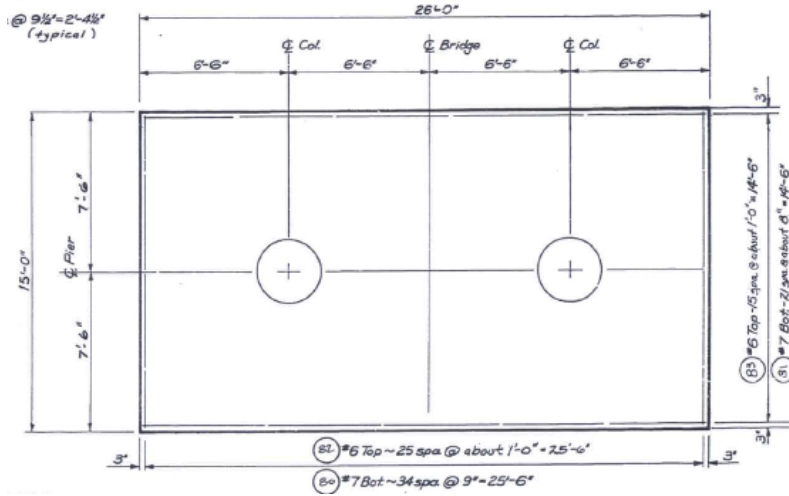


Figure 4.5.12: Bridge Foundation Spread Footing for Bents

Both abutments are about 6 m (20 ft) deep. Due to no endwall being on the abutments, there is no transverse resistance in the event of an earthquake. A footing measuring 8.84 m (29 ft) in length, 5.48 m (18 ft) in width, and 0.76 m (2.5 ft) in depth is located directly underneath the abutment-deck seating block. The elevation view of the west and east abutments is shown in Figures 4.5.13, 4.5.14 and 4.5.15.

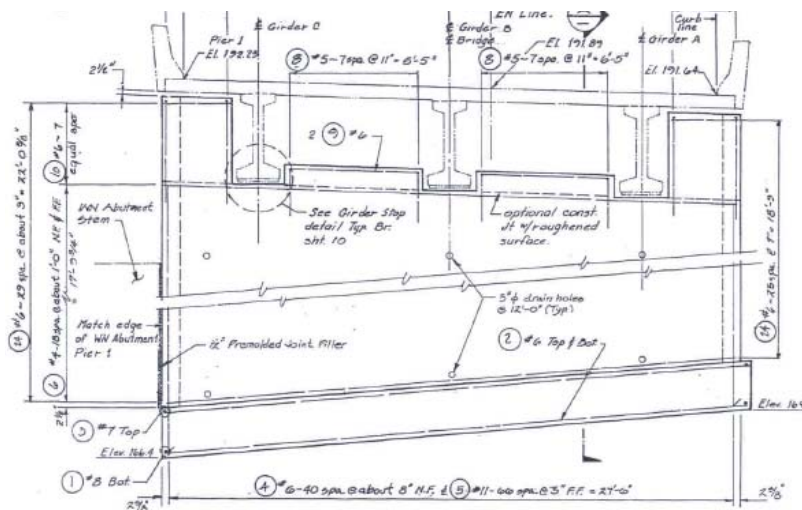


Figure 4.5.13: Bridge 520 West Abutment and Deck Elevation View

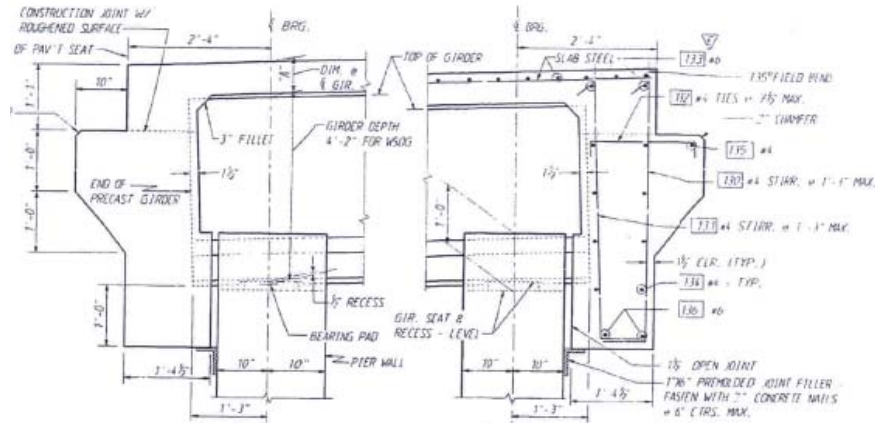


Figure 4.5.14: Bridge 520 East and West Abutments

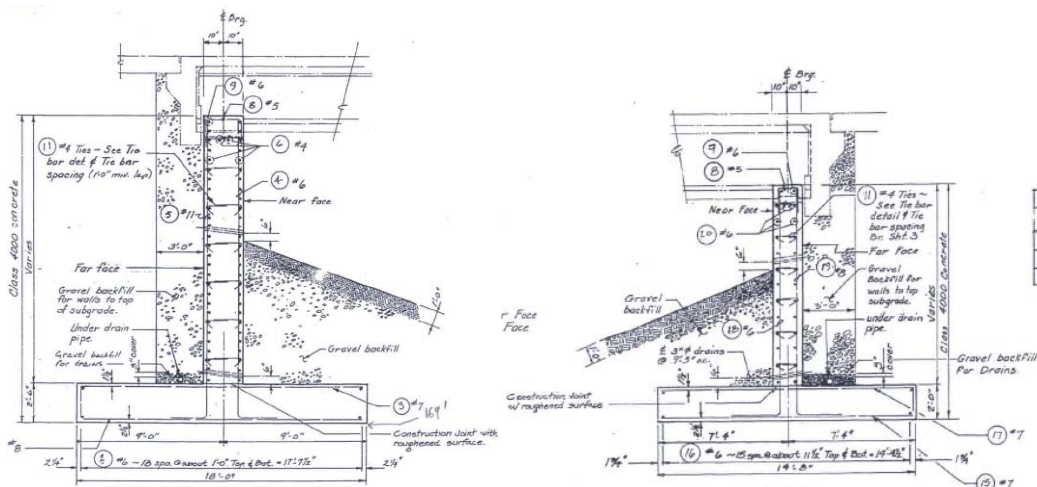


Figure 4.5.15: Bridge 520 East and West Abutments

The footings and abutment walls were constructed with WSDOT Class 4000 mix concrete providing a compressive strength of $f'_c = 27.6$ MPa (4 ksi). The concrete in the prestressed girders, columns, crossbeam, diaphragms, and slabs was specified to be class 5000. The reinforcing steel conforms to ASSHTO M31 Grade 60 with a yield strength of $f_y = 413.6$ MPa (60 ksi).

4.5.2) Structural Model

The Finite Element Model was built similarly to that of Bridge 405. See section 4.4.2.

4.5.2.1) Bridge Frequency Content

Table 4.5.1 summarizes the frequency content of Bridge 520. The first mode of vibration of Bridge 520 is in its longitudinal direction with a frequency of 1.25 Hz (period, $T = 0.8$ sec). The bridge transverse direction is excited by its fourth mode of vibration with a frequency of 6 Hz ($T = 0.165$ sec). The mode shapes are similar to those of Bridge 405.

Table 4.5.1: Frequency content of Bridge 520

Eigenvalue Output						
Mode No	Eigenvalue	Frequency		Generalized Mass	Governing DOF	
		(Rad/Time)	(Cycles/Time)			
1	61.88	7.8664	1.252	4.36E+05	X-Component	
2	869.69	29.491	4.6936	1.01E+07	X,Z-Rotation	
3	1237.8	35.182	5.5994	9.92E+06	X,Z-Rotation	
4	1434.8	37.879	6.0287	2.46E+05	Y-Component	
5	1844.5	42.948	6.8354	1.28E+07		
6	3163.8	56.248	8.9522	97266		
Participation Factors						
Mode No	X-Component	Y-Component	Z-Component	X-Rotation	Y-Rotation	Z-Rotation
1	1.018	1.68E-15	9.82E-15	2.94E-14	-0.1071	8.52E-14
2	1.67E-14	1.56E-02	-3.87E-06	0.35949	8.96E-05	0.37407
3	-1.20E-14	1.55E-02	-2.95E-06	0.27272	1.36E-04	0.50582
4	4.84E-14	1.2805	-5.93E-07	-6.86E-02	-2.69E-05	31.189
5	-2.45E-14	1.41E-03	-2.15E-06	0.23298	6.73E-06	-7.83E-02
6	1.96E-13	2.07E-05	0.51242	2.18E-05	-5.184	5.83E-04
Effective Mass						
Mode No	X-Component	Y-Component	Z-Component	X-Rotation	Y-Rotation	Z-Rotation
1	4.52E+05	1.23E-24	4.20E-23	3.77E-22	5002.9	3.17E-21
2	2.80E-21	2452.6	1.51E-04	1.31E+06	8.12E-02	1.41E+06
3	1.43E-21	2377.3	8.61E-05	7.38E+05	0.18399	2.54E+06
4	5.76E-22	4.03E+05	8.65E-08	1156.4	1.77E-04	2.39E+08
5	7.70E-21	25.45	5.93E-05	6.95E+05	5.79E-04	78459
6	3.74E-21	4.18E-05	25540	4.63E-05	2.61E+06	3.31E-02

4.6) WSDOT Bridge 90/26A

4.6.1) Geometry and reinforcement

Bridge 90/26A is an overpass located on Mercer Island near Seattle, Washington. In 1992, the bridge was built to service traffic on 72nd avenue SE. The I-90 underground Express Lane passes under the bridge (Figure 4.6.1). By today's standards, the columns are considered well-reinforced, well-confined and adequately lap-spliced.



Figure 4.6.1: Bridge 90 Aerial View



Figure 4.6.2: Bridge 90 Aerial Views

The bridge length is 91 m (298.5 ft) back to back of pavement seats and consists of five spans. The ramps are 16.3 m (53.5 ft), 19.35 m (63.5 ft), 16 m (52.5 ft), 24 m (78.7 ft), and 15 m (49.2 ft) long from South to North, respectively. The bridge has no skew to it. Plan and elevation views are shown below in Figures 4.6.3 and 4.6.4.

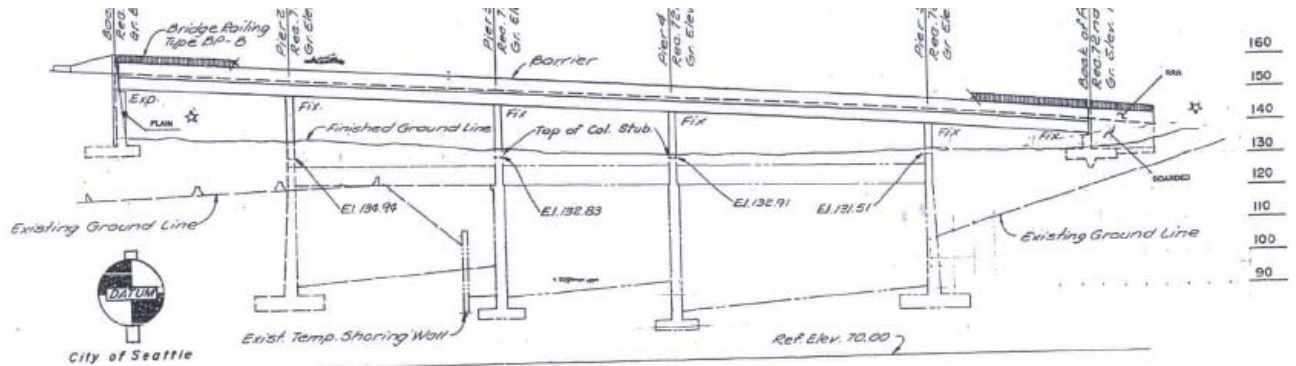


Figure 4.6.3: Bridge 90 Elevation

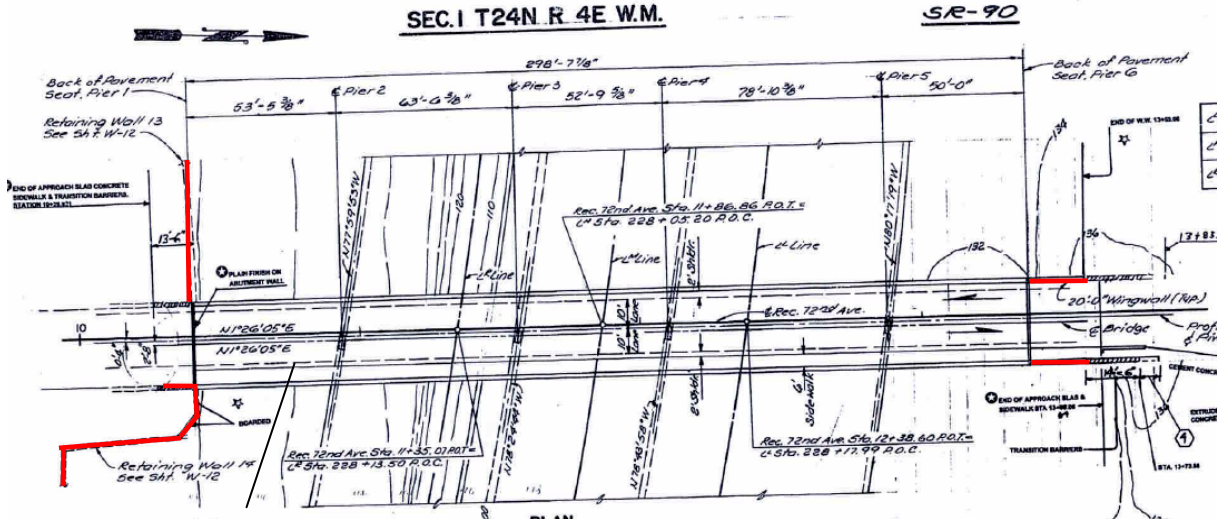


Figure 4.6.4: Bridge 90 Plan

The deck is composed of a reinforced concrete box girder. The width of the deck is 10.2 m (33.5 ft) and the depth is 1.37 m (4.5 ft). The columns and concrete box girder were cast monolithically, as shown in Figure 4.6.5.

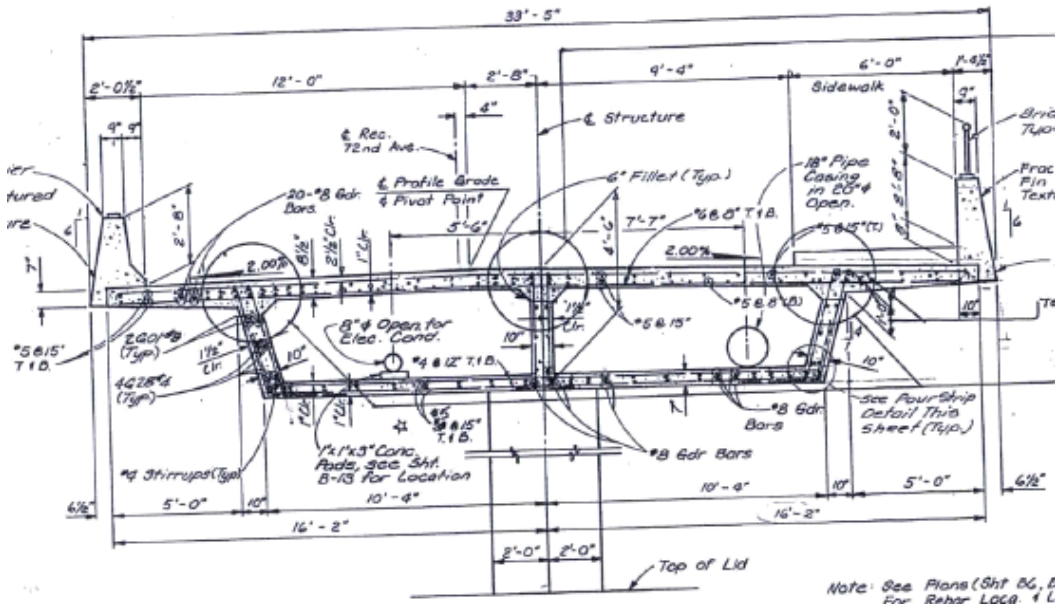
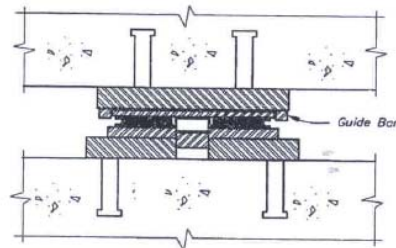


Figure 4.6.5: Bridge 90 Concrete box girder cross-section

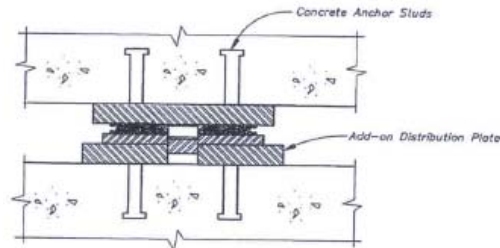
The concrete box rests upon laminated elastomeric fixed and guided bearing pads located on top of the North and South abutment seats, respectively. They are restrained in

the transverse direction by wing and retaining walls, respectively, that can be seen in solid red on Figure 4.6.4 (plan). Figures 4.6.6 and 4.6.7 show the elastomeric bearing pads.



GUIDED BEARING (1)
INCLUDING ADD-ON DISTRIBUTION PLATE

Figure 4.6.6: Guided Bearing Pad



FIXED BEARING (6)

Figure 4.6.7: Fixed Bearing Pad

At each bent, the bridge deck is monolithically constructed. The clear height of the columns is 6.10 m (20 ft), 7.21 m (23.6 ft), 5.97 m (19.7 ft), and 4.33 m (14.2 ft), from south to north, respectively. Each column has a rectangular cross-section, 0.61x1.22 m (2x4 ft). Twenty two No. 11 bars provide the longitudinal reinforcement within each column. This provides a longitudinal reinforcing ratio of 3%. The clear cover measures 3.8 cm (1.5 in.). Transverse reinforcement is provided by No. 4 bars spaced at 30.5 cm (12 in.) on center. Figure 4.6.8 shows a view of the columns. Supporting each column is a pile shaft. The pile shaft lengths are respectively 16.15 m (53 ft), 15.5 m (50.8 ft), 16 m (52.5 ft), and 14.4 m (47.25 ft) from south to north. At the bottom of each pile shaft is a spread footing.

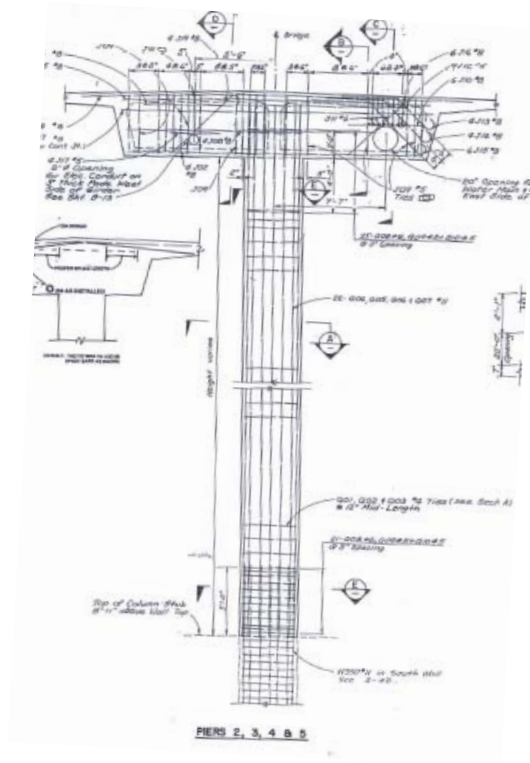


Figure 4.6.8: Bridge 90 columns

Each pile shaft has the same longitudinal reinforcement and the same cross-section as that of its column, although the transverse reinforcement is made up of No. 5 and 6 rebars. The south abutment is about 6 m (20 ft) deep. It is restrained transversely by retaining walls (see Figure 4.6.3 plan in red). A footing measuring 9.7 m (32 ft) in length, 3.8 m (12 ft) in width, and 0.91 m (3 ft) in depth is located directly underneath the abutment-deck seating block.

The north abutment is about 2.4 m (8 ft) deep. It is restrained transversely by wing walls as shown in Figure 4.6.9. A footing measuring 9.7 m (32 ft) in length, 4.8 m (16 ft) in width, and 0.91 m (3 ft) in depth is located directly underneath the abutment-deck seating block. The elevation views of the south and north abutments are shown in Figure 4.6.10 and 4.6.11.

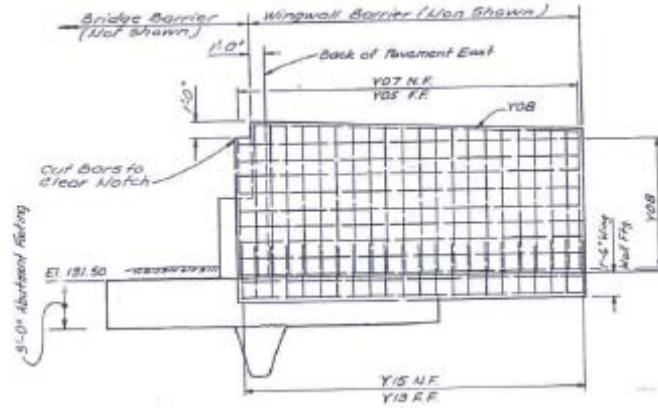


Figure 4.6.9: Wing Wall

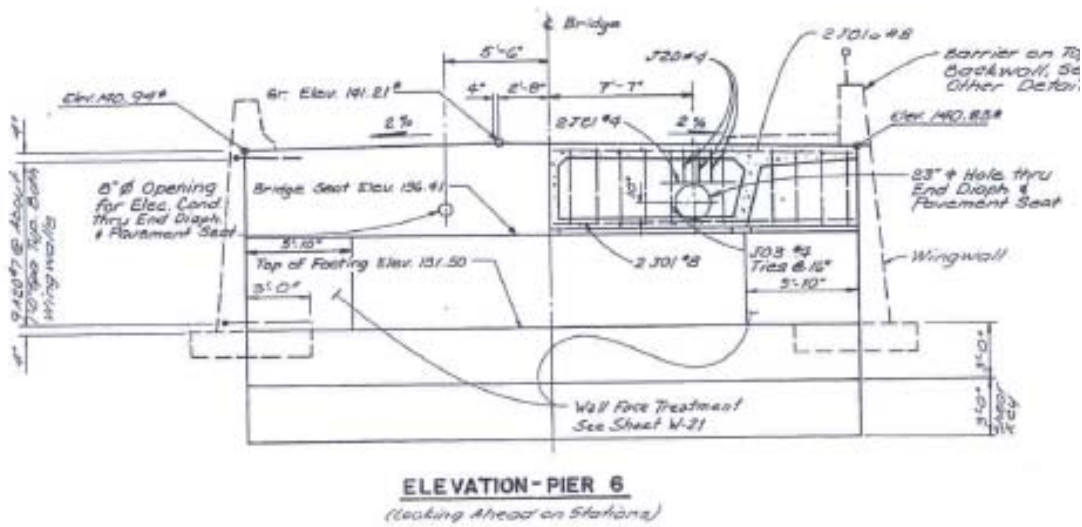


Figure 4.6.10: Bridge 90 Abutment and Deck Elevation View

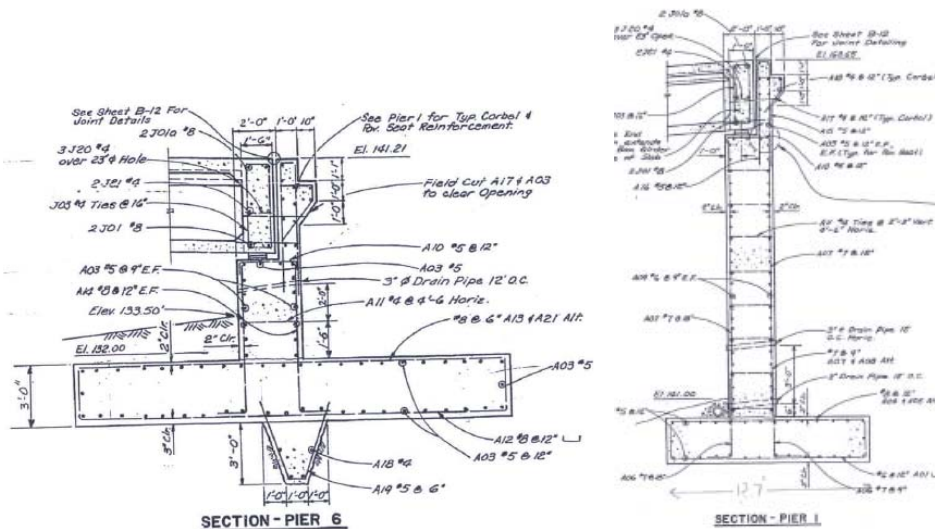


Figure 4.6.11: Bridge 90 East and West Abutments

The footings, wing walls, and abutment walls were constructed with WSDOT Class “B” mix concrete providing a compressive strength of $f'_c = 20.7$ MPa (3 ksi). The concrete for the superstructure (slabs, girders, diaphragms, and barriers) was class AX, providing a compressive strength of $f'_c = 27.6$ MPa (4 ksi). The concrete in the columns was specified to be class RC, providing a compressive strength of $f'_c = 34.47$ MPa (5 ksi). The reinforcing steel conforms to AASHTO M31 Grade 60 with a yield strength of $f_y = 413.6$ MPa (60 ksi).

4.6.2) Structural Model

As with the previous models, this bridge was discretized by 3-node quadratic Timoshenko (shear flexible) beam elements, resulting in a so-called spine model, as shown in Figure 4.6.12. The bridge has a 4° slope downward from south to north.

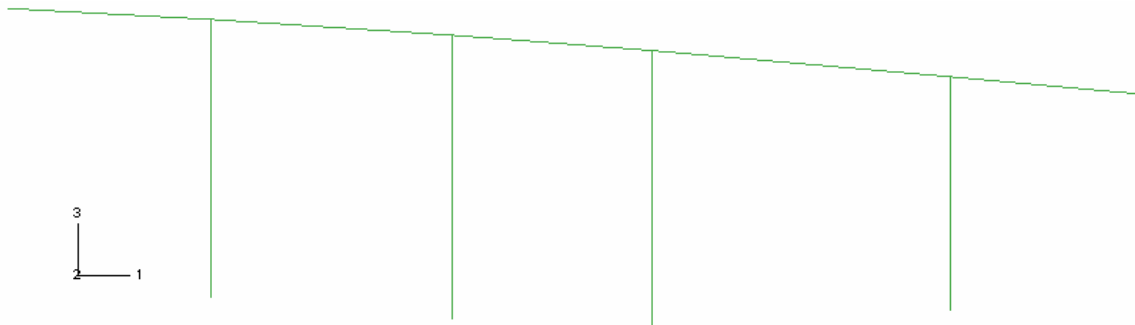


Figure 4.6.12: Bridge 90 Spine Model

Figure 4.6.13 shows the assigned deck cross-section, for the computation of cross sectional properties.

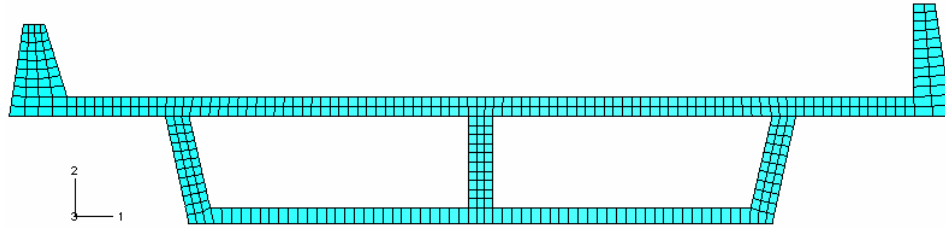


Figure 4.6.13: Bridge 405 deck meshed cross-section

A solid Finite Element Model (FEM) of the Bridge 90 deck, shown in Figure 4.6.14, was created to confirm the torsional properties. As expected for a closed cross section, the warping effects were much less significant than for the previous two bridge decks. Thus, the torsional stiffness that was used for the spine FEM of Bridge 90 was taken as the original torsional stiffness value computed by ABAQUS.

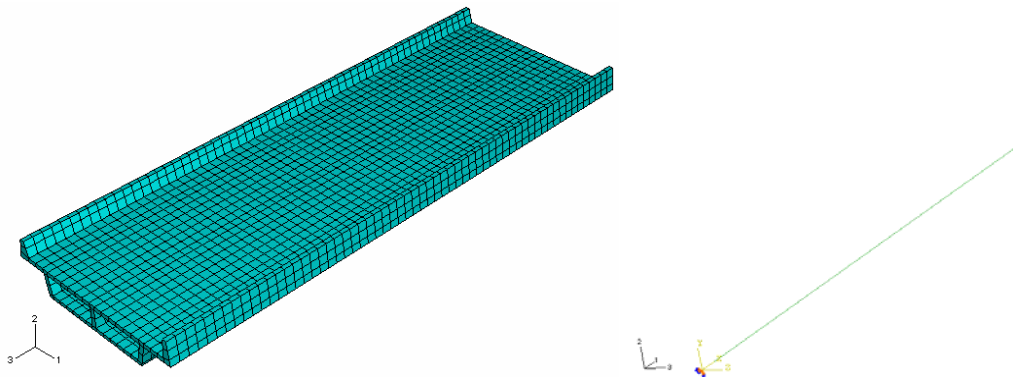


Figure 4.6.14: Bridge 90 Deck FEMs

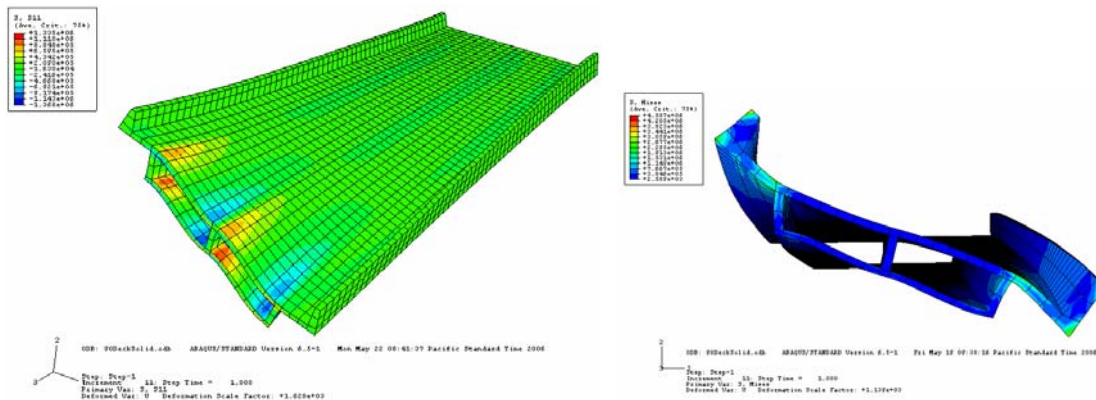


Figure 4.6.15: Output Results of Bridge 90 Deck FEM – Torsion Model

The bending characteristics in both directions were also compared. The results (horizontal and vertical displacements) for both models were in close agreement, matching within 5% error. The modeling of the bridge columns was similar to that of the previous bridge models. The rebars were distributed through the cross-section as shown on Figure 4.6.16.

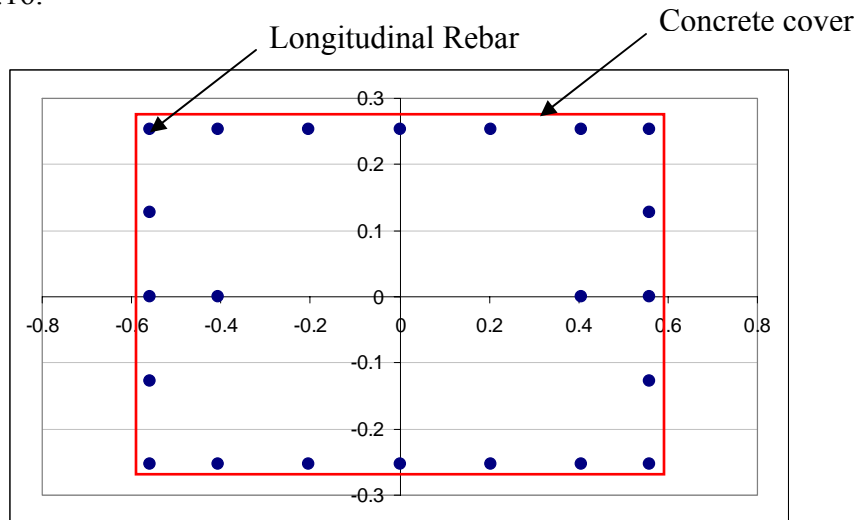


Figure 4.6.16: Rebar locations in the column cross-section

4.6.2.1) Boundary and Connectivity Conditions

The Bridge 90 north abutment is connected to the deck with a compression seal and fixed bearings restraining the longitudinal deck movement. The south abutment is connected to the deck with a strip seal (gap = 7 cm), and guided bearings allowing longitudinal deck movement. The abutments were modeled as a single node with a lumped mass. Linear springs connected the soil to the abutments to represent the Soil-Structure Interaction (SSI). The SSI was determined following the FEMA 356 (2000) procedure (See Appendix A.2), based on the geometric characteristics of the abutment footing.

The longitudinal stiffness of the fixed bearing pads was based on equation 4.3. In

the longitudinal direction, a nonlinear gap spring and a connector element were added in parallel to the bearing pad spring to model the 7.6 cm (3 in) gap between the south abutment and the deck. The north abutment was modeled similarly but did not have a bearing pad spring in parallel (see Figure 4.6.17). The connector was defined as a nonlinear spring including the plasticity effect to model the damage of the abutment resulting from pounding. The connector force-displacement curve was determined following the Caltrans – Seismic Design Criteria procedure (see Appendix A.3).



Figure 4.6.17: FE model of the soil, abutments, and deck interaction in the longitudinal direction

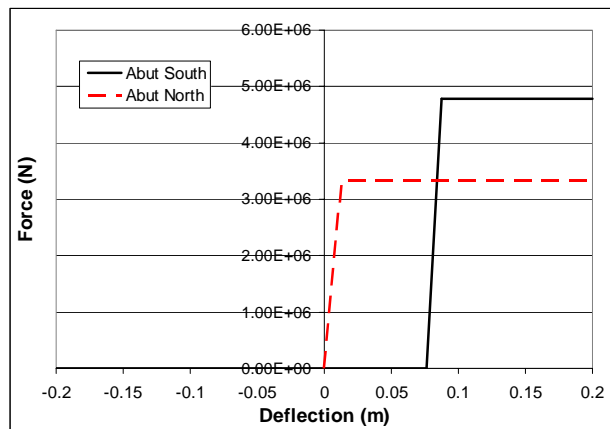


Figure 4.6.18: Abutment Force-Displacement Curves

The columns were considered fixed with the deck. The abutment and column footing soil springs were applied at the abutment and column footing nodes. Nonlinear springs along the pile shafts were used to model the resistance provided by the

surrounding soil. The L-Pile software (2002) was used to compute the P - Y curves, based on the stiff clay soil model without free water at 6 depths. The results were verified and compared to the procedure of Welch and Reese (1972) (Figure 4.6.19). Figure 4.6.20 shows a summary of the different applied boundary conditions.

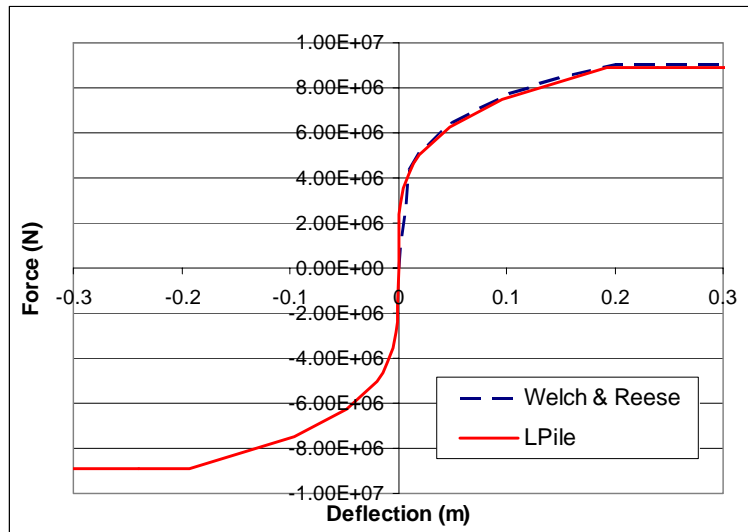


Figure 4.6.19: P-Y curve comparison example

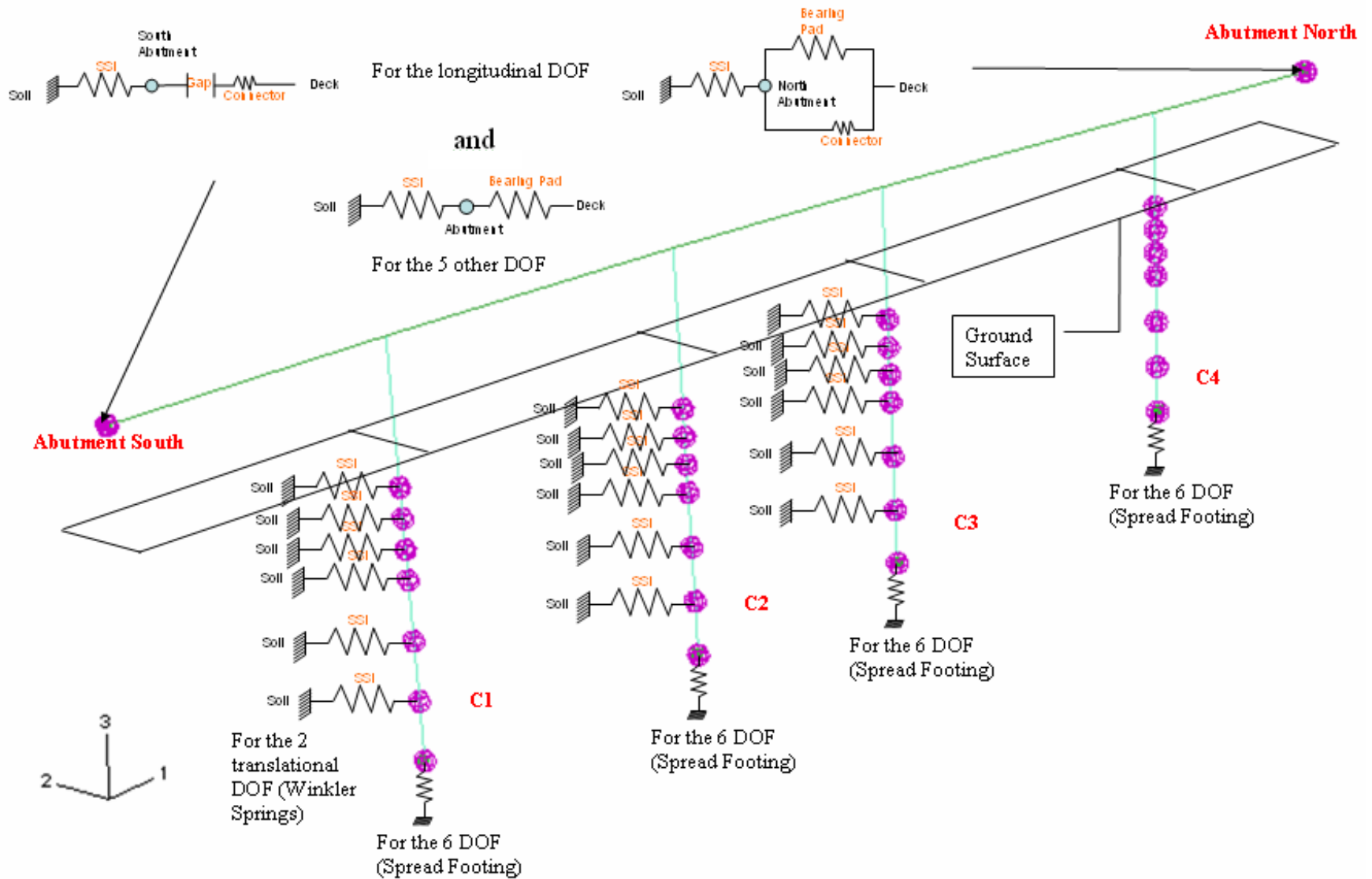


Figure 4.6.20: Bridge 90 Model Boundary Conditions

4.6.2.2) Loading and Ground Motions

The ground motions were applied at the foundation nodes in the transverse, vertical, and longitudinal directions. If not known, the vertical components of the ground motions were taken as 66% of the respective fault normal components. Figure 4.6.21 shows the earthquake applied to the model including SSI.

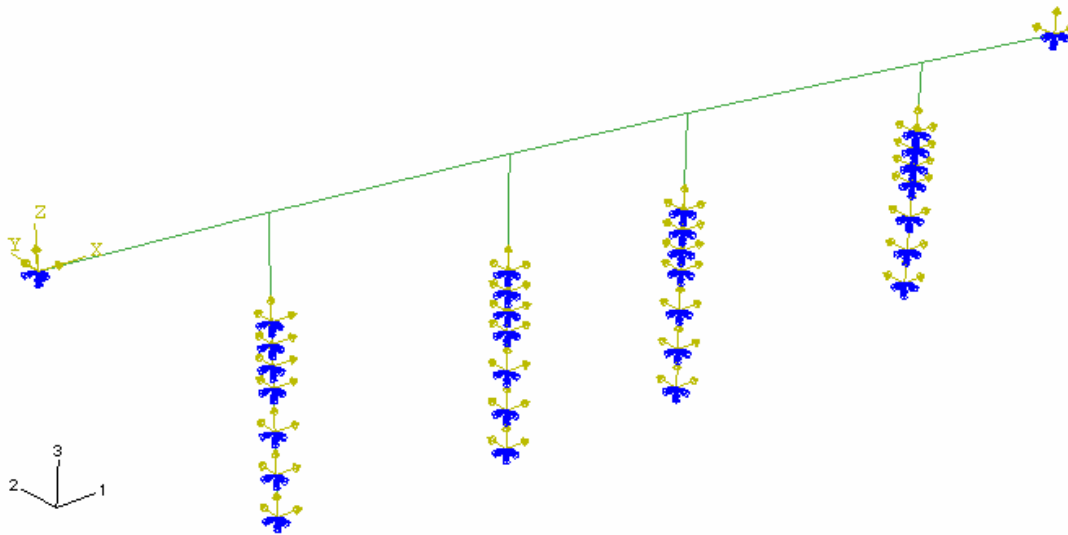


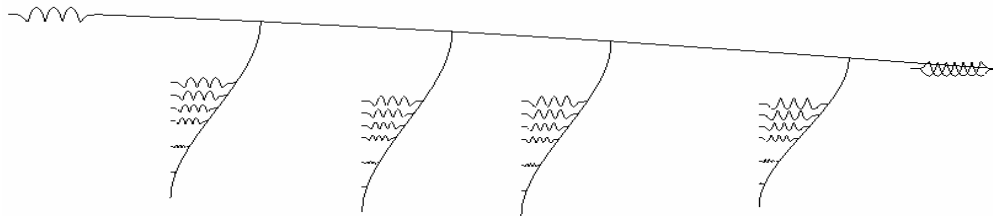
Figure 4.6.21: Applied earthquake at the foundation nodes.

4.6.2.3) Bridge Frequency Content

Table 4.6.1 summarizes the frequency content of Bridge 90. The first mode of vibration of Bridge 90 is in its longitudinal direction with a frequency of 1.22 Hz (period, $T = 0.82$ sec). The bridge transverse direction is excited by its second mode of vibration with a frequency of 2.11 Hz ($T = 0.47$ sec). Figures 4.6.22 and 4.6.23 show the two modes of deformation.

Table 4.6.1: Frequency content of Bridge 90

Eigenvalue Output						
Mode No	Eigenvalue	Frequency		Generalized Mass	Governing DOF	
		(Rad/Time)	(Cycles/Time)			
1	58.485	7.6476	1.2171	1.05E+06	X-Component	
2	176.4	13.281	2.1138	5.97E+05	Y-Component	
3	906.86	30.114	4.7928	1.13E+06		
4	1544.7	39.302	6.2552	1.11E+06		
5	1616.4	40.204	6.3987	1.60E+05		
6	2545.6	50.454	8.0301	1.76E+05		
7	2573.4	50.729	8.0737	8.19E+05		
Participation Factors						
Mode No	X-Component	Y-Component	Z-Component	X-Rotation	Y-Rotation	Z-Rotation
1	1.01E+00	-5.08E-02	1.46E-03	-1.91E-01	-3.17E+00	-2.32E+00
2	6.52E-02	1.14E+00	1.13E-04	2.27E+00	-1.98E-01	5.14E+01
3	2.88E-02	2.97E-01	-4.38E-03	3.47E+00	2.41E-01	1.32E+01
4	4.00E-04	6.08E-03	3.10E-02	1.17E+00	-2.22E+00	1.47E+01
5	-8.84E-03	5.65E-03	1.22E+00	-1.32E-01	-8.06E+01	-2.62E+00
6	-9.57E-04	-2.72E-03	1.53E+00	6.69E-01	-4.26E+01	9.43E+00
7	-1.67E-03	9.61E-03	1.79E-01	-1.23E+00	-5.10E+00	-1.68E+01
Effective Mass						
Mode No	X-Component	Y-Component	Z-Component	X-Rotation	Y-Rotation	Z-Rotation
1	1.06E+06	2.71E+03	2.22E+00	3.82E+04	1.06E+07	5.64E+06
2	2.54E+03	7.71E+05	7.67E-03	3.07E+06	2.34E+04	1.58E+09
3	9.37E+02	9.99E+04	2.17E+01	1.37E+07	6.56E+04	1.97E+08
4	1.78E-01	4.11E+01	1.07E+03	1.52E+06	5.49E+06	2.41E+08
5	1.25E+01	5.12E+00	2.39E+05	2.81E+03	1.04E+09	1.10E+06
6	1.61E-01	1.30E+00	4.10E+05	7.88E+04	3.20E+08	1.57E+07
7	2.29E+00	7.57E+01	2.63E+04	1.23E+06	2.13E+07	2.32E+08



ODB: 90bridge odb ABAQUS/STANDARD Version 5.5-1 Fri Jul 07 13:01:04 Pacific Standard Time 2006
 Step: Step-2
 Mode 1: Value = 9.8996 Freq = 0.49924 (cycles/time)
 Deformed Var: U Deformation Scale Factor: +9.110e+00

Figure 4.6.22: Bridge 90 Longitudinal mode of vibration

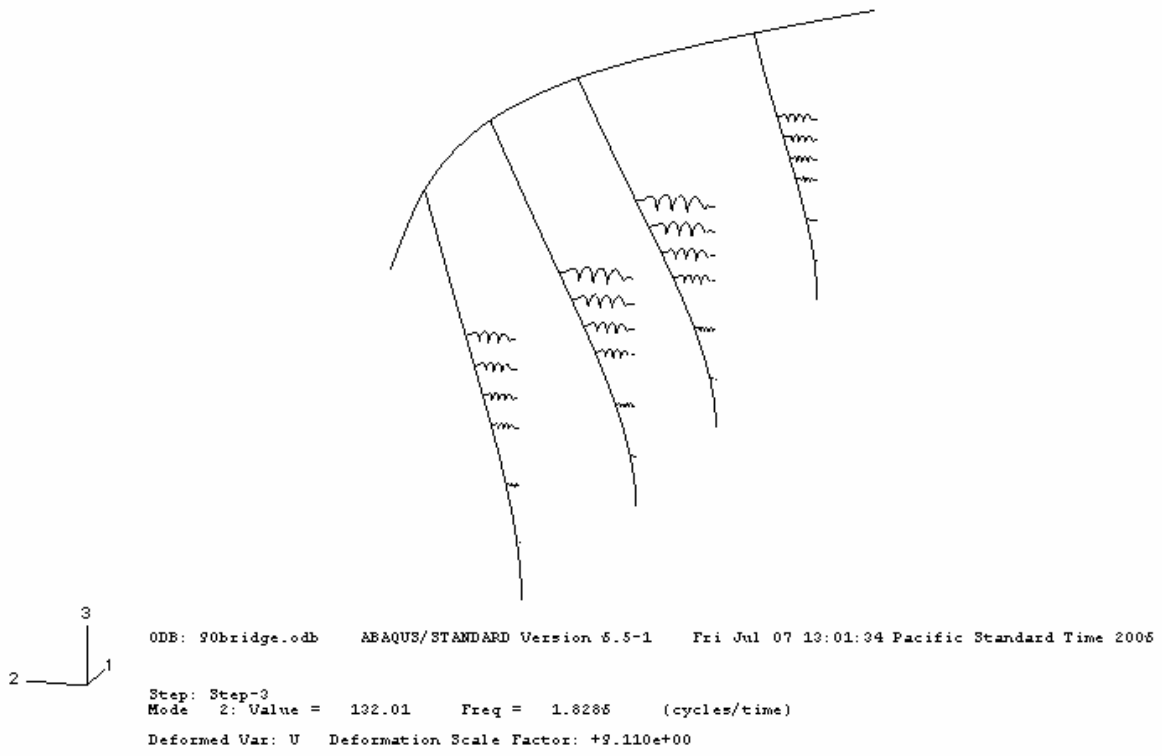


Figure 4.6.23: Bridge 90 Transverse mode of vibration

CHAPTER 5: WSDOT Bridge Results

Presented here are time-history analysis results from the nonlinear finite element analyses of the three WSDOT bridges. The results include figures showing the hysteretic response of columns, time-history responses, abutment behavior, and tables describing maximum column relative displacements, shears, moments, and curvatures. The terms “Regular” and “Inverse” refer to how the two ground motion components were applied to the bridge. “Regular” means that the FN and FP components were applied to the bridge transverse and longitudinal directions, respectively, and vice versa for “Inverse”.

The ground motions were applied to the Finite Element Model (FEM) of each bridge. In the following paragraphs, the results are analyzed by describing the general behavior of the bridges and the effect of forward directivity, and velocity pulse period. Result comparisons with the provisions of AASHTO design methods and with those of a SDOF system are also presented.

5.1) General Bridge Behavior

5.1.1) Bridge 405 and Bridge 520

Bridge 405 behavior will be described through its response to the non-FDGM recorded at Moquegua City during the southern Peru earthquake of June 23, 2001 ($M_w = 8.4$). The earthquake resulted from thrust faulting on the boundary between the Nazca and South American plates. The Moquegua ground motion lasted about 2 min. The FN and FP acceleration time histories are shown in Figure 5.1.1. Figure 5.1.2 shows the earthquake effect on the Cathedral in Moquegua.

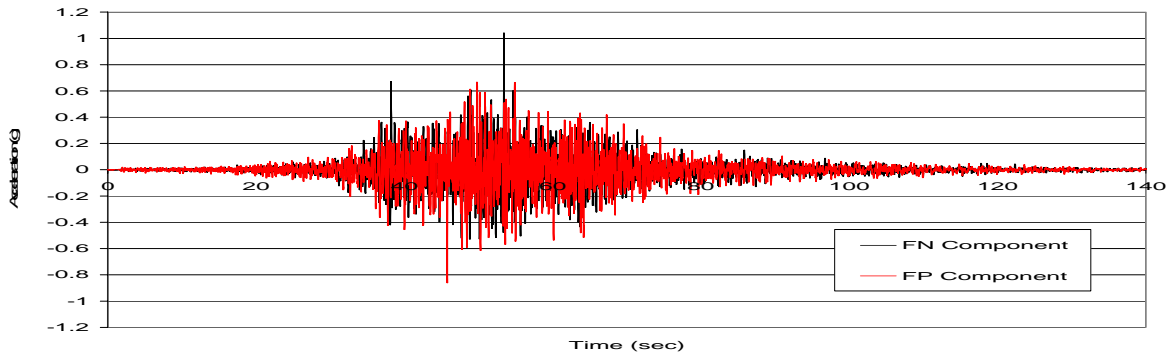


Figure 5.1.1: Moquegua GM Time History



Figure 5.1.2: Cathedral in Moquegua, a stone structure with stone walls and stone vaults, sustained damage and lost one of its vaults (Photo by E. Fierro)

The bridge, due to the boundary conditions and to its geometry, showed different responses in its transverse and longitudinal directions. The bridge was very stiff in its transverse direction because of the high resistance provided by the bents. The moment-curvature relationship for the southwest column is shown in Figure 5.1.3. One can observe the pinching behavior and the decreasing stiffness of the column in the longitudinal direction. For comparison purposes, the backbone curve (in dashed green) was computed from a freeware program (USC_RC, Asadollah Esmaily) which based the analysis on a cross-section fiber model. The computed curve closely matches the backbone curve from the ABAQUS model.

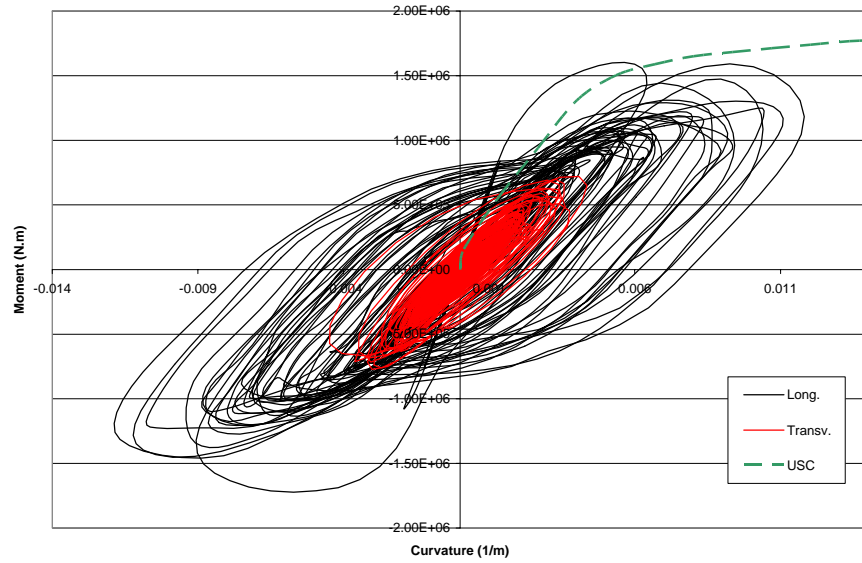


Figure 5.1.3: Moment-Curvature hysteresis curves in the transverse (red) and longitudinal (black) column direction

The columns were in double curvature in the transverse direction due to the two columns per bent and single curvature in the longitudinal direction. A plot of lateral force versus relative displacement for the southwest column is shown in Figure 5.1.4. The longitudinal component of the column relative displacement was higher than the transverse one as shown in Figure 5.1.5. But, the column base shears were of the similar amplitude (Figure 5.1.6).

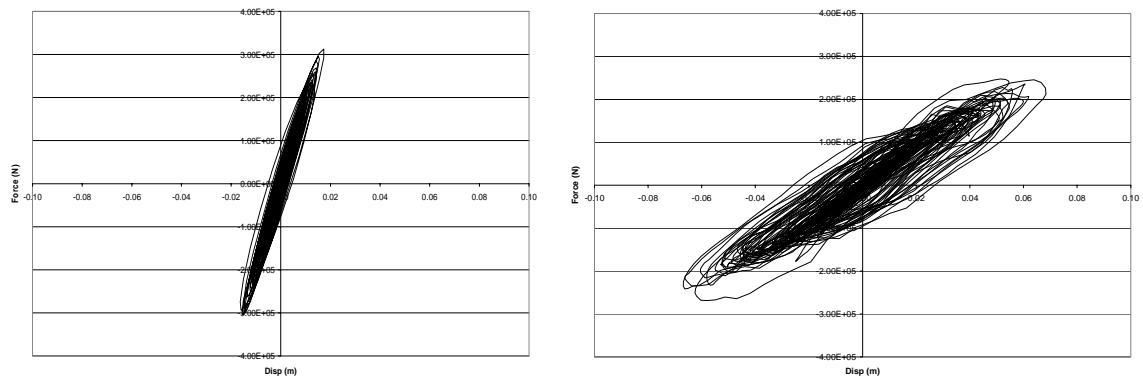


Figure 5.1.4: Force-Displacement hysteresis curves in the transverse (left) and longitudinal (right) direction

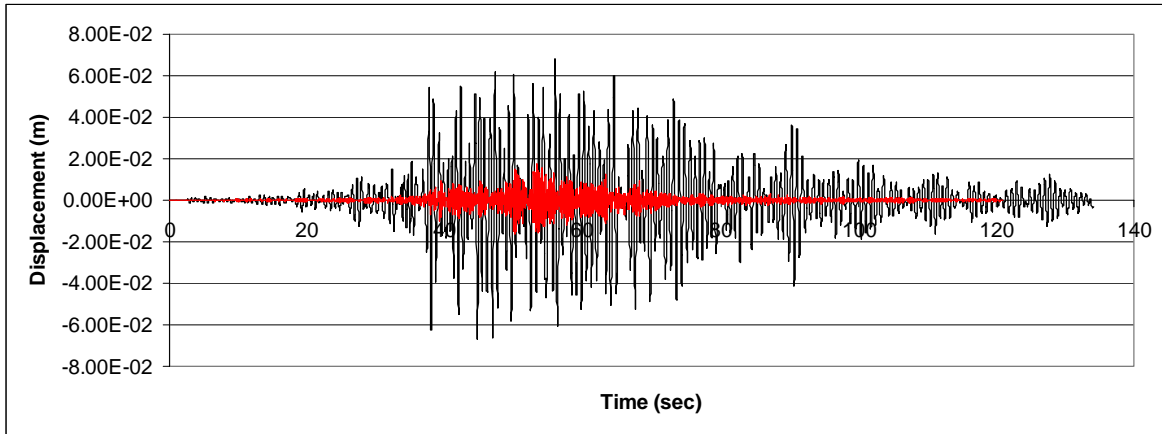


Figure 5.1.5: Transverse (red) and longitudinal (black) column displacement time history

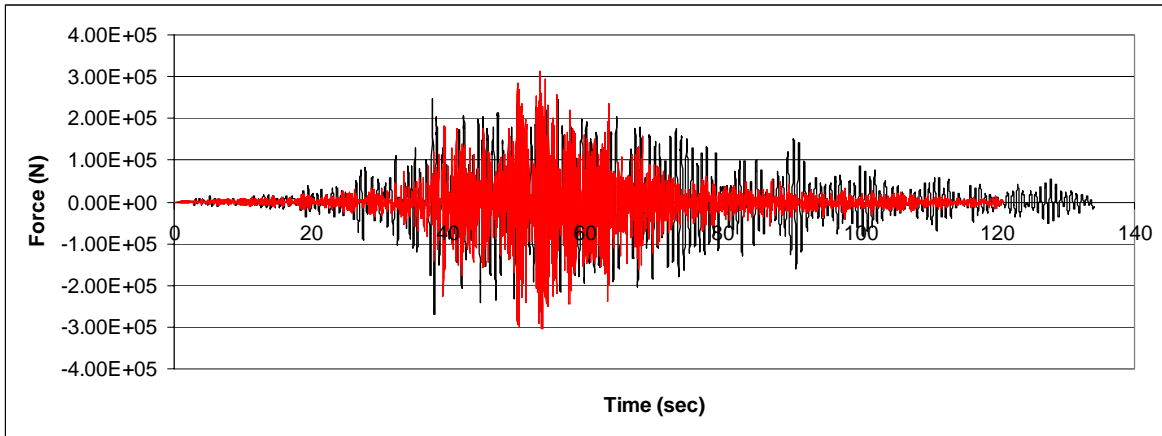


Figure 5.1.6: Transverse (red) and longitudinal (black) column base shear time history

A plot of force versus displacement is shown in Figure 5.1.7 for Bridge 405. In dashed green, the shear capacity envelope proposed by Kowalsky and Priestley (2000) is shown (see Appendix A.1). The column base shears never cross the shear capacity envelope. There is, therefore, very little risk of brittle shear failure in the columns.

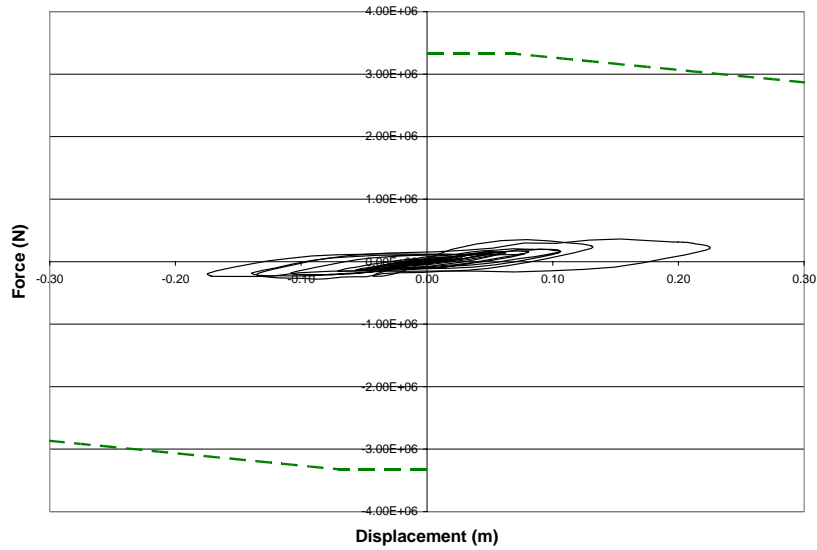


Figure 5.1.7: Bridge 405 Force – Displacement hysteresis curve, in the longitudinal direction, including the column shear capacity in dashed green

The ABAQUS output variable defined as the internal energy (or total strain energy) sums the energy dissipated by plastic deformation and the kinetic energy. The internal energy in the system increases gradually during the earthquake (see Figure 5.1.8).

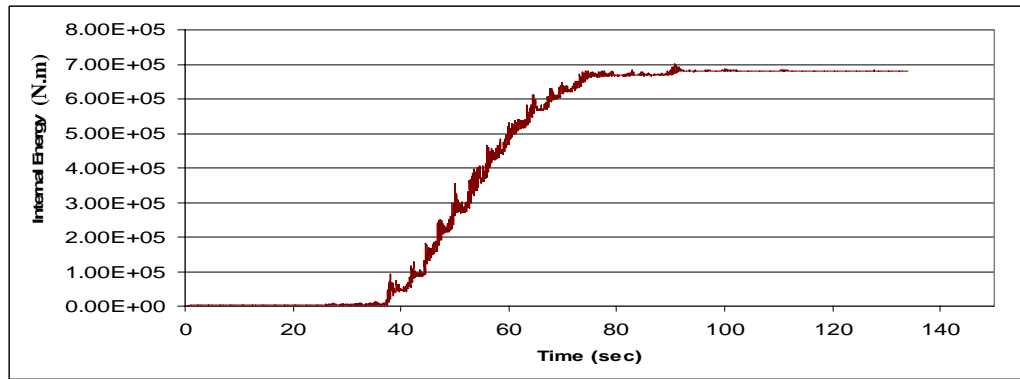


Figure 5.1.8: Total Strain Energy in the system

Figure 5.1.9 shows the longitudinal force response of the abutments from the Moquegua ground motion. At abutments, the deck was restrained only by the bearing pad's shear resistance when pushed toward the soil (negative displacement value on the Force-Displacement curve). See Figure 4.4.13. But, when pushed in the opposite direction, one can see the high stiffness provided by the abutment when the 5 cm (2 in) gap closes

(positive displacement value on the Force-Displacement curve). The north and south abutments experience pounding several times (Figure on the right), but do not reach their maximum allowable compressive force.

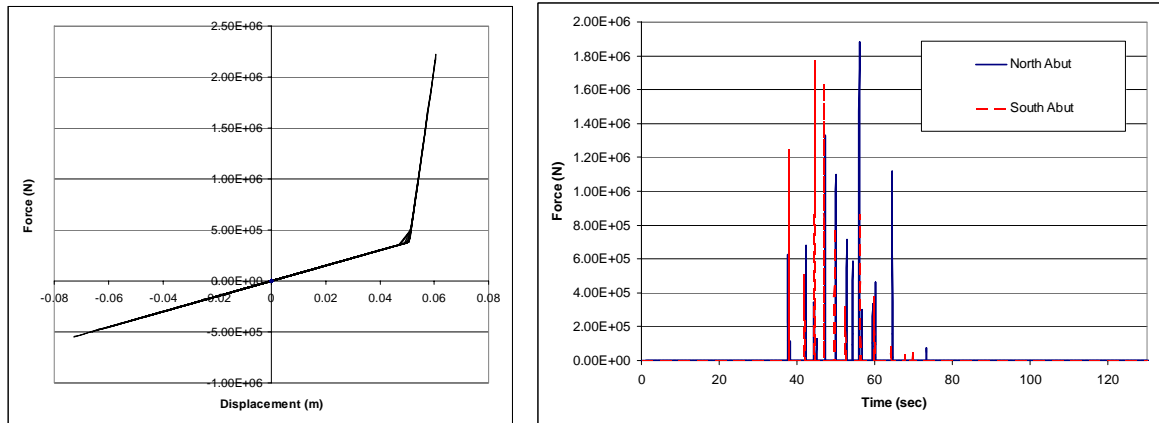


Figure 5.1.9: Abutment Hysteresis Force-Displacement (left) and Force Time History curve (right)

The general behavior of Bridge 520 was similar to that of Bridge 405 since the geometry and the boundary conditions were similar. Further details on the analysis of Bridge 520 will be presented in future sections in Chapter 5.

5.1.2) Bridge 90

The behavior of Bridge 90 is described through its response to the non FDGM recorded in the Izmit Gulf during the $M_w = 7.4$ Kocaeli, Turkey, earthquake of August 17, 1999. The earthquake resulted from strike-slip faulting on the east-west North Anatolian fault. The FN and FP acceleration time histories are shown in Figure 5.1.10. Figure 5.1.11 shows the effect of the earthquake on the surrounding buildings of the mosque in the town of Golcuk.

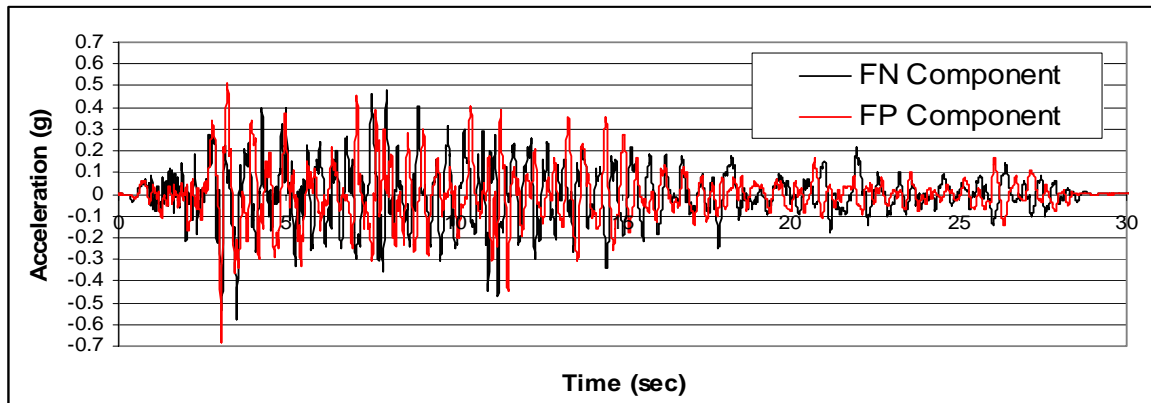


Figure 5.1.10: Izmit GM Time History



Figure 5.1.11: A mosque stood with a few other structures amid the rubble of collapsed buildings in the town of Golcuk, 60 miles east of Istanbul (Associated Press Photo, Enric Marti, 1999).

The longitudinal moment-curvature relationship at two locations of the northern column is shown in Figure 5.1.12. The moment-curvature seen at the top of the column is shown in blue and the moment-curvature seen at about 3 m (10 ft) below the ground level is shown in red where the maximum moment and curvature were recorded.

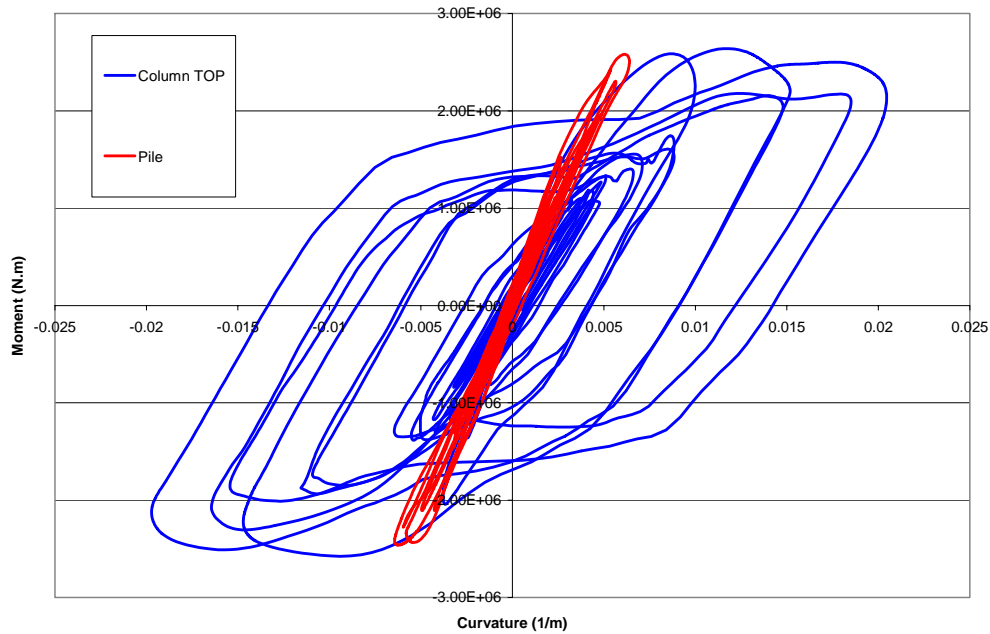


Figure 5.1.12: Moment-Curvature hysteresis curves at the column top (blue) and at the pile (red) in the longitudinal direction

A plot of lateral force versus relative displacement for the four columns is shown on Figure 5.1.13. The maximum forces were experienced at the column tops. The relative displacements were computed between the column top and the ground level. The four columns did not have the same response to the ground motions since they have different heights and Bridge 90 is not symmetric. The column C_1 is the southern column, C_4 is the northern one. The tallest column (C_2 , in green) experienced the highest relative displacement and the lowest resisting force. Conversely, the smallest column (C_4 , in red) experienced the lowest relative displacement and the highest resisting force.

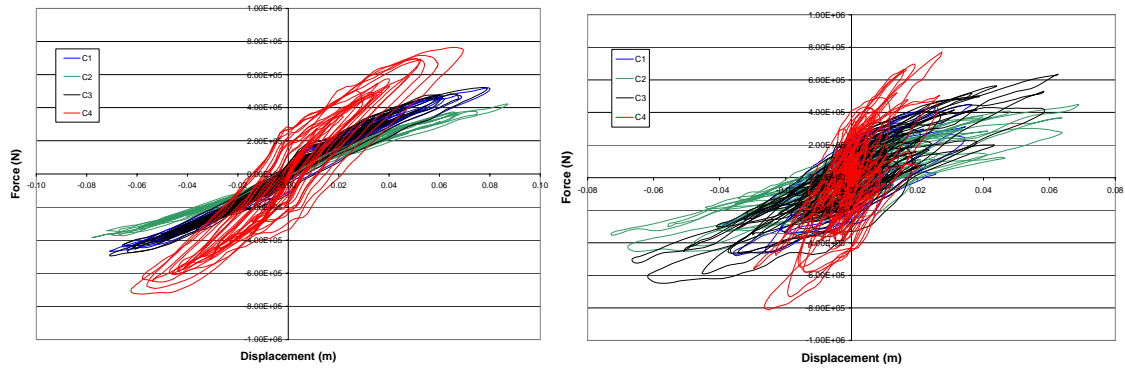


Figure 5.1.13: Column Force-Displacement hysteresis curves in the longitudinal (left) and transverse (right) direction

A plot of force versus displacement is shown in Figure 5.1.14 for Bridge 90. In purple, the shear capacity envelope proposed by Kowalsky and Priestley (2000) is shown (see Appendix A.1). The column base shears never cross their shear capacity envelope. There is very little risk of brittle shear failure in the columns.

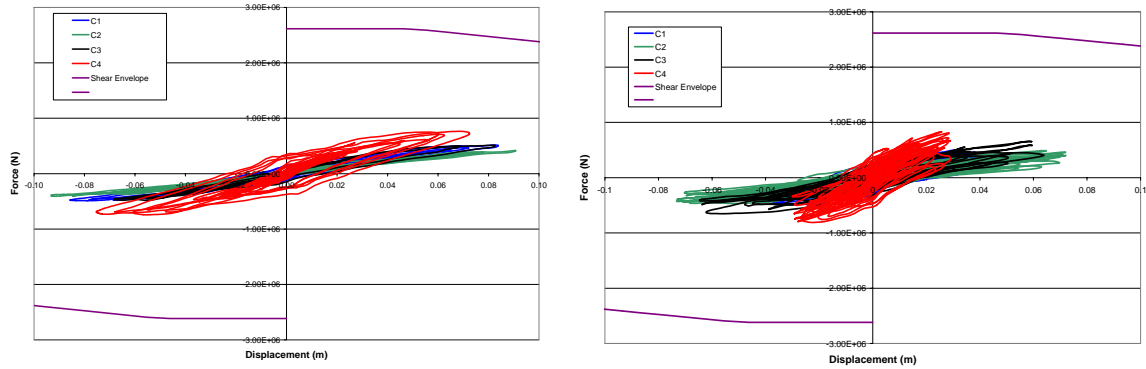


Figure 5.1.14: Force-Displacement hysteresis curves in the longitudinal (left) and transverse (right) direction

The internal energy in the system increases gradually during the earthquake due to the energy dissipated by the columns (see Figure 5.1.15).

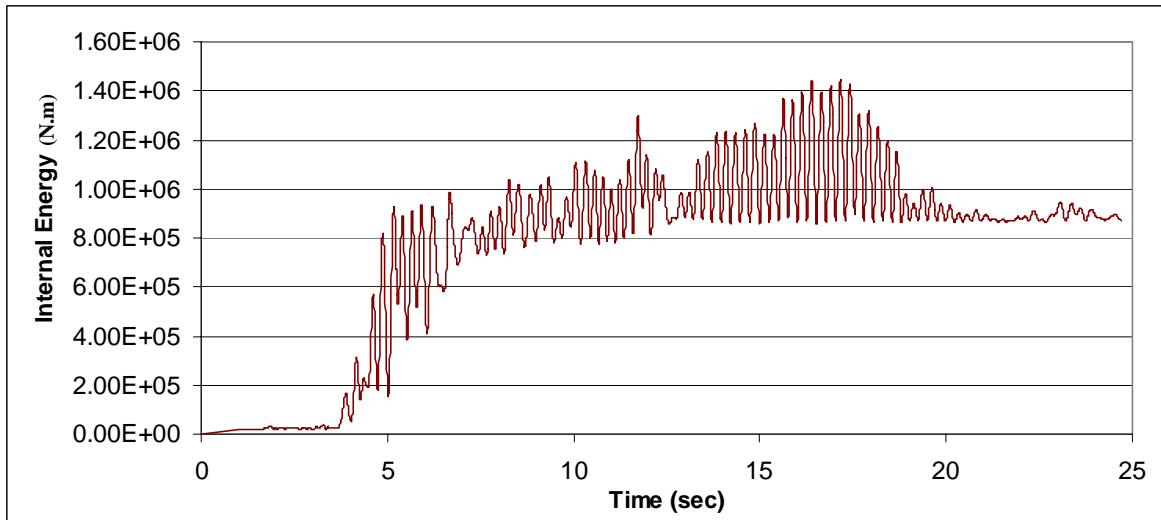


Figure 5.1.15: Total Strain Energy in the system

Figure 5.1.16 shows the longitudinal force response of the abutments from the Izmit ground motion. The abutments experienced pounding several times. Note also that they reached their maximum allowable compression force and experienced several cycles of plastic behavior.

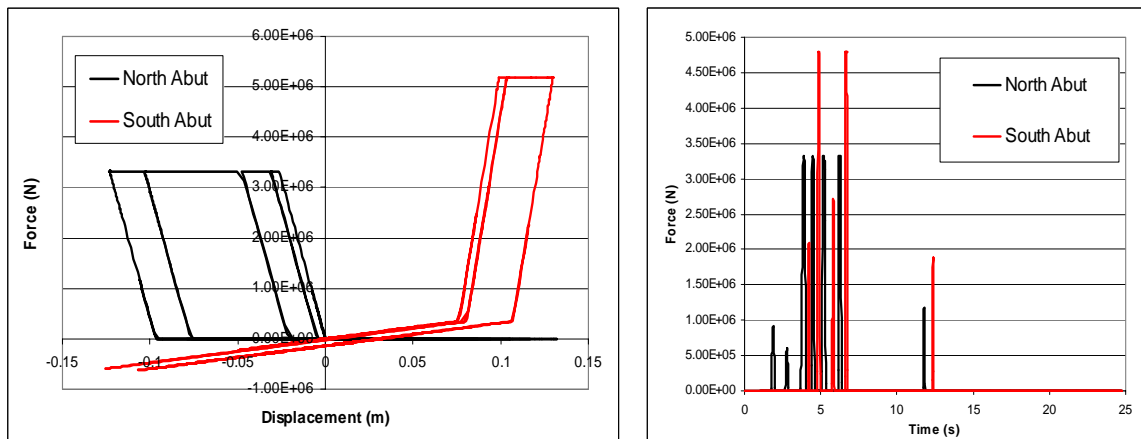
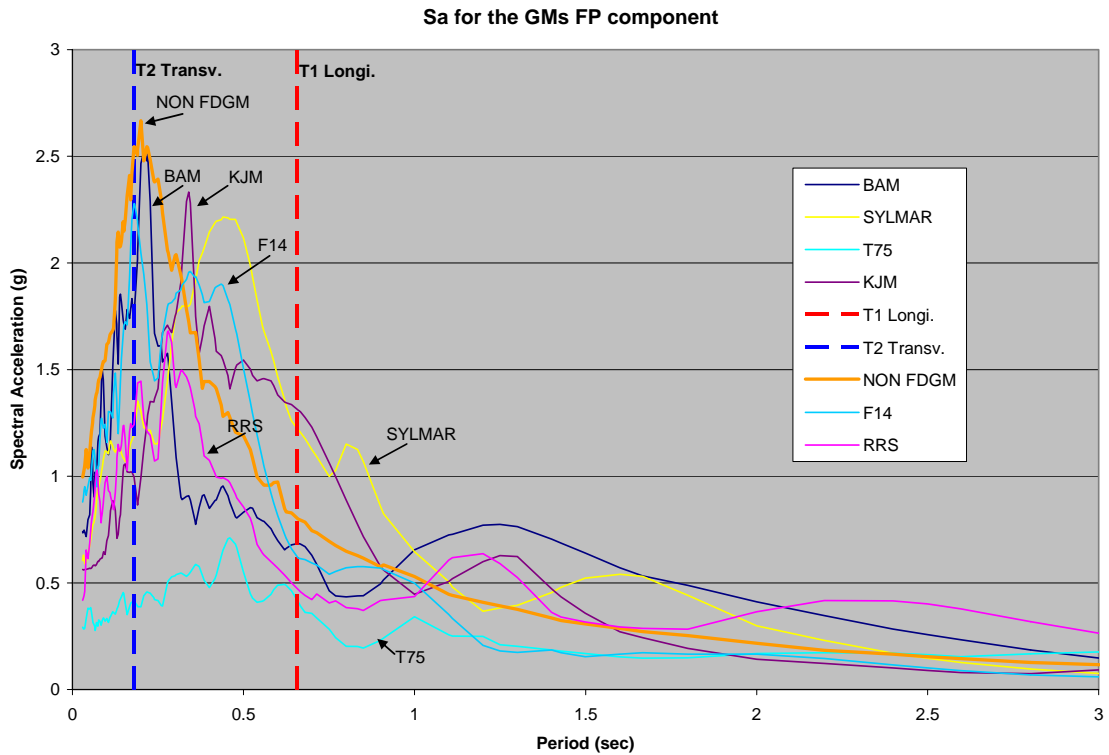
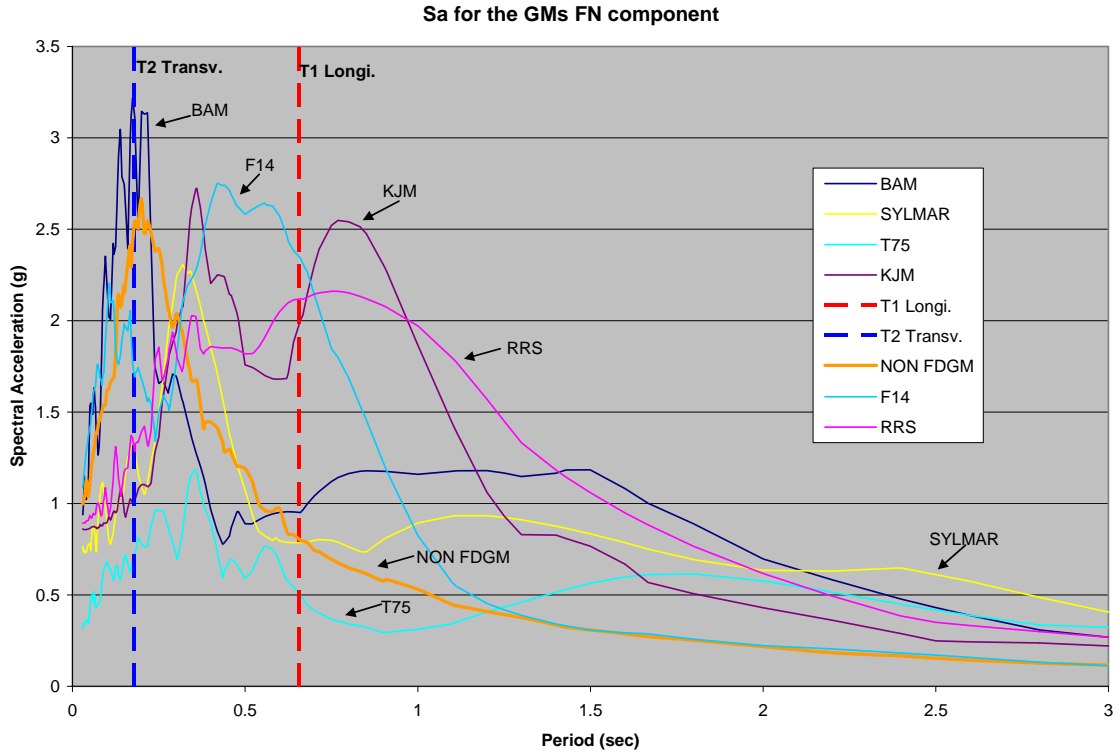


Figure 5.1.16: Abutment Hysteresis Force-Displacement (left) and Force Time History curve (right)

5.2) Forward Directivity Effect – Frequency Content

Significant seismic damage may occur if the structure response is 'in tune' with components of the ground motion (resonance), which may be identified from the response spectrum. Figures 5.2.1 to 5.2.6 show the acceleration response spectra (ARS) of the FN and FP ground motion's component for each bridge. The blue and red vertical dashed lines are, respectively, the transverse and longitudinal fundamental mode shape periods. The forward directivity “bump” effect is visible on the acceleration response spectra (ARS) of the FN ground motion components. It is created by the velocity pulse, typical of a forward directivity ground motion (Somerville et al., 1997). The ARS show only one curve for each bridge for the non-FD ground motions since they have approximately the same frequency content (see Chapter 4 - section 4.1.2).



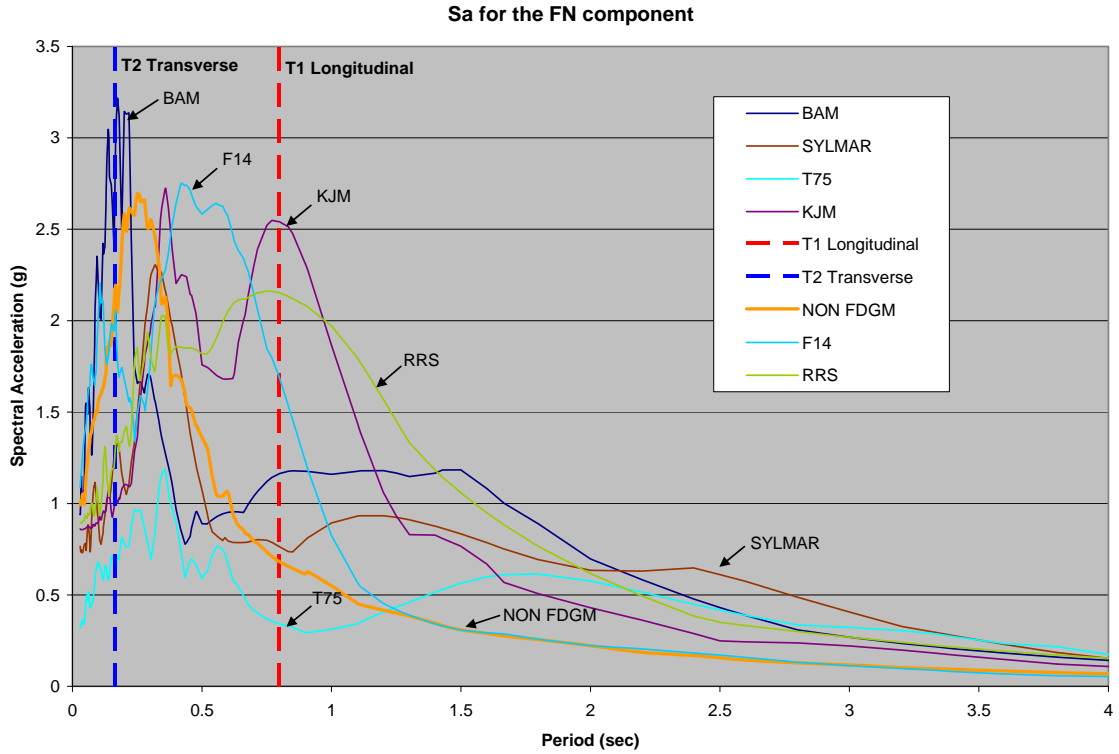


Figure 5.2.3: Bridge 520 ARS of the FN components of the Ground Motions

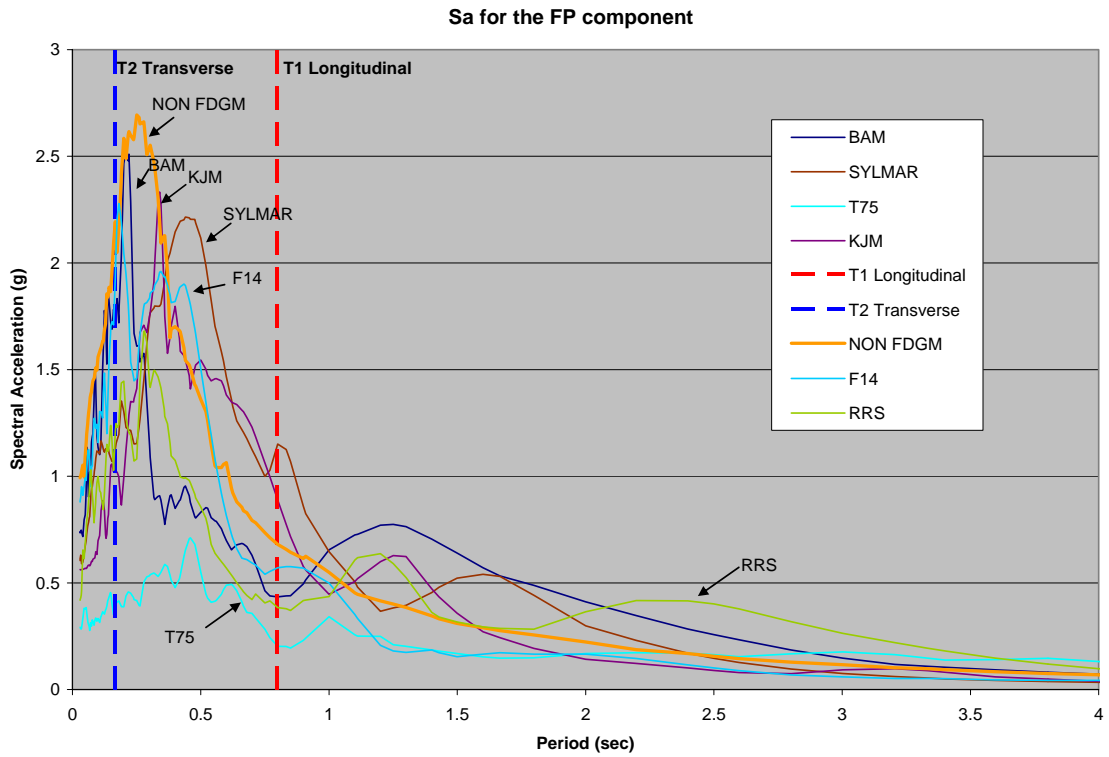


Figure 5.2.4: Bridge 520 ARS of the FP components of the Ground Motions

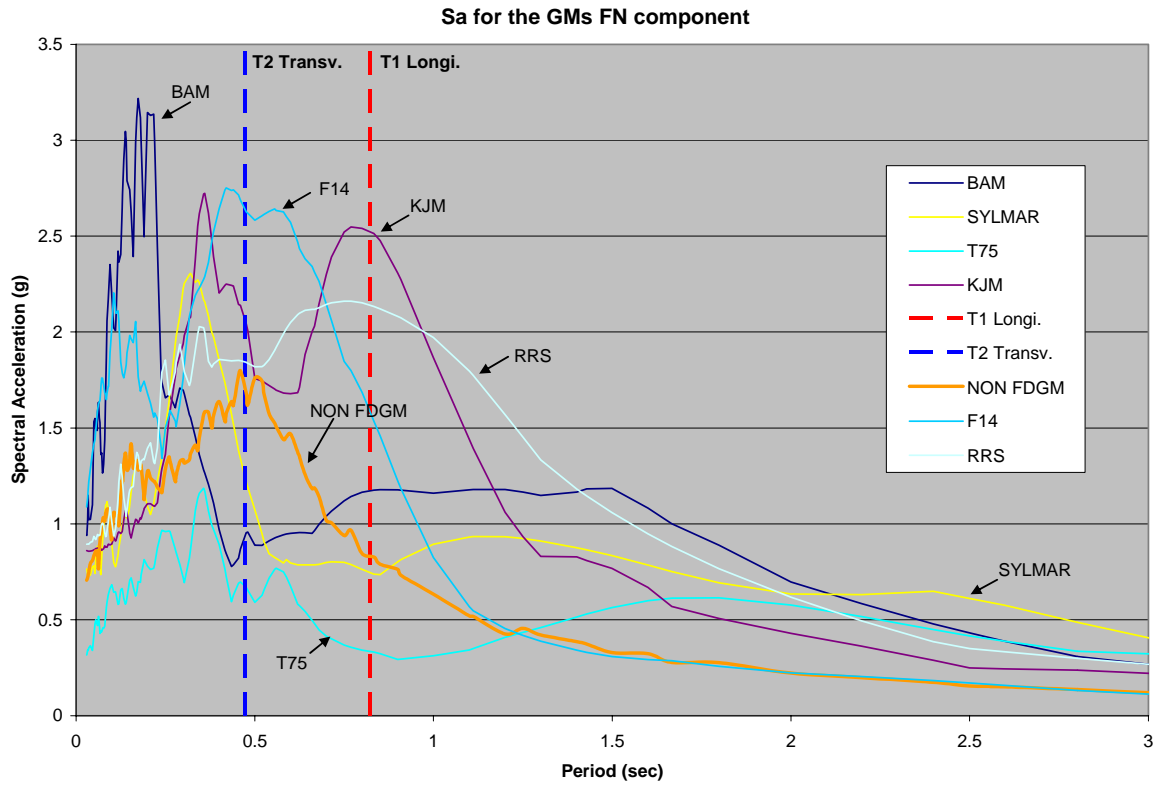


Figure 5.2.5: Bridge 90 ARS of the FN components of the Ground Motions

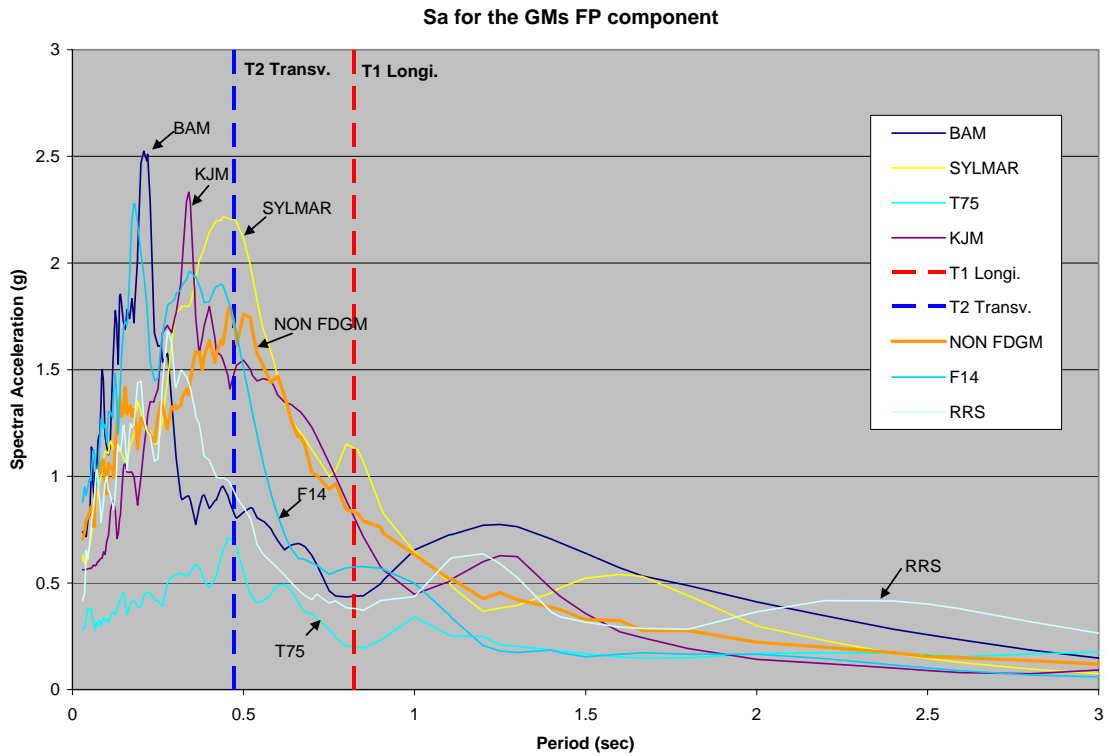


Figure 5.2.6: Bridge 90 ARS of the FP components of the Ground Motions

The ABAQUS output results (max displacement, max base shear, energy dissipated) as a function of the spectral acceleration value (S_a) were compared. Tables 5.2.1, 5.2.2, and 5.2.3 show the ground motion characteristics, including the Peak Ground Acceleration (PGA), and the spectral acceleration (S_a) value at the corresponding modes of deformation for each bridge.

Table 5.2.1: Summary of the GM characteristics and the Bridge 405 column response parameters

Type	GM	Earthquake					Regular			Inverse		
		PGA (g) FP	PGA (g) FN	Sa FN	Sa FP	Direction	Max. Base Shear (N)	Max. Disp. (m)	Plastic Energy	Max. Base Shear (N)	Max. Disp. (m)	Plastic Energy
Non FD	IZT	0.764	0.773	0.80	0.80	Longi.	2.452E+05	0.0702	5.13E+04	2.618E+05	0.0657	5.48E+04
	IZT	0.764	0.773	2.50	2.50	Transv.	4.104E+05	0.0184	5.13E+04	3.634E+05	0.0175	5.48E+04
	702	0.846	0.942	0.80	0.80	Longi.	2.708E+05	0.0615	5.42E+04	2.621E+05	0.0664	5.36E+04
	702	0.846	0.942	2.50	2.50	Transv.	3.965E+05	0.0183	5.42E+04	3.645E+05	0.0181	5.36E+04
	MOQ	0.668	1.042	0.80	0.80	Longi.	3.126E+05	0.0173	1.70E+05	2.727E+05	0.0714	1.55E+05
	MOQ	0.668	1.042	2.50	2.50	Transv.	2.688E+05	0.0684	1.70E+05	3.624E+05	0.0192	1.55E+05
	SSU	0.725	0.828	0.80	0.80	Longi.	2.523E+05	0.0717	4.85E+04	2.522E+05	0.0791	5.52E+04
	SSU	0.725	0.828	2.50	2.50	Transv.	3.537E+05	0.0188	4.85E+04	3.659E+05	0.0188	5.52E+04
	T71	0.730	0.840	0.80	0.80	Longi.	2.737E+05	0.0701	6.91E+04	2.685E+05	0.0667	1.21E+05
T71	0.730	0.840	2.50	2.50	Transv.	3.798E+05	0.0199	6.91E+04	3.643E+05	0.0194	1.21E+05	
FD (6.5)	BAM	0.647	0.880	0.95	0.69	Longi.	2.748E+05	0.0689	1.92E+04	3.353E+05	0.0903	3.90E+04
	BAM	0.647	0.880	3.12	1.72	Transv.	4.444E+05	0.0224	1.92E+04	2.993E+05	0.0142	3.90E+04
FD (6.0)	F14	0.857	1.015	2.34	0.62	Longi.	2.497E+05	0.0605	1.71E+04	3.237E+05	0.1625	7.76E+04
	F14	0.857	1.015	1.69	2.28	Transv.	3.518E+05	0.0136	1.71E+04	3.061E+05	0.0177	7.76E+04
FD (6.9)	KJM	0.548	0.854	2.00	1.31	Longi.	3.126E+05	0.1087	6.10E+04	3.613E+05	0.2254	1.26E+05
	KJM	0.548	0.854	1.03	1.00	Transv.	2.234E+05	0.0083	6.10E+04	1.210E+05	0.0078	1.26E+05
FD (6.7)	RRS	0.390	0.887	2.12	0.47	Longi.	2.591E+05	0.0495	9.78E+03	3.305E+05	0.1976	7.86E+04
	RRS	0.390	0.887	1.28	1.24	Transv.	2.643E+05	0.0101	9.78E+03	1.764E+05	0.0108	7.86E+04
FD (6.7)	Sylmar	0.595	0.733	0.79	1.22	Longi.	3.120E+05	0.1151	6.43E+04	2.609E+05	0.0645	1.83E+04
	Sylmar	0.595	0.733	1.30	1.20	Transv.	1.733E+05	0.0102	6.43E+04	1.915E+05	0.0105	1.83E+04
FD (7.6)	T75	0.278	0.314	0.50	0.41	Longi.	2.481E+05	0.0477	2.34E+03	2.663E+05	0.0574	7.91E+03
	T75	0.278	0.314	0.70	0.42	Transv.	1.393E+05	0.0054	2.34E+03	8.702E+04	0.0032	7.91E+03
FD (7.3)	LCN	0.783	0.728	0.71	0.35	Longi.	2.312E+05	0.0374	4.19E+00	2.763E+05	0.0659	8.49E+03
	LCN	0.783	0.728	0.88	1.26	Transv.	2.293E+05	0.0076	4.19E+00	2.184E+05	0.0099	8.49E+03

Table 5.2.2: Summary of the GM characteristics and the Bridge 520 column response parameters

Type	GM	Earthquake					Regular			Inverse		
		PGA (g) FP	PGA (g) FN	S_a FN	S_a FP	Direction	Max Base Shear (N)	Max Disp (m)	Plastic Energy	Max Base Shear (N)	Max Disp (m)	Plastic Energy
Non FD	IZT	0.764	0.773	0.70	0.70	Longi.	2.140E+05	0.0970	2.77E+04	2.212E+05	0.0971	2.92E+04
	IZT	0.764	0.773	2.00	2.00	Transv.	2.097E+05	0.0151	2.77E+04	1.969E+05	0.0123	2.92E+04
	702	0.846	0.942	0.70	0.70	Longi.	2.238E+05	0.0892	2.94E+04	2.161E+05	0.0926	2.72E+04
	702	0.846	0.942	2.00	2.00	Transv.	2.040E+05	0.0142	2.94E+04	1.770E+05	0.0123	2.72E+04
	SSU	0.725	0.828	0.70	0.70	Longi.	2.211E+05	0.0957	2.16E+04	2.211E+05	0.0933	1.23E+04
	SSU	0.725	0.828	2.00	2.00	Transv.	2.237E+05	0.0136	2.16E+04	1.962E+05	0.0119	1.23E+04
	T71	0.730	0.840	0.70	0.70	Longi.	2.266E+05	0.0934	4.35E+04	2.271E+05	0.0953	6.59E+04
	T71	0.730	0.840	2.00	2.00	Transv.	2.046E+05	0.0137	4.35E+04	1.895E+05	0.0141	6.59E+04
FD (6.5)	BAM	0.647	0.880	1.16	0.43	Longi.	2.200E+05	0.0656	4.26E+02	2.707E+05	0.1027	1.88E+04
	BAM	0.647	0.880	2.39	1.78	Transv.	3.065E+05	0.0205	4.26E+02	1.764E+05	0.0118	1.88E+04
FD (6.0)	F14	0.857	1.015	1.69	0.57	Longi.	2.013E+05	0.0625	2.79E+02	2.787E+05	0.1922	5.21E+04
	F14	0.857	1.015	1.94	1.71	Transv.	2.282E+05	0.0118	2.79E+02	1.746E+05	0.0152	5.21E+04
FD (6.9)	KJM	0.548	0.854	2.54	0.89	Longi.	2.449E+05	0.1155	3.47E+04	3.018E+05	0.3140	1.64E+05
	KJM	0.548	0.854	0.98	1.02	Transv.	1.261E+05	0.0070	3.47E+04	8.270E+04	0.0070	1.64E+05
FD (6.7)	RRS	0.390	0.887	2.15	0.38	Longi.	1.935E+05	0.0589	1.52E+01	2.786E+05	0.2206	7.92E+04
	RRS	0.390	0.887	1.20	1.03	Transv.	1.573E+05	0.0083	1.52E+01	9.117E+04	0.0086	7.92E+04
FD (6.7)	Sylmar	0.595	0.733	0.76	1.15	Longi.	2.226E+05	0.0921	1.99E+04	2.161E+05	0.0717	1.53E+03
	Sylmar	0.595	0.733	1.25	1.07	Transv.	1.539E+05	0.0088	1.99E+04	2.648E+05	0.0169	1.53E+03
FD (7.6)	T75	0.278	0.314	0.34	0.20	Longi.	1.336E+05	0.0346	0.00E+00	1.837E+05	0.0533	0.00E+00
	T75	0.278	0.314	0.67	0.35	Transv.	7.139E+04	0.0042	0.00E+00	4.756E+04	0.0026	0.00E+00
FD (7.3)	LCN	0.783	0.728	0.67	0.33	Longi.	2.157E+05	0.0514	0.00E+00	2.399E+05	0.0749	6.20E+02
	LCN	0.783	0.728	1.21	1.78	Transv.	1.314E+05	0.0065	0.00E+00	1.862E+05	0.0111	6.20E+02

Table 5.2.3: Summary of the GM characteristics and the Bridge 90 column response parameters

Type	GM	Earthquake					Regular			Inverse		
		PGA (g) FP	PGA (g) FN	S_a FN	S_a FP	Direction	Max Base Shear (N)	Max Disp (m)	Plastic Energy	Max Base Shear (N)	Max Disp (m)	Plastic Energy
Non FD	IZT	0.764	0.773	0.83	0.83	Longi.	7.638E+05	0.0753	1.96E+05	7.295E+05	0.0609	1.54E+05
	IZT	0.764	0.773	1.68	1.68	Transv.	8.295E+05	0.0300	1.96E+05	8.510E+05	0.0318	1.54E+05
	702	0.846	0.942	0.83	0.83	Longi.	7.640E+05	0.0695	2.28E+05	7.455E+05	0.0641	1.12E+05
	702	0.846	0.942	1.68	1.68	Transv.	8.121E+05	0.0297	2.28E+05	9.084E+05	0.0336	1.12E+05
	MOQ	0.668	1.042	0.83	0.83	Longi.	7.773E+05	0.0753	2.23E+05	7.773E+05	0.0758	2.60E+05
	MOQ	0.668	1.042	1.68	1.68	Transv.	8.166E+05	0.0258	2.23E+05	8.818E+05	0.0298	2.60E+05
	SSU	0.725	0.828	0.83	0.83	Longi.	7.791E+05	0.0702	1.24E+05	8.049E+05	0.0788	1.83E+05
	SSU	0.725	0.828	1.68	1.68	Transv.	7.060E+05	0.0329	1.24E+05	8.788E+05	0.0359	1.83E+05
	T71	0.730	0.840	0.83	0.83	Longi.	7.647E+05	0.0704	1.89E+05	7.537E+05	0.0764	3.25E+05
T71	0.730	0.840	1.68	1.68	Transv.	7.081E+05	0.0296	1.89E+05	8.605E+05	0.0311	3.25E+05	
FD (6.5)	BAM	0.647	0.880	1.18	0.44	Longi.	7.398E+05	0.0466	1.28E+04	7.949E+05	0.0921	1.61E+05
	BAM	0.647	0.880	0.95	0.81	Transv.	6.776E+05	0.0178	1.28E+04	7.070E+05	0.0184	1.61E+05
FD (6.0)	F14	0.857	1.015	1.54	0.58	Longi.	6.674E+05	0.0509	5.74E+04	9.239E+05	0.1274	1.40E+05
	F14	0.857	1.015	2.63	1.69	Transv.	1.142E+06	0.0494	5.74E+04	6.574E+05	0.0314	1.40E+05
FD (6.9)	KJM	0.548	0.854	2.51	0.77	Longi.	7.049E+05	0.0677	1.19E+05	9.454E+05	0.2053	5.29E+02
	KJM	0.548	0.854	2.04	1.51	Transv.	8.997E+05	0.0320	1.19E+05	6.061E+05	0.0366	5.29E+02
FD (6.7)	RRS	0.390	0.887	2.13	0.38	Longi.	6.455E+05	0.0515	2.61E+04	8.586E+05	0.1887	3.81E+04
	RRS	0.390	0.887	1.84	0.91	Transv.	9.938E+05	0.0333	2.61E+04	5.770E+05	0.0186	3.81E+04
FD (6.7)	Sylmar	0.595	0.733	0.74	1.13	Longi.	7.749E+05	0.0783	1.09E+05	7.016E+05	0.0623	7.12E+04
	Sylmar	0.595	0.733	1.22	2.20	Transv.	7.307E+05	0.0241	1.09E+05	1.072E+06	0.0383	7.12E+04
FD (7.6)	T75	0.278	0.314	0.33	0.20	Longi.	6.680E+05	0.0402	4.18E+03	6.816E+05	0.0461	1.48E+04
	T75	0.278	0.314	0.67	0.68	Transv.	4.080E+05	0.0125	4.18E+03	4.729E+05	0.0132	1.48E+04
FD (7.3)	LCN	0.783	0.728	0.59	0.30	Longi.	6.988E+05	0.0462	6.64E+03	6.883E+05	0.0439	7.95E+03
	LCN	0.783	0.728	0.64	0.42	Transv.	4.829E+05	0.0102	6.64E+03	4.156E+05	0.0092	7.95E+03

5.1.2.1) Longitudinal Response

The Figures 5.2.7 to 5.2.12 below show the effect of the spectral acceleration at the bridge fundamental longitudinal frequency on the peak column response in the longitudinal direction. The pink triangles represent the response from the FDGMs and the blue diamonds represent the response from the Non-FDGMs. For the “Regular” plots (on the figure’s left), the FP ground motion component was applied to the bridge longitudinal direction, and for the “Inverse” plots (on the figure’s right), the FN ground motion component was applied to the bridge longitudinal direction. Consequently, the range of spectral acceleration values (X axes) was higher for “Inverse” than for “Regular” since the FD effect is seen only in the FN ground motion component.

The column’s maximum base shear increases slightly with the spectral acceleration due to the strain hardening effect after the column yielded. A similar trend is seen for maximum column displacements, but its effect is more pronounced. Since the column behaves plastically, the displacements increase rapidly in the plastic plateau region. The maximum displacements for the FDGMs can be significantly higher than those for the non-FDGMs due to their high relative value of spectral acceleration at this period. The FD effect is seen in the intermediate period range for the selected motions ($0.5s < T < 1s$, see Figures 5.2.1 to 5.2.6) of the FN GM component (“Inverse” plots). The range of spectral acceleration values is smaller for the FP component since the FD effect is less pronounced.

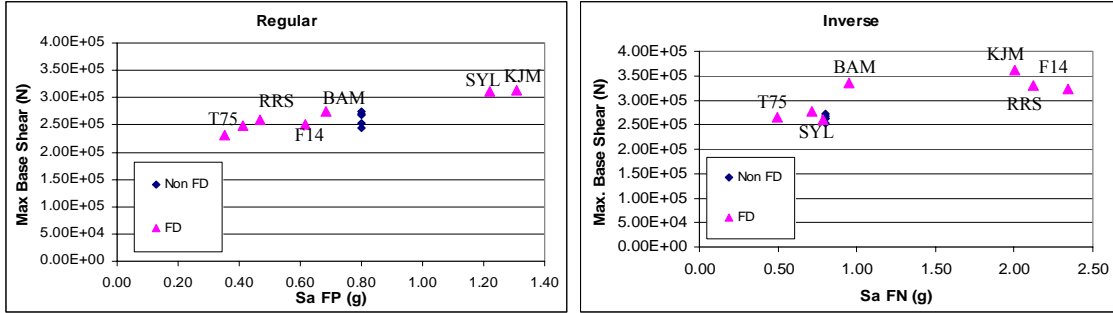


Figure 5.2.7: Bridge 405 Max Longitudinal Base Shear, S_a 's at $T_l = 0.65s$

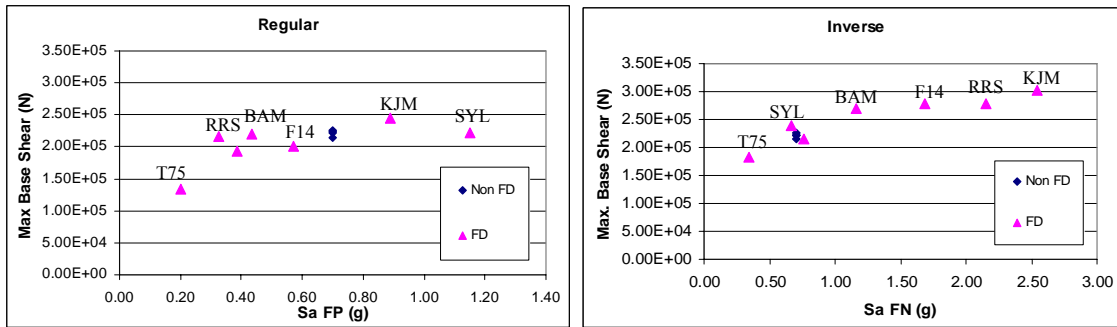


Figure 5.2.8: Bridge 520 Max Longitudinal Base Shear, S_a 's at $T_l = 0.80s$

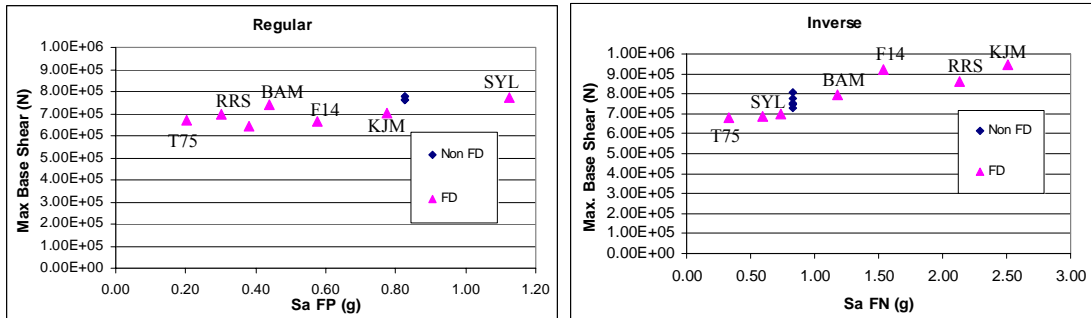


Figure 5.2.9: Bridge 90 Max Longitudinal Column Shear, S_a 's at $T_l = 0.82s$

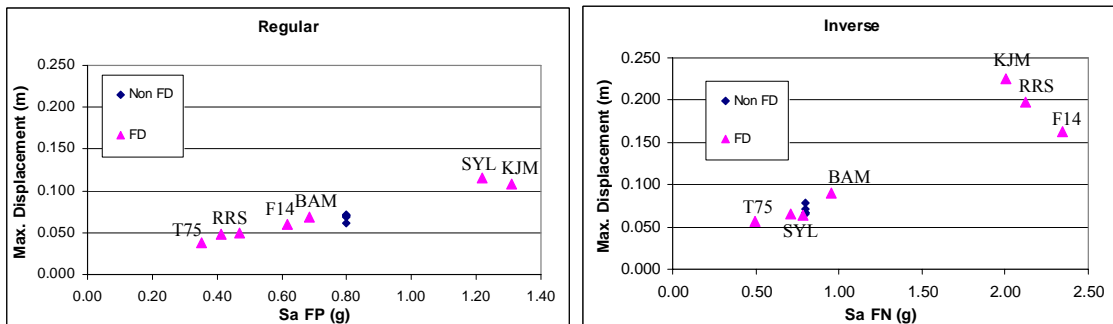


Figure 5.2.10: Bridge 405 Max Longitudinal relative Displacement, S_a 's at $T_l = 0.65s$

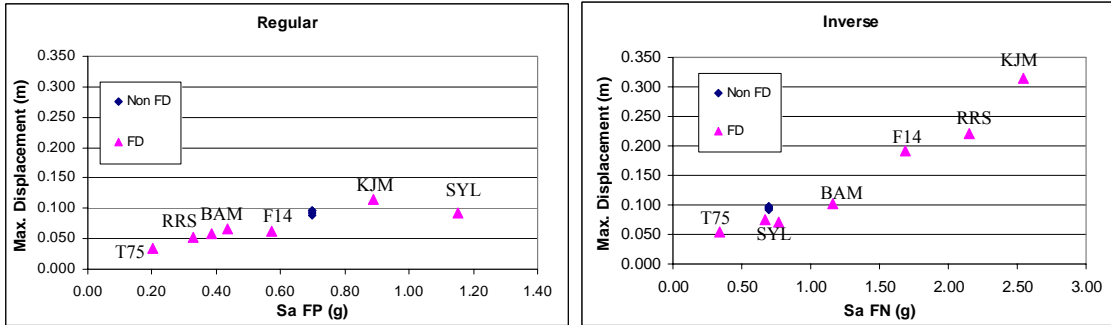


Figure 5.2.11: Bridge 520 Max Longitudinal relative Displacement, S_a 's at $T_l = 0.80s$

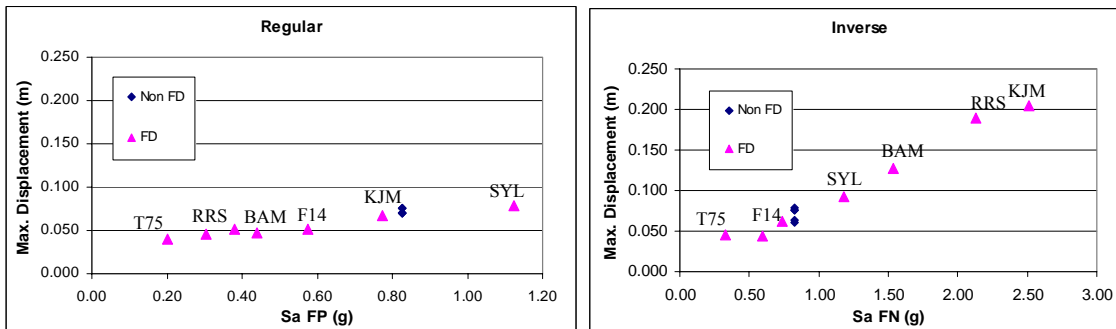


Figure 5.2.12: Bridge 90 Max Longitudinal relative Displacement, S_a 's at $T_l = 0.82s$

The energy dissipated by plastic deformation in the system often increases abruptly during a FDGM, as shown on Figures 5.2.13, 5.2.14, and 5.2.15. It is interesting to note that the level of damage is highly dependent upon the period of the bridge versus that of the forward directivity pulse. Table 5.2.4 summarizes the different fundamental bridge periods and velocity pulse periods of the FN ground motion component. When the two periods are close, most of the damage occurs during the pulse, as in the KJM Inv, RRS Inv, and F14 Inv earthquakes. For cases in which there is no pulse or the pulse period does not match the fundamental period of the bridge, the damage is much lower and it increases gradually. The damage curve for the KJM Inv and RRS Inv ground motions for Bridge 90 did not reach a very high level since one of the columns failed during the first seconds of the record, which made the finite element analysis terminate.

Table 5.2.4: fundamental bridge periods and FDGM's velocity pulse periods (T_v)

Period (sec)	bridge 405	bridge 520	bridge 90
$T_{longitudinal}$	0.66	0.80	0.82
$T_{transverse}$	0.18	0.17	0.47

FDGM	T_v (sec)
BAM	2.065
F14	0.75
KJM	1
RRS	1.25
Sylmar	2.32
T75	2.5
LCN	5.5

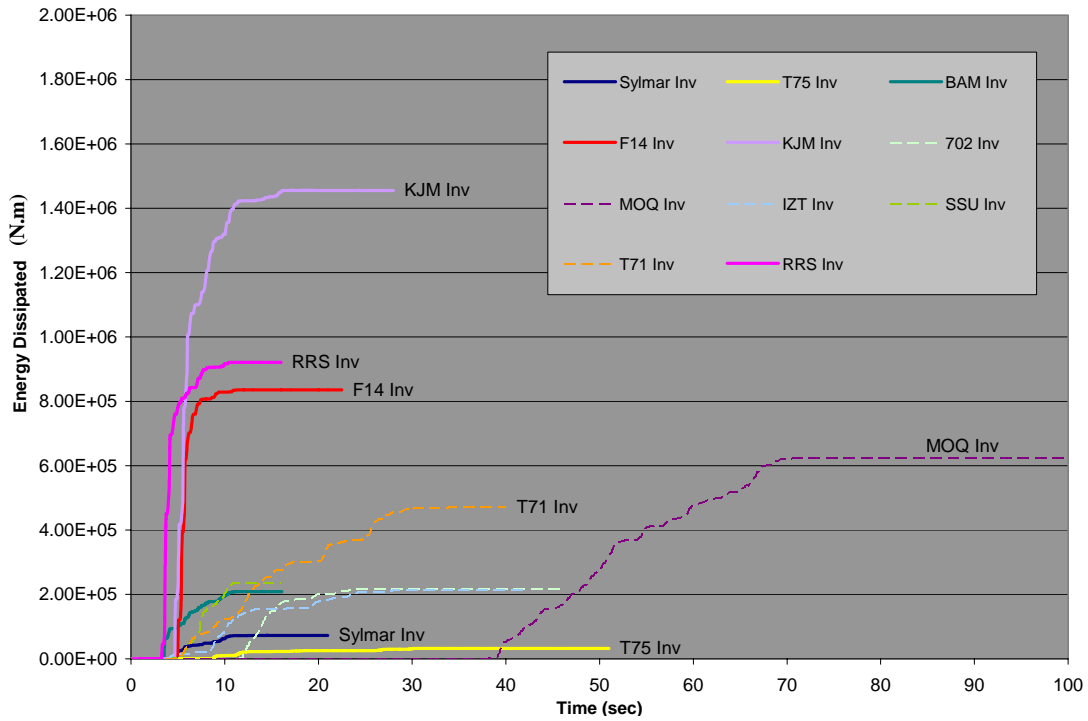


Figure 5.2.13: Bridge 405 Energy dissipated by plastic deformation in the system through time for the non-FD (dashed) and FDGMs (solid)

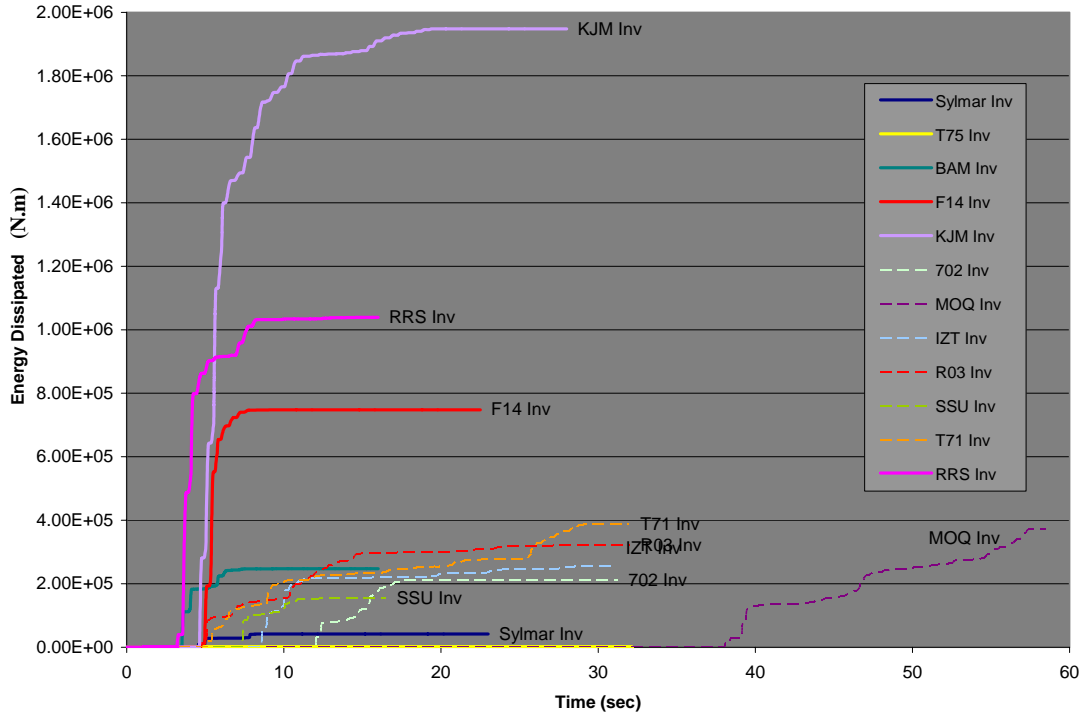


Figure 5.2.14: Bridge 520 Energy dissipated by plastic deformation in the system through time for the non-FD (dashed) and FDGMs (solid)

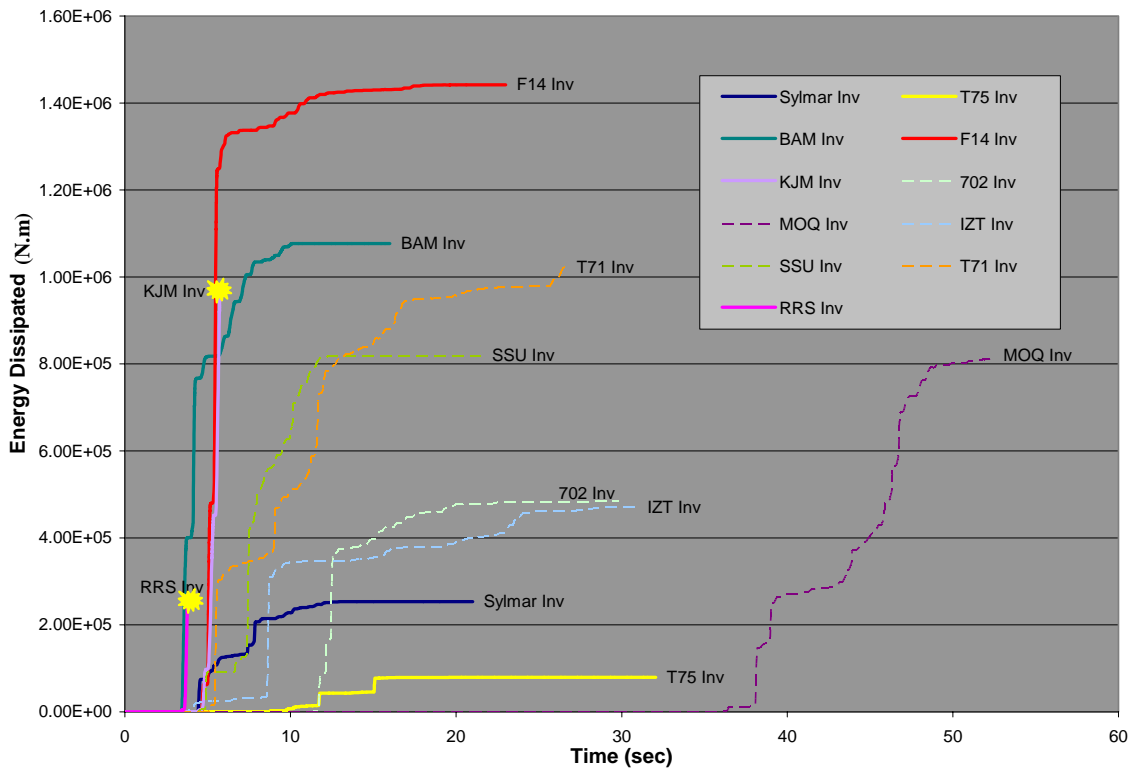


Figure 5.2.15: Bridge 90 Energy dissipated by plastic deformation in the system through time for the non-FD (dashed) and FDGMs (solid). Column failure noted for KJM Inv and RRS Inv records.

Plots of force versus displacement and moment versus curvature are shown in Figure 5.2.16 for the most damaging ground motion considered on Bridge 405. The hysteretic curves show the expected pinching behavior and decreased column stiffness and strength due to the double-sided velocity pulse of the FDGM. From the plots, one can see that the majority of plasticity and damage results from only a few large cycles.

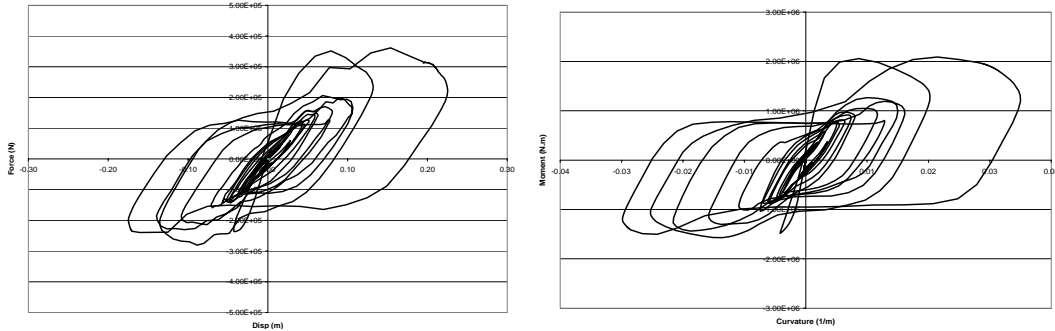


Figure 5.2.16: Bridge 405 Force-Displacement and Moment-Curvature hysteresis curve from the FD KJM GM, in the longitudinal direction

A plot of moment versus curvature is shown in Figure 5.2.17 for the most damaging ground motion considered for Bridge 90. In dashed red, the backbone curve was computed from the cross-section analysis freeware (USC_RC, Asadollah Esmaeily). The end of the curve indicates the failure of the column cross-section. The peak spectral acceleration closely matched the longitudinal fundamental period of vibration of the structure. This ground motion induced the bending failure of the shortest column (C_4). ABAQUS stopped the analysis when the maximum material capacity was reached at the top of the column. It does not indicate the overall failure of the bridge but, rather, a local failure. One can note that the column did not fail when it reached its first maximum curvature at the end of the USC curve, but the second time. The maximum curvature capacity from ABAQUS was slightly higher than the USC one. A plot of force versus displacement is shown in Figure 5.2.18. The column reached its maximum displacement

capacity of approximately 20 cm (8 in). In dashed green, the shear capacity envelope proposed by Kowalsky and Priestley (2000) is shown (see Appendix A.1). The column shear capacity is shown to be higher than its bending capacity for any displacement level.

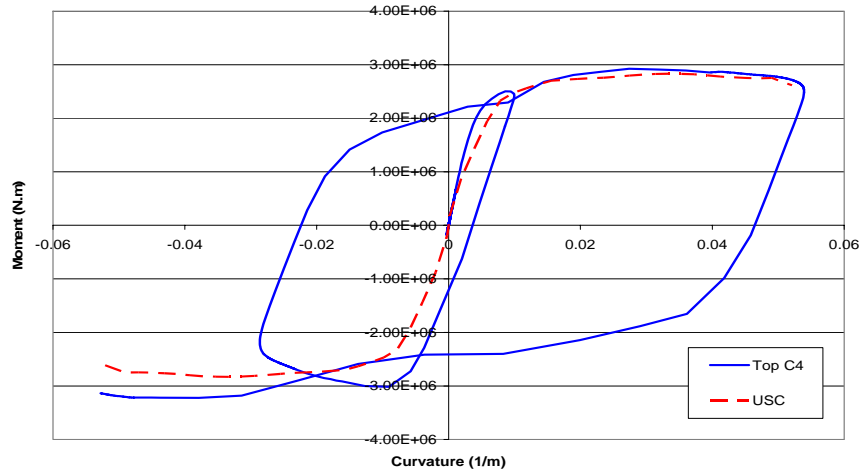


Figure 5.2.17: Bridge 90 Moment-Curvature hysteresis curve of column C_4 from the FD KJM ground motion, in the longitudinal direction, including the USC prediction curve in dashed red

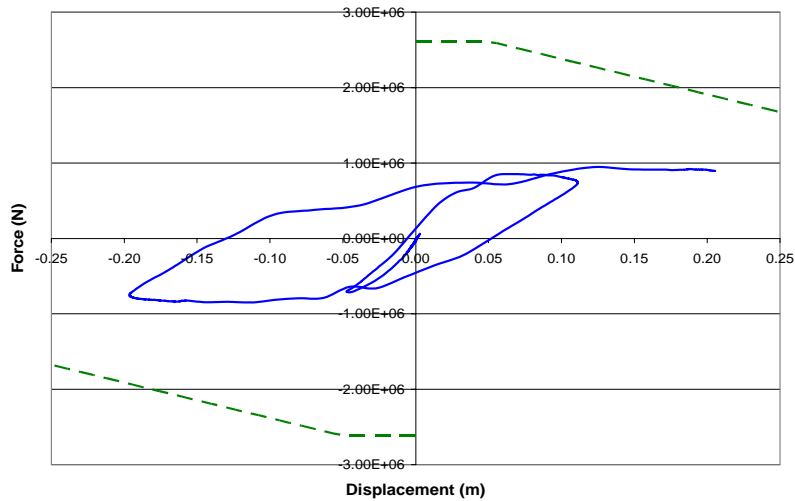


Figure 5.2.18: Bridge 90 Force – Displacement hysteresis curve of column C_4 from the FD KJM GM, in the longitudinal direction, including the column shear capacity in dashed green

Tables 5.2.5, 5.2.6 and, 5.2.7 summarize the response of the abutments during the earthquakes. “Pounding” indicates that the gap closed, “# max pressure” is the number of times the abutment reaches its maximum allowable pressure force, and “Deformation” is

the maximum plastic deformation in the springs. For Bridge 405, the non-FDGM's did not induce any damage in the abutments, but the FDGM BAM, Sylmar, F14, and KJM did. Again, note that pounding only occurred once or twice, indicating that it results from the forward directivity pulse. For Bridge 520, the non-FDGMs SSU and T71 induced four to five repeated poundings of the abutments, but the level of damage is small. On the other hand, the FDGMs KJM Inv and RRS Inv induced during only one pounding (even though they touched twice) a much larger plastic deformation caused by the pulse. The abutments of Bridge 405 and Bridge 520 behaved differently since their geometry and, subsequently, their strength capacity were unique. The bearing pad displacement capacity, never reached, of 50 cm (20 in) was the same, however. For Bridge 90, the non-FDGMs induced repeated poundings of the abutments with varying levels of damage. On the other hand, the FDGMs KJM Inv and RRS Inv induced during only one pounding a much larger plastic deformation of 33 cm caused by the pulse.

Table 5.2.5: Bridge 405 Abutment pounding

Type (M_w)	GM	Regular			Inverse		
		Pounding	# max pressure	Deformation (m)	Pounding	# max pressure	Deformation (m)
Non FD	702	yes	0	0	yes	0	0
	IZT	yes	0	0	yes	0	0
	MOQ	yes	0	0	yes	0	0
	SSU	yes	0	0	yes	0	0
	T71	yes	0	0	yes	0	0
FD (6.9)	KJM	yes	1	0.014	yes	2	0.16
FD (6.5)	BAM	yes	0	0	yes	1	0.017
FD (6.2)	LCN	yes	0	0	yes	0	0
FD (6.0)	F14	yes	0	0	yes	2	0.09
FD (6.7)	RRS	yes	0	0	yes	1	0.13
FD (7.2)	Sylmar	yes	2	0.04	yes	0	0
	T75	yes	0	0	no	0	0

Table 5.2.6: Bridge 520 Abutment pounding

Type (M_w)	GM	Regular			Inverse		
		Pounding	# max pressure	Deformation (m)	Pounding	# max pressure	Deformation (m)
Non FD	702	yes	2	0.03	yes	1	0.014
	IZT	yes	2	0.03	yes	2	0.024
	SSU	yes	4	0.03	yes	2	0.012
	T71	yes	4	0.034	yes	5	0.036
FD (6.9)	KJM	yes	1	0.056	yes	2	0.18
FD (6.5)	BAM	yes	1	0.004	yes	2	0.043
FD (6.2)	LCN	yes	0	0	yes	1	0.015
FD (6.0)	F14	yes	1	0.001	yes	2	0.014
FD (6.7)	RRS	yes	0	0	yes	1	0.17
FD (7.2)	Sylmar	yes	3	0.03	yes	2	0.011
	T75	yes	0	0	yes	0	0

Table 5.2.7: Bridge 90 Abutment pounding

Type (M_w)	GM	Regular			Inverse		
		Pounding	# max pressure	Deformation (m)	Pounding	# max pressure	Deformation (m)
Non FD	702	yes	3	0.09	yes	2	0.08
	IZT	yes	5	0.1	yes	2	0.08
	MOQ	yes	8	0.08	yes	7	0.1
	SSU	yes	4	0.065	yes	4	0.1
	T71	yes	2	0.09	yes	3	0.1
FD (6.9)	KJM	yes	1	0.065	yes	1	0.33
FD (6.5)	BAM	yes	2	0.005	yes	1	0.11
FD (6.2)	LCN	yes	3	0.007	yes	1	0.07
FD (6.0)	F14	yes	3	0.04	yes	1	0.19
FD (6.7)	RRS	yes	4	0.007	yes	1	0.33
FD (7.2)	Sylmar	yes	4	0.06	yes	2	0.027
	T75	yes	1	0.001	yes	4	0.02

5.1.2.2) Transverse Response

Figures 5.2.19 to 5.2.24 show the effect of the spectral acceleration on the column response in the transverse direction. The column's maximum base shears and displacements increase nearly linearly with S_a . The bridge response is mainly governed by the frequency content of the ground motion. The transverse fundamental periods of Bridge 405 and 520 are around 0.2 sec. At this short period range ($0 < T < 0.5s$), the Forward Directivity “bump” effect does not appear in the ARS and the non-FDGMs had a greater spectral acceleration value. Consequently, the non-FDGMs often induced higher maximum base shears and displacements.

As in the longitudinal direction, the maximum column responses were governed by the ARS value but, in the transverse direction, those values were generally higher for the non-FDGMs than those of the FDGMs because the fundamental bridge periods were different. For the “Regular” plots (on the figures’ left), the FN ground motion component was applied to the bridge transverse direction, and for the “Inverse” plots (on the figures’ right), the FP ground motion component was applied to the bridge transverse direction.

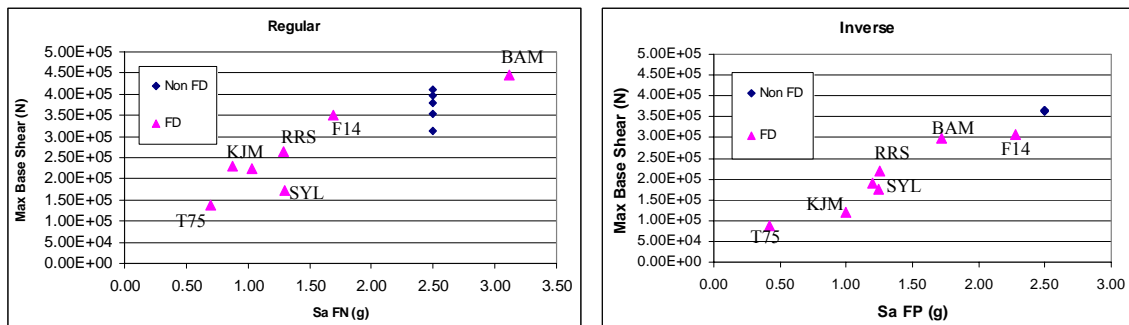


Figure 5.2.19: Bridge 405 Max Transverse Base Shear, S_a 's at $T_t = 0.18$ s

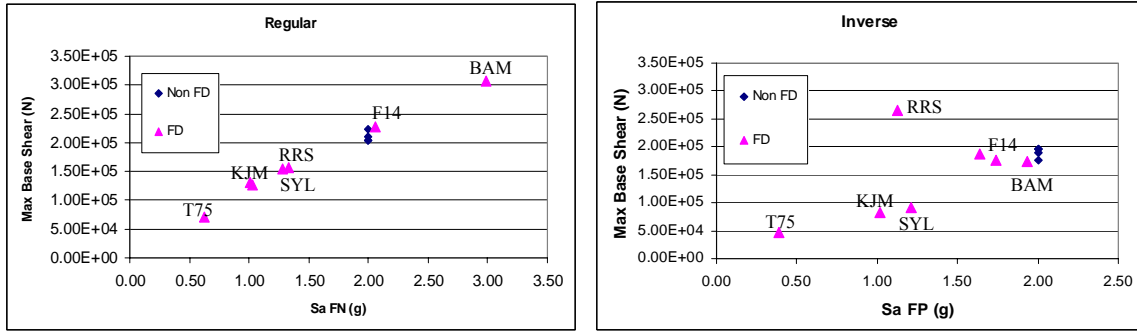


Figure 5.2.20: Bridge 520 Max Transverse Base Shear, S_a 's at $T_t = 0.17$ s

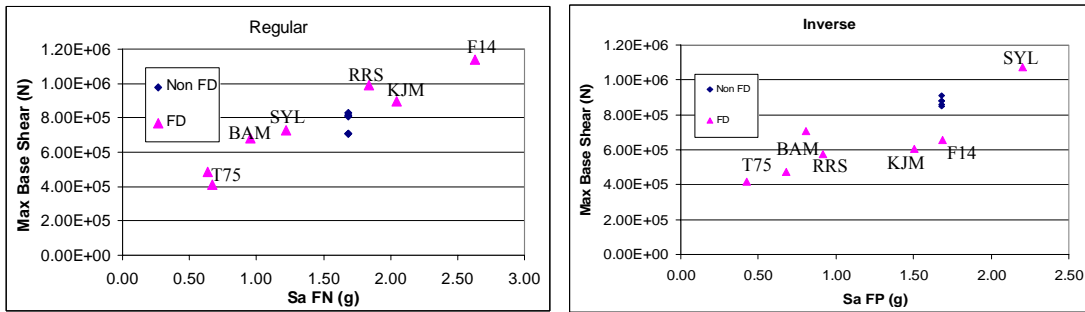


Figure 5.2.21: Bridge 90 Max Transverse Column (C_4) Shear, S_a 's at $T_t = 0.47$ s

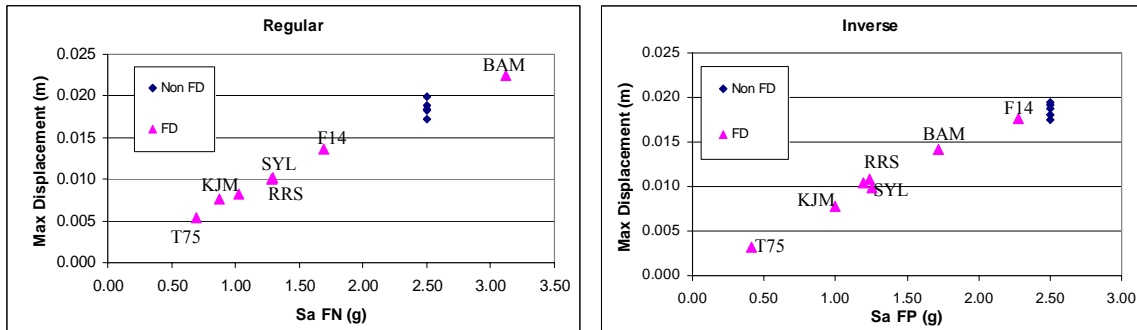


Figure 5.2.22: Bridge 405 Max Transverse relative Displacement, S_a 's at $T_t = 0.18$ s

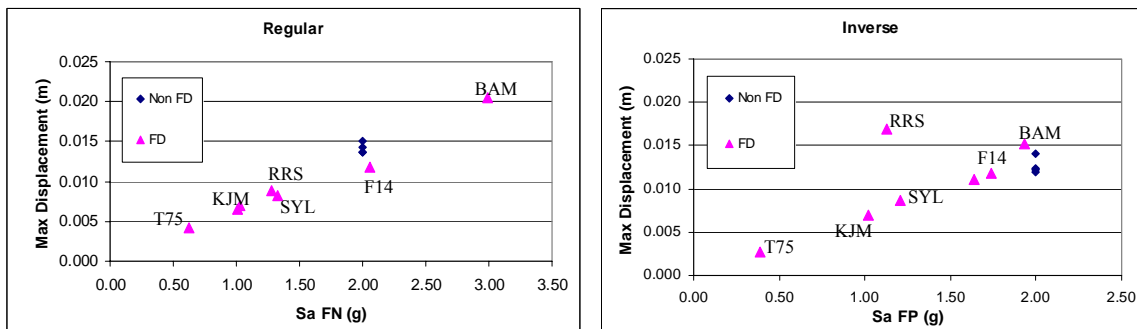


Figure 5.2.23: Bridge 520 Max Transverse relative Displacement, S_a 's at $T_t = 0.17$ s

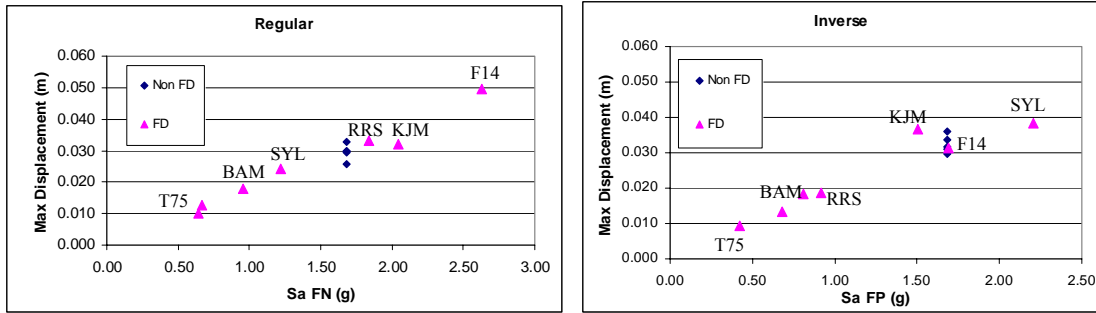


Figure 5.2.24: Bridge 90 Max Transverse Column (C_4) relative Displacement, S_a 's at $T_t = 0.47$ s

5.3) Velocity Pulse Period Effect

The effect of the velocity pulse period was investigated. A plot of maximum longitudinal displacement from the FN component of the FDGMs versus velocity pulse period is shown on Figure 5.3.1. Table 5.1.4 gives the different fundamental bridge periods (T_{long} and T_{trans}) and the FDGM velocity pulse periods (T_v). One can see that the maximum displacement in the governing columns is much higher when the velocity pulse period is close to the fundamental longitudinal periods (in dashed red in the Figures) of the bridges. These results were expected and agree with the results of section 5.2 since the “bumps” seen in the FN FDGM response spectra (ARS) correspond to their pulse period, or periods (Somerville et al., 1997). The pulse period range that is the most influential on the bridge response does not exceed ± 0.5 sec from the fundamental bridge period. The severity of the demand was controlled by the ratio of the pulse period to system period.

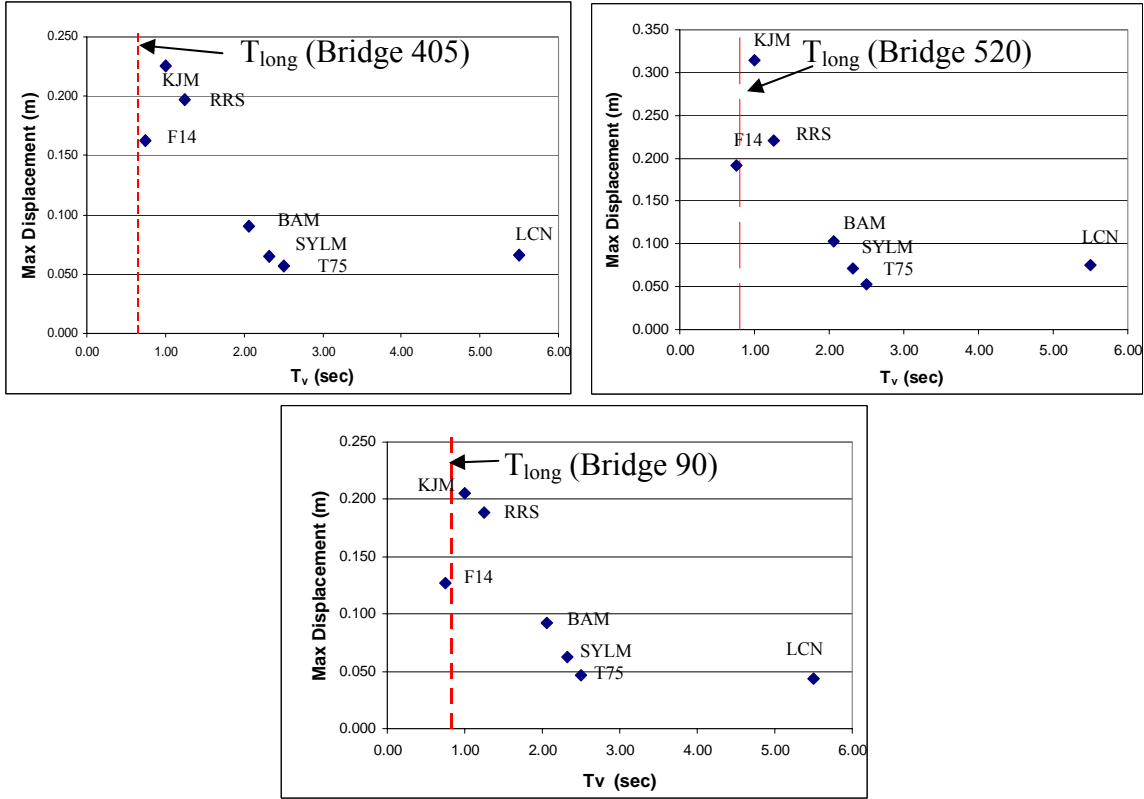


Figure 5.3.1: Bridge 405 (left), Bridge 520 (right), and Bridge 90 (down) Max Displacement Vs. Velocity Pulse Period

A plot of maximum longitudinal displacement from the FN component of the FDGMs versus peak ground acceleration (PGA) is shown on Figure 5.3.2. The maximum displacements increase with the PGA but not uniformly. Figure 5.3.2 shows a general trend but not a clear relationship. A ground motion with a high PGA value may induce high damage in the columns, but not necessarily. A plot of maximum longitudinal displacement from the FN component of the FDGMs versus peak ground velocity (PGV) is shown on Figure 5.3.3. It shows scattered data points, leading to the conclusion that the damage in the column is not a function of the PGV. Again, a ground motion with high PGV value may induce high damage in the columns, but not necessarily.

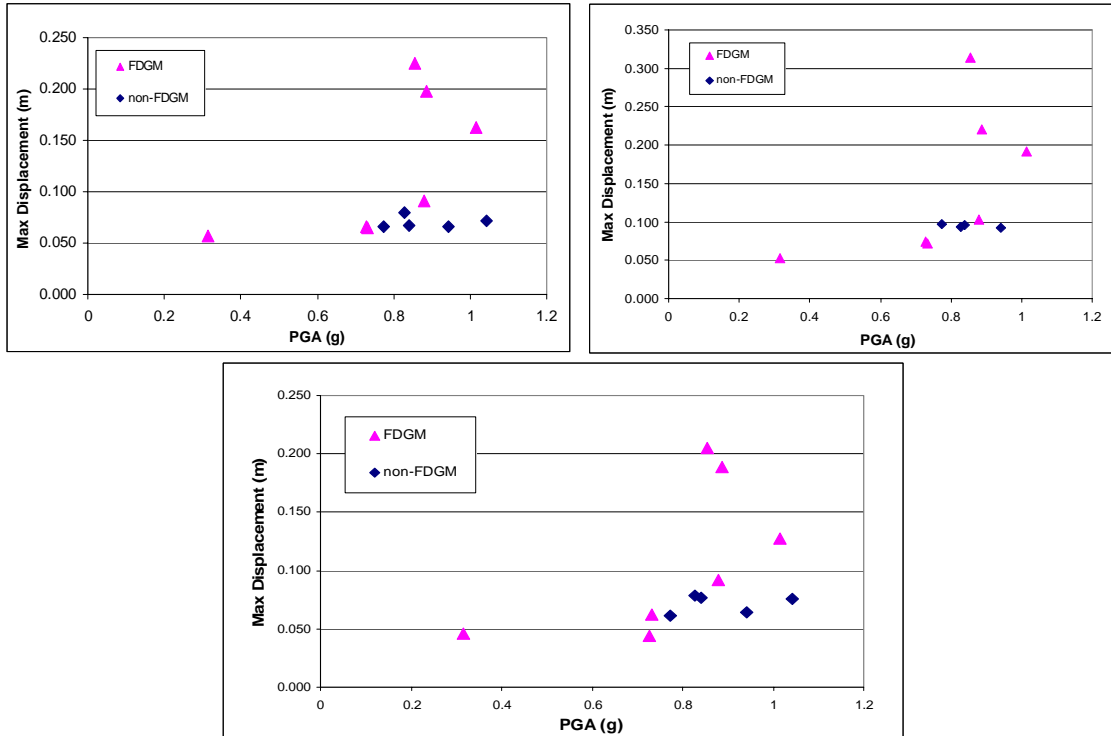


Figure 5.3.2: Bridge 405 (left), Bridge 520 (right), and Bridge 90 (down) Max Displacement Vs. Peak Ground Acceleration (PGA)

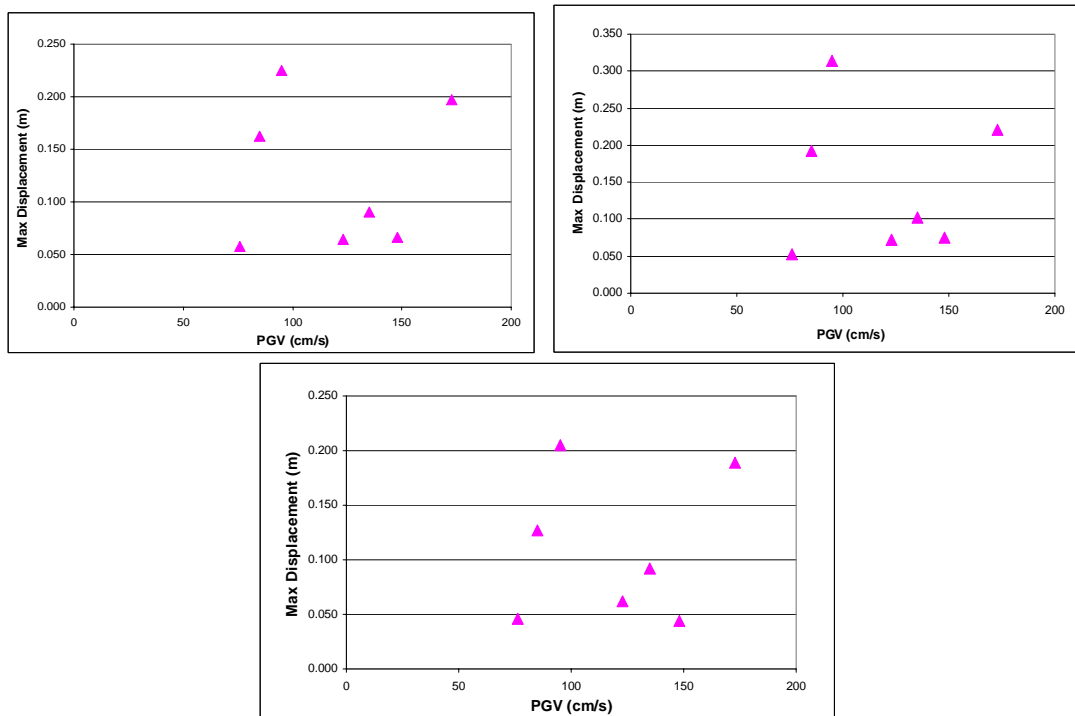


Figure 5.3.3: Bridge 405 (left), Bridge 520 (right), and Bridge 90 (down) Max Displacement Vs. Peak Ground Velocity (PGV) of the FDGMs

The FDGM pulse period is proportional to the earthquake magnitude, lengthening as the earthquake magnitude increases (Somerville 1998, Rodriguez-Marek 2000, and Alavi and Krawinkler 2000) as shown in Figure 5.3.4. As a result, damage due to smaller magnitude earthquakes can be more significant for short period structures than damage due to larger magnitude earthquakes, since the near-fault pulse period is closer to the fundamental period of the structure in the smaller magnitude earthquake. It was the case in this research. The KJM ground motion recorded from the magnitude 6.9 Kobe earthquake induced significantly higher damage to the columns than that from the LCN ground motion recorded from a magnitude 7.3 earthquake. The uncertainty associated with the pulse period determination is very high, however. At the current state of knowledge on the FDGMs, it is hard to predict the velocity pulse period. The probability of occurrence of a FDGM with a specific velocity pulse period is also difficult to predict. To be conservative, a designer may choose to consider a FD ground motion with a velocity pulse period matching the fundamental bridge period. However, such a choice could be greatly conservative.

Since the bridge response is mainly governed by the first velocity pulse, a simple ground motion consisting of a single pulse may be sufficient to evaluate bridge performance for forward directivity ground motions.

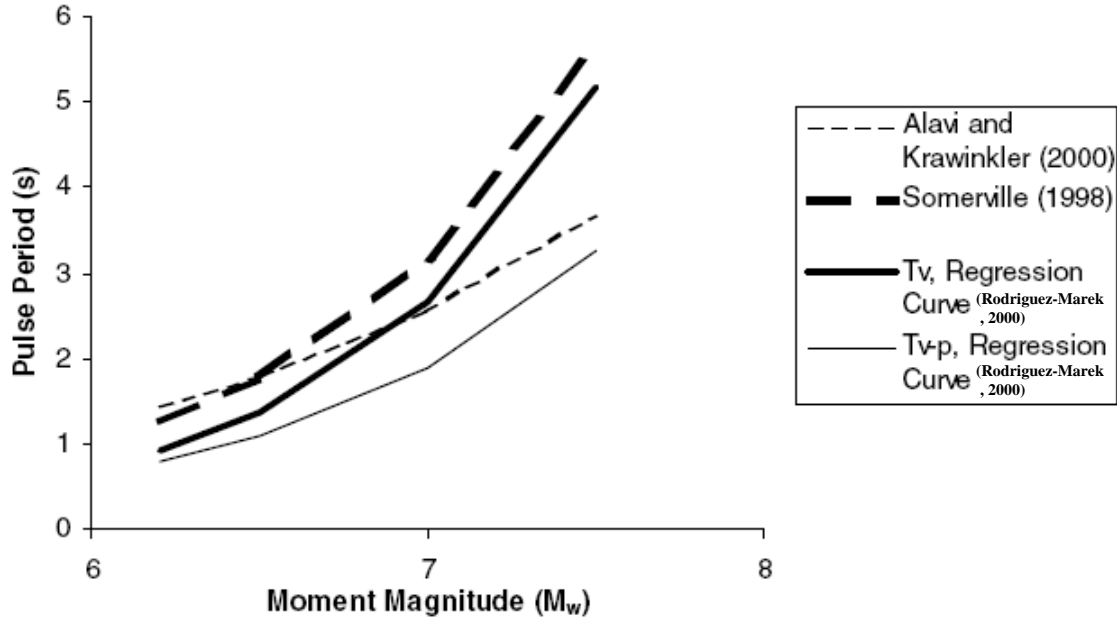


Figure 5.3.4: Velocity Pulse Period Models Vs. Moment Magnitude (from Rodriguez-Marek, 2000)

5.4) Soil-Structure Interaction Effect

The Soil-Structure Interaction (SSI) effect was investigated through a comparison of the response of Bridge 520 with and without foundation flexibility. The effect of site response on the ground motions was already taken into account (see section 4.1.1). Without SSI effects, the ground motions were applied directly to the footing nodes, the deck was unrestrained, and the abutments were not considered. Figures 5.4.1 and 5.4.2 show the maximum base shear and displacement, respectively, in the two bridge directions for different ground motions when foundation flexibility was included (blue diamonds) and when it was not (pink triangles). The results show that the bridge is much more sensitive to the effects in the transverse direction than in the longitudinal direction. The model with SSI has stiff springs in the transverse direction at both the abutments and the footings that connect to the soil. The deck in the model without SSI is free to move,

as opposed to the restraint provided with SSI included. This lack of restraint increases the demand on the columns. In the longitudinal direction, the maximum base shears are shown to be slightly decreased without SSI effects. There is no significant difference because in both cases the column yield point was reached. The maximum relative displacements generally increased when the SSI was not included, especially for the FDGMs. Consequently, the damage on the columns also increased. The SSI should be included by engineers in bridge design to avoid over-conservatism, especially when forward directivity ground motions are taken into account.

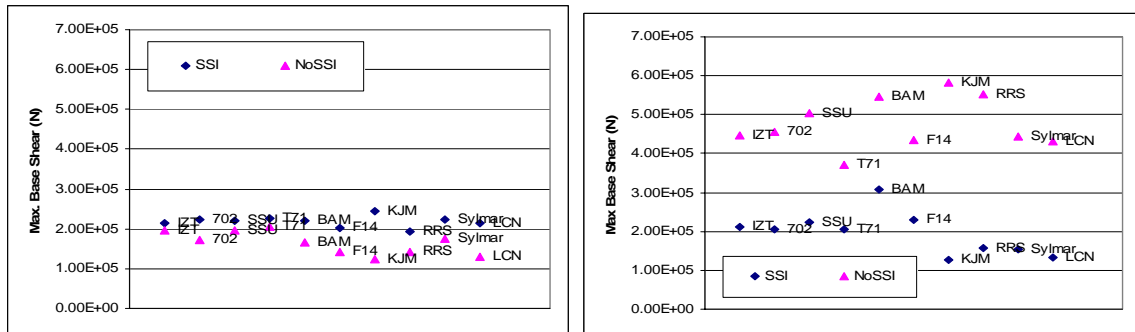


Figure 5.4.1: Bridge 520 longitudinal (left) and transverse (right) Max Base Shear, with or without SSI

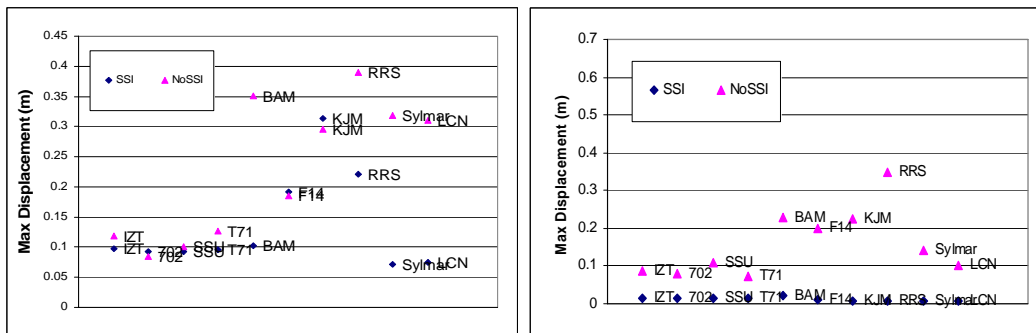


Figure 5.4.2: Bridge 520 longitudinal (left) and transverse (right) Max Column Displacement, with or without SSI

5.5) Comparison with a SDOF system

In her research on FD ground motions, Gillie (2005) utilized the time-stepping Newmark's method to compute the nonlinear response of a SDOF system when subjected

to the fault normal ground motion component. All FD and non-FD motions were run using a Wen (1976) hysteretic relationship calibrated to a typical concrete hysteresis loop. A comparison of the multi-degree-of-freedom (MDOF) models of Bridge 520 and Bridge 405 was made to the nonlinear SDOF analyses by Gillie (2005). A comparison to SDOF analyses was not possible for Bridge 90 because its column yielding force was significantly different from those of the SDOF models. The comparison was also not possible for the bridge transverse responses because the nonlinear SDOF system did not show realistic results at low period values. The non-FDGMs did not include spectral matching or modification for site response, therefore, the non-FDGM ABAQUS analyses were rerun without spectral matching or site response modification for comparison to the non-FDGM SDOF analyses. The SDOF maximum displacements were those computed in the case where the SDOF natural period matches the longitudinal bridge mode of vibration. Being able to accurately evaluate the modes of vibration of a structure is a key aspect to predicting its response using a nonlinear SDOF analysis. Figures 5.5.1 and 5.5.2 show the comparison, for each ground motion, of the maximum displacements found from the following models: nonlinear SDOF in pink circles, nonlinear MDOF (ABAQUS) including SSI in red diamonds, and nonlinear MDOF (ABAQUS) without SSI in blue squares. The SDOF maximum displacements are always unconservative with regard to the ones computed with the ABAQUS bridge models for the non-FDGMs, while the results for the FDGMs were mixed. The use of a simple SDOF system to predict the response of a complex structure under forward directivity ground motions is not recommended since the results were not consistent. The variation of the axial load on the columns is not taken into account in the SDOF system and the P-Delta effect is not

included. Moreover, the SDOF hysteretic model could not match the ABAQUS one. There was also a slight uncertainty concerning the determination of the SDOF model yielding force.

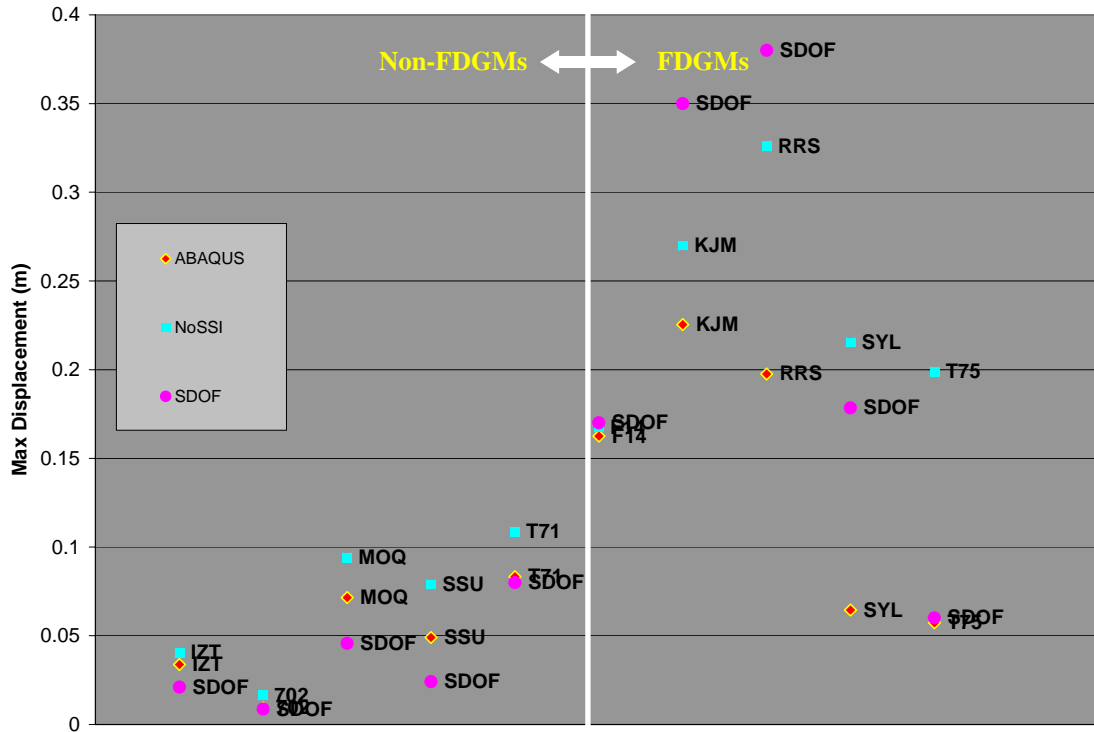


Figure 5.5.1: (Bridge 405) Maximum SDOF displacement compared to the longitudinal ABAQUS model response

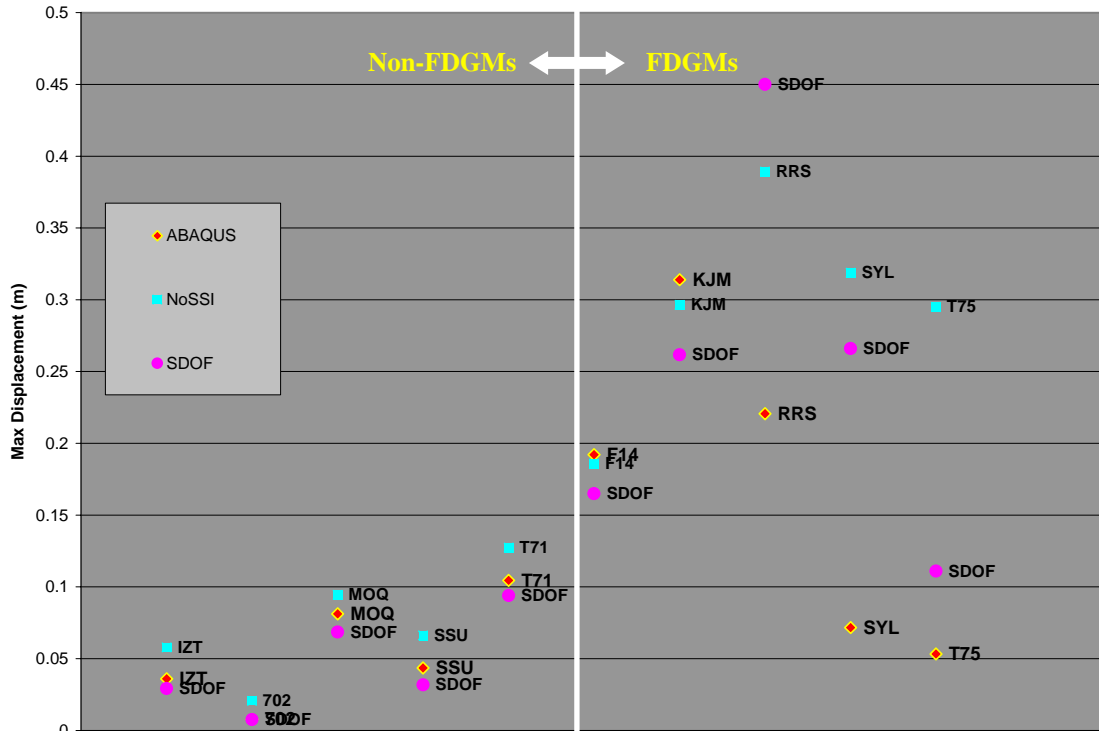


Figure 5.5.2: (Bridge 520) Maximum SDOF displacement compared to the longitudinal ABAQUS model response

5.6) AASHTO prediction comparison

Bridges in the United States are usually designed using the *Standard Specifications for Highway Bridges*, which was written by the American Association of State Highway and Transportation Officials (AASHTO). Following the AASHTO (LRFD Bridge Design Specifications, 2004) procedure, the maximum base shear was computed and compared to those of the finite element model. See Appendix A.4. A multimode linear response spectrum analysis was performed to obtain an approximate upper bound to the peak significant response (column maximum base shear, column max. relative displacement) of the WSDOT bridges to a user-supplied input spectrum as a function of period (given by the WSDOT). Figures 5.6.2 to 5.6.7 show the ARS of the FN and FP

component of the non-FD and FD ground motions for each bridge. Moreover, the figures show the target ARS found from the PSHA (Gillie, 2005) and the AASHTO ARS used by the WSDOT. One can see that the AASHTO curve was lower than the target ARS. The AASHTO procedure uses an outdated acceleration coefficient map created in 1988 by the United States Geological Survey (USGS). Moreover, the USGS PSHA (Gillie, 2005) was based on 2 percent probability of exceedance in 50 years which corresponds to a collapse protection, rare but possible. On the other hand, the AASHTO contour maps of the acceleration coefficient were based on 10 percent probability of exceedance in 50 years which corresponds to the design level. Figure 5.6.1 shows the ARS for 2 and 10% probability of exceedance. One can see that the spectrum for 10% probability of exceedance is below the other spectrum. A factor of 1.5 that is used in the building codes to compute the collapse level from the design spectrum was applied to the AASHTO ARS.

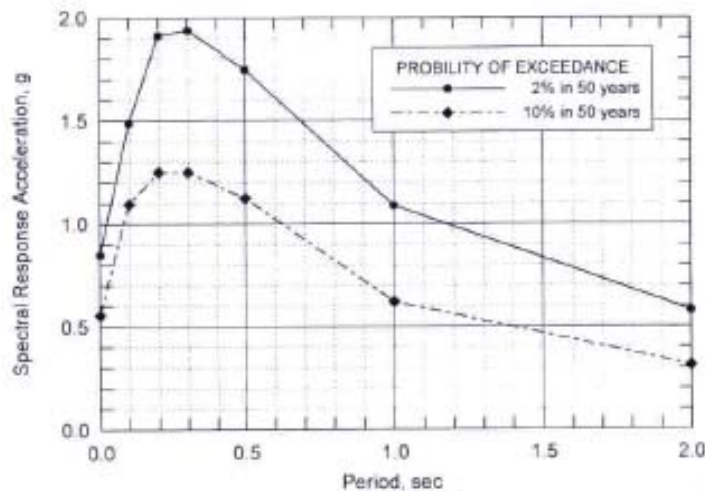


Figure 5.6.1: Uniform hazard response spectra for 2% and 10% probability of exceedance in 50 years for San Francisco, California

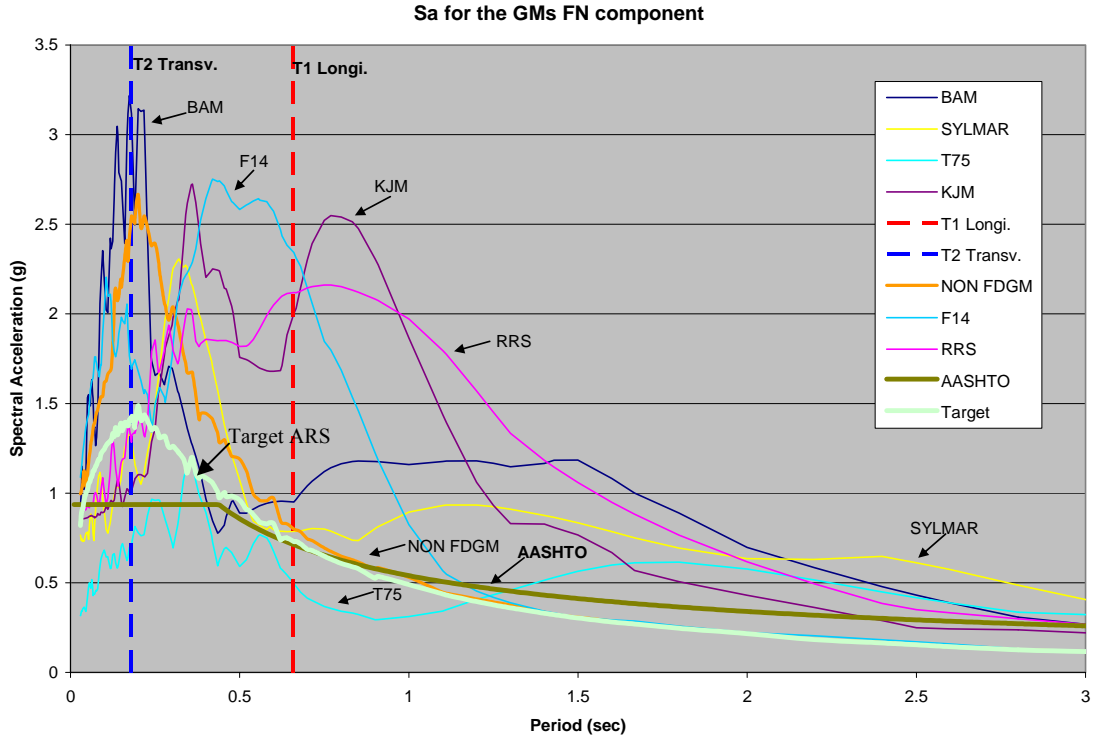


Figure 5.6.2: Bridge 405 ARS of the FN components of the ground motions, and the one used for the AASHTO design procedure

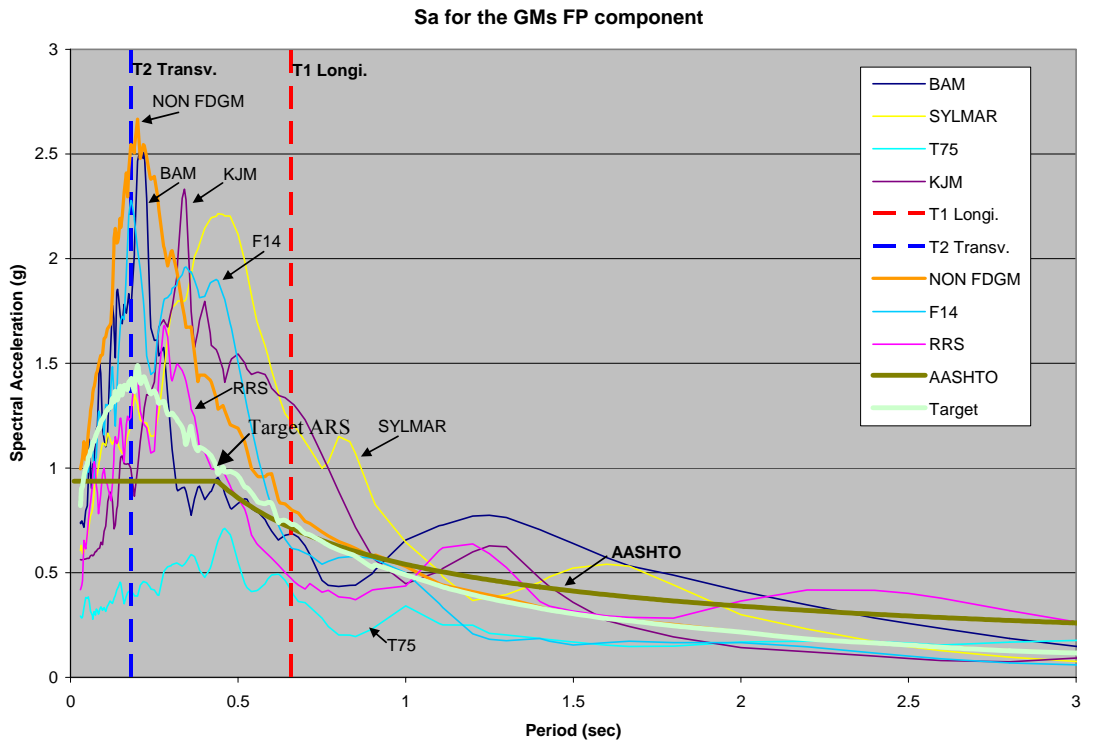


Figure 5.6.3: Bridge 405 ARS of the FP components of the GMs, and the one used for the AASHTO design procedure

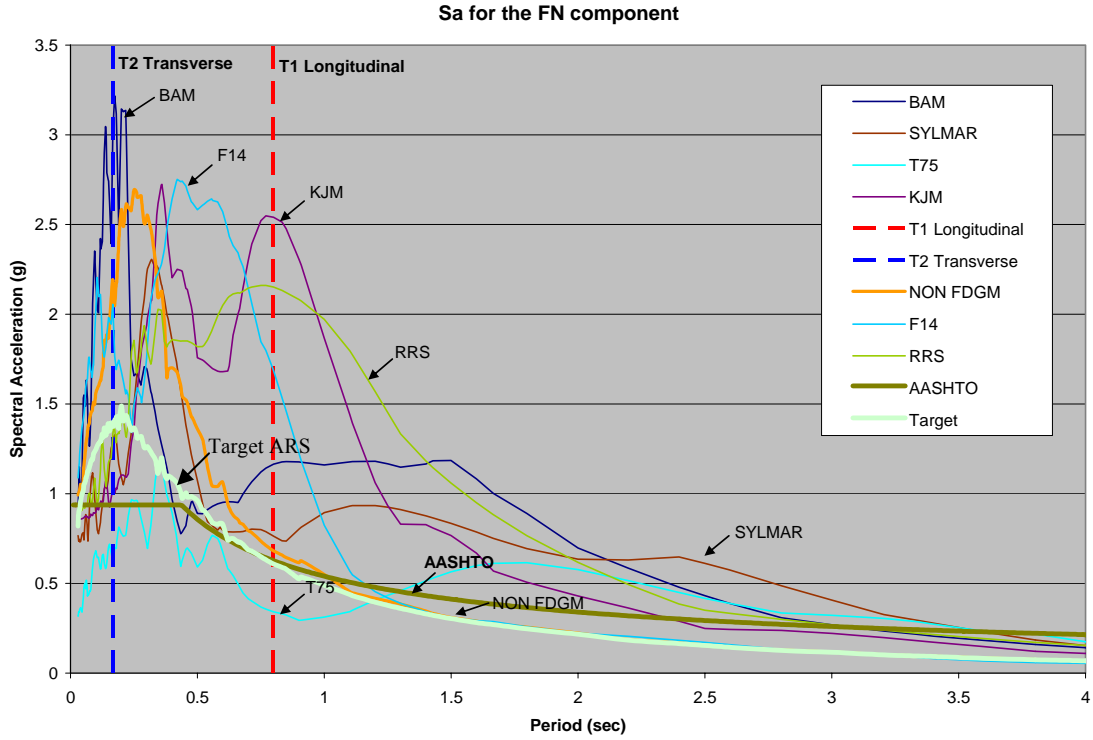


Figure 5.6.4: Bridge 520 ARS of the FN component of the GMs, and the one used for the AASHTO design procedure

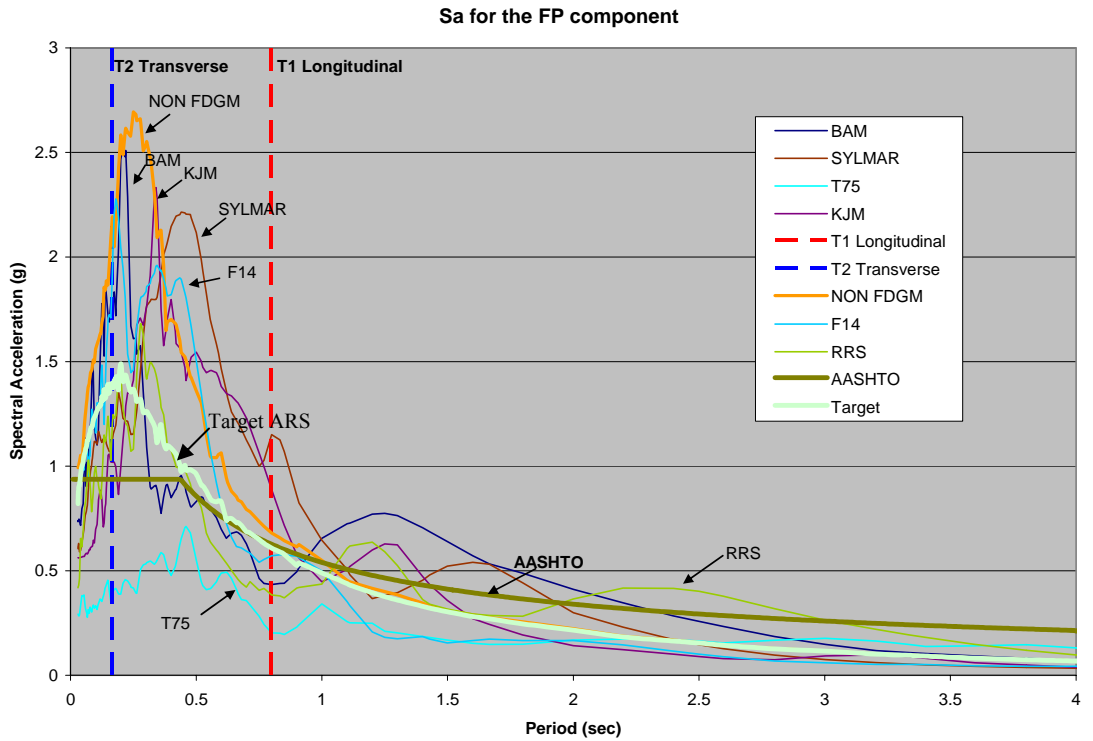


Figure 5.6.5: Bridge 520 ARS of the FP component of the GMs, and the one used for the AASHTO design procedure

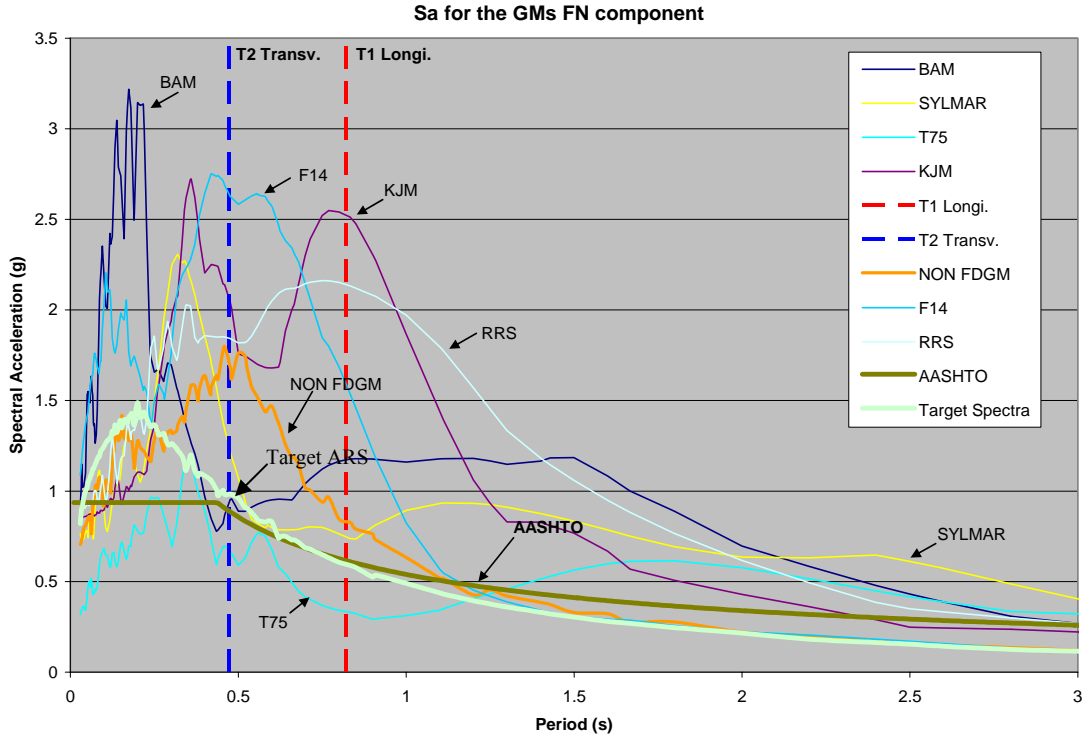


Figure 5.6.6: Bridge 90 ARS of the FN component of the GMs, and the one used for the AASHTO design procedure

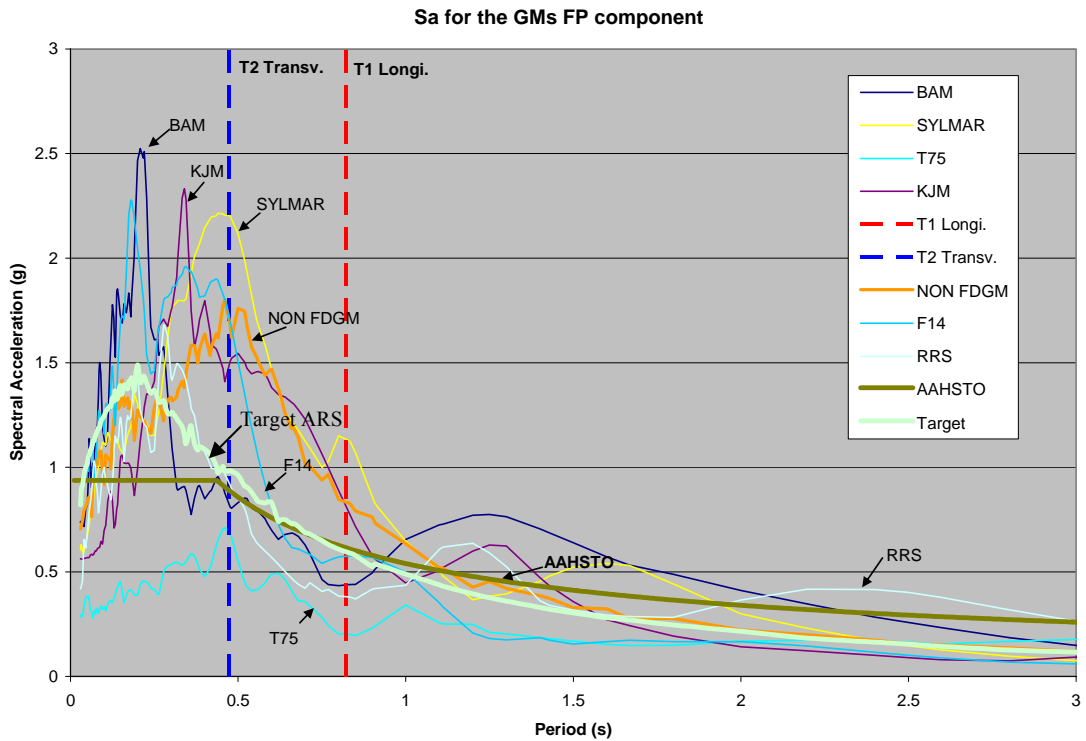


Figure 5.6.7: Bridge 90 ARS of the FP component of the GMs, and the one used for the AASHTO design procedure

The maximum base shear comparisons are shown in Figures 5.6.8 to 5.6.10 for each bridge. A Response Modification factor to take into account the inelastic effect of 3.5 for multiple columns per bent and 2.0 for single column was subsequently applied to the AASHTO maximum base shears assuming that the bridges were of the “essential” importance category. The AASHTO predicted maximum base shears were always unconservative in comparison to the non-FDGMs and FDGMs for Bridge 405 and 520, and were always conservative for Bridge 90. Figure 5.6.11 shows the comparison between the FEM displacements and the design AASHTO displacements. AASHTO (2004) results are found to be unconservative in that respect, predominantly for the FDGMs. This is expected since AASHTO requires that bridges near faults use a site specific ground motion assessment.

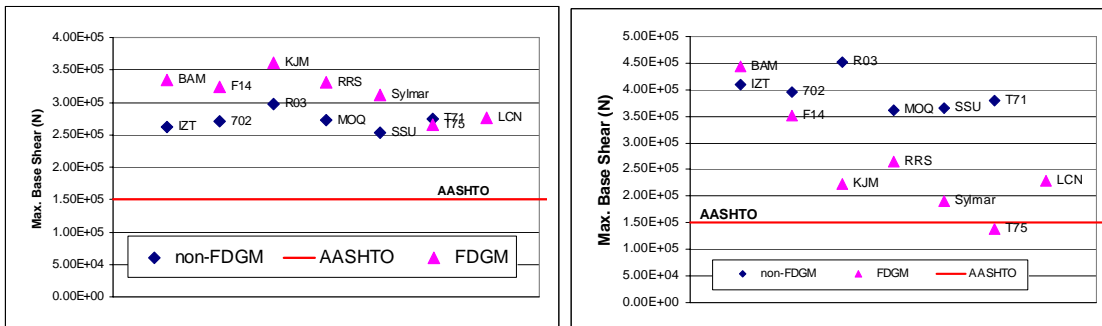


Figure 5.6.8: Bridge 405 Maximum longitudinal (left) and transverse (right) governing column base shears compared to the AASHTO (2004) design prediction

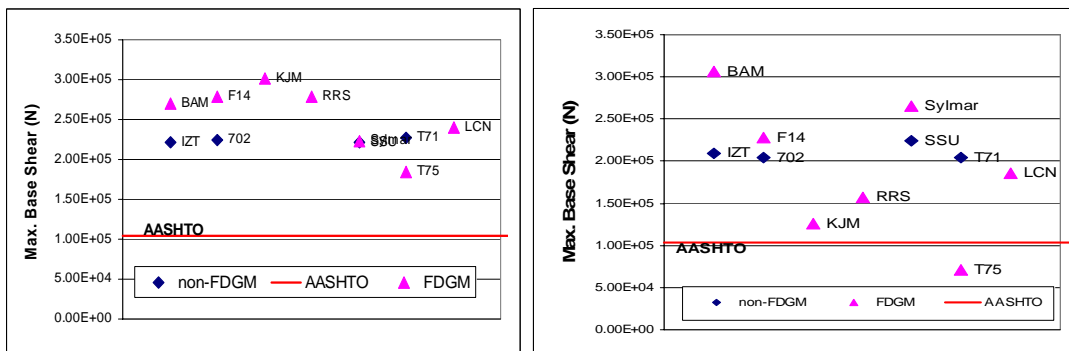


Figure 5.6.9: Bridge 520 Maximum longitudinal (left) and transverse (right) governing column base shears compared to the AASHTO (2004) design prediction

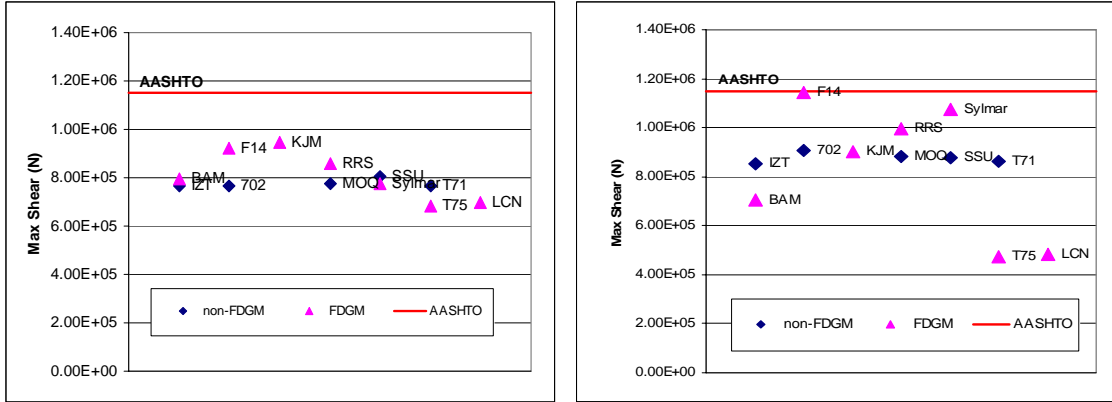


Figure 5.6.10: Bridge 90 Maximum longitudinal (left) and transverse (right) column shears (column C_4) compared to the AASHTO (2004) design prediction

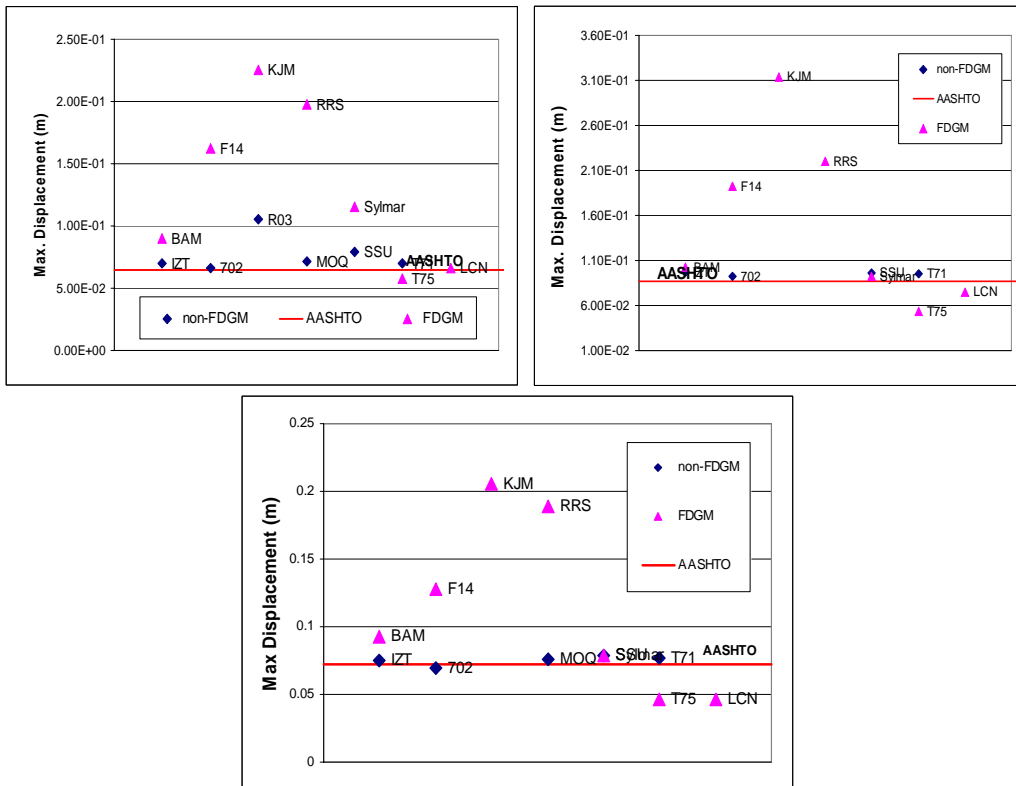


Figure 5.6.11: Bridge 405 (left), Bridge 520 (right) and Bridge 90 (down) maximum governing column displacements compared to the AASHTO (2004) design prediction

5.7) Acceleration Spectra prediction comparison

Using the Acceleration Response Spectra (ARS), the values of maximum base shear and maximum relative displacement for the governing column of each bridge were computed and compared to the ABAQUS results. The ARS are based on the response of a linear SDOF to the different ground motions. The maximum base shear and the maximum relative displacement predicted by the ARS are given by Equation 5.1 and 5.2, respectively:

$$F = m \times S_a \quad (5.1)$$

$$S_d = S_a / \omega_n^2 \quad (5.2)$$

Where F is the maximum base shear (in N), m the mass applied to the column (in kg), S_a the ARS value at the fundamental longitudinal period of the bridge (in g), ω_n is the fundamental longitudinal angular frequency of the bridge (in rad/sec), and S_d the maximum relative displacement (in m). Figures 5.7.1 and 5.7.2 show the comparison between the ABAQUS model and the prediction from the acceleration spectra for the maximum base shears and maximum governing column displacement, respectively. One can see that the ARS prediction is shown to be conservative for the maximum base shears, especially for non-forward directivity ground motions for all three bridges. The level of conservatism varies greatly concerning the predicted maximum base shears for the forward directivity ground motions. The maximum displacements could not be compared accurately for Bridge 90 since its column heights varied significantly. For Bridge 405 and 520, the predicted maximum relative displacements in Figure 5.7.2 were found to be, for most of the records, very close to the ABAQUS results. However, the maximum predicted displacement of Bridge 520 was over-conservative for the Sylmar

ground motion. An *R*-factor to take into account the inelasticity effects is needed to better approximate the maximum base shears. The use of the ARS to compute the expected maximum base shears and displacements is recommended for both non-forward directivity and forward directivity ground motions.

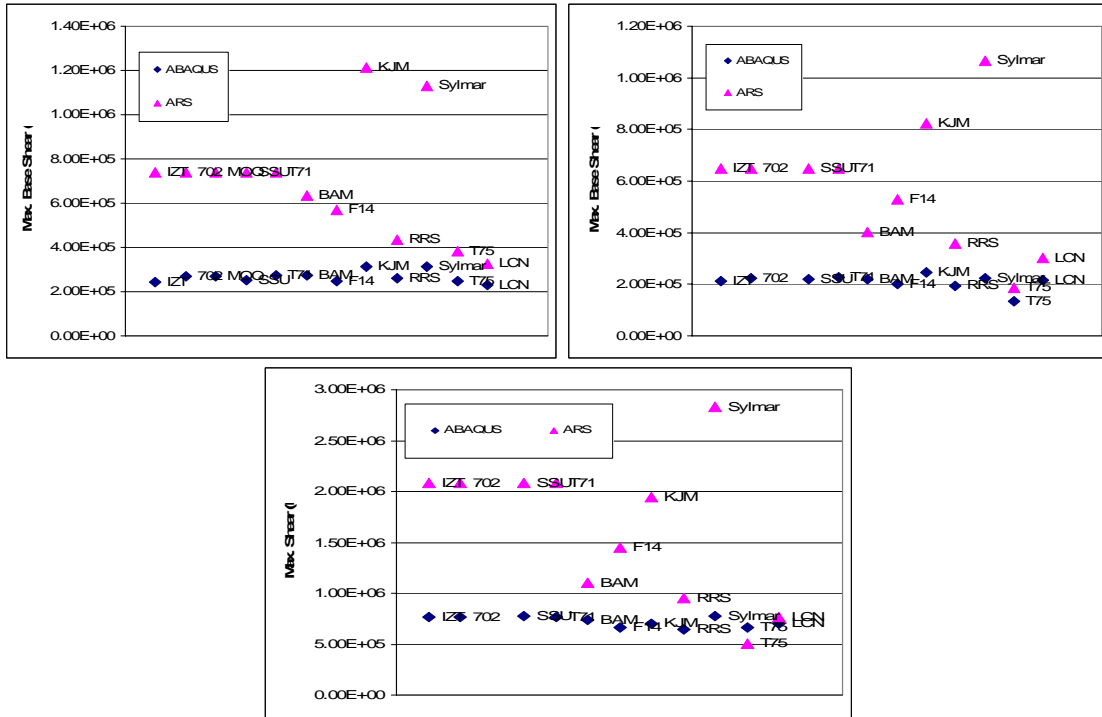


Figure 5.7.1: Bridge 405 (left), Bridge 520 (right) and Bridge 90 (down) maximum governing column shears compared to the ARS

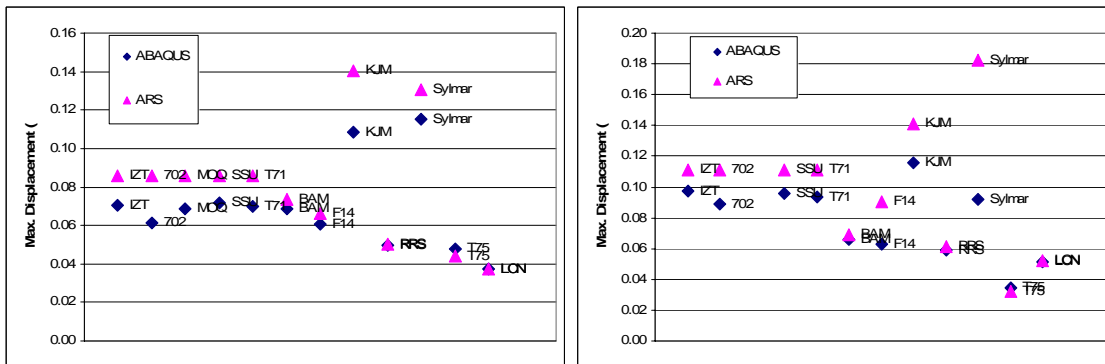


Figure 5.7.2: Bridge 405 (left) and Bridge 520 (right) maximum governing column displacement compared to the ARS

CHAPTER 6: Conclusion

Three typical post-1990 Washington State Department of Transportation (WSDOT) monolithic concrete bridges were chosen for nonlinear seismic evaluation under both forward directivity and non-forward directivity ground motions. Additionally, comparisons with results of a nonlinear and linear single-degree-of-freedom (SDOF) analysis and those of the American Association of State Highway and Transportation Officials (AASHTO) design provisions were made. The effects of soil-structure-interaction (SSI) were investigated as well.

Significant seismic damage may occur if the structure response is in tune with components of the forward directivity ground motion. The forward directivity effects may be identified from the response spectrum of the fault-normal component by the “bump” that is created by the ground motion velocity pulse (Somerville et al., 1997). The response of bridges to forward directivity ground motions is highly dependent upon the period content of this velocity pulse. If the period of the pulse is close to the bridge fundamental periods, significant damage can occur during a few cycles. The severity of the demand is controlled by the ratio of the pulse period to bridge fundamental periods.

The nonlinear time history analysis results from ABAQUS showed that most of the damage in the bridge columns during forward directivity ground motions occurred at the beginning of the record in response to the double-sided velocity pulse. Therefore, a simple ground motion consisting of a sinusoidal single pulse may be sufficient to evaluate bridge performance for forward directivity ground motions.

The forward directivity velocity pulse period is proportional to the earthquake magnitude, lengthening as the earthquake magnitude increases. As a result, damage due

to smaller magnitude earthquakes can be more significant for shorter period structures than damage resulting in larger magnitude earthquakes, since the near-fault pulse period is closer to the fundamental period of the structure in ground motions generated by the smaller magnitude earthquake. This was the case for both the MDOF and SDOF analyses all three bridges in this research. The results showed also that high peak ground acceleration (PGA) and/or peak ground velocity (PGV) is only one of several conditions that can cause high demand on the bridges.

The three bridges considered, Bridge 90/26A, Bridge 405/46N-E, and Bridge 520/19E-N, all typical concrete overpasses ranging from 50 m (162 ft) to 91 m (298 ft) in length, generally survived the earthquake motions without significant damage to the columns. However, column flexural failure was predicted for the Bridge 90 model when subjected to two of the forward directivity ground motions where the ground motion velocity pulse period was similar to the bridge fundamental period. In both cases, the maximum curvature capacity of one of the columns was reached. The bridge models often indicated distress at the abutments, including pounding, exceedance of abutment strength limits, and significant movement at the bearing pads. The risk of the deck exceeding the abutment bearing pad displacement capacity was high for Bridge 90 under forward directivity ground motion. The abutment strength limit was often reached, corresponding to an excessive pressure from the abutment on its surrounding soil.

The effect of Soil-Structure-Interaction (SSI) was studied through the response of the bridge models, with and without foundation flexibility. When the SSI was not included in the bridge analysis, by replacing the abutment/soil springs with rollers and the column footing springs with fixed bases, the bridge maximum base shears did not change

significantly in the longitudinal direction, while the base shears in the transverse direction were affected greatly. When the SSI was not included in the bridge models, the bridge maximum displacements in both directions increased significantly as well. This increase was particularly over-conservative for the forward directivity ground motions which already have a high displacement demand in many cases.

The use of the acceleration response spectra to compute the expected response of the bridges in terms of maximum base shears and relative displacements was found to be quite successful for both non-forward directivity and forward directivity ground motions. Care must be taken in the choice of the response modification factor (or *R*-factor) to include the inelasticity effect on the maximum base shear in the columns.

The performance of the nonlinear SDOF bridge models were always slightly unconservative compared to that of the full bridge models under non-forward directivity ground motion. The results of a simple SDOF bridge model to predict the response of a bridge under forward directivity ground motions ranged from very conservative for some ground motions to slightly unconservative for other ground motions. Therefore, nonlinear SDOF analyses are specifically not recommended in the case of forward directivity ground motions since the results were not consistent. A more detailed multiple-degree-of-freedom (MDOF) model should be used to assess bridge seismic performance so that SSI and the interaction of the longitudinal and transverse responses of the bridges can be included, particularly if a performance based design or assessment of the bridge is required.

The AASHTO (2004) bridge design procedure using the *ATC-6* collapse level acceleration response spectra, assuming that the bridges were categorized as “essential”,

was very unconservative for Bridge 405 and 520 with regard to the predicted maximum base shears in comparison to the nonlinear time history results for the non-forward directivity and forward directivity ground motions. The predicted AASHTO maximum base shears were found to be slightly conservative for Bridge 90 for both the forward directivity and non-forward directivity ground motions. The maximum AASHTO displacements for the non-forward directivity ground motions were found to be close to those from the nonlinear time history analyses. However, the maximum displacements from the AASHTO procedure were found to be unconservative for all three bridges for most of the forward directivity ground motions. This was expected since AASHTO requires that bridges near faults use a site specific ground motion assessment to assess the uncertainty in the forward directivity ground motions. Due to the variation in the acceleration response spectra with period due to forward directivity ground motions, to amplify the design spectra to implicitly consider the inelastic demands does not provide a reliable basis for representing near-fault, forward directivity ground motions.

Depending on the importance of the bridge being designed or assessed, the appropriate approach taken with forward directivity ground motions should be carefully considered by the designer. To follow the current AASHTO code provisions may lead to unconservative displacement ductility demand unless the required site specific analysis, for sites located close to an active fault, is performed. On the other hand, design for a forward directivity ground motion with a velocity pulse period matching the fundamental bridge period will require the bridge to resist very large demands. It must be kept in mind that the predicted velocity pulse period is still subject to significant uncertainty, therefore

it is difficult from the current state of knowledge to include forward directivity ground motion parameters within a probabilistic seismic hazard analysis.

REFERENCE

- ABAQUS Software & Documentation, Version 6.5-1 (2004)
©ABAQUS, Inc.
- Abrahamson Norman A. (1998)
“Statistical properties of peak ground accelerations recorded by SMART 1 array”,
Bull. Seismo. Soc. Am., Volume 78, Issue 1, pp.26-41
- Alavi Babak and Helmut Krawinkler (2004)
“Behavior of moment-resisting frame structures subjected to near-fault ground motions”,
Earthquake Engng Struct. Dyn. ; 33:687–706 (DOI: 10.1002/eqe.369)
- Alavi, B. and Krawinkler, H. (2000)
“Consideration of near-fault ground motion effects in seismic design”,
Proceedings, 12th World Conference on Earthquake Engineering, New Zealand.
- Alavi B., Krawinkler H. (2001)
“Effects of near-fault ground motions on frame structures”,
Earthquake Engineering Center Report No. 138., Department of Civil Engineering, Stanford University, February.
- Alhamany A., J. Chicois, R. Fougères and A. Hamel (1992)
“Effet Bauschinger lors de la plasticité cyclique de l'aluminium pur monocristallin”,
J. Phys., III France 2,1491-1508
- American Association of State Highway and Transportation Officials AASHTO LRFD
Bridge Design Specifications (2004), Third Edition
- Anderson J. C. and F. Naeim, (1984)
“Design criteria and ground motion effects in the seismic response of multi-story buildings”,
Proc. Applied technology Council, AC 10-1, Seminar on Earthquake Ground Motion and Building Damage Potential, San Francisco.
- Anderson J. C., Bertero VV. (1987)
“Uncertainties in establishing design earthquake”,
Journal of Structural Engineering, ASCE; 113(8):1709–24.
- Attalla, M. R., T.F. Paret, and S.A. Freeman, (1998)
“Near-Source Behavior of Buildings under Pulse-Type Earthquakes”,
Proceedings of the sixth US National Conference on Earthquake Engineering, Seattle, Washington.

- Bertero, V. V., S.A. Mahin, and R.A. Herrera, (1978)
 “A Seismic Design Implication of Near-fault San Fernando Earthquake Records”,
Earthquake Engineering and Structural Dynamics, Vol.6, pp. 31-34.
- Bertero , V. V. et al. (1976)
 “Establishment of design earthquakes: evaluation of present methods”,
Proceedings, Int. Symp. On Earthquake Structural Engineering, V. 1, St. Louis,
 pp. 551-580.
- Bielak J., Loukakis K., Hisada Y., Yoshimura C. (2003)
 “Domain reduction method for three-dimensional earthquake modeling in
 localized regions. Part I: Theory”,
Bulletin of the Seismological Society of America;93(2):817–24.
- Bray Jonathan D., Rodriguez-Marek Adrian (2004)
 “Characterization of forward-directivity ground motions in the near-fault region”,
Soil Dyn. And Earthq. Engineering 24, 815-828
- Brocher Thomas M., Richard J. Blakely, and Ray E. Wells (Aug. 2004)
 “Interpretation of the Seattle Uplift, Washington, as a Passive-Roof Duplex”,
Bulletin of the Seismological Society of America, Vol. 94, No. 4, pp. 1379–1401
- Brocher Thomas M., T. Parsons, R. J. Blakely, Christensen, M. A. Fisher, Wells (2001)
 “Upper crustal structure in Puget Lowland, Washington: results from the 1998
 Seismic Hazards Investigation in Puget Sound”,
J. Geophys. Res. 106, 13,541–13,564.
- Caltrans Seismic Design Criteria (2004)
 February 2004 Version 1.3, Section 6.1.2.2 and 2.1
- Calvert, A. J., M. A. Fisher, and the SHIPS working group (2001)
 “Imaging the Seattle Fault zone with high-resolution seismic tomography”,
Geophys. Res. Lett. 28, 2337–2340.
- Carr, A.J., (1996)
 “Ruaumoko – Program for Inelastic Dynamic Analysis”,
 Department of Civil Engineering, University of Canterbury, New Zealand.
- Chai J.F., Loh CH. (1999)
 “Near-fault ground motion and its effect on civil structures”,
*Proceedings of the International Workshop on Mitigation of Seismic Effects on
 Transportation Structures*, Taiwan. , p. 70–81
- Chen M.A., Penzien, J. (1977)
 “Nonlinear soil–structure interaction of skew highway bridge”,
Report UCB/EERC-77/24, Earthquake Engineering Research Center.

- Chopra A. K. and C. Chintanapakdee, (1998)
“Accuracy of response spectrum estimates of structural response to near-field earthquake ground motions: preliminary results”,
ASCE Structures world Conf., San Francisco, Paper No. T136-1
- Chopra Anil K., and Chatpan Chintanapakdee (2001)
“Comparing response of SDOF systems to near-fault and far-fault earthquake motions in the context of spectral regions”,
Earthquake Engng Struct. Dyn.; 30:1769–1789 (DOI: 10.1002/eqe.92)
- Ciampoli M., Pinto PE. (1995)
“Effects of soil–structure interaction on inelastic seismic response of bridge piers”,
ASCE Journal of structural Engineering ;121(5):806–14.
- Cofer, W. F., McLean, D. I., and McGuire, J. W. (1994)
“Analytical Modeling of Foundations for Seismic Analysis of Bridges”,
Final Technical Report No. WA-RD 328.1, Washington State Department of Transportation, February
- Cofer, W. F., and Modak, S. (1997)
“Modeling Pile Foundations for Seismic Analysis”,
Final Technical Report No. WA-RD 406.1 & 406.2, Washington State Transportation Center, June
- Dameron R. A., V. P. Sobash and I. P. Lam (1997)
“Nonlinear Seismic Analysis of Bridge Structures. Foundation-Soil Representation and Ground Motion Input”,
Computers & Structures Vol. 64, No. 516, pp. 1251-1269
- Dendrou B., Werner S.D., Toridis T. (1985)
”Three dimensional response of a concrete bridge system to traveling seismic waves”,
Computers and Structures ;20:593–603.
- Derecho, A. T. and Huckelbridge, A. A. (1991)
“Soil-structure interaction – a brief overview”, in S. K. Ghosh, ed., “Earthquake-Resistant Concrete Structures: Inelastic Response and Design”, SP 127,
American Concrete Institute, Detroit, Michigan, pp239-259
- Dicleli Murat, Buddaram Srikanth (2006)
“Equivalent linear analysis of seismic-isolated bridges subjected to near-fault ground motions with forward rupture directivity effect”,
Engineering Structures, January

- Federal Emergency Management Agency, FEMA 356 (2000)
Prestandard and commentary for the seismic rehabilitation of buildings
- Filiatrault, A., Trembley, R. (1998)
“Seismic Retrofit of Steel Moment Resisting Frames with Passive Friction Energy Dissipating Systems”,
Proceedings of NEHRP Conference and Workshop on Research on the Northridge, California Earthquake of January 17, 1994, Vol. 3. pp 554-561.
- Gazetas G., Mylonakis G. (1998)
“Seismic soil–structure interaction: new evidence and emerging issues”,
Proceedings of a Specialty Conference: Geotechnical Earthquake Engineering and Soil Dynamics III, August 1998. ASCE, p. 1119–74 Geotechnical Special Publication No. 75.
- Ghasemi Hamid, Hisanori Otsuka, James D. Cooper, and Hiroyuki Nakajima (1996)
“Aftermath of the Kobe Earthquake”,
FHWA, fall 1996, Vol. 60, No. 2
- Gillie Joanna Lynn (2005)
“Nonlinear Response Spectra of Forward-Directivity Ground Motions”,
Masters of Science in Civil Engineering, Washington State University, Dec 2005
- Hall, J. F., T.H. Heaton, M.W. Halling, and D.J. Wald, (1995)
“Near-Source Ground Motion and its Effects on Flexible Buildings”,
Earthquake Spectra, Vol. 11, pp. 569-605.
- Hall, J. F., and B.T. Aagaard, (1998)
“Fundamentals of the Near-Source Problem”,
5th Caltrans Seismic Research Workshop, Sacramento, California, June.
- Ingham Tim J., Santiago Rodriguez, Roupem Donikian, John Chan (1999)
“Seismic analysis of bridges with pile foundations”,
Computers and Structures 72, 49±62
- Iwan, W.D., (1996)
“Implications of Measured Near-Field Ground Motion on Structural Response”,
Building an International Community of Structural Engineering Proceedings of Structures Congress XIV, Chicago, Illinois.
- Jeremic Boris, Sashi Kunnath, Feng Xiong (2004)
“Influence of soil–foundation–structure interaction on seismic response of the I-880 viaduct”,
Engineering Structures 26, 391–402

- Johnson, S. Y., C. J. Potter, and J. M. Armentrout (1994)
“Origin and evolution of the Seattle fault and Seattle Basin”,
Washington, *Geology* 22,71–74.
- Johnson, S. Y., C. J. Potter, J. M. Armentrout, J. J. Miller, C. A. Finn, and Weaver (1996)
“The southern Whidbey Island fault: an active structure in the Puget Lowland”,
Washington, *Geol. Soc. Am. Bull.* 108, 334–354.
- Kalkan E., Kunnath S. (2006)
“Effects of Fling Step and Forward Directivity on Seismic Response of
Buildings”,
Earthquake Spectra, Vol. 22, No. 2, pages 367-390, May 2006
- Kappos A.J., Manolis G.D., Moschonas I.F.
“Seismic assessment and design of R/C bridges with irregular configuration,
including SSI effects”,
International Journal of Engineering Structures; 24:1337–48.
- Kowalsky, M.J., Priestley, M.J.N. (2000)
“Improved Analytical Model for Shear Strength of Circular Reinforced Concrete
Columns in Seismic Regions”,
ACI Structural Journal, 97(3), 388-397.
- Krawinkler, H. and Alavi, B. (1998)
“Development of improved design procedures for near-fault ground motions”,
SMIP 98, Seminar on Utilization of Strong Motion Data: Oakland, CA.
- Krawinkler, H. (2003)
“Matching of Equivalent Pulses to Near-Fault Ground Motions”,
Report to the *Pacific Earthquake Engineering Research Center (PEER)*.
http://www.peertestbeds.net/Cct/Krawinkler_Pulse_Matching_Description.doc.
- L-Pile Plus 4, (2002)
ENSOFIT, INC.'s
- Lam, I., and G.R. Martin, (1986)
“Seismic design of highway bridge foundations”,
FHWA-RD-86-103. U. S. Department of Transportation, FHA, R&D, McLean,
VA
- Légeron Frederic, Paultre P., Mazars J. (2005)
“Damage Mechanics Modeling of Nonlinear Seismic Behavior of Concrete
Structures”
J. of Structural Engineering, ASCE, June

- Lehman Dawn E., Moehle Jack P. (2000)
 “Seismic performance of well-confined concrete bridge columns”,
PEER Report 1998/01, University of California, Berkeley, December
- Liao W.I., Loh CH., Wan S., Jean W.Y., Chai J.F. (2000)
 “Dynamic responses of bridges subjected to near-fault ground motions”,
Journal of the Chinese Institute of Engineers; 23(4):455–64.
- Liao Wen-I, Chin-Hsiung Loh, Bor-Han Lee (2004)
 “Comparison of dynamic response of isolated and non-isolated continuous girder bridges subjected to near-fault ground motions”,
Engineering Structures 26; 2173–2183, July
- Loh CH., Wan S., Liao WI. (2002)
 “Effects of hysteretic model on seismic demands: consideration of near-fault ground motions”,
The Structural Design of Tall Buildings; 11:115–69.
- Makley, B. (2001)
 “Seismic behavior of bridge shear columns subjected to near-field pulse loading”,
 Report presented to the University of California at San Diego, La Jolla, CA.
- Makris N., Badoni D., Delis E., Gazetas G. (1995)
 « Prediction of observed bridge response with soil–pile–structure interaction”,
ASCE Journal of Structural Engineering; 120(10):2992– 3011.
- Makris N., Black Cameron J. (2004)
 “Evaluation of Peak Ground Velocity as a “Good” Intensity Measure for Near-Source Ground Motions”,
Journal of Engineering Mechanics, ASCE, September 2004
- Malhotra Praveen K. (1999)
 “Response of Buildings to Near-Field Pulse-like Ground Motions”,
Earthquake Engng. Struct. Dyn. 28, 1309, 1326
- Mander, J.B., Priestley, M.J.N., Park, R. (1988)
 “Theoretical Stress-Strain Model for Confined Concrete”,
Journal of Structural Engineering, 11(8), 1804-1826.
- Maragakis E.A., Jennings P.C. (1987)
 “Analytical models for the rigid body motions of skew bridges”,
Earthquake Engineering and Structural Dynamics; 15(8):923–44.
- Matlock, H., SHC Foo, and Cheang, (1981)
 “Soil-pile interaction in liquefiable cohesionless soils during earthquake loading”,
ICRAGEESD, Uni. Of Missouri, Rolla, MO

- Mavroeidis, G. P., and Papageorgiou A. S. (2003)
 “A mathematical representation of near-fault ground motions”,
Bulletin of the Seismological Society of America, 93(3), 1999-1131.
- Mayes, R. L., and A. Shaw, (1997)
 “The Effects of Near Fault Ground Motions on Bridge Columns”,
*Proceedings of the FHWA/NCEER Workshop on the National Representation of
 Seismic Ground Motion for New and Existing Highway Facilities.*
 Burlingame, California, May
- Mazars J., Pijaudier-Cabot G. (1989)
 “Continuum Damage Theory – Application to Concrete”,
J. of Engng Mechanics, Vol. 115, No.2. February
- McCallen D.B., Romstadt K.M. (1994)
 “Analysis of a skewed short span, box girder overpass”,
Earthquake Spectra; 10(4):729–55.
- McDaniel Cole, Rodriguez-Marek Adrian (2004)
 “Dynamic Response of Bridges to Near-Fault, Forward Directivity Ground
 Motions”, Proposal for the project.
- McGuire Jeffrey W., Cofer, W. F., McLean, D.I., and Marsh, M. L. (1994)
 “Analytical Modeling of Spread Footing Foundations for Seismic Analysis of
 Bridges”,
Transportation Research Record No. 1447, TRB, pp. 80-92
- Modak Sukomal (1995)
 “Determination of Rheological parameters of pile foundations for bridges for
 earthquake analysis”,
 Master of Science in Civil engineering, WSU
- Modak Sukomal (1997)
 “Determination of Rheological parameters of pile foundations for bridges for
 earthquake analysis”,
WA-RD 406.2 WSDOT Technical Report
- Molzer P. C., M. A. Fisher, R. J. Blakely, R. C. Bucknam, T. Parsons, R. S. Crosson, and
 K. C. Creager
 “Subsurface Geometry and Evolution of the Seattle Fault Zone and the Seattle
 Basin, Washington”,
 by U. S. ten Brink

- Mylonakis George, Dimitri Papastamatiou, John Psycharis, and Khaled Mahmoud (2001)
 “Simplified Modeling of Bridge Response on Soft Soil to nonuniform seismic excitation”,
Journal of Bridge Engineering
- Nakashima M., Matsumiya T., Asano K. (2000)
 “Comparison in earthquake responses of steel moment frames subjected to near-fault strong motions recorded in Japan, Taiwan and the US”,
Proceedings of the International Workshop on Annual Commemoration of Chi-Chi Earthquake, Technology Aspect, Taiwan, vol. II, p. 112–23.
- Orozco Greg L. and Scott A. Ashford (2002)
 “Effects of Large Velocity Pulses on Reinforced Concrete Bridge Columns”,
PEER Report 2002/23, University of California, Berkeley, April
- Park S. W., H. Ghasemi, J. Shen, P. G. Somerville, W. Yen and M. Yashinsky, (2004)
 “Simulation of the seismic performance of the Bolu Viaduct subjected to near-fault ground motions”,
Earthquake Engng Struct. Dyn; 33:1249–1270 (DOI: 10.1002/eqe.395)
- Pacific Earthquake Engineering Research Center (PEER). (2000)
PEER Strong Motion Database [Online]. <<http://peer.berkeley.edu/smcat/>>
- Pratt, T. L., S. Y. Johnson, C. J. Potter, W. J. Stephenson, and C. A. Finn (1997)
 “Seismic reflection images beneath Puget Sound, western Washington State: the Puget Lowland thrust sheet hypothesis”,
J. Geophys. Res., 102, 27,469–27,489.
- Priestley, M. J. N., Seible F., Calvi G. M. (1996)
 “Seismic Design and Retrofit of bridges”,
John Wiley & sons, Inc., NYC
- Priestley, M. J. N. (2003)
 “Myths and fallacies in earthquake engineering, revisited: The Malley-Milne lecture”,
 Rose School, Collegio Alessandro Volta, Pavia, Italy.
- Reese, L. C. (1977)
 “Laterally loaded piles: program documentation”,
ASCE 287-305
- Reese L.C. (2000)
 LPILE plus 4.0 technical manual. Ensoft, Inc., Harpenden, U.K.

- Rodriguez-Marek, A. (2000)
“Near-Fault Seismic Site Response”,
Ph. D. Dissertation, University of California at Berkeley, Fall 2000.
- Rodriguez-Marek, A., J.D. Bray and N.A. Abrahamson, (2001)
“An Empirical Geotechnical Seismic Site Response Procedure”,
Earthquake Spectra, The Professional Journal of the Earthquake Engineering Research Institute, V. 17, No. 1, Feb., pp. 65-87.
- Seed H.B., Wong R.T., Idriss I.M., Tokimatsu K. (1984)
“Moduli and damping factors for dynamic analysis of cohesionless soils”,
Earthquake Engineering Research Center Report UCB/EERC- 84/14,
University of California at Berkeley
- Shen J.; Meng-Hao Tsai; Kuo-Chun Chang; and George C. Lee (2004)
“Performance of a Seismically Isolated Bridge under Near-Fault Earthquake Ground Motions”,
J. Structural Engng © ASCE, June
- Somerville, P. G. (1993)
“Engineering applications of strong ground motion simulation”,
Tectonophysics, 218 (1-3), 195-219.
- Somerville, P.G. (1998)
“Development of an improved representation of near fault ground motions”,
Proc. SMIP98 Seminar on Utilization of Strong Motion Data, California Strong Motion Instrumentation Program, Sacramento, CA, 1-20.
- Somerville, P.G. (2000)
“Magnitude scaling of near fault ground motion”,
Proc. Int. Workshop on Annual Commemoration of Chi-Chi earthquake, Vol. 1, 59-70.
- Somerville, P.G., Saikia, C., Wald, D., Graves, R. (1996)
“Implications of the Northridge earthquake for strong ground motions from thrust faults”,
Bull. Seism. Soc. Am., 86, S115-S125.
- Somerville, P.G., Smith, N.F., Graves, R.W. and Abrahamson, N.A. (1997)
“Modification of empirical strong ground motion attenuation relations to include the amplitude and duration effects of rupture directivity”,
Seismological Research Letters 68, 199-222.

- Somerville, P. G. (2003)
“Characterizing Near-Fault ground motions for the design and evaluation of bridges”,
Pacific Earthquake Engineering Research Center (PEER)
Available at <http://www.peertestbeds.net/ucs.htm>.
- Spyrakos C.C. (1992)
“Seismic behavior of bridge piers including soil–structure interaction”,
Computers and Structures; 43(2): 373–84.
- Stewart Jonathan P. (2001)
“Characteristics of Near-Fault Ground Motions”,
PEER report
- Sucuogly H., Erberik, and Yucemen (1999)
“Influence of peak ground velocity on seismic failure probability”
4th Int. Conf. Of the European Association for Structural Dynamics, Prague
- Sweet J. (1993)
“A technique for nonlinear soil–structure interaction”,
Technical Report CAI-093-100, Caltrans, Sacramento, California.
- Symans, M., Cofer, W., Du, Y., Fridley, K. (2003)
“Evaluation of Fluid Dampers for Seismic Energy Dissipation of Woodframe Structures”,
CUREE Report No. W-20, Consortium of Universities for Research in Earthquake Engineering, Richmond, CA.
- Tongaonkar N.P., R.S. Jangid (2003)
“Seismic response of isolated bridges with soil–structure interaction”,
Soil Dynamics and Earthquake Engineering 23, 287–302
- Tseng W-S, Penzien J. (2000)
“Soil–foundation–structure interaction”,
Bridge Engineering Handbook (Chapter 42), CRC Press: Boca Raton, FL.
- Uniform Building Code, UBC. Structural engineering design provisions (1997)
International Conference of Building Officials, vol. 2. 1997.
- USGS Website
Partial Report for Seattle fault zone (Class A) No. 570
1.0: U.S. Geological Survey Open-File Report 03-417
<http://qfaults.cr.usgs.gov>.

- Veletsos A.S. and B. Verbic. (1973)
 “Vibration of viscoelastic foundations”,
Earthq. Engin. Struct. Dyn., Vol. 2, pp 87-102
- van Wagoner, T. M., R. S. Crosson, K. Creager, G. Medema, L. Preston, Symons, and T. M. Brocher (2002)
 “Crustal structure and relocated earthquakes in the Puget Lowland, Washington from high-resolution seismic tomography”,
J. Geophys. Res. (in press)
- Welch, R. C. and Reese, L. C. (1972)
 “Laterally loaded behavior of drilled shafts”,
Research Report 3-5-65-89, Center for Highway Research, University of Texas, Austin.
- Wen, Y. (1976)
 “Method for random vibration of hysteretic systems”,
Journal of the Engineering Mechanics Division ASCE, 102(EM2): 249-263.
- Wolf, J.P. (1988)
 “Dynamic soil-structure interaction”,
Prentice-hall, inc, Englewood cliffs, new jersey
- Yashinsky M., M. J. Karshenas, (2003)
 “Fundamentals of seismic protection for bridges “,
EERI
- Yoshimura C., Bielak J., Hisada Y. (2003)
 “Domain reduction method for three-dimensional earthquake modeling in localized regions. Part II: Verification and examples”,
Bulletin of the Seismological Society of America; 93(2):825–40.
- Zhang J., Makris N. (2001)
 “Seismic response analysis of highway overcrossings including soil–structure interaction”,
PEER 2001/02, March 2001
- Zhang, Y. and Iwan, W. D. (2002)
 “Active interaction control of tall buildings subjected to near-field ground motions”,
Journal of Structural Engineering, ASCE; 128, 69-79.

APPENDIX

APPENDIX A

A.1 Shear Capacity Degradation Model

To capture strength degradation resulting from shear action, the method proposed by Kowalsky and Priestley (2000) was used. According to the authors, the nominal shear capacity of a reinforced concrete member is the summation of three components.

$$V_A = V_S + V_P + V_C \quad (\text{A.1})$$

Where V_S is the contributing shear capacity from the steel truss mechanism, V_P is the contribution from the compressively applied axial load, and V_C is the contribution from the concrete mechanism. Each shear component is represented below mathematically for circular columns.

$$V_S = \frac{\pi}{2} A_{sp} f_y \frac{D - c - cov}{s} \cot(\theta) \quad (\text{A.2})$$

$$V_P = P \tan \alpha = P \frac{D - c}{2L} \quad (\text{Single Bending}) \quad (\text{A.3})$$

$$V_P = P \tan \alpha = P \frac{D - c}{L} \quad (\text{Double Bending}) \quad (\text{A.4})$$

$$V_C = \alpha \beta k \sqrt{f'_c} (0.8 A_g) \quad (\text{A.5})$$

$$1 \leq \alpha = 3 - \frac{M}{VD} \leq 1.5 \quad (\text{A.6})$$

$$\beta = 0.5 + 20 \rho_l \leq 1 \quad (\text{A.7})$$

In the above equations, D is the column diameter, c is the location of the neutral axis, cov is the cover distance, P is the applied axial load, and ρ_l is the longitudinal

reinforcing steel ratio. The term k is determined from Figure A.1-1 below. There was originally a uniaxial and a biaxial curve produced by Kowalsky and Priestley, but for this research, to be conservative, the biaxial curve was used for the shear envelope, and it is shown in Figure A.1-1.

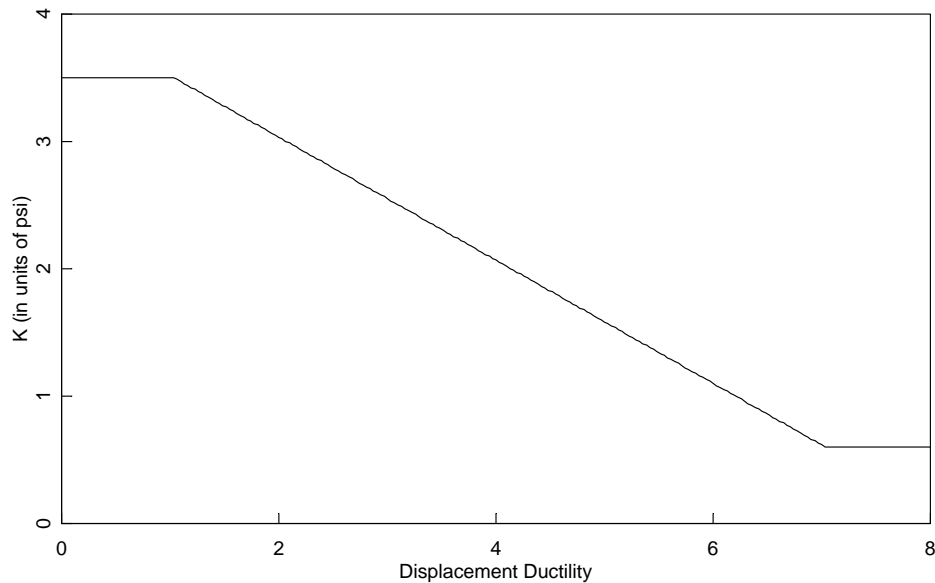


Figure A.1-1: k curve

A.2 Foundation Stiffnesses – FEMA 356 (2000)

The footing spring stiffnesses were computed following FEMA 356 recommendations as described in Figure A.2-1. The computed spring stiffnesses are shown on Table A.2-1.

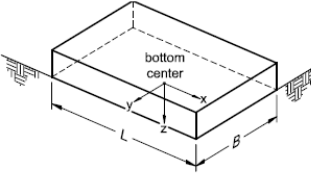
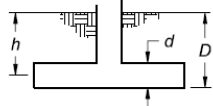
Degree of Freedom	Stiffness of Foundation at Surface	Note
Translation along x-axis	$K_{x,sur} = \frac{GB}{2-\nu} \left[3.4 \left(\frac{L}{B} \right)^{0.65} + 1.2 \right]$	 <p>Orient axes such that $L \geq B$</p>
Translation along y-axis	$K_{y,sur} = \frac{GB}{2-\nu} \left[3.4 \left(\frac{L}{B} \right)^{0.65} + 0.4 \frac{L}{B} + 0.8 \right]$	
Translation along z-axis	$K_{z,sur} = \frac{GB}{1-\nu} \left[1.55 \left(\frac{L}{B} \right)^{0.75} + 0.8 \right]$	
Rocking about x-axis	$K_{xx,sur} = \frac{GB^3}{1-\nu} \left[0.4 \left(\frac{L}{B} \right) + 0.1 \right]$	
Rocking about y-axis	$K_{yy,sur} = \frac{GB^3}{1-\nu} \left[0.47 \left(\frac{L}{B} \right)^{2.4} + 0.034 \right]$	
Torsion about z-axis	$K_{zz,sur} = GB^3 \left[0.53 \left(\frac{L}{B} \right)^{2.45} + 0.51 \right]$	
Degree of Freedom	Correction Factor for Embedment	Note
Translation along x-axis	$\beta_x = \left(1 + 0.21 \sqrt{\frac{D}{B}} \right) \cdot \left[1 + 1.6 \left(\frac{hd(B+L)}{BL^2} \right)^{0.4} \right]$	 <p>d = height of effective sidewall contact (may be less than total foundation height) h = depth to centroid of effective sidewall contact</p> <p>For each degree of freedom, calculate $K_{emb} = \beta K_{sur}$</p>
Translation along y-axis	$\beta_y = \beta_x$	
Translation along z-axis	$\beta_z = \left[1 + \frac{1}{21} \frac{D}{B} \left(2 + 2.6 \frac{B}{L} \right) \right] \cdot \left[1 + 0.32 \left(\frac{d(B+L)}{BL} \right)^{2/3} \right]$	
Rocking about x-axis	$\beta_{xx} = 1 + 2.5 \frac{d}{B} \left[1 + \frac{2d}{B} \left(\frac{d}{D} \right)^{-0.2} \sqrt{\frac{B}{L}} \right]$	
Rocking about y-axis	$\beta_{yy} = 1 + 1.4 \left(\frac{d}{L} \right)^{0.6} \left[1.5 + 3.7 \left(\frac{d}{L} \right)^{1.9} \left(\frac{d}{D} \right)^{-0.6} \right]$	
Torsion about z-axis	$\beta_{zz} = 1 + 2.6 \left(1 + \frac{B}{L} \right) \left(\frac{d}{B} \right)^{0.9}$	

Figure A.2-1: Elastic Solutions for Rigid Footing Spring Constraints (FEMA 356, 2000)

Table A.2 -1 Bridge 405 Footing Spring stiffnesses

$G =$	2.15E+08	Pa	shear modulus of the soil
$K_{11} =$	6.06E+09	N/m	X Axis
$K_{22} =$	6.39E+09	N/m	Y Axis
$K_{33} =$	5.34E+09	N/m	Vertical translation Z
$K_{44} =$	3.5E+10	N-m/rad	X Axis Rocking
$K_{55} =$	7.86E+10	N-m/rad	Y Axis Rocking
$K_{66} =$	9.79E+10	N-m/rad	Torsion Z

Table A.2 -2 Bridge 520 Footing Spring stiffnesses

$G =$	1.47E+08	Pa	shear modulus of the soil
$K_{11} =$	4.64E+09	N/m	X Axis
$K_{22} =$	4.87E+09	N/m	Y Axis
$K_{33} =$	3.87E+09	N/m	Vertical translation Z
$K_{44} =$	2.71E+10	N-m/rad	X Axis Rocking
$K_{55} =$	5.66E+10	N-m/rad	Y Axis Rocking
$K_{66} =$	7.07E+10	N-m/rad	Torsion Z

Table A.2 -3 Bridge 90 Footing Spring stiffnesses

	Foot 1	Foot 2	Foot 3	Foot 4	Unit	
$G =$	2.01E+08	2.01E+08	2.01E+08	2.01E+08	Pa	shear modulus of the soil
$K_{11} =$	1.21E+10	1.07E+10	1.03E+10	1.17E+10	N/m	X Axis
$K_{22} =$	1.25E+10	1.13E+10	1.09E+10	1.21E+10	N/m	Y Axis
$K_{33} =$	8.88E+09	7.71E+09	7.27E+09	8.59E+09	N/m	Vertical translation Z
$K_{44} =$	8.74E+10	4.01E+10	2.93E+10	8.72E+10	N-m/rad	X Axis Rocking
$K_{55} =$	1.64E+11	9.94E+10	7.01E+10	1.64E+11	N-m/rad	Y Axis Rocking
$K_{66} =$	1.98E+11	1.16E+11	8.25E+10	1.98E+11	N-m/rad	Torsion Z

A.3 Longitudinal Abutment Response – Caltrans (2004)

Caltrans (Seismic Design Criteria, Feb. 2004, Version 1.3) states that the linear elastic demand model shall include an effective abutment stiffness, K_{eff} , that accounts for expansion gaps, and incorporates a realistic value for the embankment fill response. The abutment embankment fill stiffness is nonlinear and is dependent upon on the material properties of the abutment backfill. Based on passive earth pressure tests and the force deflection results from large-scale abutment testing at UC Davis, the initial embankment fill stiffness is $K_i \approx 20$ kip.in/ft (11.5 kN.mm/m). The initial stiffness shall be adjusted proportional to the backwall/diaphragm height, as documented in the following equation.

$$K_{abut} = \begin{cases} K_i \times w \times \left(\frac{h}{5.5} \right) & \text{U.S. units} \\ K_i \times w \times \left(\frac{h}{1.7} \right) & \text{S.I. units} \end{cases} \quad (A.8)$$

Where, w is the width of the backwall or the diaphragm for seat and diaphragm abutments, respectively.

The passive pressure resisting the movement at the abutment increases linearly with the displacement, as shown in Figure A.3-1. The maximum passive pressure of 5.0

ksf (239 kPa), presented in the following equations is based on the ultimate static force developed in the full scale abutment testing conducted at UC Davis [Maroney, 1995].

$$P_{bw} \text{ or } P_{dia} = \begin{cases} A_e \times 5.0 \text{ ksf} \times \left(\frac{h_{bw} \text{ or } h_{dia}}{5.5}\right) & (\text{ft, kip}) \\ A_e \times 239 \text{ kPa} \times \left(\frac{h_{bw} \text{ or } h_{dia}}{1.7}\right) & (\text{m, kN}) \end{cases} \quad (\text{A.9})$$

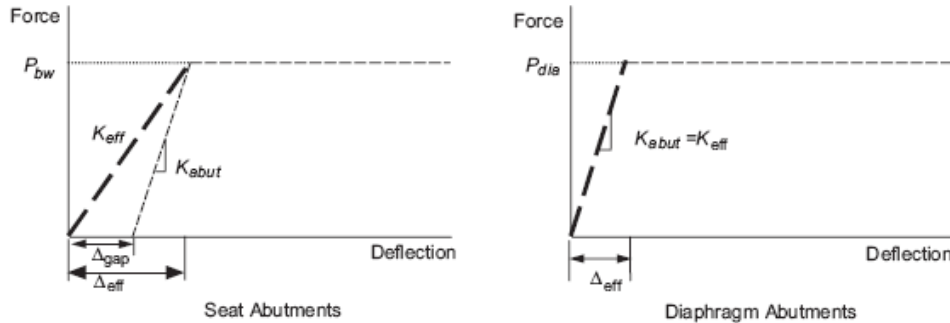


Figure A.3-1: Effective Abutment Stiffness

The effective abutment area for calculating the ultimate longitudinal force capacity of an abutment is presented in the following equation.

$$A_e = \begin{cases} h_{bw} \times w_{bw} & \text{Seat Abutments} \\ h_{dia} \times w_{dia} & \text{Diaphragm Abutments} \end{cases} \quad (\text{A.10})$$

$h_{dia} = h_{dia}^*$ = Effective height if the diaphragm is not designed for full soil pressure

$h_{dia} = h_{dia}^{**}$ = Effective height if the diaphragm is designed for full soil pressure

For seat abutments, the backwall is typically designed to break off in order to protect the foundation from inelastic action. The area considered effective for mobilizing the backfill longitudinally is equal to the area of the backwall. See Figure A.3-2.

For diaphragm abutments the entire diaphragm is typically designed to engage the backfill immediately when the bridge is displaced longitudinally. Therefore, the effective abutment area is equal to the entire area of the diaphragm. If the diaphragm has not been designed to resist the passive earth pressure exerted by the abutment backfill, the

effective abutment area is limited to the portion of the diaphragm above the soffit of the girders. See Figure A.3-2.

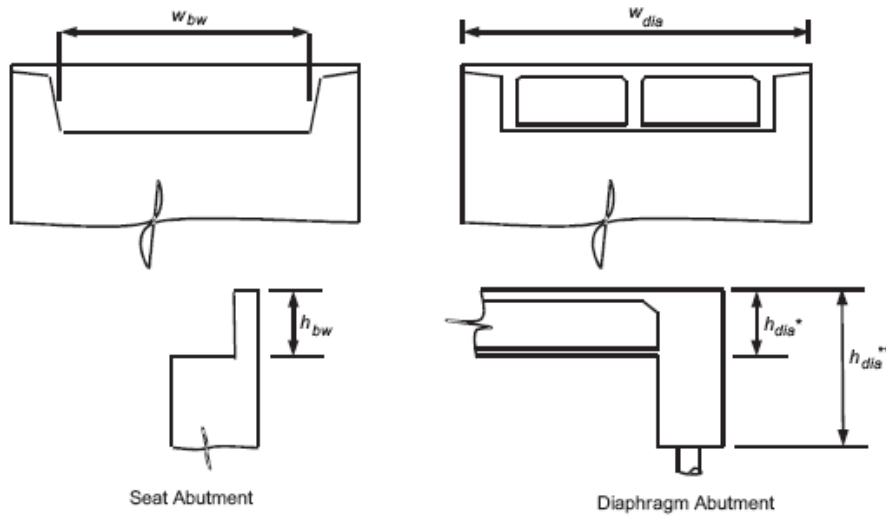


Figure A.3-2: Effective Abutment Area

Finally, Bridge 405 abutments were modeled with the following nonlinear force-displacement curve, including plasticity effect. See Figure A.3-3. Bridge 520 had a similar force-displacement curve.

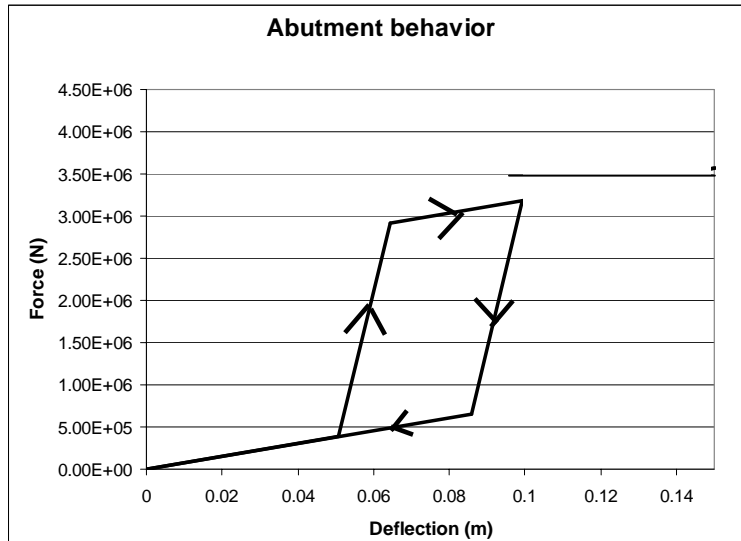


Figure A.3-3 Bridge 405 Abutments force-displacement curve

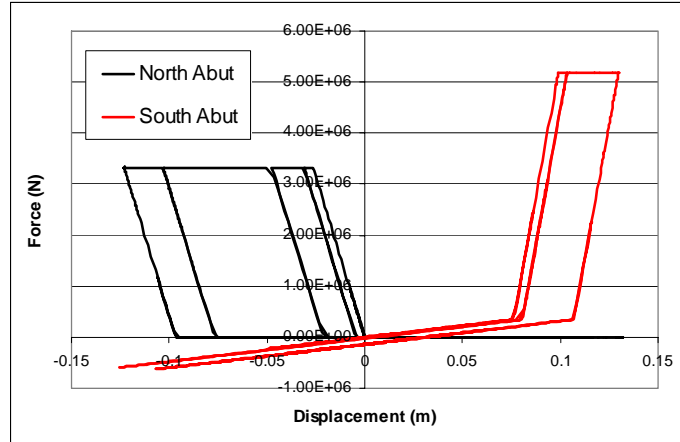


Figure A.3-4 Bridge 90 Abutments force-displacement curve

A.4 AASHTO (2004) procedure

Figure A.3-1 shows the seismic design procedure followed to determine the forces and displacements in the bridge.

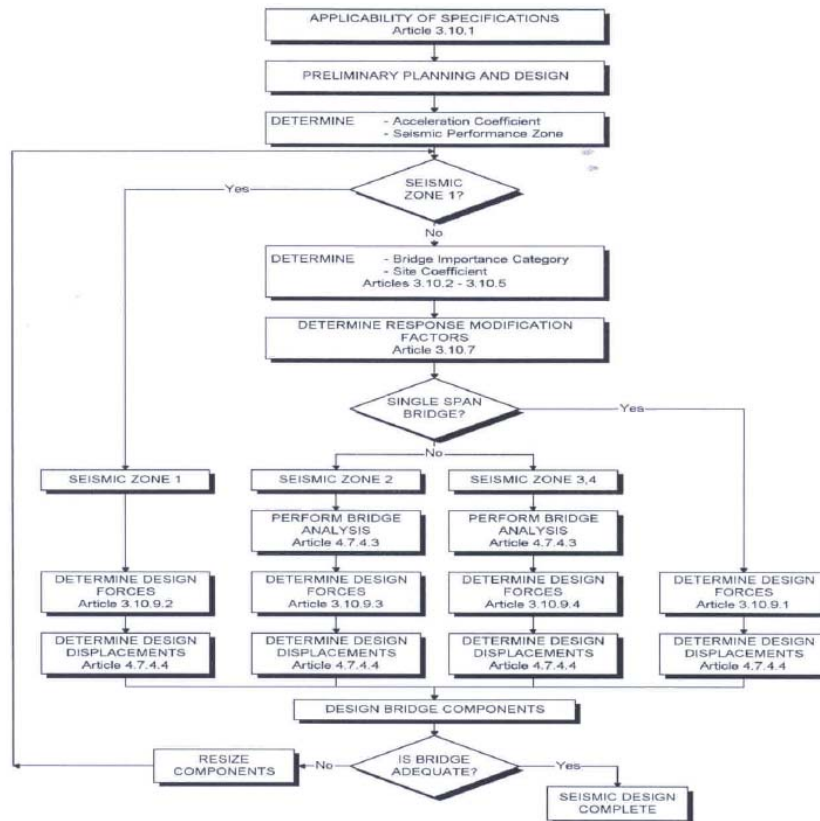


Figure A.3-1: AASHTO bridge seismic design procedure chart

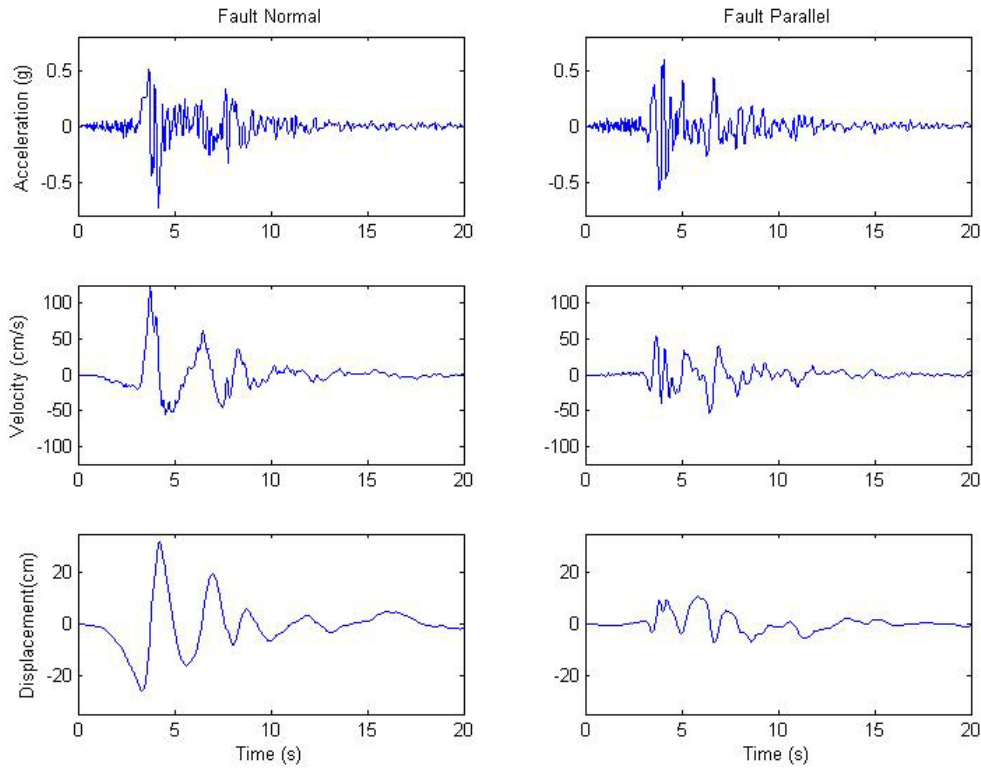
The bridges were located in Seismic Zone 3. The Multimode Spectral Method (Article 4.7.4.3.3) was used with ABAQUS to compute the seismic design forces and displacements. The elastic seismic response spectra were given by the WSDOT. Two load cases were computed from the previous analysis (Article 3.10.8). The maximum one was selected:

- 100% of the absolute value of the force effects in one of the perpendicular directions combined with 30% of the absolute value of the force effects in the second perpendicular direction
- 100% of the absolute value of the force effects in the second perpendicular direction combined with 30% of the absolute value of the force effects in the first perpendicular direction.

APPENDIX B

B.1 Ground Motions Characteristics

The forward directivity ground motions (FDGM) and the non FDGMs of Bridge 405 are listed below. Presented are the acceleration, velocity, and displacement time histories for both fault normal (FN) and fault parallel (FP) ground motion components.

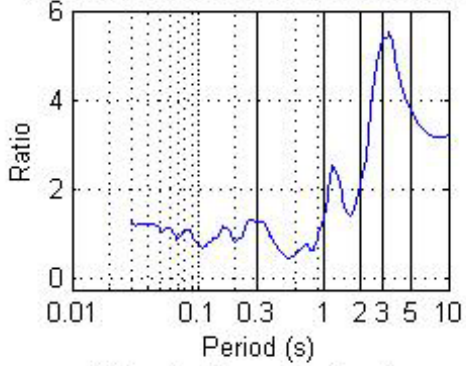


PACIFIC ENGINEERING AND ANALYSIS STRONG-MOTION DATA

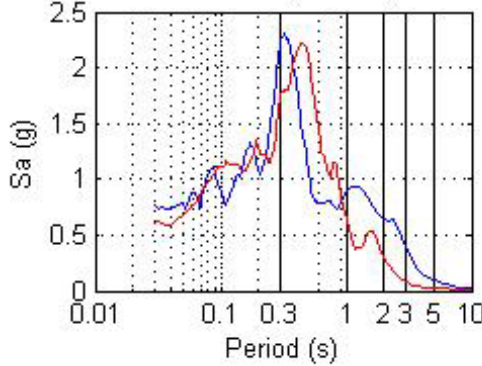
Thick lines are Fault Normal,
Thin lines are Fault Parallel
Reference Line is FN/FP Ratio from
Somerville et al.(1997) for
Mw=7.5,R=0 (Maximum Directivity Conditions)

Period for Svfn(max)
2.40 [2.20, 2.50] s
Period for Svfp(max)
0.50 [0.48, 0.52] s

Acceleration Response Spectral Ratios



Acceleration Response Spectra



Velocity Response Spectra

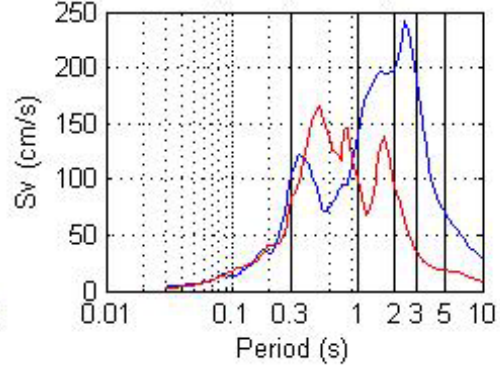
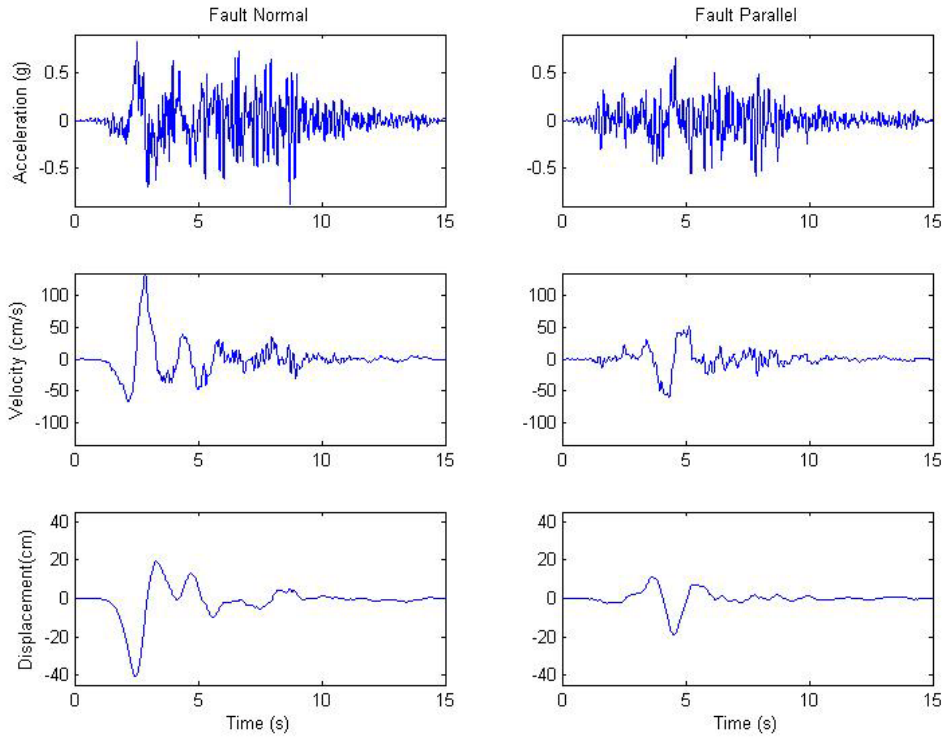


Figure B.1-1: Characteristics of SYL - Sylmar - Olive View Med FF



BHRC Strong Motion Data
 Thick lines are Fault Normal,
 Thin lines are Fault Parallel
 Reference Line is FN/FP Ratio from
 Somerville et al.(1997) for
 $M_w=7.5, R=0$ (Maximum Directivity Conditions)

Period for $S_{vfn}(\max)$
 1.50 [1.43, 1.60] s
 Period for $S_{vfp}(\max)$
 1.30 [1.25, 1.40] s

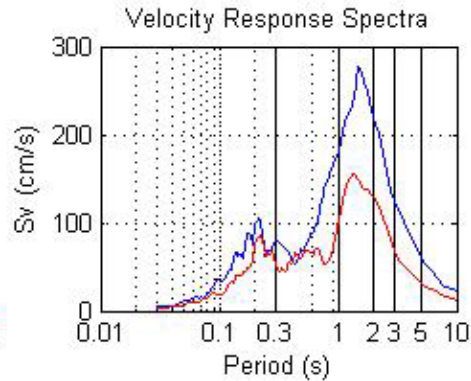
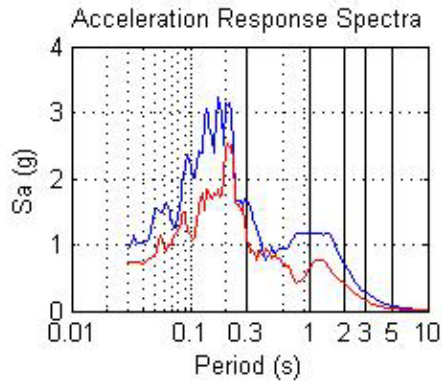
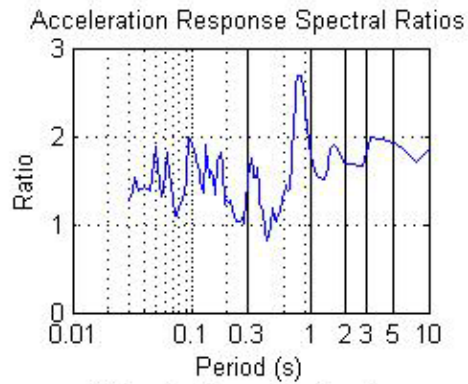
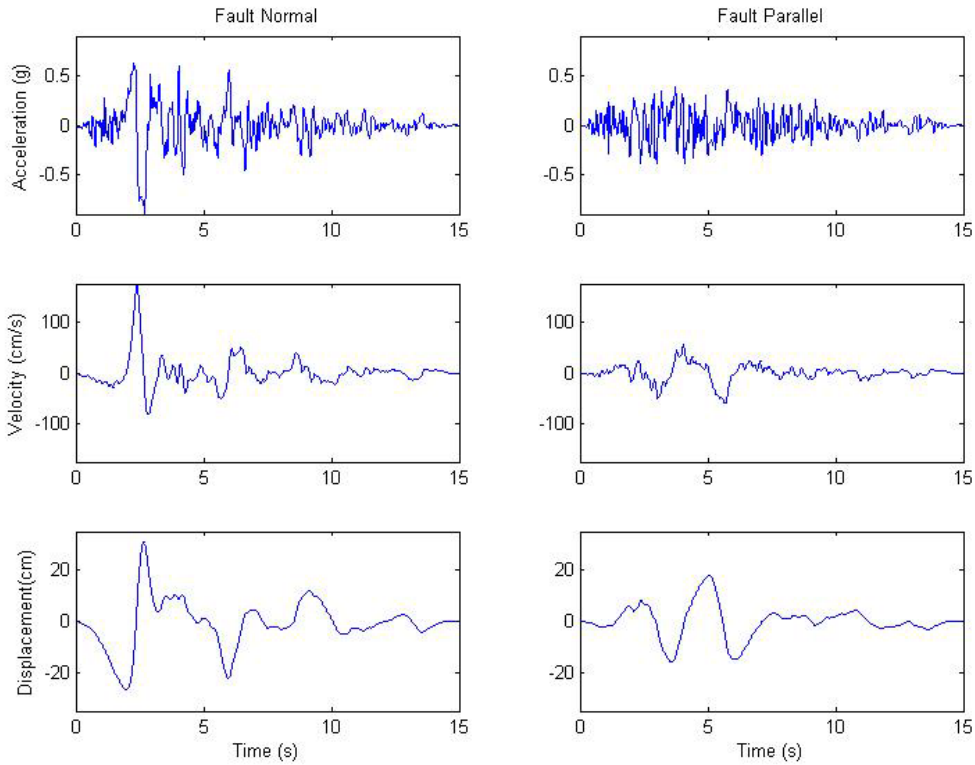


Figure B.1-2: Characteristics of BAM - Bam Station



PACIFIC ENGINEERING AND ANALYSIS STRONG-MOTION DATA
 Thick lines are Fault Normal,
 Thin lines are Fault Parallel
 Reference Line is FN/FP Ratio from
 Somerville et al.(1997) for
 Mw=7.5,R=0 (Maximum Directivity Conditions)

Period for Svfn(max)
 1.10 [1.00, 1.11] s
 Period for Svfp(max)
 2.50 [2.40, 2.60] s

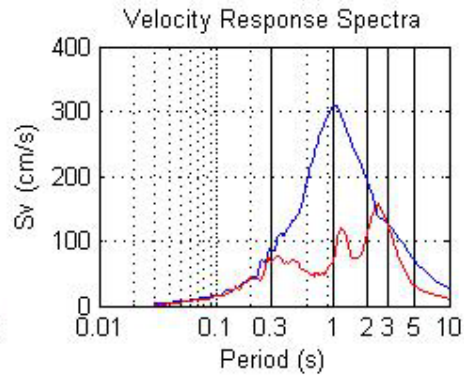
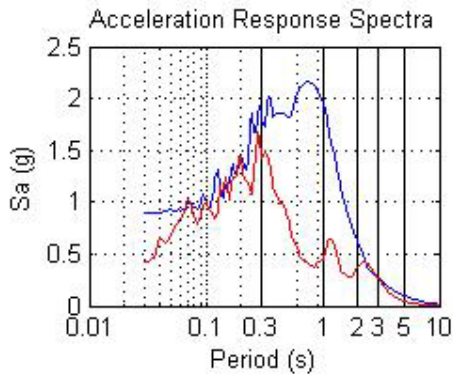
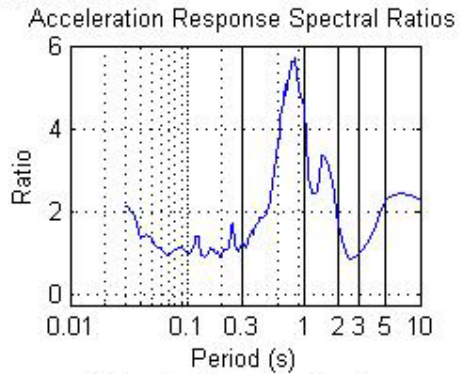
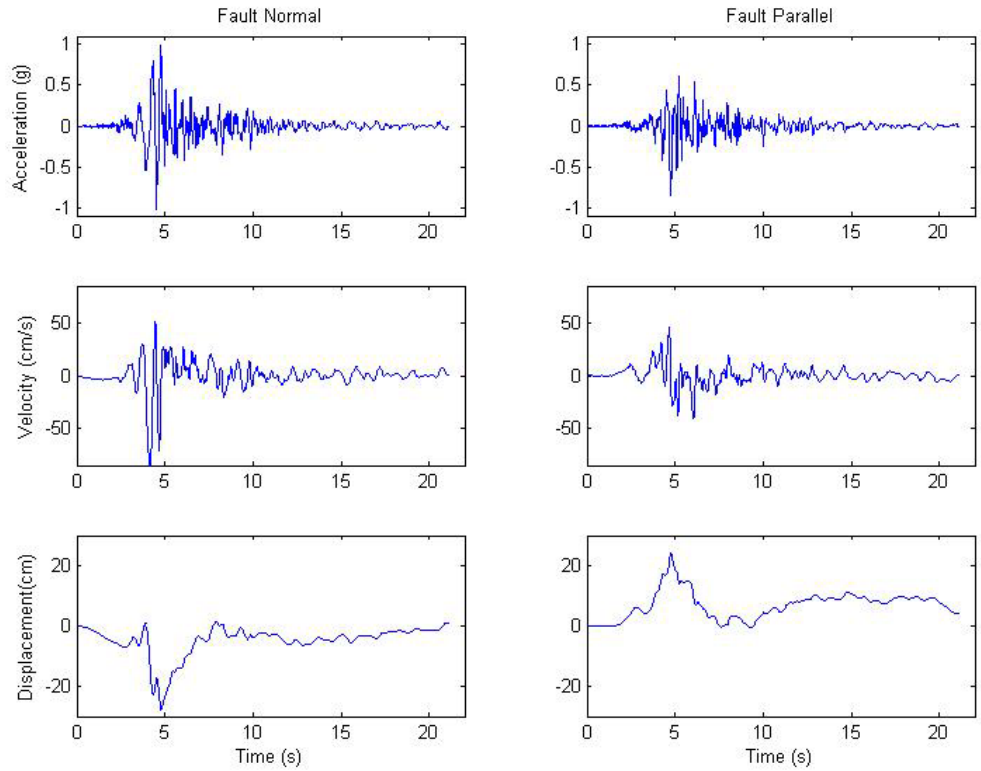


Figure B.1-3: Characteristics of RRS - 5968 (77) Rinaldi Receiving Sta



CSMIP Strong Motion Data
 Thick lines are Fault Normal,
 Thin lines are Fault Parallel
 Reference Line is FN/FP Ratio from
 Somerville et al.(1997) for
 $M_w=7.5, R=0$ (Maximum Directivity Conditions)

Period for $S_{vfn}(\max)$
 0.66 [0.64, 0.67] s
 Period for $S_{vfp}(\max)$
 0.44 [0.43, 0.45] s

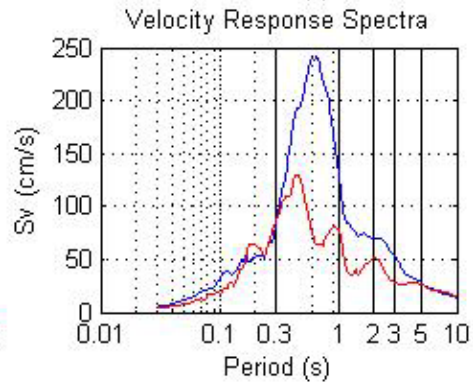
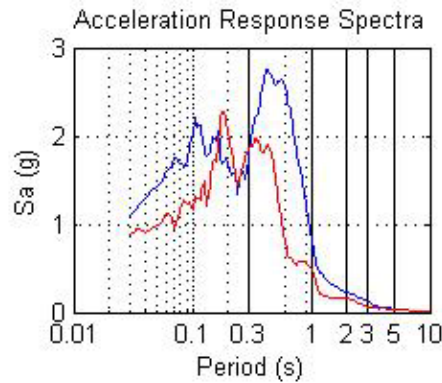
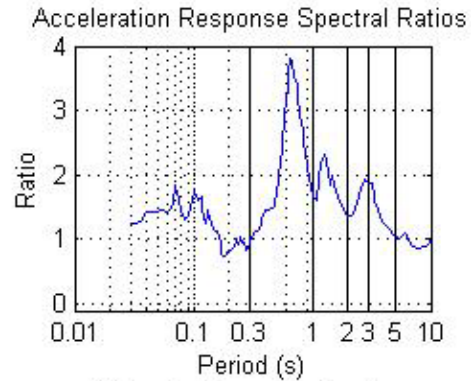
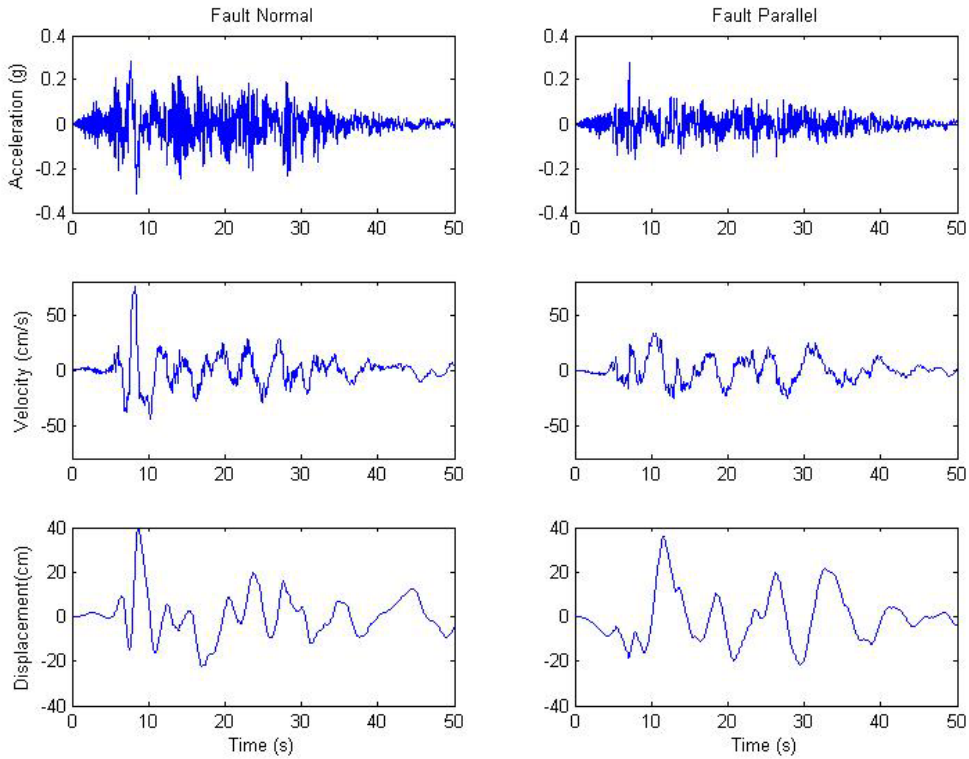


Figure B.1-4: Characteristics of F14 - Fault Zone14



PACIFIC ENGINEERING AND ANALYSIS STRONG-MOTION DATA
 Thick lines are Fault Normal,
 Thin lines are Fault Parallel
 Reference Line is FN/FP Ratio from
 Somerville et al.(1997) for
 $M_w=7.5, R=0$ (Maximum Directivity Conditions)

Period for $S_{vfn}(max)$
 2.00 [1.80, 2.20] s
 Period for $S_{vfp}(max)$
 6.99 [5.99, 8.00] s

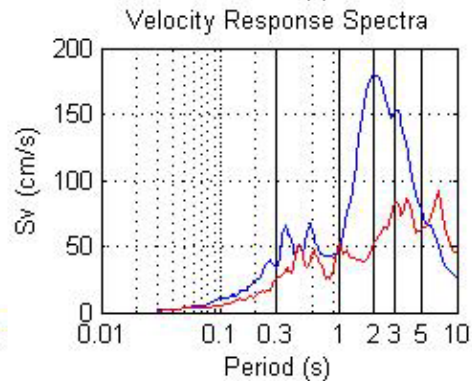
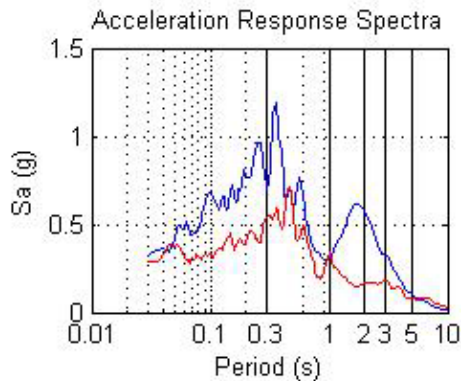
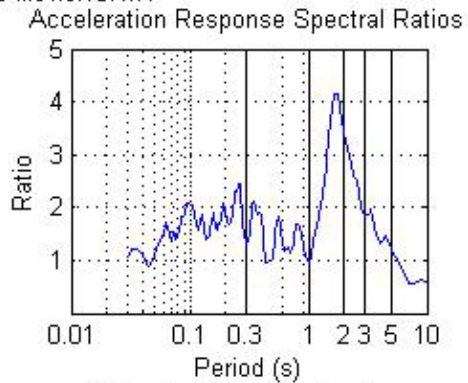
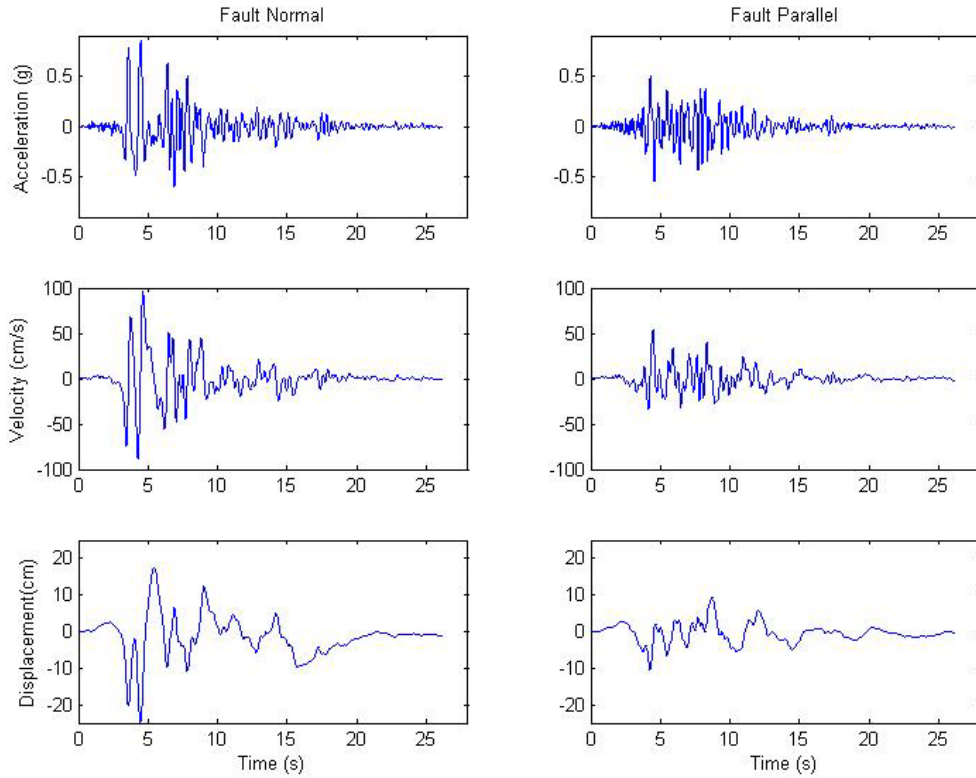


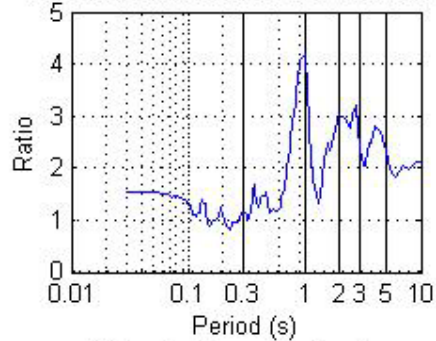
Figure B.1-5: Characteristics of T75 - TCU075-W (g)



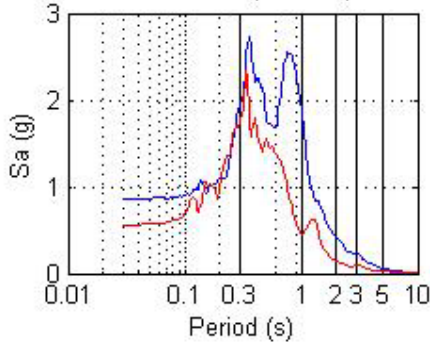
PACIFIC ENGINEERING AND ANALYSIS STRONG-MOTION DATA
 Thick lines are Fault Normal,
 Thin lines are Fault Parallel
 Reference Line is FN/FP Ratio from
 Somerville et al.(1997) for
 $M_w=7.5, R=0$ (Maximum Directivity Conditions)

Period for $S_{vfn}(\max)$
 0.85 [0.83, 0.90] s
 Period for $S_{vfp}(\max)$
 0.67 [0.66, 0.68] s

Acceleration Response Spectral Ratios



Acceleration Response Spectra



Velocity Response Spectra

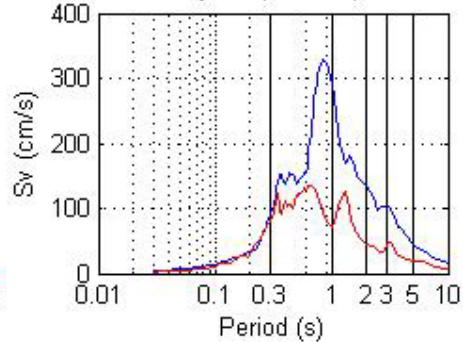
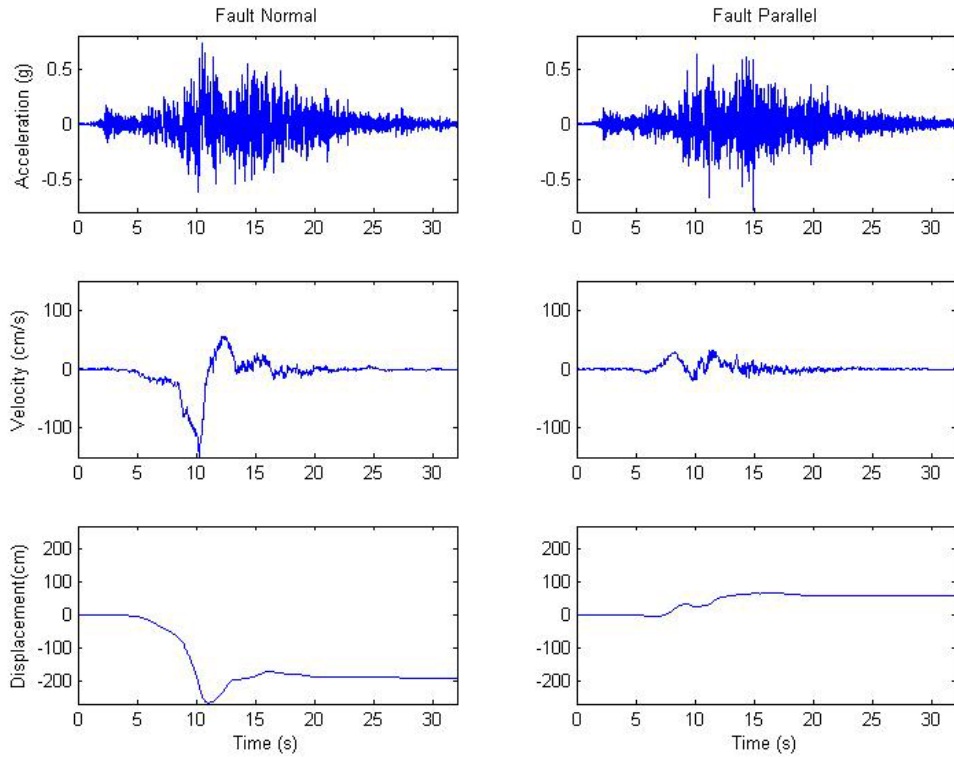


Figure B.1-6: Characteristics of KJM - Kobe



PACIFIC ENGINEERING AND ANALYSIS STRONG-MOTION DATA
 Thick lines are Fault Normal,
 Thin lines are Fault Parallel
 Reference Line is FN/FP Ratio from
 Somerville et al.(1997) for
 Mw=7.5,R=0 (Maximum Directivity Conditions)

Period for Svfn(max)
 4.00 [3.80, 4.50] s
 Period for Svfp(max)
 3.40 [3.33, 3.60] s

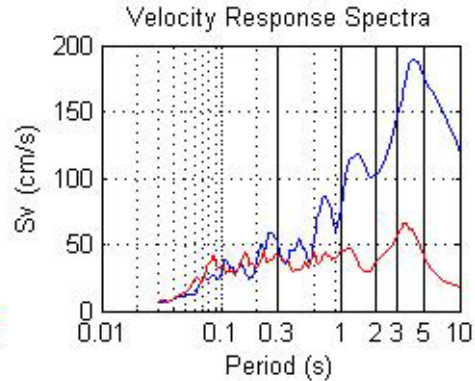
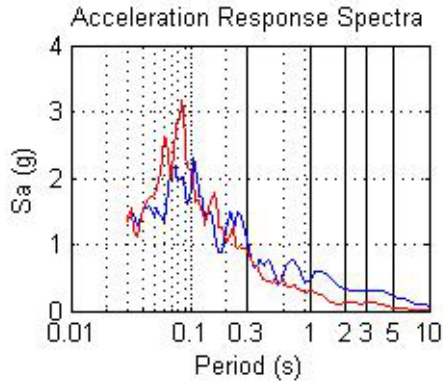
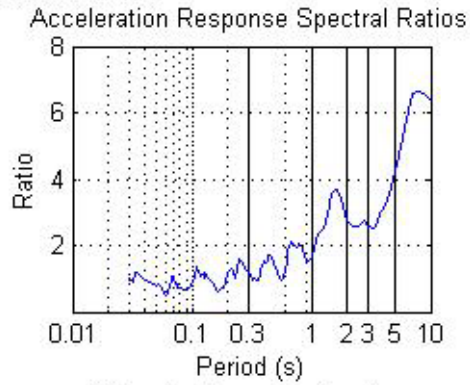
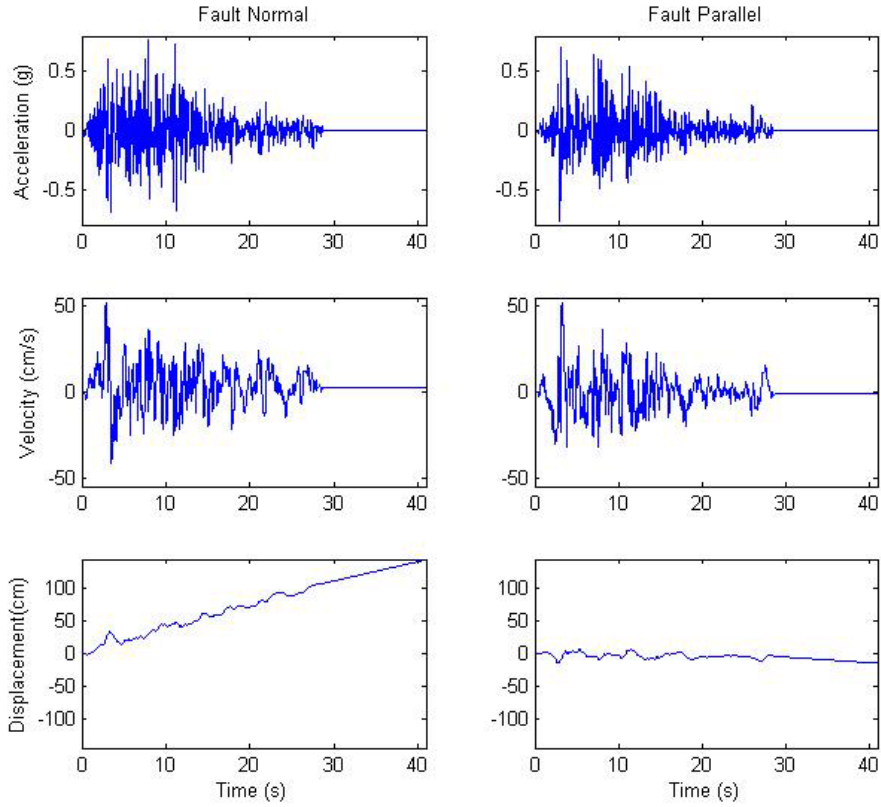


Figure B.1-7: Characteristics of LCN – 24 Lucerne



Site Response Results for Bridge 405 46NE
 Thick lines are Fault Normal,
 Thin lines are Fault Parallel
 Reference Line is FN/FP Ratio from
 Somerville et al.(1997) for
 Mw=7.5,R=0 (Maximum Directivity Conditions)

Period for Svfn(max)
 0.32 [0.32, 0.33] s
 Period for Svfp(max)
 0.30 [0.29, 0.30] s

Acceleration Response Spectral Ratios

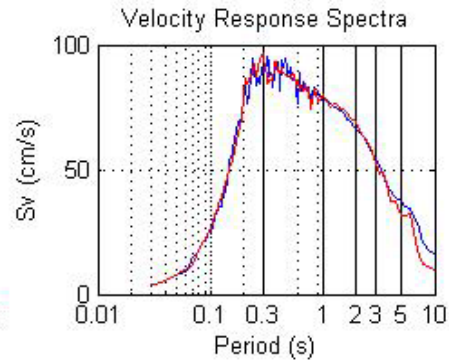
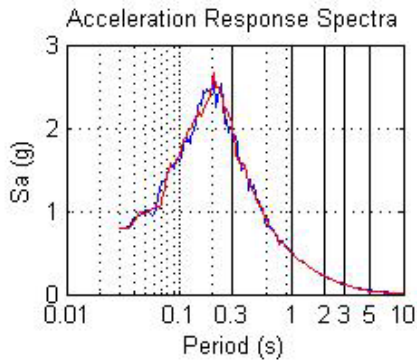
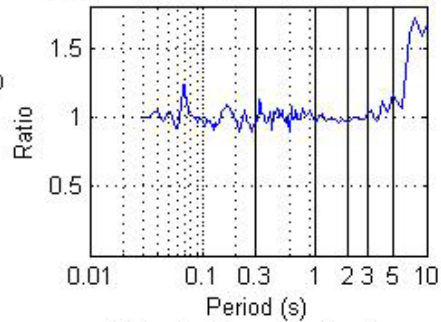
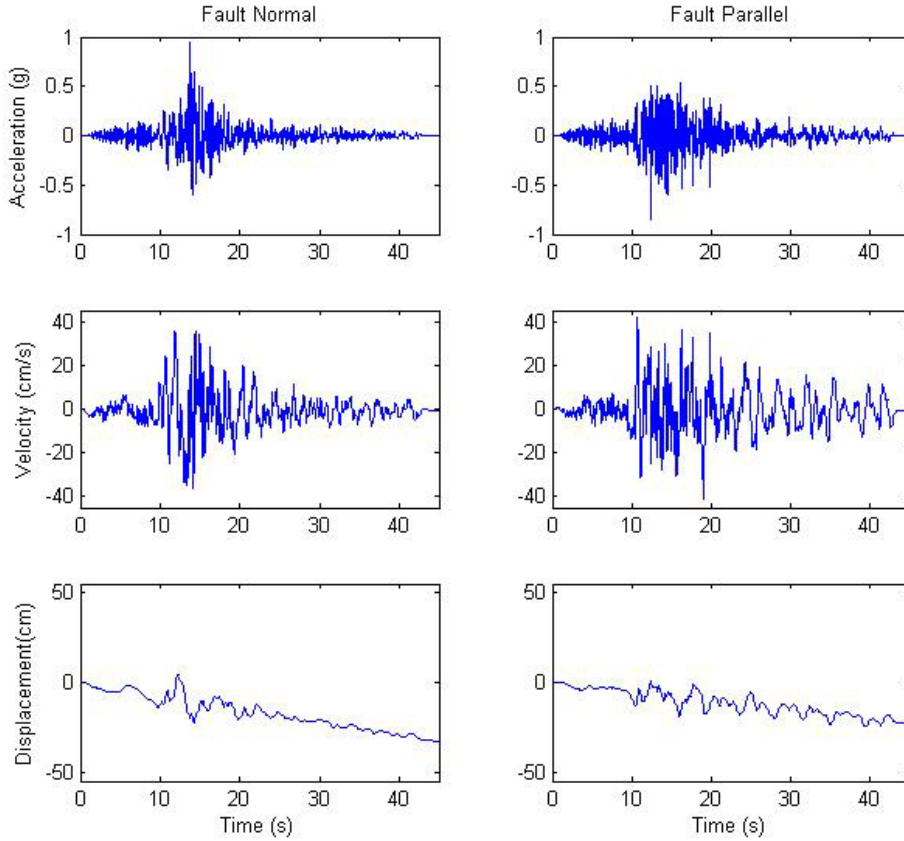


Figure B.1-8: Characteristics of IZT - Izmit, Kocaeli 1999



Site Response Results for Bridge 405 46NE
 Thick lines are Fault Normal,
 Thin lines are Fault Parallel
 Reference Line is FN/FP Ratio from
 Somerville et al.(1997) for
 Mw=7.5,R=0 (Maximum Directivity Conditions)

Period for Svfn(max)
 0.30 [0.30, 0.32] s
 Period for Svfp(max)
 0.36 [0.36, 0.37] s

Acceleration Response Spectral Ratios

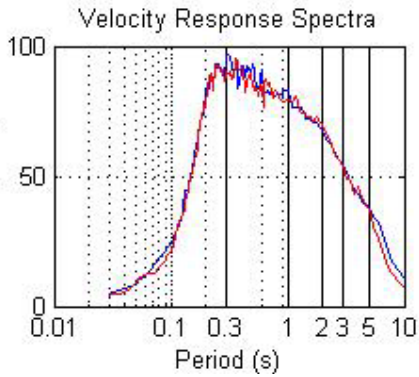
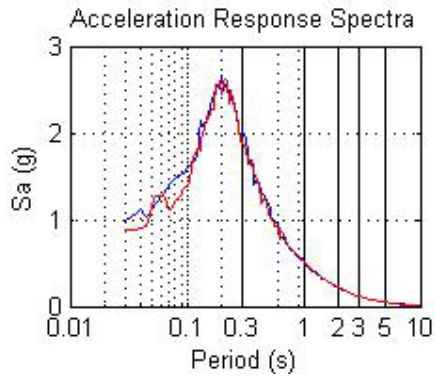
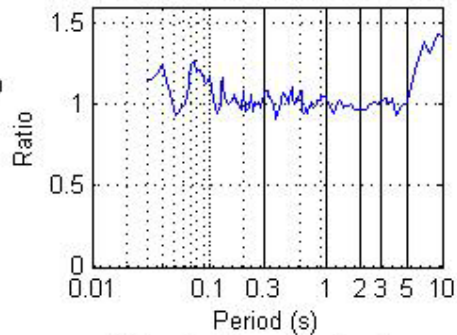
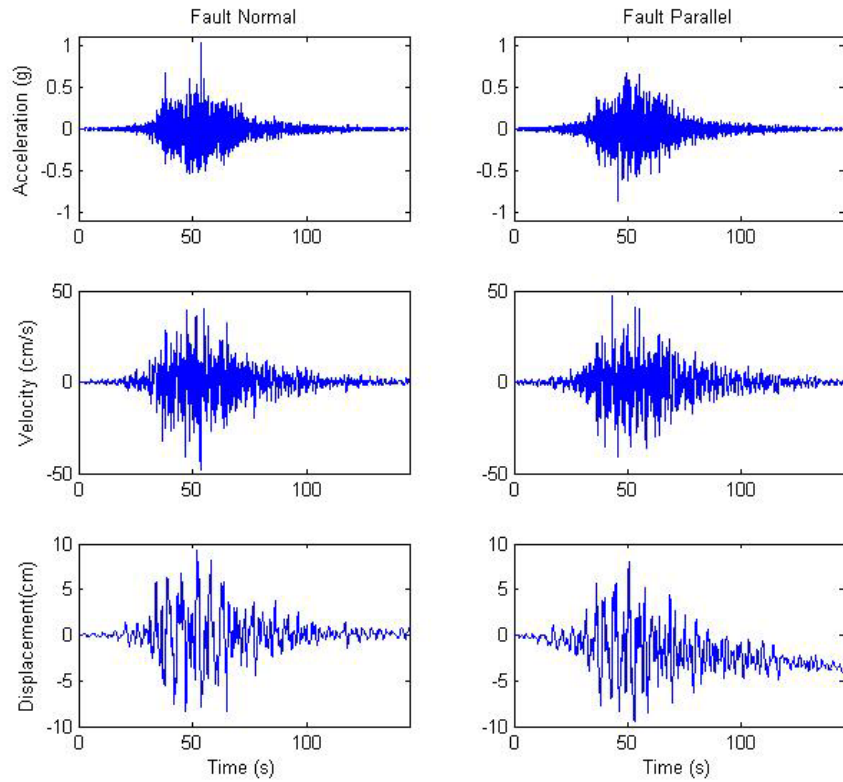


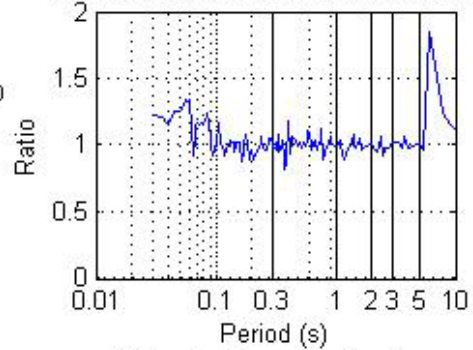
Figure B.1-9: Characteristics of 702 - Fire Station #28, Nisqually 2001



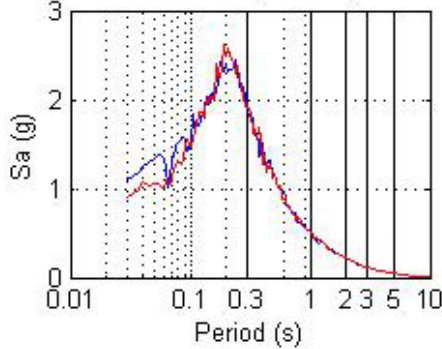
Site Response Results for Bridge 405 46NE
 Thick lines are Fault Normal,
 Thin lines are Fault Parallel
 Reference Line is FN/FP Ratio from
 Somerville et al.(1997) for
 Mw=7.5,R=0 (Maximum Directivity Conditions)

Period for Svfn(max)
 0.40 [0.38, 0.42] s
 Period for Svfp(max)
 0.38 [0.37, 0.38] s

Acceleration Response Spectral Ratios



Acceleration Response Spectra



Velocity Response Spectra

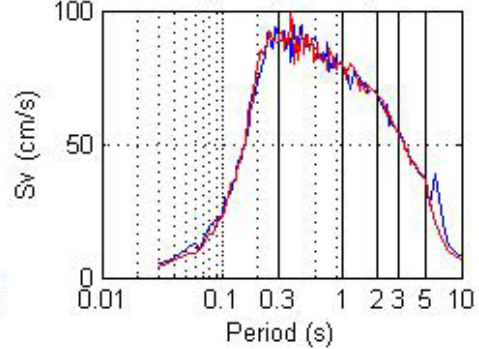
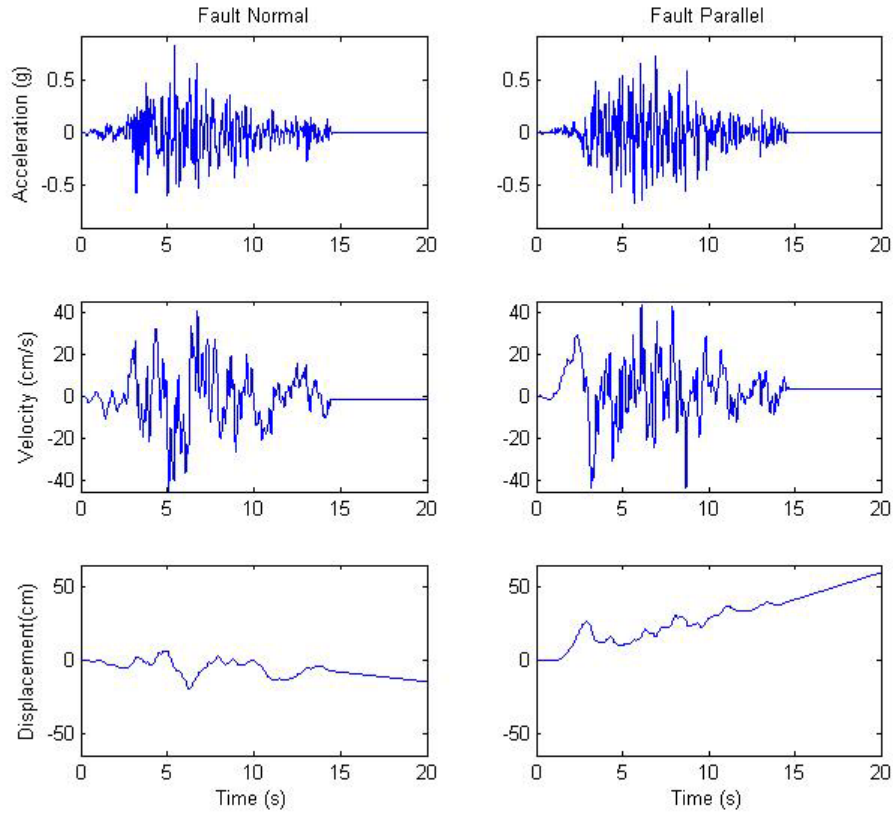


Figure B.1-10: Characteristics of MOQ – Moquegua, Peru 2001



Site Response Results for Bridge 405 46NE
 Thick lines are Fault Normal,
 Thin lines are Fault Parallel
 Reference Line is FN/FP Ratio from
 Somerville et al.(1997) for
 $M_w=7.5, R=0$ (Maximum Directivity Conditions)

Period for $Sv_{fn}(max)$
 0.38 [0.37, 0.38] s
 Period for $Sv_{fp}(max)$
 0.25 [0.24, 0.26] s

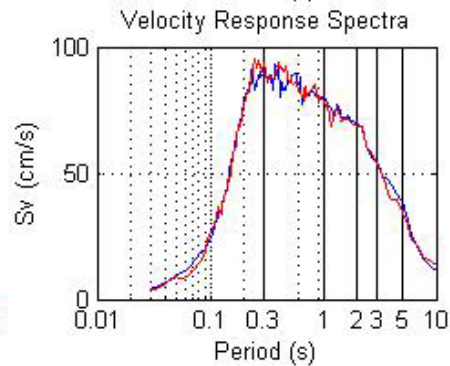
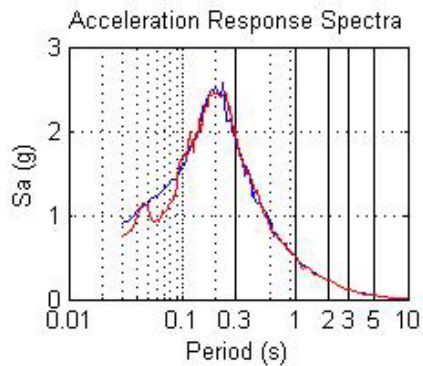
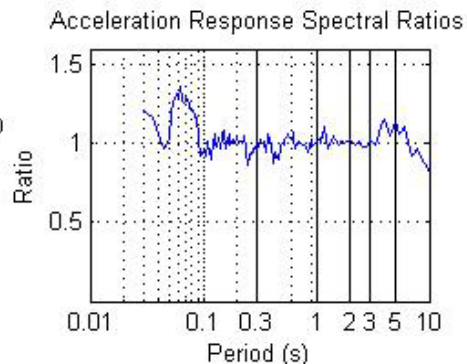
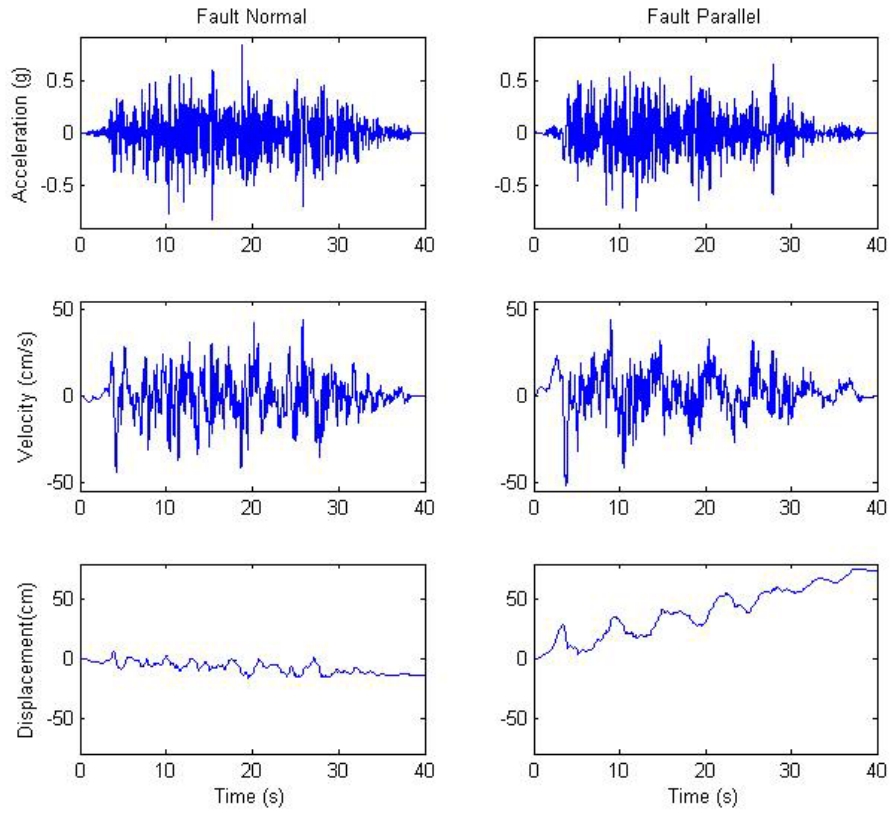


Figure B.1-11: Characteristics of SSU - Santa Susana, Northridge 1994



Site Response Results for Bridge 405 46NE
 Thick lines are Fault Normal,
 Thin lines are Fault Parallel
 Reference Line is FN/FP Ratio from
 Somerville et al.(1997) for
 $M_w=7.5, R=0$ (Maximum Directivity Conditions)

Period for $S_{vfn}(max)$
 0.28 [0.26, 0.28] s
 Period for $S_{vfp}(max)$
 0.44 [0.43, 0.45] s

Acceleration Response Spectral Ratios

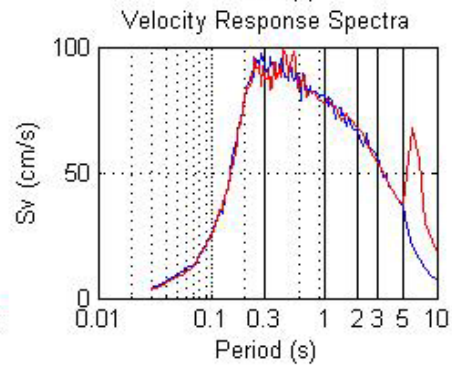
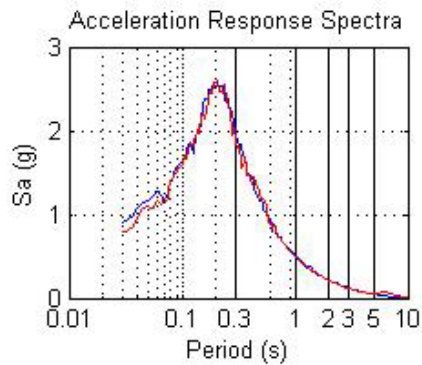
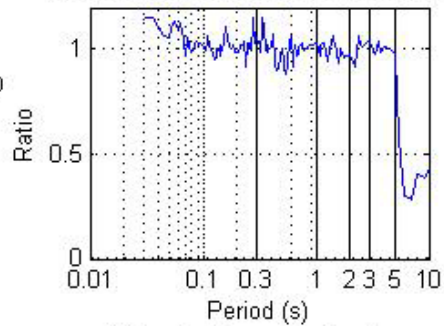


Figure B.1-12: Characteristics of T71 - TCU-071, Chi Chi 1999

B.2 Bridge 405 Input Data

B.2.1 Material Properties

The above stress-strain curves were implemented in the ABAQUS Bridge 405 model. Figures B.2-1 to B.2-3 show the concrete compressive, tensile, and steel strain-stress curves respectively. Table B.2-1 summarizes the material densities used in the models.

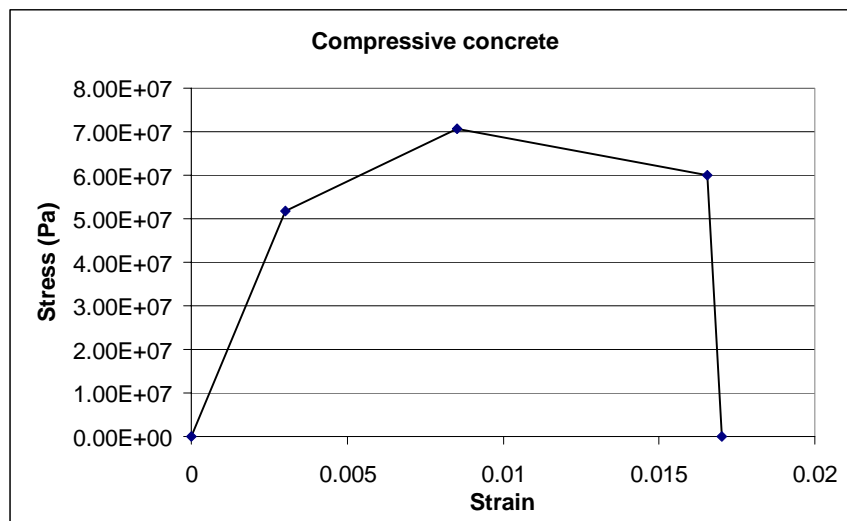


Figure B.2-1: Compressive stress-strain concrete curve

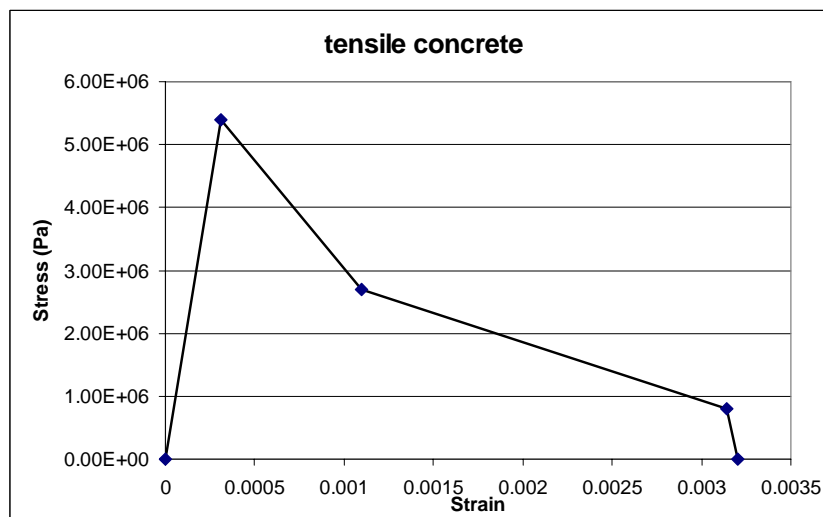


Figure B.2-2: Tensile stress-strain concrete curve

Table B.2-1: Material densities

Densities	
Concrete	2400 kg/m ³
Steel	7500 kg/m ³

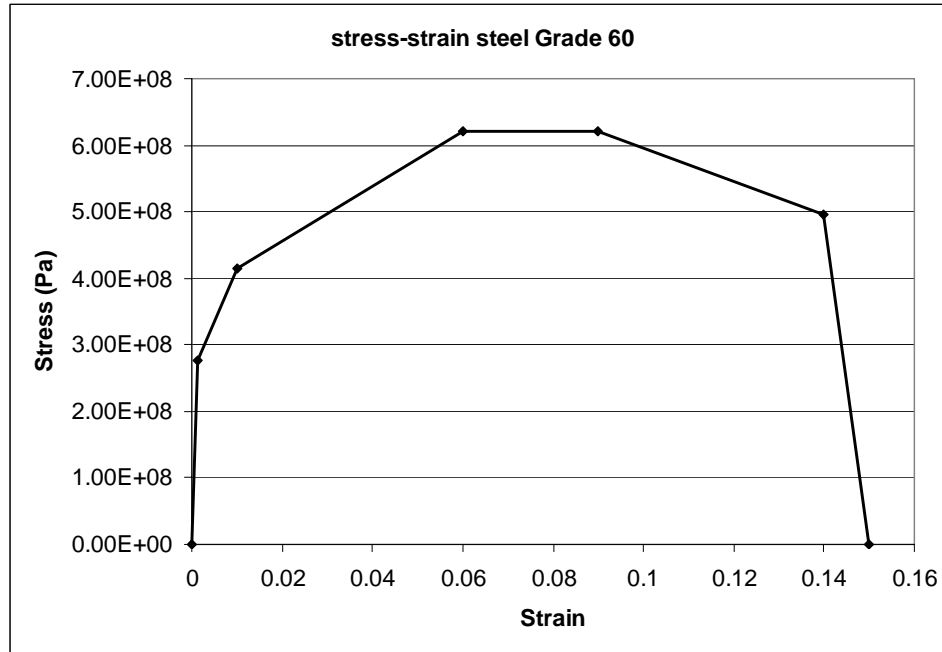


Figure B.2-3: Compressive stress-strain steel 60 curve

B.3 Bridge Output Data

Tables B.3-1, B.3-2, and B.3-3 show the bridge analysis results on the columns, including the maximum curvature, moment, base shear, relative displacement and damage when the GMs were applied in the “Regular” and “Inverse” fashion.

Table B.3-1: Bridge 405 results for the northwest column

Earthquake			Regular					Inverse				
Type	GM	Direction	Max Curvature (1/m)	Max Moment (N.m)	Max Base Shear (N)	Max Disp (m)	Damage	Max Curvature (1/m)	Max Moment (N.m)	Max Base Shear (N)	Max Disp (m)	Damage
Non FD	IZT	Longi.	0.0125	1.502E+06	2.452E+05	0.0702	5.13E+04	0.0113	1.678E+06	2.618E+05	0.0657	5.48E+04
	IZT	Transv.	0.0046	1.101E+06	4.104E+05	0.0184	5.13E+04	0.0035	9.085E+05	3.634E+05	0.0175	5.48E+04
	702	Longi.	0.0109	1.652E+06	2.708E+05	0.0615	5.42E+04	0.0119	1.589E+06	2.621E+05	0.0664	5.36E+04
	702	Transv.	0.0036	1.033E+06	3.965E+05	0.0183	5.42E+04	0.0048	8.906E+05	3.645E+05	0.0181	5.36E+04
	MOQ	Longi.	0.0119	1.722E+06	2.688E+05	0.0684	1.70E+05	0.0119	1.680E+06	2.727E+05	0.0714	1.55E+05
	MOQ	Transv.	0.0045	7.721E+05	3.126E+05	0.0173	1.70E+05	0.0054	8.668E+05	3.624E+05	0.0192	1.55E+05
	SSU	Longi.	0.0130	1.579E+06	2.523E+05	0.0717	4.85E+04	0.0154	1.609E+06	2.522E+05	0.0791	5.52E+04
	SSU	Transv.	0.0042	8.875E+05	3.537E+05	0.0188	4.85E+04	0.0043	8.986E+05	3.659E+05	0.0188	5.52E+04
	T71	Longi.	0.0122	1.601E+06	2.737E+05	0.0701	6.91E+04	0.0123	1.592E+06	2.685E+05	0.0667	1.21E+05
T71	Transv.	0.0045	9.688E+05	3.798E+05	0.0199	6.91E+04	0.0044	9.102E+05	3.643E+05	0.0194	1.21E+05	
FD (6.5)	BAM	Longi.	0.0115	1.607E+06	2.748E+05	0.0689	1.92E+04	0.0156	1.901E+06	3.353E+05	0.0903	3.90E+04
	BAM	Transv.	0.0052	1.120E+06	4.444E+05	0.0224	1.92E+04	0.0031	7.411E+05	2.993E+05	0.0142	3.90E+04
FD (6.0)	F14	Longi.	0.0089	1.565E+06	2.497E+05	0.0605	1.71E+04	0.0299	1.870E+06	3.237E+05	0.1625	7.76E+04
	F14	Transv.	0.0024	8.969E+05	3.518E+05	0.0136	1.71E+04	0.0041	6.093E+05	3.061E+05	0.0177	7.76E+04
FD (6.9)	KJM	Longi.	0.0202	1.903E+06	3.126E+05	0.1087	6.10E+04	0.0350	2.089E+06	3.613E+05	0.2254	1.26E+05
	KJM	Transv.	0.0020	6.027E+05	2.234E+05	0.0083	6.10E+04	0.0020	2.370E+05	1.210E+05	0.0078	1.26E+05
FD (6.7)	RRS	Longi.	0.0073	1.623E+06	2.591E+05	0.0495	9.78E+03	0.0361	1.824E+06	3.305E+05	0.1976	7.86E+04
	RRS	Transv.	0.0026	7.088E+05	2.643E+05	0.0101	9.78E+03	0.0037	4.579E+05	1.764E+05	0.0108	7.86E+04
FD (6.7)	Sylmar	Longi.	0.0199	1.752E+06	3.120E+05	0.1151	6.43E+04	0.0112	1.710E+06	2.609E+05	0.0645	1.83E+04
	Sylmar	Transv.	0.0038	4.273E+05	1.733E+05	0.0102	6.43E+04	0.0027	4.057E+05	1.915E+05	0.0105	1.83E+04
FD (7.6)	T75	Longi.	0.0052	1.552E+06	2.481E+05	0.0477	2.34E+03	0.0078	1.626E+06	2.663E+05	0.0574	7.91E+03
	T75	Transv.	0.0009	3.742E+05	1.393E+05	0.0054	2.34E+03	0.0005	2.386E+05	8.702E+04	0.0032	7.91E+03
FD (7.3)	LCN	Longi.	0.0032	1.415E+06	2.312E+05	0.0374	4.19E+00	0.0105	1.579E+06	2.763E+05	0.0659	8.49E+03
	LCN	Transv.	0.0010	5.782E+05	2.293E+05	0.0076	4.19E+00	0.0020	5.855E+05	2.184E+05	0.0099	8.49E+03

Table B.3-2: Bridge 520 results for the northwest column

Earthquake			Regular					Inverse				
Type	GM	Direction	Max Curvature (1/m)	Max Moment (N.m)	Max Base Shear (N)	Max Disp (m)	Damage	Max Curvature (1/m)	Max Moment (N.m)	Max Base Shear (N)	Max Disp (m)	Damage
Non FD	IZT	Longi.	0.0084	1.716E+06	2.140E+05	0.0970	2.77E+04	0.0086	1.721E+06	2.212E+05	0.0971	2.92E+04
	IZT	Transv.	0.0020	6.729E+05	2.097E+05	0.0151	2.77E+04	0.0016	5.998E+05	1.969E+05	0.0123	2.92E+04
	702	Longi.	0.0072	1.716E+06	2.238E+05	0.0892	2.94E+04	0.0082	1.683E+06	2.161E+05	0.0926	2.72E+04
	702	Transv.	0.0019	5.647E+05	2.040E+05	0.0142	2.94E+04	0.0017	5.219E+05	1.770E+05	0.0123	2.72E+04
	SSU	Longi.	0.0086	1.687E+06	2.211E+05	0.0957	2.16E+04	0.0071	1.738E+06	2.211E+05	0.0933	1.23E+04
	SSU	Transv.	0.0011	7.426E+05	2.237E+05	0.0136	2.16E+04	0.0014	6.420E+05	1.962E+05	0.0119	1.23E+04
	T71	Longi.	0.0079	1.653E+06	2.266E+05	0.0934	4.35E+04	0.0089	1.707E+06	2.271E+05	0.0953	6.59E+04
	T71	Transv.	0.0019	5.564E+05	2.046E+05	0.0137	4.35E+04	0.0021	5.554E+05	1.895E+05	0.0141	6.59E+04
FD (6.5)	BAM	Longi.	0.0037	1.573E+06	2.200E+05	0.0656	4.26E+02	0.0088	1.877E+06	2.707E+05	0.1027	1.88E+04
	BAM	Transv.	0.0022	9.855E+05	3.065E+05	0.0205	4.26E+02	0.0019	5.257E+05	1.764E+05	0.0118	1.88E+04
FD (6.0)	F14	Longi.	0.0035	1.518E+06	2.013E+05	0.0625	2.79E+02	0.0204	1.976E+06	2.787E+05	0.1922	5.21E+04
	F14	Transv.	0.0011	6.737E+05	2.282E+05	0.0118	2.79E+02	0.0026	4.272E+05	1.746E+05	0.0152	5.21E+04
FD (6.9)	KJM	Longi.	0.0115	1.870E+06	2.449E+05	0.1155	3.47E+04	0.0312	2.151E+06	3.018E+05	0.3140	1.64E+05
	KJM	Transv.	0.0011	3.711E+05	1.261E+05	0.0070	3.47E+04	0.0013	1.463E+05	8.270E+04	0.0070	1.64E+05
FD (6.7)	RRS	Longi.	0.0030	1.472E+06	1.935E+05	0.0589	1.52E+01	0.0233	1.860E+06	2.786E+05	0.2206	7.92E+04
	RRS	Transv.	0.0007	4.769E+05	1.573E+05	0.0083	1.52E+01	0.0016	2.925E+05	9.117E+04	0.0086	7.92E+04
FD (6.7)	Sylmar	Longi.	0.0081	1.683E+06	2.226E+05	0.0921	1.99E+04	0.0045	1.634E+06	2.161E+05	0.0717	1.53E+03
	Sylmar	Transv.	0.0007	5.076E+05	1.539E+05	0.0088	1.99E+04	0.0016	8.315E+05	2.648E+05	0.0169	1.53E+03
FD (7.6)	T75	Longi.	0.0015	1.046E+06	1.336E+05	0.0346	0.00E+00	0.0027	1.426E+06	1.837E+05	0.0533	0.00E+00
	T75	Transv.	0.0003	2.401E+05	7.139E+04	0.0042	0.00E+00	0.0002	1.521E+05	4.756E+04	0.0026	0.00E+00
FD (7.3)	LCN	Longi.	0.0026	1.439E+06	2.157E+05	0.0514	0.00E+00	0.0047	1.655E+06	2.399E+05	0.0749	6.20E+02
	LCN	Transv.	0.0005	3.684E+05	1.314E+05	0.0065	0.00E+00	0.0011	5.636E+05	1.862E+05	0.0111	6.20E+02

Table B.3-3: Bridge 90 results for the northern column (C₄)

Earthquake			Regular					Inverse				
Type	GM	Direction	Max Curvature (1/m)	Max Moment (N.m)	Max Base Shear (N)	Max Disp (m)	Damage	Max Curvature (1/m)	Max Moment (N.m)	Max Base Shear (N)	Max Disp (m)	Damage
Non FD	IZT	Longi.	0.0019	3.345E+06	7.638E+05	0.0753	1.96E+05	0.0150	2.653E+06	7.295E+05	0.0609	1.96E+05
	IZT	Transv.	0.1099	3.330E+06	8.295E+05	0.0300	1.96E+05	0.0030	2.393E+06	8.510E+05	0.0318	1.96E+05
	702	Longi.	0.0181	2.578E+06	7.640E+05	0.0695	2.28E+05	0.0152	2.533E+06	7.455E+05	0.0641	2.28E+05
	702	Transv.	0.0028	2.364E+06	8.121E+05	0.0297	2.28E+05	0.0025	2.635E+06	9.084E+05	0.0336	2.28E+05
	MOQ	Longi.	0.0204	2.759E+06	7.773E+05	0.0753	2.23E+05	0.0208	2.542E+06	7.773E+05	0.0758	2.60E+05
	MOQ	Transv.	0.0028	2.403E+06	8.166E+05	0.0258	2.23E+05	0.0026	2.616E+06	8.818E+05	0.0298	2.60E+05
	SSU	Longi.	0.0184	2.641E+06	7.791E+05	0.0702	1.24E+05	0.0206	2.754E+06	8.049E+05	0.0788	1.83E+05
	SSU	Transv.	0.0021	2.090E+06	7.060E+05	0.0329	1.24E+05	0.0035	2.479E+06	8.788E+05	0.0359	1.83E+05
	T71	Longi.	0.0176	2.598E+06	7.647E+05	0.0704	1.89E+05	0.0204	2.561E+06	7.537E+05	0.0764	3.25E+05
T71	Transv.	0.0024	2.114E+06	7.081E+05	0.0296	1.89E+05	0.0033	2.434E+06	8.605E+05	0.0311	3.25E+05	
FD (6.5)	BAM	Longi.	0.0103	2.622E+06	7.398E+05	0.0466	1.28E+04	0.0252	2.786E+06	7.949E+05	0.0921	1.61E+05
	BAM	Transv.	0.0020	2.626E+06	6.776E+05	0.0178	1.28E+04	0.0033	2.278E+06	7.070E+05	0.0184	1.61E+05
FD (6.0)	F14	Longi.	0.0117	2.376E+06	6.674E+05	0.0509	5.74E+04	0.0340	3.099E+06	9.239E+05	0.1274	1.40E+05
	F14	Transv.	0.0037	3.544E+06	1.142E+06	0.0494	5.74E+04	0.0047	1.949E+06	6.574E+05	0.0314	1.40E+05
FD (6.9)	KJM	Longi.	0.0160	2.609E+06	7.049E+05	0.0677	1.19E+05	0.0539	3.225E+06	9.454E+05	0.2053	1.19E+05
	KJM	Transv.	0.0041	2.856E+06	8.997E+05	0.0320	1.19E+05	0.0050	1.965E+06	6.061E+05	0.0366	1.19E+05
FD (6.7)	RRS	Longi.	0.0121	2.200E+06	6.455E+05	0.0515	2.61E+04	0.0451	2.931E+06	8.586E+05	0.1887	3.81E+04
	RRS	Transv.	0.0036	3.301E+06	9.938E+05	0.0333	2.61E+04	0.0043	1.817E+06	5.770E+05	0.0186	3.81E+04
FD (6.7)	Sylmar	Longi.	0.0199	2.910E+06	7.749E+05	0.0783	1.09E+05	0.0152	2.718E+06	7.016E+05	0.0623	1.09E+05
	Sylmar	Transv.	0.0025	2.036E+06	7.307E+05	0.0241	1.09E+05	0.0032	3.134E+06	1.072E+06	0.0383	1.09E+05
FD (7.6)	T75	Longi.	0.0080	2.356E+06	6.680E+05	0.0402	4.18E+03	0.0099	2.375E+06	6.816E+05	0.0461	1.48E+04
	T75	Transv.	0.0010	1.242E+06	4.080E+05	0.0125	4.18E+03	0.0012	1.396E+06	4.729E+05	0.0132	1.48E+04
FD (7.3)	LCN	Longi.	0.0097	2.552E+06	6.988E+05	0.0462	6.64E+03	0.0091	2.425E+06	6.883E+05	0.0439	7.95E+03
	LCN	Transv.	0.0011	1.674E+06	4.829E+05	0.0102	6.64E+03	0.0012	1.366E+06	4.156E+05	0.0092	7.95E+03

B.4 Bridges Finite Element Input Files

Bridge 405

*Heading

** Job name: 405bridge Model name: 405bridge

*Preprint, echo=NO, model=YES, history=NO, contact=NO

**

** PARTS

**

*Part, name=BRIDGE

*Node

1,	0.,	0.,	0.
2,	1.98125005,	0.,	0.
3,	3.9625001,	0.,	0.
4,	5.9437499,	0.,	0.
5,	7.92500019,	0.,	0.
6,	9.90625,	0.,	0.
7,	11.8874998,	0.,	0.
8,	13.8687496,	0.,	0.
9,	15.8500004,	0.,	0.
10,	18.1737499,	0.,	0.
11,	20.4974995,	0.,	0.
12,	22.8212509,	0.,	0.
13,	25.1450005,	0.,	0.
14,	27.46875,	0.,	0.
15,	29.7924995,	0.,	0.
16,	32.1162491,	0.,	0.
17,	34.4399986,	0.,	0.
18,	36.4212494,	0.,	0.
19,	38.4025002,	0.,	0.
20,	40.3837509,	0.,	0.
21,	42.3650017,	0.,	0.
22,	44.3462486,	0.,	0.
23,	46.3274994,	0.,	0.
24,	48.3087502,	0.,	0.
25,	50.2900009,	0.,	0.
26,	15.8500004,	-3.5,	0.
27,	15.8500004,	-2.50939989,	0.
28,	15.8500004,	-1.51880002,	0.
29,	15.8500004,	-0.75940001,	0.
30,	15.8500004,	0.,	0.
31,	15.8500004,	0.75940001,	0.
32,	15.8500004,	1.51880002,	0.
33,	15.8500004,	2.50939989,	0.
34,	15.8500004,	3.5,	0.

35,	34.4399986,	-3.5,	0.
36,	34.4399986,	-2.50939989,	0.
37,	34.4399986,	-1.51880002,	0.
38,	34.4399986,	-0.75940001,	0.
39,	34.4399986,	0.,	0.
40,	34.4399986,	0.75940001,	0.
41,	34.4399986,	1.51880002,	0.
42,	34.4399986,	2.50939989,	0.
43,	34.4399986,	3.5,	0.
44,	15.8500004,	-1.51880002,	0.
45,	15.8500004,	-1.51880002,	-0.26943332
46,	15.8500004,	-1.51880002,	-0.538866639
47,	15.8500004,	-1.51880002,	-0.808300018
48,	15.8500004,	-1.51880002,	-1.07773328
49,	15.8500004,	-1.51880002,	-1.34716666
50,	15.8500004,	-1.51880002,	-1.61660004
51,	15.8500004,	-1.51880002,	-1.8860333
52,	15.8500004,	-1.51880002,	-2.15546656
53,	15.8500004,	-1.51880002,	-2.42490005
54,	15.8500004,	-1.51880002,	-2.69433331
55,	15.8500004,	-1.51880002,	-2.96376657
56,	15.8500004,	-1.51880002,	-3.23320007
57,	15.8500004,	-1.51880002,	-3.50263333
58,	15.8500004,	-1.51880002,	-3.77206659
59,	15.8500004,	-1.51880002,	-4.04150009
60,	15.8500004,	-1.51880002,	-4.31093311
61,	15.8500004,	-1.51880002,	-4.58036661
62,	15.8500004,	-1.51880002,	-4.84980011
63,	15.8500004,	-1.51880002,	-5.11923313
64,	15.8500004,	-1.51880002,	-5.38866663
65,	15.8500004,	-1.51880002,	-5.65810013
66,	15.8500004,	-1.51880002,	-5.92753315
67,	15.8500004,	-1.51880002,	-6.19696665
68,	15.8500004,	-1.51880002,	-6.46640015
69,	15.8500004,	1.51880002,	0.
70,	15.8500004,	1.51880002,	-0.26943332
71,	15.8500004,	1.51880002,	-0.538866639
72,	15.8500004,	1.51880002,	-0.808300018
73,	15.8500004,	1.51880002,	-1.07773328
74,	15.8500004,	1.51880002,	-1.34716666
75,	15.8500004,	1.51880002,	-1.61660004
76,	15.8500004,	1.51880002,	-1.8860333
77,	15.8500004,	1.51880002,	-2.15546656
78,	15.8500004,	1.51880002,	-2.42490005
79,	15.8500004,	1.51880002,	-2.69433331
80,	15.8500004,	1.51880002,	-2.96376657
81,	15.8500004,	1.51880002,	-3.23320007

82, 15.8500004, 1.51880002, -3.50263333
83, 15.8500004, 1.51880002, -3.77206659
84, 15.8500004, 1.51880002, -4.04150009
85, 15.8500004, 1.51880002, -4.31093311
86, 15.8500004, 1.51880002, -4.58036661
87, 15.8500004, 1.51880002, -4.84980011
88, 15.8500004, 1.51880002, -5.11923313
89, 15.8500004, 1.51880002, -5.38866663
90, 15.8500004, 1.51880002, -5.65810013
91, 15.8500004, 1.51880002, -5.92753315
92, 15.8500004, 1.51880002, -6.19696665
93, 15.8500004, 1.51880002, -6.46640015
94, 34.4399986, -1.51880002, 0.
95, 34.4399986, -1.51880002, -0.26943332
96, 34.4399986, -1.51880002, -0.538866639
97, 34.4399986, -1.51880002, -0.808300018
98, 34.4399986, -1.51880002, -1.07773328
99, 34.4399986, -1.51880002, -1.34716666
100, 34.4399986, -1.51880002, -1.61660004
101, 34.4399986, -1.51880002, -1.8860333
102, 34.4399986, -1.51880002, -2.15546656
103, 34.4399986, -1.51880002, -2.42490005
104, 34.4399986, -1.51880002, -2.69433331
105, 34.4399986, -1.51880002, -2.96376657
106, 34.4399986, -1.51880002, -3.23320007
107, 34.4399986, -1.51880002, -3.50263333
108, 34.4399986, -1.51880002, -3.77206659
109, 34.4399986, -1.51880002, -4.04150009
110, 34.4399986, -1.51880002, -4.31093311
111, 34.4399986, -1.51880002, -4.58036661
112, 34.4399986, -1.51880002, -4.84980011
113, 34.4399986, -1.51880002, -5.11923313
114, 34.4399986, -1.51880002, -5.38866663
115, 34.4399986, -1.51880002, -5.65810013
116, 34.4399986, -1.51880002, -5.92753315
117, 34.4399986, -1.51880002, -6.19696665
118, 34.4399986, -1.51880002, -6.46640015
119, 34.4399986, 1.51880002, 0.
120, 34.4399986, 1.51880002, -0.26943332
121, 34.4399986, 1.51880002, -0.538866639
122, 34.4399986, 1.51880002, -0.808300018
123, 34.4399986, 1.51880002, -1.07773328
124, 34.4399986, 1.51880002, -1.34716666
125, 34.4399986, 1.51880002, -1.61660004
126, 34.4399986, 1.51880002, -1.8860333
127, 34.4399986, 1.51880002, -2.15546656
128, 34.4399986, 1.51880002, -2.42490005

129, 34.4399986, 1.51880002, -2.69433331
 130, 34.4399986, 1.51880002, -2.96376657
 131, 34.4399986, 1.51880002, -3.23320007
 132, 34.4399986, 1.51880002, -3.50263333
 133, 34.4399986, 1.51880002, -3.77206659
 134, 34.4399986, 1.51880002, -4.04150009
 135, 34.4399986, 1.51880002, -4.31093311
 136, 34.4399986, 1.51880002, -4.58036661
 137, 34.4399986, 1.51880002, -4.84980011
 138, 34.4399986, 1.51880002, -5.11923313
 139, 34.4399986, 1.51880002, -5.38866663
 140, 34.4399986, 1.51880002, -5.65810013
 141, 34.4399986, 1.51880002, -5.92753315
 142, 34.4399986, 1.51880002, -6.19696665
 143, 34.4399986, 1.51880002, -6.46640015
 144, 15.8500004, -3.96239996, -6.46640015
 145, 15.8500004, -2.74060011, -6.46640015
 146, 15.8500004, -1.51880002, -6.46640015
 147, 15.8500004, -0.75940001, -6.46640015
 148, 15.8500004, 0., -6.46640015
 149, 15.8500004, 0.75940001, -6.46640015
 150, 15.8500004, 1.51880002, -6.46640015
 151, 15.8500004, 2.74060011, -6.46640015
 152, 15.8500004, 3.96239996, -6.46640015
 153, 34.4399986, -3.96239996, -6.46640015
 154, 34.4399986, -2.74060011, -6.46640015
 155, 34.4399986, -1.51880002, -6.46640015
 156, 34.4399986, -0.75940001, -6.46640015
 157, 34.4399986, 0., -6.46640015
 158, 34.4399986, 0.75940001, -6.46640015
 159, 34.4399986, 1.51880002, -6.46640015
 160, 34.4399986, 2.74060011, -6.46640015
 161, 34.4399986, 3.96239996, -6.46640015
 162, -0.0500000007, 0., 0.
 163, 50.3400002, 0., 0.
 164, 15.8500004, 0., -6.51640034
 165, 34.4399986, 0., -6.51640034
 166, -0.0500000007, 0., 0.
 167, 50.3400002, 0., 0.
 168, -0.0250000004, 0., 0.
 169, 50.3149986, 0., 0.

*Element, type=B32

1, 1, 2, 3
 2, 3, 4, 5
 3, 5, 6, 7
 4, 7, 8, 9
 5, 9, 10, 11

6, 11, 12, 13
7, 13, 14, 15
8, 15, 16, 17
9, 17, 18, 19
10, 19, 20, 21
11, 21, 22, 23
12, 23, 24, 25
13, 26, 27, 28
14, 28, 29, 30
15, 30, 31, 32
16, 32, 33, 34
17, 35, 36, 37
18, 37, 38, 39
19, 39, 40, 41
20, 41, 42, 43
21, 44, 45, 46
22, 46, 47, 48
23, 48, 49, 50
24, 50, 51, 52
25, 52, 53, 54
26, 54, 55, 56
27, 56, 57, 58
28, 58, 59, 60
29, 60, 61, 62
30, 62, 63, 64
31, 64, 65, 66
32, 66, 67, 68
33, 69, 70, 71
34, 71, 72, 73
35, 73, 74, 75
36, 75, 76, 77
37, 77, 78, 79
38, 79, 80, 81
39, 81, 82, 83
40, 83, 84, 85
41, 85, 86, 87
42, 87, 88, 89
43, 89, 90, 91
44, 91, 92, 93
45, 94, 95, 96
46, 96, 97, 98
47, 98, 99, 100
48, 100, 101, 102
49, 102, 103, 104
50, 104, 105, 106
51, 106, 107, 108
52, 108, 109, 110

53, 110, 111, 112
54, 112, 113, 114
55, 114, 115, 116
56, 116, 117, 118
57, 119, 120, 121
58, 121, 122, 123
59, 123, 124, 125
60, 125, 126, 127
61, 127, 128, 129
62, 129, 130, 131
63, 131, 132, 133
64, 133, 134, 135
65, 135, 136, 137
66, 137, 138, 139
67, 139, 140, 141
68, 141, 142, 143
69, 144, 145, 146
70, 146, 147, 148
71, 148, 149, 150
72, 150, 151, 152
73, 153, 154, 155
74, 155, 156, 157
75, 157, 158, 159
76, 159, 160, 161
*Elset, elset=DECK, generate
1, 12, 1
*BEAM GENERAL SECTION, elset=DECK, SECTION=MESHED
0.0,1.0,0.0
*INCLUDE, INPUT=Model405SectionGood.bsp
*Elset, elset=XBEAM2, generate
13, 16, 1
*Elset, elset=XBEAM3, generate
17, 20, 1
*Elset, elset=COLUMNS, generate
21, 68, 1
*Elset, elset=FOOT2, generate
69, 72, 1
*Elset, elset=FOOT3, generate
73, 76, 1
*Nset, nset=NFOOT2
164,
*Nset, nset=NFOOT3
165,
*Nset, nset=NSABUTW
162,
*Nset, nset=NSABUTE
163,


```

*Nset, nset=NABUTW
166,
*Nset, nset=NABUTE
167,
*Nset, nset=NGAPW
168,
*Nset, nset=NGAPE
169,
*Nset, nset=NSABUTSANDFOOT, generate
162, 165, 1
*Nset, nset=NBFOOT2
148,
*Nset, nset=NBFOOT3
157,
*Nset, nset=NBABUTW
1,
*Nset, nset=NBABUTE
25,
*Nset, nset=NBABUTSANDFOOT
1, 25, 148, 157
*Nset, nset=RPXB2
30,
*Nset, nset=RPXB3
39,
*Nset, nset=RPF2
148,
*Nset, nset=RPF3
157,
*Nset, nset=TIENODEF2
144, 145, 147, 149, 151, 152
*Nset, nset=TIENODEF3
153, 154, 156, 158, 160, 161
*Elset, elset="COLUMN SW", generate
21, 32, 1
*Nset, nset=BOTTOM
67,
** Region: (Section-1-XBEAM2:XBEAM2), (Beam Orientation:XBEAM2)
** Section: Section-1-XBEAM2 Profile: Profile-1
*Beam Section, elset=XBEAM2, material=CONCRETE, temperature=GRADIENTS,
section=RECT
1.2192, 1.2192
0.,0.,-1.
** Region: (Section-2-XBEAM3:XBEAM3), (Beam Orientation:XBEAM3)
** Section: Section-2-XBEAM3 Profile: Profile-2
*Beam Section, elset=XBEAM3, material=CONCRETE, temperature=GRADIENTS,
section=RECT
1.2192, 1.2192

```

0.,0.,-1.
 ** Region: (Section-3-COLUMNS:COLUMNS), (Beam Orientation:COLUMNS)
 ** Section: Section-3-COLUMNS Profile: Profile-3
 *Beam Section, elset=COLUMNS, material="CONCRETE COLUMN",
 temperature=GRADIENTS, section=CIRC
 0.4572
 0.,1.,0.
 5, 12
 ** Region: (Section-4-FOOT2:FOOT2), (Beam Orientation:FOOT2)
 ** Section: Section-4-FOOT2 Profile: Profile-4
 *Beam Section, elset=FOOT2, material=CONCRETE, temperature=GRADIENTS,
 section=RECT
 0.9144, 4.2672
 0.,0.,-1.
 ** Region: (Section-5-FOOT3:FOOT3), (Beam Orientation:FOOT3)
 ** Section: Section-5-FOOT3 Profile: Profile-5
 *Beam Section, elset=FOOT3, material=CONCRETE, temperature=GRADIENTS,
 section=RECT
 0.9144, 4.2672
 0.,0.,-1.
 *Element, type=MASS, elset="_PickedSet38_ABUTE MASS_"
 77, 167
 *Mass, elset="_PickedSet38_ABUTE MASS_"
 31715.,
 *Element, type=MASS, elset="_PickedSet39_ABUTW MASS_"
 78, 166
 *Mass, elset="_PickedSet39_ABUTW MASS_"
 31715.,
 *Element, type=Spring2, elset="FOOTS DOF1-spring"
 79, 164, 148
 80, 165, 157
 *Spring, elset="FOOTS DOF1-spring"
 1, 1
 6.06e+09
 *Element, type=Spring2, elset="FOOTS DOF2-spring"
 81, 164, 148
 82, 165, 157
 *Spring, elset="FOOTS DOF2-spring"
 2, 2
 6.39e+09
 *Element, type=Spring2, elset="FOOTS DOF3-spring"
 83, 164, 148
 84, 165, 157
 *Spring, elset="FOOTS DOF3-spring"
 3, 3
 5.34e+09
 *Element, type=Spring2, elset="FOOTS DOF4-spring"

```

85, 164, 148
86, 165, 157
*Spring, elset="FOOTS DOF4-spring"
4, 4
3.5e+10
*Element, type=Spring2, elset="FOOTS DOF5-spring"
87, 164, 148
88, 165, 157
*Spring, elset="FOOTS DOF5-spring"
5, 5
7.86e+10
*Element, type=Spring2, elset="FOOTS DOF6-spring"
89, 164, 148
90, 165, 157
*Spring, elset="FOOTS DOF6-spring"
6, 6
9.79e+10
*End Part
**
**
** ASSEMBLY
**
*Assembly, name=Assembly
**
*Instance, name=BRIDGE-1, part=BRIDGE
** REBAR FOR WHOLE COLUMNS
**
*REBAR,ELEMENT=BEAM,MATERIAL="Steel Rebar",NAME=RB1
COLUMNS, 0.00064473, 0.36295125, 0.20955
*REBAR,ELEMENT=BEAM,MATERIAL="Steel Rebar",NAME=RB2
COLUMNS,0.00064473, 0.20955, 0.36295125
*REBAR,ELEMENT=BEAM,MATERIAL="Steel Rebar",NAME=RB3
COLUMNS,0.00064473, 0, 0.4191
*REBAR,ELEMENT=BEAM,MATERIAL="Steel Rebar",NAME=RB4
COLUMNS,0.00064473, -0.20955, 0.36295125
*REBAR,ELEMENT=BEAM,MATERIAL="Steel Rebar",NAME=RB5
COLUMNS,0.00064473, -0.36295125, 0.20955
*REBAR,ELEMENT=BEAM,MATERIAL="Steel Rebar",NAME=RB6
COLUMNS,0.00064473, -0.4191, 0
*REBAR,ELEMENT=BEAM,MATERIAL="Steel Rebar",NAME=RB7
COLUMNS,0.00064473, -0.36295125, -0.20955
*REBAR,ELEMENT=BEAM,MATERIAL="Steel Rebar",NAME=RB8
COLUMNS,0.00064473, -0.20955, -0.36295125
*REBAR,ELEMENT=BEAM,MATERIAL="Steel Rebar",NAME=RB9
COLUMNS,0.00064473, 0, -0.4191
*REBAR,ELEMENT=BEAM,MATERIAL="Steel Rebar",NAME=RB10
COLUMNS,0.00064473, 0.20955, -0.36295125

```

```

*REBAR,ELEMENT=BEAM,MATERIAL="Steel Rebar",NAME=RB11
COLUMNS,0.00064473, 0.36295125, -0.20955
*REBAR,ELEMENT=BEAM,MATERIAL="Steel Rebar",NAME=RB12
COLUMNS,0.00064473, 0.4191, 0.0
*End Instance
**
*Nset, nset=_PickedSet71, internal, instance=BRIDGE-1
13,
*Orientation, name="DATUM CSYS-1"
1., 0., 0., 0., 1., 0.
1, 0.
*Orientation, name="DATUM CSYS-XBEAM3"
0., 1., 0., -1., 0., 0.
1, 0.
*Orientation, name="DATUM CSYS-XBEAM2"
0., 1., 0., 1., 0., 0.
1, 0.
** Constraint: Constraint-1
*Rigid Body, ref node=_PickedSet72, elset=BRIDGE-1.XBEAM2, position=CENTER OF
MASS
** Constraint: Constraint-2
*Rigid Body, ref node=_PickedSet73, elset=BRIDGE-1.XBEAM3, position=CENTER OF
MASS
** Constraint: Constraint-3
*Rigid Body, ref node=_PickedSet74, elset=BRIDGE-1.FOOT2, position=CENTER OF
MASS
** Constraint: Constraint-4
*Rigid Body, ref node=_PickedSet75, elset=BRIDGE-1.FOOT3, position=CENTER OF
MASS
**
** CONNECTORS
**
*Element, type=CONN3D2, elset=_Conn-1_CnSet_
1, BRIDGE-1.159, BRIDGE-1.143
*Connector Section, elset=_Conn-1_CnSet_
Beam,
"DATUM CSYS-1",
*Element, type=CONN3D2, elset=_Conn-10_CnSet_
2, BRIDGE-1.39, BRIDGE-1.17
*Connector Section, elset=_Conn-10_CnSet_
Hinge,
"DATUM CSYS-XBEAM3",
*Element, type=CONN3D2, elset=_Conn-2_CnSet_
3, BRIDGE-1.119, BRIDGE-1.41
*Connector Section, elset=_Conn-2_CnSet_
Beam,
"DATUM CSYS-1",

```

*Element, type=CONN3D2, elset=_Conn-3_CnSet_
 4, BRIDGE-1.150, BRIDGE-1.93
 *Connector Section, elset=_Conn-3_CnSet_
 Beam,
 "DATUM CSYS-1",
 *Element, type=CONN3D2, elset=_Conn-4_CnSet_
 5, BRIDGE-1.69, BRIDGE-1.32
 *Connector Section, elset=_Conn-4_CnSet_
 Beam,
 "DATUM CSYS-1",
 *Element, type=CONN3D2, elset=_Conn-5_CnSet_
 6, BRIDGE-1.155, BRIDGE-1.118
 *Connector Section, elset=_Conn-5_CnSet_
 Beam,
 "DATUM CSYS-1",
 *Element, type=CONN3D2, elset=_Conn-6_CnSet_
 7, BRIDGE-1.94, BRIDGE-1.37
 *Connector Section, elset=_Conn-6_CnSet_
 Beam,
 "DATUM CSYS-1",
 *Element, type=CONN3D2, elset=_Conn-7_CnSet_
 8, BRIDGE-1.146, BRIDGE-1.68
 *Connector Section, elset=_Conn-7_CnSet_
 Beam,
 "DATUM CSYS-1",
 *Element, type=CONN3D2, elset=_Conn-8_CnSet_
 9, BRIDGE-1.44, BRIDGE-1.28
 *Connector Section, elset=_Conn-8_CnSet_
 Beam,
 "DATUM CSYS-1",
 *Element, type=CONN3D2, elset=_Conn-9_CnSet_
 10, BRIDGE-1.30, BRIDGE-1.9
 *Connector Section, elset=_Conn-9_CnSet_
 Hinge,
 "DATUM CSYS-XBEAM2",
 *Element, type=CONN3D2, elset="_Conn-Abut E_CnSet_"
 11, BRIDGE-1.169, BRIDGE-1.167
 *Connector Section, elset="_Conn-Abut E_CnSet_", behavior=ConnProp-AbutPlastic
 Axial,
 "DATUM CSYS-1",
 *Element, type=CONN3D2, elset="_Conn-Abut W_CnSet_"
 12, BRIDGE-1.168, BRIDGE-1.166
 *Connector Section, elset="_Conn-Abut W_CnSet_", behavior=ConnProp-AbutPlastic
 Axial,
 "DATUM CSYS-1",
 *Element, type=Spring2, elset="AD DOF1 BEARING-spring"
 13, BRIDGE-1.167, BRIDGE-1.25

14, BRIDGE-1.166, BRIDGE-1.1
 *Spring, elset="AD DOF1 BEARING-spring"
 1, 1
 7.53e+06
 *Element, type=Spring2, elset="AD DOF1 GAP-spring"
 15, BRIDGE-1.169, BRIDGE-1.25
 16, BRIDGE-1.1, BRIDGE-1.168
 *Spring, elset="AD DOF1 GAP-spring", nonlinear
 1, 1
 0,0
 0,0.0508
 5000000, 0.07867
 *Element, type=Spring2, elset="AD DOF2-spring"
 17, BRIDGE-1.167, BRIDGE-1.25
 18, BRIDGE-1.166, BRIDGE-1.1
 *Spring, elset="AD DOF2-spring"
 2, 2
 4.38e+10
 *Element, type=Spring2, elset="AD DOF3-spring"
 19, BRIDGE-1.167, BRIDGE-1.25
 20, BRIDGE-1.166, BRIDGE-1.1
 *Spring, elset="AD DOF3-spring"
 3, 3
 3e+11
 *Element, type=Spring2, elset="AD DOF4-spring"
 21, BRIDGE-1.167, BRIDGE-1.25
 22, BRIDGE-1.166, BRIDGE-1.1
 *Spring, elset="AD DOF4-spring"
 4, 4
 1e+11
 *Element, type=Spring2, elset="AD DOF5-spring"
 23, BRIDGE-1.167, BRIDGE-1.25
 24, BRIDGE-1.166, BRIDGE-1.1
 *Spring, elset="AD DOF5-spring"
 5, 5
 1e+08
 *Element, type=Spring2, elset="AD DOF6-spring"
 25, BRIDGE-1.167, BRIDGE-1.25
 26, BRIDGE-1.166, BRIDGE-1.1
 *Spring, elset="AD DOF6-spring"
 6, 6
 1e+08
 *Element, type=Spring2, elset="SA DOF1-spring"
 27, BRIDGE-1.162, BRIDGE-1.166
 28, BRIDGE-1.163, BRIDGE-1.167
 *Spring, elset="SA DOF1-spring"
 1, 1

```

5.16e+09
*Element, type=Spring2, elset="SA DOF2-spring"
29, BRIDGE-1.162, BRIDGE-1.166
30, BRIDGE-1.163, BRIDGE-1.167
*Spring, elset="SA DOF2-spring"
2, 2
5.87e+09
*Element, type=Spring2, elset="SA DOF3-spring"
31, BRIDGE-1.162, BRIDGE-1.166
32, BRIDGE-1.163, BRIDGE-1.167
*Spring, elset="SA DOF3-spring"
3, 3
4.55e+09
*Element, type=Spring2, elset="SA DOF4-spring"
33, BRIDGE-1.162, BRIDGE-1.166
34, BRIDGE-1.163, BRIDGE-1.167
*Spring, elset="SA DOF4-spring"
4, 4
7.59e+09
*Element, type=Spring2, elset="SA DOF5-spring"
35, BRIDGE-1.162, BRIDGE-1.166
36, BRIDGE-1.163, BRIDGE-1.167
*Spring, elset="SA DOF5-spring"
5, 5
5.27e+10
*Element, type=Spring2, elset="SA DOF6-spring"
37, BRIDGE-1.162, BRIDGE-1.166
38, BRIDGE-1.163, BRIDGE-1.167
*Spring, elset="SA DOF6-spring"
6, 6
6.44e+10
*End Assembly
**
** MATERIALS
**
*Material, name=CONCRETE
*Damping, alpha=0.72, beta=0.003
*Density
2400.,
*Elastic
2e+10, 0.18
*Material, name="CONCRETE COLUMN"
*Concrete
5.17e+07, 0.
7.07e+07, 0.0055
6.01e+07, 0.0135
0., 0.02

```

```

*Tension Stiffening
  1., 0.
  0.5, 0.00078
  0.15, 0.00282
  0., 0.004
*Damping, alpha=0.72, beta=0.003
*Density
2400.,
*Elastic
  1.4e+10, 0.18
*Material, name="STEEL REBAR"
*Damping, alpha=0.72, beta=0.003
*Elastic
  2e+11, 0.3
*Plastic, hardening=COMBINED
  2.76e+08, 0.
  4.14e+08, 0.00862069
  6.21e+08, 0.0586207
  6.21e+08, 0.0886207
  4.96e+08, 0.138621
  0., 0.15
*Connector Behavior, name=ConnProp-AbutPlastic
*Connector Elasticity, component=1
  1.79e+08,
*Connector Plasticity, component=1
*Connector Hardening, definition=Tabular
  2.44e+06, 0., 0.
  2.44e+06, 0.9, 0.
**
** BOUNDARY CONDITIONS
**
** Name: BC-FIXE Type: Displacement/Rotation
*Boundary
BRIDGE-1.NSABUTSANDFOOT, 1, 1
BRIDGE-1.NSABUTSANDFOOT, 2, 2
BRIDGE-1.NSABUTSANDFOOT, 3, 3
BRIDGE-1.NSABUTSANDFOOT, 4, 4
BRIDGE-1.NSABUTSANDFOOT, 5, 5
BRIDGE-1.NSABUTSANDFOOT, 6, 6
** Name: BC-Fix GE Type: Displacement/Rotation
*Boundary
BRIDGE-1.NGAPE, 2, 2
BRIDGE-1.NGAPE, 3, 3
BRIDGE-1.NGAPE, 4, 4
BRIDGE-1.NGAPE, 5, 5
BRIDGE-1.NGAPE, 6, 6
** Name: BC-Fix GW Type: Displacement/Rotation

```



```

*Boundary
BRIDGE-1.NGAPW, 2, 2
BRIDGE-1.NGAPW, 3, 3
BRIDGE-1.NGAPW, 4, 4
BRIDGE-1.NGAPW, 5, 5
BRIDGE-1.NGAPW, 6, 6
** -----
**
** STEP: Step-1 - Gravity
**
*Step, name="Step-1 - Gravity"
*Static, stabilize=0.0002
1., 1., 1e-05, 1.
**
** LOADS
**
** Name: Load-1  Type: Gravity
*Dload
, GRAV, 9.81, 0., 0., -1.
**
** OUTPUT REQUESTS
**
*Restart, write, frequency=0
*Monitor, dof=2, node=_PickedSet71, frequency=1
**
** FIELD OUTPUT: F-Output-2
**
*Output, field
*Element Output, directions=YES
SF,
**
** FIELD OUTPUT: F-Output-1
**
*Node Output
UT,
**
** FIELD OUTPUT: F-Output-3
**
*Element Output, elset=BRIDGE-1."COLUMN SW", directions=YES
E, SE
**
** HISTORY OUTPUT: H-Output-1
**
*Output, history
*Energy Output
ALLIE, ALLKE, ALLPD
**

```

```

** HISTORY OUTPUT: H-Output-5
**
*Element Output, elset="AD DOF1 GAP-spring"
E11, S11
**
** HISTORY OUTPUT: H-Output-2
**
*Element Output, elset="_Conn-Abut E_CnSet_"
CTF1, CU1
**
** HISTORY OUTPUT: H-Output-3
**
*Element Output, elset=BRIDGE-1."COLUMN SW"
ELKE, ELPD, ELSE
**
** HISTORY OUTPUT: H-Output-4
**
*Output, history, frequency=10
*Element Output, elset="_Conn-Abut W_CnSet_"
CTF1, CU1
*End Step
** -----
**
** STEP: Step-2 - EQ
**
*Step, name="Step-2 - EQ", amplitude=RAMP, inc=2000000
Submit the bridge to the earthquake
*Dynamic,alpha=-0.05,haftol=1e+08
0.005,26.1,4.5e-10,0.02
*Solution technique, type=quasi-newton, reform kernel=15
**
** BOUNDARY CONDITIONS
**
** Name: Acc DOF1 Type: Acceleration/Angular acceleration
*Boundary, op=NEW, amplitude=KjmFN, type=ACCELERATION
BRIDGE-1.NSABUTSANDFOOT, 1, 1, 9.81
** Name: Acc DOF2 Type: Acceleration/Angular acceleration
*Boundary, op=NEW, amplitude=KjmFP, type=ACCELERATION
BRIDGE-1.NSABUTSANDFOOT, 2, 2, 9.81
** Name: Acc DOF3 Type: Acceleration/Angular acceleration
*Boundary, op=NEW, amplitude=KjmFN, type=ACCELERATION
BRIDGE-1.NSABUTSANDFOOT, 3, 3, 6.54
** Name: BC-FIXE Type: Displacement/Rotation
*Boundary, op=NEW
** Name: BC-Fix GE Type: Displacement/Rotation
*Boundary, op=NEW
** Name: BC-Fix GW Type: Displacement/Rotation

```

```

*Boundary, op=NEW
** Name: BC-FixRot Type: Displacement/Rotation
*Boundary, op=NEW
BRIDGE-1.NSABUTSANDFOOT, 4, 4
BRIDGE-1.NSABUTSANDFOOT, 5, 5
BRIDGE-1.NSABUTSANDFOOT, 6, 6
** Name: BC-FixRot GE Type: Displacement/Rotation
*Boundary, op=NEW
BRIDGE-1.NGAPE, 4, 4
BRIDGE-1.NGAPE, 5, 5
BRIDGE-1.NGAPE, 6, 6
** Name: BC-FixRot GW Type: Displacement/Rotation
*Boundary, op=NEW
BRIDGE-1.NGAPW, 4, 4
BRIDGE-1.NGAPW, 5, 5
BRIDGE-1.NGAPW, 6, 6
** Name: BC-GE DOF2 Type: Acceleration/Angular acceleration
*Boundary, op=NEW, amplitude=KjmFP, type=ACCELERATION
BRIDGE-1.NGAPE, 2, 2, 9.81
** Name: BC-GE DOF3 Type: Acceleration/Angular acceleration
*Boundary, op=NEW, amplitude=KjmFN, type=ACCELERATION
BRIDGE-1.NGAPE, 3, 3, 6.54
** Name: BC-GW DOF2 Type: Acceleration/Angular acceleration
*Boundary, op=NEW, amplitude=KjmFP, type=ACCELERATION
BRIDGE-1.NGAPW, 2, 2, 9.81
** Name: BC-GW DOF3 Type: Acceleration/Angular acceleration
*Boundary, op=NEW, amplitude=KjmFN, type=ACCELERATION
BRIDGE-1.NGAPW, 3, 3, 6.54
**
** CONTROLS
**
*Controls, reset
*Controls, analysis=discontinuous
*Controls, parameters=constraints
1e-05, 1e-05, 1e-05, 0.005, 0.1, 1e-05, 1e-05
**
** OUTPUT REQUESTS
**
*Restart, write, frequency=0
**
** FIELD OUTPUT: F-Output-2
**
*Output, field, frequency=1
*Element Output, directions=YES
SF,
**
** FIELD OUTPUT: F-Output-1

```

```

**
*Node Output
UT,
**
** FIELD OUTPUT: F-Output-3
**
*Element Output, elset=BRIDGE-1."COLUMN SW", directions=YES
E, SE
**
** HISTORY OUTPUT: H-Output-1
**
*Output, history, frequency=1
*Energy Output
ALLIE, ALLKE, ALLPD
**
** HISTORY OUTPUT: H-Output-5
**
*Element Output, elset="AD DOF1 GAP-spring"
E11, S11
**
** HISTORY OUTPUT: H-Output-2
**
*Element Output, elset="_Conn-Abut E_CnSet_"
CTF1, CU1
**
** HISTORY OUTPUT: H-Output-3
**
*Element Output, elset=BRIDGE-1."COLUMN SW"
ELKE, ELPD, ELSE
**
** HISTORY OUTPUT: H-Output-4
**
*Output, history
*Element Output, elset="_Conn-Abut W_CnSet_"
CTF1, CU1
*End Step

```

Bridge 520

```

*Heading
** Job name: 520bridgeGap2 Model name: 520bridgeGap2
*Preprint, echo=NO, model=YES, history=NO, contact=YES
**
** PARTS
**
*Part, name=BRIDGE
*Node

```

1,	0.,	0.,	0.
2,	1.67639995,	0.,	0.
3,	3.35279989,	0.,	0.
4,	5.02920008,	0.,	0.
5,	6.70559978,	0.,	0.
6,	8.38199997,	0.,	0.
7,	10.0584002,	0.,	0.
8,	11.7348003,	0.,	0.
9,	13.4111996,	0.,	0.
10,	15.8495998,	0.,	0.
11,	18.2880001,	0.,	0.
12,	20.7264004,	0.,	0.
13,	23.1648006,	0.,	0.
14,	25.6032009,	0.,	0.
15,	28.0415993,	0.,	0.
16,	30.4799995,	0.,	0.
17,	32.9183998,	0.,	0.
18,	34.9757996,	0.,	0.
19,	37.0331993,	0.,	0.
20,	39.0905991,	0.,	0.
21,	41.1479988,	0.,	0.
22,	43.2053986,	0.,	0.
23,	45.2627983,	0.,	0.
24,	47.3202019,	0.,	0.
25,	49.3776016,	0.,	0.
26,	13.4111996,	-3.5,	0.
27,	13.4111996,	-2.74060011,	0.
28,	13.4111996,	-1.98119998,	0.
29,	13.4111996,	-0.99059999,	0.
30,	13.4111996,	0.,	0.
31,	13.4111996,	0.99059999,	0.
32,	13.4111996,	1.98119998,	0.
33,	13.4111996,	2.74060011,	0.
34,	13.4111996,	3.5,	0.
35,	32.9183998,	-3.5,	0.
36,	32.9183998,	-2.74060011,	0.
37,	32.9183998,	-1.98119998,	0.
38,	32.9183998,	-0.99059999,	0.
39,	32.9183998,	0.,	0.
40,	32.9183998,	0.99059999,	0.
41,	32.9183998,	1.98119998,	0.
42,	32.9183998,	2.74060011,	0.
43,	32.9183998,	3.5,	0.
44,	13.4111996,	-1.98119998,	0.
45,	13.4111996,	-1.98119998,	-0.357441515
46,	13.4111996,	-1.98119998,	-0.714883029
47,	13.4111996,	-1.98119998,	-1.07232451

48, 13.4111996, -1.98119998, -1.42976606
49, 13.4111996, -1.98119998, -1.78720748
50, 13.4111996, -1.98119998, -2.14464903
51, 13.4111996, -1.98119998, -2.50209045
52, 13.4111996, -1.98119998, -2.85953212
53, 13.4111996, -1.98119998, -3.21697354
54, 13.4111996, -1.98119998, -3.57441497
55, 13.4111996, -1.98119998, -3.93185639
56, 13.4111996, -1.98119998, -4.28929806
57, 13.4111996, -1.98119998, -4.64673948
58, 13.4111996, -1.98119998, -5.00418091
59, 13.4111996, -1.98119998, -5.36162233
60, 13.4111996, -1.98119998, -5.71906424
61, 13.4111996, -1.98119998, -6.07650566
62, 13.4111996, -1.98119998, -6.43394709
63, 13.4111996, -1.98119998, -6.79138851
64, 13.4111996, -1.98119998, -7.14882994
65, 13.4111996, -1.98119998, -7.50627136
66, 13.4111996, -1.98119998, -7.86371279
67, 13.4111996, -1.98119998, -8.22115421
68, 13.4111996, -1.98119998, -8.57859612
69, 13.4111996, 1.98119998, 0.
70, 13.4111996, 1.98119998, -0.357441515
71, 13.4111996, 1.98119998, -0.714883029
72, 13.4111996, 1.98119998, -1.07232451
73, 13.4111996, 1.98119998, -1.42976606
74, 13.4111996, 1.98119998, -1.78720748
75, 13.4111996, 1.98119998, -2.14464903
76, 13.4111996, 1.98119998, -2.50209045
77, 13.4111996, 1.98119998, -2.85953212
78, 13.4111996, 1.98119998, -3.21697354
79, 13.4111996, 1.98119998, -3.57441497
80, 13.4111996, 1.98119998, -3.93185639
81, 13.4111996, 1.98119998, -4.28929806
82, 13.4111996, 1.98119998, -4.64673948
83, 13.4111996, 1.98119998, -5.00418091
84, 13.4111996, 1.98119998, -5.36162233
85, 13.4111996, 1.98119998, -5.71906424
86, 13.4111996, 1.98119998, -6.07650566
87, 13.4111996, 1.98119998, -6.43394709
88, 13.4111996, 1.98119998, -6.79138851
89, 13.4111996, 1.98119998, -7.14882994
90, 13.4111996, 1.98119998, -7.50627136
91, 13.4111996, 1.98119998, -7.86371279
92, 13.4111996, 1.98119998, -8.22115421
93, 13.4111996, 1.98119998, -8.57859612
94, 32.9183998, 1.98119998, 0.

95, 32.9183998, 1.98119998, -0.357441515
96, 32.9183998, 1.98119998, -0.714883029
97, 32.9183998, 1.98119998, -1.07232451
98, 32.9183998, 1.98119998, -1.42976606
99, 32.9183998, 1.98119998, -1.78720748
100, 32.9183998, 1.98119998, -2.14464903
101, 32.9183998, 1.98119998, -2.50209045
102, 32.9183998, 1.98119998, -2.85953212
103, 32.9183998, 1.98119998, -3.21697354
104, 32.9183998, 1.98119998, -3.57441497
105, 32.9183998, 1.98119998, -3.93185639
106, 32.9183998, 1.98119998, -4.28929806
107, 32.9183998, 1.98119998, -4.64673948
108, 32.9183998, 1.98119998, -5.00418091
109, 32.9183998, 1.98119998, -5.36162233
110, 32.9183998, 1.98119998, -5.71906424
111, 32.9183998, 1.98119998, -6.07650566
112, 32.9183998, 1.98119998, -6.43394709
113, 32.9183998, 1.98119998, -6.79138851
114, 32.9183998, 1.98119998, -7.14882994
115, 32.9183998, 1.98119998, -7.50627136
116, 32.9183998, 1.98119998, -7.86371279
117, 32.9183998, 1.98119998, -8.22115421
118, 32.9183998, 1.98119998, -8.57859612
119, 32.9183998, -1.98119998, 0.
120, 32.9183998, -1.98119998, -0.357441515
121, 32.9183998, -1.98119998, -0.714883029
122, 32.9183998, -1.98119998, -1.07232451
123, 32.9183998, -1.98119998, -1.42976606
124, 32.9183998, -1.98119998, -1.78720748
125, 32.9183998, -1.98119998, -2.14464903
126, 32.9183998, -1.98119998, -2.50209045
127, 32.9183998, -1.98119998, -2.85953212
128, 32.9183998, -1.98119998, -3.21697354
129, 32.9183998, -1.98119998, -3.57441497
130, 32.9183998, -1.98119998, -3.93185639
131, 32.9183998, -1.98119998, -4.28929806
132, 32.9183998, -1.98119998, -4.64673948
133, 32.9183998, -1.98119998, -5.00418091
134, 32.9183998, -1.98119998, -5.36162233
135, 32.9183998, -1.98119998, -5.71906424
136, 32.9183998, -1.98119998, -6.07650566
137, 32.9183998, -1.98119998, -6.43394709
138, 32.9183998, -1.98119998, -6.79138851
139, 32.9183998, -1.98119998, -7.14882994
140, 32.9183998, -1.98119998, -7.50627136
141, 32.9183998, -1.98119998, -7.86371279

142, 32.9183998, -1.98119998, -8.22115421
 143, 32.9183998, -1.98119998, -8.57859612
 144, 13.4111996, -3.96239996, -8.57859612
 145, 13.4111996, -2.74060011, -8.57859612
 146, 13.4111996, -1.51880002, -8.57859612
 147, 13.4111996, -0.75940001, -8.57859612
 148, 13.4111996, 0., -8.57859612
 149, 13.4111996, 0.75940001, -8.57859612
 150, 13.4111996, 1.51880002, -8.57859612
 151, 13.4111996, 2.74060011, -8.57859612
 152, 13.4111996, 3.96239996, -8.57859612
 153, 32.9183998, -3.96239996, -8.57859612
 154, 32.9183998, -2.74060011, -8.57859612
 155, 32.9183998, -1.51880002, -8.57859612
 156, 32.9183998, -0.75940001, -8.57859612
 157, 32.9183998, 0., -8.57859612
 158, 32.9183998, 0.75940001, -8.57859612
 159, 32.9183998, 1.51880002, -8.57859612
 160, 32.9183998, 2.74060011, -8.57859612
 161, 32.9183998, 3.96239996, -8.57859612
 162, -0.0500000007, 0., 0.
 163, 49.4276009, 0., 0.
 164, 13.4111996, 0., -8.57859612
 165, 32.9183998, 0., -8.57859612
 166, -0.0500000007, 0., 0.
 167, 49.4276009, 0., 0.
 168, -0.0250000004, 0., 0.
 169, 49.4025993, 0., 0.

*Element, type=B32

1, 1, 2, 3
 2, 3, 4, 5
 3, 5, 6, 7
 4, 7, 8, 9
 5, 9, 10, 11
 6, 11, 12, 13
 7, 13, 14, 15
 8, 15, 16, 17
 9, 17, 18, 19
 10, 19, 20, 21
 11, 21, 22, 23
 12, 23, 24, 25
 13, 26, 27, 28
 14, 28, 29, 30
 15, 30, 31, 32
 16, 32, 33, 34
 17, 35, 36, 37
 18, 37, 38, 39

19, 39, 40, 41
20, 41, 42, 43
21, 44, 45, 46
22, 46, 47, 48
23, 48, 49, 50
24, 50, 51, 52
25, 52, 53, 54
26, 54, 55, 56
27, 56, 57, 58
28, 58, 59, 60
29, 60, 61, 62
30, 62, 63, 64
31, 64, 65, 66
32, 66, 67, 68
33, 69, 70, 71
34, 71, 72, 73
35, 73, 74, 75
36, 75, 76, 77
37, 77, 78, 79
38, 79, 80, 81
39, 81, 82, 83
40, 83, 84, 85
41, 85, 86, 87
42, 87, 88, 89
43, 89, 90, 91
44, 91, 92, 93
45, 94, 95, 96
46, 96, 97, 98
47, 98, 99, 100
48, 100, 101, 102
49, 102, 103, 104
50, 104, 105, 106
51, 106, 107, 108
52, 108, 109, 110
53, 110, 111, 112
54, 112, 113, 114
55, 114, 115, 116
56, 116, 117, 118
57, 119, 120, 121
58, 121, 122, 123
59, 123, 124, 125
60, 125, 126, 127
61, 127, 128, 129
62, 129, 130, 131
63, 131, 132, 133
64, 133, 134, 135
65, 135, 136, 137

66, 137, 138, 139
67, 139, 140, 141
68, 141, 142, 143
69, 144, 145, 146
70, 146, 147, 148
71, 148, 149, 150
72, 150, 151, 152
73, 153, 154, 155
74, 155, 156, 157
75, 157, 158, 159
76, 159, 160, 161
*Elset, elset=DECK, generate
1, 12, 1
*BEAM GENERAL SECTION,elset=DECK, SECTION=MESHED
0.0,1.0,0.0
*INCLUDE, INPUT=Model520SectionGood.bsp
*Elset, elset=XBEAM2, generate
13, 16, 1
*Elset, elset=XBEAM3, generate
17, 20, 1
*Elset, elset=COLUMNS, generate
21, 68, 1
*Elset, elset=FOOT2, generate
69, 72, 1
*Elset, elset=FOOT3, generate
73, 76, 1
*Nset, nset=NFOOT2
164,
*Nset, nset=NFOOT3
165,
*Nset, nset=NSABUTS
162,
*Nset, nset=NSABUTN
163,
*Nset, nset=NABUTS
166,
*Nset, nset=NABUTN
167,
*Nset, nset=NGAPS
168,
*Nset, nset=NGAPN
169,
*Nset, nset=NSABUTSANDFOOT, generate
162, 165, 1
*Nset, nset=NBFOOT2
148,
*Nset, nset=NBFOOT3

157,
 *Nset, nset=NBABUTS
 1,
 *Nset, nset=NBABUTN
 25,
 *Nset, nset=NBABUTSANDFOOT
 1, 25, 148, 157
 *Nset, nset=RPXB2
 30,
 *Nset, nset=RPXB3
 39,
 *Nset, nset=RPF2
 148,
 *Nset, nset=RPF3
 157,
 *Nset, nset=TIENODEF2
 144, 145, 147, 149, 151, 152
 *Nset, nset=TIENODEF3
 153, 154, 156, 158, 160, 161
 *Elset, elset="COLUMN SW", generate
 21, 32, 1
 *Nset, nset=BOTTOM
 67,
 ** Region: (Section-1-XBEAM2:XBEAM2), (Beam Orientation:XBEAM2)
 ** Section: Section-1-XBEAM2 Profile: Profile-1
 *Beam Section, elset=XBEAM2, material=CONCRETE, temperature=GRADIENTS,
 section=RECT
 1.2192, 1.2192
 0.,0.,-1.
 ** Region: (Section-2-XBEAM3:XBEAM3), (Beam Orientation:XBEAM3)
 ** Section: Section-2-XBEAM3 Profile: Profile-2
 *Beam Section, elset=XBEAM3, material=CONCRETE, temperature=GRADIENTS,
 section=RECT
 1.2192, 1.2192
 0.,0.,-1.
 ** Region: (Section-3-COLUMNS:COLUMNS), (Beam Orientation:COLUMNS)
 ** Section: Section-3-COLUMNS Profile: Profile-3
 *Beam Section, elset=COLUMNS, material="CONCRETE COLUMN",
 temperature=GRADIENTS, section=CIRC
 0.4572
 0.,1.,0.
 5,12
 ** Region: (Section-4-FOOT2:FOOT2), (Beam Orientation:FOOT2)
 ** Section: Section-4-FOOT2 Profile: Profile-4
 *Beam Section, elset=FOOT2, material=CONCRETE, temperature=GRADIENTS,
 section=RECT
 0.9144, 4.572

0.,0.,-1.
 ** Region: (Section-5-FOOT3:FOOT3), (Beam Orientation:FOOT3)
 ** Section: Section-5-FOOT3 Profile: Profile-5
 *Beam Section, elset=FOOT3, material=CONCRETE, temperature=GRADIENTS,
 section=RECT
 0.9144, 4.572
 0.,0.,-1.
 *Element, type=MASS, elset="_PickedSet38__PICKEDSET36_NABUTN_ABUTN
 MASS____"
 77, 167
 *Mass, elset="_PickedSet38__PICKEDSET36_NABUTN_ABUTN MASS____"
 104000.,
 *Element, type=MASS, elset="_PickedSet39__PICKEDSET37_NABUTS_ABUTS
 MASS____"
 78, 166
 *Mass, elset="_PickedSet39__PICKEDSET37_NABUTS_ABUTS MASS____"
 145000.,
 *Element, type=Spring2, elset="FOOTS DOF1-spring"
 79, 164, 148
 80, 165, 157
 *Spring, elset="FOOTS DOF1-spring"
 1, 1
 4.64e+09
 *Element, type=Spring2, elset="FOOTS DOF2-spring"
 81, 164, 148
 82, 165, 157
 *Spring, elset="FOOTS DOF2-spring"
 2, 2
 4.87e+09
 *Element, type=Spring2, elset="FOOTS DOF3-spring"
 83, 164, 148
 84, 165, 157
 *Spring, elset="FOOTS DOF3-spring"
 3, 3
 3.87e+09
 *Element, type=Spring2, elset="FOOTS DOF4-spring"
 85, 164, 148
 86, 165, 157
 *Spring, elset="FOOTS DOF4-spring"
 4, 4
 2.71e+10
 *Element, type=Spring2, elset="FOOTS DOF5-spring"
 87, 164, 148
 88, 165, 157
 *Spring, elset="FOOTS DOF5-spring"
 5, 5
 5.66e+10

```

*Element, type=Spring2, elset="FOOTS DOF6-spring"
89, 164, 148
90, 165, 157
*Spring, elset="FOOTS DOF6-spring"
6, 6
7.07e+10
*End Part
**
**
** ASSEMBLY
**
*Assembly, name=Assembly
**
*Instance, name=BRIDGE-1, part=BRIDGE
** REBAR FOR WHOLE COLUMNS
**
*REBAR,ELEMENT=BEAM,MATERIAL="Steel Rebar",NAME=RB1
COLUMNS, 0.00064473, 0.377596053, 0.181840675
*REBAR,ELEMENT=BEAM,MATERIAL="Steel Rebar",NAME=RB2
COLUMNS,0.00064473, 0.261304576 ,0.327665574
*REBAR,ELEMENT=BEAM,MATERIAL="Steel Rebar",NAME=RB3
COLUMNS,0.00064473,0.093258523 ,0.408592288
*REBAR,ELEMENT=BEAM,MATERIAL="Steel Rebar",NAME=RB4
COLUMNS,0.00064473,-0.093258523 ,0.408592288
*REBAR,ELEMENT=BEAM,MATERIAL="Steel Rebar",NAME=RB5
COLUMNS,0.00064473,-0.261304576 ,0.327665574
*REBAR,ELEMENT=BEAM,MATERIAL="Steel Rebar",NAME=RB6
COLUMNS,0.00064473,-0.377596053 ,0.181840675
*REBAR,ELEMENT=BEAM,MATERIAL="Steel Rebar",NAME=RB7
COLUMNS,0.00064473,-0.4191, 0
*REBAR,ELEMENT=BEAM,MATERIAL="Steel Rebar",NAME=RB8
COLUMNS,0.00064473,-0.377596053 ,-0.181840675
*REBAR,ELEMENT=BEAM,MATERIAL="Steel Rebar",NAME=RB9
COLUMNS,0.00064473,-0.261304576 ,-0.327665574
*REBAR,ELEMENT=BEAM,MATERIAL="Steel Rebar",NAME=RB10
COLUMNS,0.00064473,-0.093258523 ,-0.408592288
*REBAR,ELEMENT=BEAM,MATERIAL="Steel Rebar",NAME=RB11
COLUMNS,0.00064473,0.093258523 ,-0.408592288
*REBAR,ELEMENT=BEAM,MATERIAL="Steel Rebar",NAME=RB12
COLUMNS,0.00064473,0.261304576 ,-0.327665574
*REBAR,ELEMENT=BEAM,MATERIAL="Steel Rebar",NAME=RB13
COLUMNS,0.00064473,0.377596053 ,-0.181840675
*REBAR,ELEMENT=BEAM,MATERIAL="Steel Rebar",NAME=RB14
COLUMNS,0.00064473,0.4191, 0
*End Instance
**
*Nset, nset=Monitor-1, instance=BRIDGE-1

```

```

30,
*Orientation, name="DATUM CSYS-1"
    1.,    0.,    0.,    0.,    1.,    0.
1, 0.
*Orientation, name="DATUM CSYS-XBEAM2"
    0.,    1.,    0.,    1.,    0.,    0.
1, 0.
*Orientation, name="DATUM CSYS-XBEAM3"
    0.,    1.,    0.,   -1.,    0.,    0.
1, 0.
** Constraint: RigidBody-1
*Rigid Body, ref node=_PickedSet28, elset=BRIDGE-1.FOOT2, position=CENTER OF
MASS
** Constraint: RigidBody-2
*Rigid Body, ref node=_PickedSet29, elset=BRIDGE-1.FOOT3, position=CENTER OF
MASS
** Constraint: RigidBody-3
*Rigid Body, ref node=_PickedSet30, elset=BRIDGE-1.XBEAM2, position=CENTER OF
MASS
** Constraint: RigidBody-4
*Rigid Body, ref node=_PickedSet31, elset=BRIDGE-1.XBEAM3, position=CENTER OF
MASS
**
** CONNECTORS
**
*Element, type=CONN3D2, elset=_Conn-10_CnSet_
1, BRIDGE-1.68, BRIDGE-1.146
*Connector Section, elset=_Conn-10_CnSet_
Beam,
"DATUM CSYS-1",
*Element, type=CONN3D2, elset=_Conn-11_CnSet_
2, BRIDGE-1.44, BRIDGE-1.28
*Connector Section, elset=_Conn-11_CnSet_
Beam,
"DATUM CSYS-1",
*Element, type=CONN3D2, elset=_Conn-12_CnSet_
3, BRIDGE-1.30, BRIDGE-1.9
*Connector Section, elset=_Conn-12_CnSet_
Hinge,
"DATUM CSYS-XBEAM2",
*Element, type=CONN3D2, elset=_Conn-3_CnSet_
4, BRIDGE-1.143, BRIDGE-1.155
*Connector Section, elset=_Conn-3_CnSet_
Beam,
"DATUM CSYS-1",
*Element, type=CONN3D2, elset=_Conn-4_CnSet_
5, BRIDGE-1.39, BRIDGE-1.17

```

*Connector Section, elset=_Conn-4_CnSet_
 Hinge,
 "DATUM CSYS-XBEAM3",
 *Element, type=CONN3D2, elset=_Conn-5_CnSet_
 6, BRIDGE-1.119, BRIDGE-1.37
 *Connector Section, elset=_Conn-5_CnSet_
 Beam,
 "DATUM CSYS-1",
 *Element, type=CONN3D2, elset=_Conn-6_CnSet_
 7, BRIDGE-1.93, BRIDGE-1.150
 *Connector Section, elset=_Conn-6_CnSet_
 Beam,
 "DATUM CSYS-1",
 *Element, type=CONN3D2, elset=_Conn-7_CnSet_
 8, BRIDGE-1.69, BRIDGE-1.32
 *Connector Section, elset=_Conn-7_CnSet_
 Beam,
 "DATUM CSYS-1",
 *Element, type=CONN3D2, elset=_Conn-8_CnSet_
 9, BRIDGE-1.118, BRIDGE-1.159
 *Connector Section, elset=_Conn-8_CnSet_
 Beam,
 "DATUM CSYS-1",
 *Element, type=CONN3D2, elset=_Conn-9_CnSet_
 10, BRIDGE-1.94, BRIDGE-1.41
 *Connector Section, elset=_Conn-9_CnSet_
 Beam,
 "DATUM CSYS-1",
 *Element, type=CONN3D2, elset="_Conn-Abut N_CnSet_"
 11, BRIDGE-1.169, BRIDGE-1.167
 *Connector Section, elset="_Conn-Abut N_CnSet_", behavior=ConnProp-AbutPlastic
 Axial,
 "DATUM CSYS-1",
 *Element, type=CONN3D2, elset="_Conn-Abut S_CnSet_"
 12, BRIDGE-1.168, BRIDGE-1.166
 *Connector Section, elset="_Conn-Abut S_CnSet_", behavior=ConnProp-AbutPlastic
 Axial,
 "DATUM CSYS-1",
 *Element, type=Spring2, elset="AD DOF1-spring"
 13, BRIDGE-1.167, BRIDGE-1.25
 14, BRIDGE-1.166, BRIDGE-1.1
 *Spring, elset="AD DOF1-spring"
 1, 1
 6.52e+06
 *Element, type=Spring2, elset="AD DOF1 GAP N-spring"
 15, BRIDGE-1.169, BRIDGE-1.25
 *Spring, elset="AD DOF1 GAP N-spring", nonlinear

```

1, 1
0,0
0,0.0508
5000000,0.0663
*Element, type=Spring2, elset="AD DOF1 GAP S-spring"
16, BRIDGE-1.1, BRIDGE-1.168
*Spring, elset="AD DOF1 GAP S-spring",nonlinear
1, 1
0,0
0,0.0508
5000000,0.0663
*Element, type=Spring2, elset="AD DOF2-spring"
17, BRIDGE-1.167, BRIDGE-1.25
18, BRIDGE-1.166, BRIDGE-1.1
*Spring, elset="AD DOF2-spring"
2, 2
4.38e+10
*Element, type=Spring2, elset="AD DOF3-spring"
19, BRIDGE-1.167, BRIDGE-1.25
20, BRIDGE-1.166, BRIDGE-1.1
*Spring, elset="AD DOF3-spring"
3, 3
3e+11
*Element, type=Spring2, elset="AD DOF4-spring"
21, BRIDGE-1.167, BRIDGE-1.25
22, BRIDGE-1.166, BRIDGE-1.1
*Spring, elset="AD DOF4-spring"
4, 4
1e+11
*Element, type=Spring2, elset="AD DOF5-spring"
23, BRIDGE-1.167, BRIDGE-1.25
24, BRIDGE-1.166, BRIDGE-1.1
*Spring, elset="AD DOF5-spring"
5, 5
1e+08
*Element, type=Spring2, elset="AD DOF6-spring"
25, BRIDGE-1.167, BRIDGE-1.25
26, BRIDGE-1.166, BRIDGE-1.1
*Spring, elset="AD DOF6-spring"
6, 6
1e+10
*Element, type=Spring2, elset="SA DOF1-spring"
27, BRIDGE-1.162, BRIDGE-1.166
28, BRIDGE-1.163, BRIDGE-1.167
*Spring, elset="SA DOF1-spring"
1, 1
5.64e+09

```



```

*Element, type=Spring2, elset="SA DOF2-spring"
29, BRIDGE-1.162, BRIDGE-1.166
30, BRIDGE-1.163, BRIDGE-1.167
*Spring, elset="SA DOF2-spring"
2, 2
5.94e+09
*Element, type=Spring2, elset="SA DOF3-spring"
31, BRIDGE-1.162, BRIDGE-1.166
32, BRIDGE-1.163, BRIDGE-1.167
*Spring, elset="SA DOF3-spring"
3, 3
4.5e+09
*Element, type=Spring2, elset="SA DOF4-spring"
33, BRIDGE-1.162, BRIDGE-1.166
34, BRIDGE-1.163, BRIDGE-1.167
*Spring, elset="SA DOF4-spring"
4, 4
3.13e+10
*Element, type=Spring2, elset="SA DOF5-spring"
35, BRIDGE-1.162, BRIDGE-1.166
36, BRIDGE-1.163, BRIDGE-1.167
*Spring, elset="SA DOF5-spring"
5, 5
7.35e+10
*Element, type=Spring2, elset="SA DOF6-spring"
37, BRIDGE-1.162, BRIDGE-1.166
38, BRIDGE-1.163, BRIDGE-1.167
*Spring, elset="SA DOF6-spring"
6, 6
8.48e+10
*End Assembly
**
** MATERIALS
**
*Material, name=CONCRETE
*Damping, alpha=0.6, beta=0.003
*Density
2400.,
*Elastic
2e+10, 0.18
*Material, name="CONCRETE COLUMN"
*Concrete
5.17e+07, 0.
7.06e+07, 0.0055
6e+07, 0.0134
0., 0.02
*Tension Stiffening

```

```

1., 0.
0.5, 0.00078
0.15, 0.00282
0., 0.004
*Damping, alpha=0.6, beta=0.003
*Density
2400.,
*Elastic
1.72e+10, 0.18
*Material, name="STEEL REBAR"
*Damping, alpha=0.6, beta=0.003
*Elastic
2e+11, 0.3
*Plastic, hardening=COMBINED
2.76e+08, 0.
4.14e+08, 0.00862069
6.21e+08, 0.0586207
6.21e+08, 0.0886207
4.96e+08, 0.138621
0., 0.15
*Connector Behavior, name=ConnProp-AbutPlastic
*Connector Elasticity, component=1
3.22e+08,
*Connector Plasticity, component=1
*Connector Hardening, definition=Tabular
2.3e+06, 0., 0.
2.3e+06, 0.85, 0.
**
** BOUNDARY CONDITIONS
**
** Name: BC-Fix GN Type: Displacement/Rotation
*Boundary
BRIDGE-1.NGAPN, 2, 2
BRIDGE-1.NGAPN, 3, 3
BRIDGE-1.NGAPN, 4, 4
BRIDGE-1.NGAPN, 5, 5
BRIDGE-1.NGAPN, 6, 6
** Name: BC-Fix GS Type: Displacement/Rotation
*Boundary
BRIDGE-1.NGAPS, 2, 2
BRIDGE-1.NGAPS, 3, 3
BRIDGE-1.NGAPS, 4, 4
BRIDGE-1.NGAPS, 5, 5
BRIDGE-1.NGAPS, 6, 6
** Name: Disp-BC-FIXE Type: Displacement/Rotation
*Boundary
BRIDGE-1.NSABUTSANDFOOT, 1, 1

```

```

BRIDGE-1.NSABUTSANDFOOT, 2, 2
BRIDGE-1.NSABUTSANDFOOT, 3, 3
BRIDGE-1.NSABUTSANDFOOT, 4, 4
BRIDGE-1.NSABUTSANDFOOT, 5, 5
BRIDGE-1.NSABUTSANDFOOT, 6, 6
** -----
**
** STEP: Step-1 - Gravity
**
*Step, name="Step-1 - Gravity", nlgeom=YES
*Static, stabilize=0.0002
1., 1., 1e-05, 1.
**
** LOADS
**
** Name: Load-1  Type: Gravity
*Dload
, GRAV, 9.81, 0., 0., -1.
**
** OUTPUT REQUESTS
**
*Restart, write, frequency=0
*Monitor, dof=2, node=Monitor-1, frequency=1
**
** FIELD OUTPUT: F-Output-2
**
*Output, field
*Element Output, directions=YES
SF,
**
** FIELD OUTPUT: F-Output-1
**
*Node Output
UT,
**
** FIELD OUTPUT: F-Output-3
**
*Element Output, elset=BRIDGE-1."COLUMN SW", directions=YES
E, SE
**
** HISTORY OUTPUT: H-Output-3
**
*Output, history
*Energy Output
ALLIE, ALLKE, ALLPD
**
** HISTORY OUTPUT: H-Output-5

```

```

**
*Element Output, elset="AD DOF1 GAP N-spring"
E11, S11
**
** HISTORY OUTPUT: H-Output-6
**
*Element Output, elset="AD DOF1 GAP S-spring"
E11, S11
**
** HISTORY OUTPUT: H-Output-4
**
*Element Output, elset="_Conn-Abut N_CnSet_"
CP1, CTF1, CU1
**
** HISTORY OUTPUT: H-Output-1
**
*Element Output, elset="_Conn-Abut S_CnSet_"
CP1, CTF1, CU1
**
** HISTORY OUTPUT: H-Output-2
**
*Element Output, elset=BRIDGE-1."COLUMN SW"
ELKE, ELPD, ELSE
*End Step
** -----
**
** STEP: Step-2 EQ
**
*Step, name="Step-2 EQ", nlgeom=YES, amplitude=RAMP, inc=20000000
Submit EQ
*Dynamic,alpha=-0.05,haftol=1e+08
0.005,30.,4e-10,0.005
**
** BOUNDARY CONDITIONS
**
** Name: Acc-BC-1 Type: Acceleration/Angular acceleration
*Boundary, op=NEW, amplitude=IztFN, type=ACCELERATION
BRIDGE-1.NSABUTSANDFOOT, 1, 1, 9.81
** Name: Acc-BC-2 Type: Acceleration/Angular acceleration
*Boundary, op=NEW, amplitude=IztFP, type=ACCELERATION
BRIDGE-1.NSABUTSANDFOOT, 2, 2, 9.81
** Name: Acc-BC-3 Type: Acceleration/Angular acceleration
*Boundary, op=NEW, amplitude=IztFN, type=ACCELERATION
BRIDGE-1.NSABUTSANDFOOT, 3, 3, 6.54
** Name: BC-Fix GN Type: Displacement/Rotation
*Boundary, op=NEW
** Name: BC-Fix GS Type: Displacement/Rotation

```

```

*Boundary, op=NEW
** Name: BC-FixRot N Type: Displacement/Rotation
*Boundary, op=NEW
BRIDGE-1.NGAPN, 4, 4
BRIDGE-1.NGAPN, 5, 5
BRIDGE-1.NGAPN, 6, 6
** Name: BC-FixRot S Type: Displacement/Rotation
*Boundary, op=NEW
BRIDGE-1.NGAPS, 4, 4
BRIDGE-1.NGAPS, 5, 5
BRIDGE-1.NGAPS, 6, 6
** Name: BC-GN DOF2 Type: Acceleration/Angular acceleration
*Boundary, op=NEW, amplitude=IztFP, type=ACCELERATION
BRIDGE-1.NGAPN, 2, 2, 9.81
** Name: BC-GN DOF3 Type: Acceleration/Angular acceleration
*Boundary, op=NEW, amplitude=IztFN, type=ACCELERATION
BRIDGE-1.NGAPN, 3, 3, 6.54
** Name: BC-GS DOF2 Type: Acceleration/Angular acceleration
*Boundary, op=NEW, amplitude=IztFP, type=ACCELERATION
BRIDGE-1.NGAPS, 2, 2, 9.81
** Name: BC-GS DOF3 Type: Acceleration/Angular acceleration
*Boundary, op=NEW, amplitude=IztFN, type=ACCELERATION
BRIDGE-1.NGAPS, 3, 3, 6.54
** Name: Disp-BC-FIXE Type: Displacement/Rotation
*Boundary, op=NEW
** Name: Disp-BC-Fix Rot Type: Displacement/Rotation
*Boundary, op=NEW
BRIDGE-1.NSABUTSANDFOOT, 4, 4
BRIDGE-1.NSABUTSANDFOOT, 5, 5
BRIDGE-1.NSABUTSANDFOOT, 6, 6
**
** OUTPUT REQUESTS
**
*Restart, write, frequency=0
*Monitor, dof=2, node=Monitor-1, frequency=1
**
** FIELD OUTPUT: F-Output-2
**
*Output, field, frequency=1
*Element Output, directions=YES
SF,
**
** FIELD OUTPUT: F-Output-1
**
*Node Output
UT,
**

```

```

** FIELD OUTPUT: F-Output-3
**
*Element Output, elset=BRIDGE-1."COLUMN SW", directions=YES
E, SE
**
** HISTORY OUTPUT: H-Output-3
**
*Output, history, frequency=1
*Energy Output
ALLIE, ALLKE, ALLPD
**
** HISTORY OUTPUT: H-Output-5
**
*Element Output, elset="AD DOF1 GAP N-spring"
E11, S11
**
** HISTORY OUTPUT: H-Output-6
**
*Element Output, elset="AD DOF1 GAP S-spring"
E11, S11
**
** HISTORY OUTPUT: H-Output-4
**
*Element Output, elset="_Conn-Abut N_CnSet_"
CP1, CTF1, CU1
**
** HISTORY OUTPUT: H-Output-1
**
*Element Output, elset="_Conn-Abut S_CnSet_"
CP1, CTF1, CU1
**
** HISTORY OUTPUT: H-Output-2
**
*Element Output, elset=BRIDGE-1."COLUMN SW"
ELKE, ELPD, ELSE
*End Step

```

Bridge 90

```

*Heading
** Job name: 90bridge Model name: 90bridge
*Preprint, echo=NO, model=NO, history=NO, contact=NO
**
** PARTS
**
*Part, name=BRIDGE
*Node

```

1,	0.,	0.,	0.
2,	2.03800011,	0.,	-0.108999997
3,	4.07499981,	0.,	-0.218999997
4,	6.11299992,	0.,	-0.328000009
5,	8.14999962,	0.,	-0.437000006
6,	10.1879997,	0.,	-0.546999991
7,	12.2259998,	0.,	-0.656000018
8,	14.2629995,	0.,	-0.764999986
9,	16.3010006,	0.,	-0.875
10,	18.7199993,	0.,	-1.03199995
11,	21.1389999,	0.,	-1.18900001
12,	23.559,	0.,	-1.347
13,	25.9780006,	0.,	-1.50399995
14,	28.3969994,	0.,	-1.66199994
15,	30.8169994,	0.,	-1.81900001
16,	33.2360001,	0.,	-1.97599995
17,	35.6559982,	0.,	-2.13400006
18,	37.6650009,	0.,	-2.28699994
19,	39.6749992,	0.,	-2.44099998
20,	41.6850014,	0.,	-2.59400001
21,	43.6949997,	0.,	-2.74799991
22,	45.7039986,	0.,	-2.90100002
23,	47.7140007,	0.,	-3.05500007
24,	49.723999,	0.,	-3.20799994
25,	51.7340012,	0.,	-3.36199999
26,	54.7369995,	0.,	-3.625
27,	57.7410011,	0.,	-3.88800001
28,	60.7439995,	0.,	-4.15199995
29,	63.7470016,	0.,	-4.41499996
30,	66.7509995,	0.,	-4.67799997
31,	69.7539978,	0.,	-4.94199991
32,	72.7580032,	0.,	-5.20499992
33,	75.7610016,	0.,	-5.46799994
34,	77.6660004,	0.,	-5.63999987
35,	79.5709991,	0.,	-5.81099987
36,	81.4759979,	0.,	-5.98199987
37,	83.3809967,	0.,	-6.15399981
38,	85.2860031,	0.,	-6.32499981
39,	87.1910019,	0.,	-6.49700022
40,	89.0960007,	0.,	-6.66800022
41,	91.0009995,	0.,	-6.84000015
42,	16.3010006,	0.,	-0.875
43,	16.3010006,	0.,	-1.17999995
44,	16.3010006,	0.,	-1.48399997
45,	16.3010006,	0.,	-1.78900003
46,	16.3010006,	0.,	-2.09400001
47,	16.3010006,	0.,	-2.39899993

48,	16.3010006,	0.,	-2.704
49,	16.3010006,	0.,	-3.0079999
50,	16.3010006,	0.,	-3.31299996
51,	16.3010006,	0.,	-3.61800003
52,	16.3010006,	0.,	-3.9230001
53,	16.3010006,	0.,	-4.22800016
54,	16.3010006,	0.,	-4.53200006
55,	16.3010006,	0.,	-4.83699989
56,	16.3010006,	0.,	-5.1420002
57,	16.3010006,	0.,	-5.44700003
58,	16.3010006,	0.,	-5.75199986
59,	16.3010006,	0.,	-6.05600023
60,	16.3010006,	0.,	-6.36100006
61,	16.3010006,	0.,	-6.66599989
62,	16.3010006,	0.,	-6.97100019
63,	16.3010006,	0.,	-8.58600044
64,	16.3010006,	0.,	-10.2010002
65,	16.3010006,	0.,	-11.816
66,	16.3010006,	0.,	-13.4309998
67,	16.3010006,	0.,	-15.0459995
68,	16.3010006,	0.,	-16.6609993
69,	16.3010006,	0.,	-18.2759991
70,	16.3010006,	0.,	-19.8910007
71,	16.3010006,	0.,	-21.5060005
72,	16.3010006,	0.,	-23.1210003
73,	35.6559982,	0.,	-2.13400006
74,	35.6559982,	0.,	-2.46099997
75,	35.6559982,	0.,	-2.78900003
76,	35.6559982,	0.,	-3.1170001
77,	35.6559982,	0.,	-3.44400001
78,	35.6559982,	0.,	-3.77200007
79,	35.6559982,	0.,	-4.0999999
80,	35.6559982,	0.,	-4.42700005
81,	35.6559982,	0.,	-4.75500011
82,	35.6559982,	0.,	-5.08300018
83,	35.6559982,	0.,	-5.40999985
84,	35.6559982,	0.,	-5.73799992
85,	35.6559982,	0.,	-6.06599998
86,	35.6559982,	0.,	-6.39300013
87,	35.6559982,	0.,	-6.72100019
88,	35.6559982,	0.,	-7.04899979
89,	35.6559982,	0.,	-7.37599993
90,	35.6559982,	0.,	-7.704
91,	35.6559982,	0.,	-8.03100014
92,	35.6559982,	0.,	-8.35900021
93,	35.6559982,	0.,	-8.68700027
94,	35.6559982,	0.,	-9.01399994

95,	35.6559982,	0.,	-9.34200001
96,	35.6559982,	0.,	-10.8940001
97,	35.6559982,	0.,	-12.4460001
98,	35.6559982,	0.,	-13.9969997
99,	35.6559982,	0.,	-15.5489998
100,	35.6559982,	0.,	-17.1009998
101,	35.6559982,	0.,	-18.6520004
102,	35.6559982,	0.,	-20.2040005
103,	35.6559982,	0.,	-21.7560005
104,	35.6559982,	0.,	-23.3080006
105,	35.6559982,	0.,	-24.8589993
106,	51.7340012,	0.,	-3.36199999
107,	51.7340012,	0.,	-3.69400001
108,	51.7340012,	0.,	-4.02600002
109,	51.7340012,	0.,	-4.3579998
110,	51.7340012,	0.,	-4.69000006
111,	51.7340012,	0.,	-5.02099991
112,	51.7340012,	0.,	-5.35300016
113,	51.7340012,	0.,	-5.68499994
114,	51.7340012,	0.,	-6.0170002
115,	51.7340012,	0.,	-6.34899998
116,	51.7340012,	0.,	-6.68100023
117,	51.7340012,	0.,	-7.01300001
118,	51.7340012,	0.,	-7.34499979
119,	51.7340012,	0.,	-7.67700005
120,	51.7340012,	0.,	-8.00800037
121,	51.7340012,	0.,	-8.34000015
122,	51.7340012,	0.,	-8.67199993
123,	51.7340012,	0.,	-9.00399971
124,	51.7340012,	0.,	-9.33600044
125,	51.7340012,	0.,	-10.9431515
126,	51.7340012,	0.,	-12.5502787
127,	51.7340012,	0.,	-14.1574059
128,	51.7340012,	0.,	-15.764533
129,	51.7340012,	0.,	-17.3719997
130,	51.7340012,	0.,	-18.9790001
131,	51.7340012,	0.,	-20.5860004
132,	51.7340012,	0.,	-22.1930008
133,	51.7340012,	0.,	-23.7999992
134,	51.7340012,	0.,	-25.4069996
135,	75.7610016,	0.,	-5.46799994
136,	75.7610016,	0.,	-5.77699995
137,	75.7610016,	0.,	-6.08599997
138,	75.7610016,	0.,	-6.39599991
139,	75.7610016,	0.,	-6.70499992
140,	75.7610016,	0.,	-7.01399994
141,	75.7610016,	0.,	-7.32299995

142,	75.7610016,	0.,	-7.63199997
143,	75.7610016,	0.,	-7.94099998
144,	75.7610016,	0.,	-8.2510004
145,	75.7610016,	0.,	-8.56000042
146,	75.7610016,	0.,	-8.86900043
147,	75.7610016,	0.,	-9.17800045
148,	75.7610016,	0.,	-9.48700047
149,	75.7610016,	0.,	-9.79599953
150,	75.7610016,	0.,	-11.2370005
151,	75.7610016,	0.,	-12.6780005
152,	75.7610016,	0.,	-14.1190004
153,	75.7610016,	0.,	-15.5600004
154,	75.7610016,	0.,	-17.0009995
155,	75.7610016,	0.,	-18.4419994
156,	75.7610016,	0.,	-19.882
157,	75.7610016,	0.,	-21.323
158,	75.7610016,	0.,	-22.7639999
159,	75.7610016,	0.,	-24.2049999
160,	-0.0500000007,	0.,	0.
161,	91.0500031,	0.,	-6.84000015
162,	-0.0500000007,	0.,	0.
163,	91.0500031,	0.,	-6.84000015
164,	16.3010006,	0.,	-8.58600044
165,	16.3010006,	0.,	-10.2010002
166,	16.3010006,	0.,	-11.816
167,	16.3010006,	0.,	-13.4309998
168,	16.3010006,	0.,	-15.0459995
169,	16.3010006,	0.,	-16.6609993
170,	16.3010006,	0.,	-18.2759991
171,	16.3010006,	0.,	-19.8910007
172,	16.3010006,	0.,	-21.5060005
173,	16.3010006,	0.,	-23.1210003
174,	35.6559982,	0.,	-10.8940001
175,	35.6559982,	0.,	-12.4460001
176,	35.6559982,	0.,	-13.9969997
177,	35.6559982,	0.,	-15.5489998
178,	35.6559982,	0.,	-17.1009998
179,	35.6559982,	0.,	-18.6520004
180,	35.6559982,	0.,	-20.2040005
181,	35.6559982,	0.,	-21.7560005
182,	35.6559982,	0.,	-23.3080006
183,	35.6559982,	0.,	-24.8589993
184,	51.7340012,	0.,	-10.9431515
185,	51.7340012,	0.,	-12.5502787
186,	51.7340012,	0.,	-14.1574059
187,	51.7340012,	0.,	-15.764533
188,	51.7340012,	0.,	-17.3719997

189,	51.7340012,	0.,	-18.9790001
190,	51.7340012,	0.,	-20.5860004
191,	51.7340012,	0.,	-22.1930008
192,	51.7340012,	0.,	-23.7999992
193,	51.7340012,	0.,	-25.4069996
194,	75.7610016,	0.,	-11.2370005
195,	75.7610016,	0.,	-12.6780005
196,	75.7610016,	0.,	-14.1190004
197,	75.7610016,	0.,	-15.5600004
198,	75.7610016,	0.,	-17.0009995
199,	75.7610016,	0.,	-18.4419994
200,	75.7610016,	0.,	-19.882
201,	75.7610016,	0.,	-21.323
202,	75.7610016,	0.,	-22.7639999
203,	75.7610016,	0.,	-24.2049999

*Element, type=B32

1, 1, 2, 3
2, 3, 4, 5
3, 5, 6, 7
4, 7, 8, 9
5, 9, 10, 11
6, 11, 12, 13
7, 13, 14, 15
8, 15, 16, 17
9, 17, 18, 19
10, 19, 20, 21
11, 21, 22, 23
12, 23, 24, 25
13, 25, 26, 27
14, 27, 28, 29
15, 29, 30, 31
16, 31, 32, 33
17, 33, 34, 35
18, 35, 36, 37
19, 37, 38, 39
20, 39, 40, 41
21, 42, 43, 44
22, 44, 45, 46
23, 46, 47, 48
24, 48, 49, 50
25, 50, 51, 52
26, 52, 53, 54
27, 54, 55, 56
28, 56, 57, 58
29, 58, 59, 60
30, 60, 61, 62
31, 62, 63, 64

32, 64, 65, 66
33, 66, 67, 68
34, 68, 69, 70
35, 70, 71, 72
36, 73, 74, 75
37, 75, 76, 77
38, 77, 78, 79
39, 79, 80, 81
40, 81, 82, 83
41, 83, 84, 85
42, 85, 86, 87
43, 87, 88, 89
44, 89, 90, 91
45, 91, 92, 93
46, 93, 94, 95
47, 95, 96, 97
48, 97, 98, 99
49, 99, 100, 101
50, 101, 102, 103
51, 103, 104, 105
52, 106, 107, 108
53, 108, 109, 110
54, 110, 111, 112
55, 112, 113, 114
56, 114, 115, 116
57, 116, 117, 118
58, 118, 119, 120
59, 120, 121, 122
60, 122, 123, 124
61, 124, 125, 126
62, 126, 127, 128
63, 128, 129, 130
64, 130, 131, 132
65, 132, 133, 134
66, 135, 136, 137
67, 137, 138, 139
68, 139, 140, 141
69, 141, 142, 143
70, 143, 144, 145
71, 145, 146, 147
72, 147, 148, 149
73, 149, 150, 151
74, 151, 152, 153
75, 153, 154, 155
76, 155, 156, 157
77, 157, 158, 159
*Nset, nset=NABUT_SOUTH

160,
*Nset, nset=NABUT_NORTH
161,
*Nset, nset=NSOIL_SOUTH
162,
*Nset, nset=NSOIL_NORTH
163,
*Nset, nset=NF11
164,
*Nset, nset=NF12
165,
*Nset, nset=NF13
166,
*Nset, nset=NF14
167,
*Nset, nset=NF15
168,
*Nset, nset=NF16
169,
*Nset, nset=NF17
170,
*Nset, nset=NF18
171,
*Nset, nset=NF19
172,
*Nset, nset=NF110
173,
*Nset, nset=NF21
174,
*Nset, nset=NF22
175,
*Nset, nset=NF23
176,
*Nset, nset=NF24
177,
*Nset, nset=NF25
178,
*Nset, nset=NF26
179,
*Nset, nset=NF27
180,
*Nset, nset=NF28
181,
*Nset, nset=NF29
182,
*Nset, nset=NF210
183,

*Nset, nset=NF31
184,
*Nset, nset=NF32
185,
*Nset, nset=NF33
186,
*Nset, nset=NF34
187,
*Nset, nset=NF35
188,
*Nset, nset=NF36
189,
*Nset, nset=NF37
190,
*Nset, nset=NF38
191,
*Nset, nset=NF39
192,
*Nset, nset=NF310
193,
*Nset, nset=NF41
194,
*Nset, nset=NF42
195,
*Nset, nset=NF43
196,
*Nset, nset=NF44
197,
*Nset, nset=NF45
198,
*Nset, nset=NF46
199,
*Nset, nset=NF47
200,
*Nset, nset=NF48
201,
*Nset, nset=NF49
202,
*Nset, nset=NF410
203,
*Elset, elset=C1, generate
21, 30, 1
*Elset, elset=C2, generate
36, 46, 1
*Elset, elset=C3, generate
52, 60, 1
*Elset, elset=C4, generate

```

66, 72, 1
*Elset, elset=PILE1, generate
31, 35, 1
*Elset, elset=PILE2, generate
47, 51, 1
*Elset, elset=PILE3, generate
61, 65, 1
*Elset, elset=PILE4, generate
73, 77, 1
*Elset, elset=DECK, generate
1, 20, 1
*BEAM GENERAL SECTION,elset=DECK, SECTION=MESHED
0.0,1.0,0.0
*INCLUDE, INPUT=Model90Section.bsp
*Elset, elset=COLUMNSANDPILES, generate
21, 77, 1
*Nset, nset=NDECKS
1,
*Nset, nset=NDECKN
41,
*Nset, nset=NF1MASS
72,
*Nset, nset=NF2MASS
105,
*Nset, nset=NF3MASS
134,
*Nset, nset=NF4MASS
159,
*Nset, nset=NSOILABUTANDFOOT
162, 163, 173, 183, 193, 203
*Nset, nset=NBASECOLUMNS
62, 95, 124, 149
*Nset, nset=NTOPCOLUMNS
43, 74, 107, 136
*Nset, nset=NSOILSPRINGS
162, 163, 164, 165, 166, 167, 169, 171, 173, 174, 175, 176, 177, 179, 181, 183
184, 185, 186, 187, 189, 191, 193, 194, 195, 196, 197, 199, 201, 203
*Nset, nset=NColumnsBottom
61, 94, 123, 148
** Region: (Section-1-C1:Picked), (Beam Orientation:C1)
*Elset, elset=_I2, internal
21, 22, 30
** Section: Section-1-C1 Profile: Profile-1
*Beam Section, elset=_I2, material=CONCRETE_HINGE, temperature=GRADIENTS,
section=RECT
1.2192, 0.6096
0.17365,0.984807,0.

```

** Region: (Section-C1 m:Picked), (Beam Orientation:C1)
 *Elset, elset=_PickedSet367, internal, generate
 23, 29, 1
 ** Section: Section-C1 m Profile: Profile-1
 *Beam Section, elset=_PickedSet367, material=CONCRETE, temperature=GRADIENTS,
 section=RECT
 1.2192, 0.6096
 0.17365,0.984807,0.

** Region: (Section-2-PILE1:PILE1), (Beam Orientation:PILE1)
 ** Section: Section-2-PILE1 Profile: Profile-2
 *Beam Section, elset=PILE1, material=CONCRETE, temperature=GRADIENTS,
 section=RECT
 1.2192, 0.6096
 0.17365,0.984807,0.

** Region: (Section-3-C2:Picked), (Beam Orientation:C2)
 *Elset, elset=_PickedSet368, internal
 36, 37, 45, 46
 ** Section: Section-3-C2 Profile: Profile-3
 *Beam Section, elset=_PickedSet368, material=CONCRETE_HINGE,
 temperature=GRADIENTS, section=RECT
 1.2192, 0.6096
 0.17365,0.984807,0.

** Region: (Section-C2 m:Picked), (Beam Orientation:C2)
 *Elset, elset=_PickedSet371, internal, generate
 38, 44, 1
 ** Section: Section-C2 m Profile: Profile-1
 *Beam Section, elset=_PickedSet371, material=CONCRETE, temperature=GRADIENTS,
 section=RECT
 1.2192, 0.6096
 0.17365,0.984807,0.

** Region: (Section-4-PILE2:PILE2), (Beam Orientation:PILE2)
 ** Section: Section-4-PILE2 Profile: Profile-4
 *Beam Section, elset=PILE2, material=CONCRETE, temperature=GRADIENTS,
 section=RECT
 1.2192, 0.6096
 0.17365,0.984807,0.

** Region: (Section-5-C3:Picked), (Beam Orientation:C3)
 *Elset, elset=_PickedSet369, internal
 52, 53, 59, 60
 ** Section: Section-5-C3 Profile: Profile-5
 *Beam Section, elset=_PickedSet369, material=CONCRETE_HINGE,
 temperature=GRADIENTS, section=RECT
 1.2192, 0.6096
 0.17365,0.984807,0.

** Region: (Section-C3 m:Picked), (Beam Orientation:C3)
 *Elset, elset=_PickedSet372, internal, generate
 54, 58, 1

** Section: Section-C3 m Profile: Profile-1
 *Beam Section, elset=_PickedSet372, material=CONCRETE, temperature=GRADIENTS,
 section=RECT
 1.2192, 0.6096
 0.17365,0.984807,0.
 ** Region: (Section-6-PILE3:PILE3), (Beam Orientation:PILE3)
 ** Section: Section-6-PILE3 Profile: Profile-6
 *Beam Section, elset=PILE3, material=CONCRETE, temperature=GRADIENTS,
 section=RECT
 1.2192, 0.6096
 0.17365,0.984807,0.
 ** Region: (Section-7-C4:Picked), (Beam Orientation:C4)
 *Elset, elset=_PickedSet370, internal
 66, 67, 71, 72
 ** Section: Section-7-C4 Profile: Profile-7
 *Beam Section, elset=_PickedSet370, material=CONCRETE_HINGE,
 temperature=GRADIENTS, section=RECT
 1.2192, 0.6096
 0.17365,0.984807,0.
 ** Region: (Section-C4 m:Picked), (Beam Orientation:C4)
 *Elset, elset=_PickedSet373, internal, generate
 68, 70, 1
 ** Section: Section-C4 m Profile: Profile-1
 *Beam Section, elset=_PickedSet373, material=CONCRETE, temperature=GRADIENTS,
 section=RECT
 1.2192, 0.6096
 0.17365,0.984807,0.
 ** Region: (Section-8-PILE4:PILE4), (Beam Orientation:PILE4)
 ** Section: Section-8-PILE4 Profile: Profile-8
 *Beam Section, elset=PILE4, material=CONCRETE, temperature=GRADIENTS,
 section=RECT
 1.2192, 0.6096
 0.17365,0.984807,0.
 *Element, type=MASS, elset=NABUT_NORTH_MASSABUTNORTH_
 78, 161
 *Mass, elset=NABUT_NORTH_MASSABUTNORTH_
 158000.,
 *Element, type=MASS, elset=NABUT_SOUTH_MASSABUTSOUTH_
 79, 160
 *Mass, elset=NABUT_SOUTH_MASSABUTSOUTH_
 187000.,
 *Element, type=MASS, elset=_PickedSet171_MASSFOOT1_
 80, 72
 *Mass, elset=_PickedSet171_MASSFOOT1_
 140000.,
 *Element, type=MASS, elset=_PickedSet172_MASSFOOT2_
 81, 105

```

*Mass, elset=_PickedSet172_MASSFOOT2_
86000.,
*Element, type=MASS, elset=_PickedSet173_MASSFOOT3_
82, 134
*Mass, elset=_PickedSet173_MASSFOOT3_
66000.,
*Element, type=MASS, elset=_PickedSet174_MASSFOOT4_
83, 159
*Mass, elset=_PickedSet174_MASSFOOT4_
140000.,
*Element, type=Spring2, elset="AD N 1-spring"
84, 41, 161
*Spring, elset="AD N 1-spring", nonlinear
1, 1
0,-0.1
0,0
3325806.69182682,0.0131969565217391
3325806.69182682,0.15
*Element, type=Spring2, elset="AD N 1 BEARING-spring"
85, 161, 41
*Spring, elset="AD N 1 BEARING-spring"
1, 1
7.53e+06
*Element, type=Spring2, elset="AD N 2-spring"
86, 161, 41
*Spring, elset="AD N 2-spring"
2, 2
4.38e+10
*Element, type=Spring2, elset="AD N 3-spring"
87, 161, 41
*Spring, elset="AD N 3-spring"
3, 3
3e+11
*Element, type=Spring2, elset="AD N 4-spring"
88, 161, 41
*Spring, elset="AD N 4-spring"
4, 4
1e+11
*Element, type=Spring2, elset="AD N 5-spring"
89, 161, 41
*Spring, elset="AD N 5-spring"
5, 5
1e+08
*Element, type=Spring2, elset="AD N 6-spring"
90, 161, 41
*Spring, elset="AD N 6-spring"
6, 6

```

```

1e+08
*Element, type=Spring2, elset="AD S 1 GAP-spring"
91, 160, 1
*Spring, elset="AD S 1 GAP-spring", nonlinear
1, 1
0,-0.1
0,0
0,0.0762
4789161.63623063,0.0876021704347826
4789161.63623063,0.15
*Element, type=Spring2, elset="AD S 2-spring"
92, 160, 1
*Spring, elset="AD S 2-spring"
2, 2
4.38e+10
*Element, type=Spring2, elset="AD S 3-spring"
93, 160, 1
*Spring, elset="AD S 3-spring"
3, 3
3e+11
*Element, type=Spring2, elset="AD S 4-spring"
94, 160, 1
*Spring, elset="AD S 4-spring"
4, 4
1e+11
*Element, type=Spring2, elset="AD S 5-spring"
95, 160, 1
*Spring, elset="AD S 5-spring"
5, 5
1e+08
*Element, type=Spring2, elset="AD S 6-spring"
96, 160, 1
*Spring, elset="AD S 6-spring"
6, 6
1e+08
*Element, type=Spring2, elset="FOOT 11-spring"
97, 173, 72
*Spring, elset="FOOT 11-spring"
1, 1
1.3e+10
*Element, type=Spring2, elset="FOOT 12-spring"
98, 173, 72
*Spring, elset="FOOT 12-spring"
2, 2
1.38e+10
*Element, type=Spring2, elset="FOOT 13-spring"
99, 173, 72

```

*Spring, elset="FOOT 13-spring"
3, 3
9.99e+09
*Element, type=Spring2, elset="FOOT 14-spring"
100, 173, 72
*Spring, elset="FOOT 14-spring"
4, 4
1.11e+11
*Element, type=Spring2, elset="FOOT 15-spring"
101, 173, 72
*Spring, elset="FOOT 15-spring"
5, 5
3e+11
*Element, type=Spring2, elset="FOOT 16-spring"
102, 173, 72
*Spring, elset="FOOT 16-spring"
6, 6
3.32e+11
*Element, type=Spring2, elset="FOOT 21-spring"
103, 183, 105
*Spring, elset="FOOT 21-spring"
1, 1
1.07e+10
*Element, type=Spring2, elset="FOOT 22-spring"
104, 183, 105
*Spring, elset="FOOT 22-spring"
2, 2
1.13e+10
*Element, type=Spring2, elset="FOOT 23-spring"
105, 183, 105
*Spring, elset="FOOT 23-spring"
3, 3
7.71e+09
*Element, type=Spring2, elset="FOOT 24-spring"
106, 183, 105
*Spring, elset="FOOT 24-spring"
4, 4
4.01e+10
*Element, type=Spring2, elset="FOOT 25-spring"
107, 183, 105
*Spring, elset="FOOT 25-spring"
5, 5
9.94e+10
*Element, type=Spring2, elset="FOOT 26-spring"
108, 183, 105
*Spring, elset="FOOT 26-spring"
6, 6

1.16e+11
*Element, type=Spring2, elset="FOOT 31-spring"
109, 193, 134
*Spring, elset="FOOT 31-spring"
1, 1
1.03e+10
*Element, type=Spring2, elset="FOOT 32-spring"
110, 193, 134
*Spring, elset="FOOT 32-spring"
2, 2
1.09e+10
*Element, type=Spring2, elset="FOOT 33-spring"
111, 193, 134
*Spring, elset="FOOT 33-spring"
3, 3
7.27e+09
*Element, type=Spring2, elset="FOOT 34-spring"
112, 193, 134
*Spring, elset="FOOT 34-spring"
4, 4
2.93e+10
*Element, type=Spring2, elset="FOOT 35-spring"
113, 193, 134
*Spring, elset="FOOT 35-spring"
5, 5
7.01e+10
*Element, type=Spring2, elset="FOOT 36-spring"
114, 193, 134
*Spring, elset="FOOT 36-spring"
6, 6
8.25e+10
*Element, type=Spring2, elset="FOOT 41-spring"
115, 203, 159
*Spring, elset="FOOT 41-spring"
1, 1
1.26e+10
*Element, type=Spring2, elset="FOOT 42-spring"
116, 203, 159
*Spring, elset="FOOT 42-spring"
2, 2
1.33e+10
*Element, type=Spring2, elset="FOOT 43-spring"
117, 203, 159
*Spring, elset="FOOT 43-spring"
3, 3
9.69e+09
*Element, type=Spring2, elset="FOOT 44-spring"

118, 203, 159
*Spring, elset="FOOT 44-spring"
4, 4
1.11e+11
*Element, type=Spring2, elset="FOOT 45-spring"
119, 203, 159
*Spring, elset="FOOT 45-spring"
5, 5
2.99e+11
*Element, type=Spring2, elset="FOOT 46-spring"
120, 203, 159
*Spring, elset="FOOT 46-spring"
6, 6
3.32e+11
*Element, type=Spring2, elset="SA N 1-spring"
121, 163, 161
*Spring, elset="SA N 1-spring"
1, 1
6.56e+09
*Element, type=Spring2, elset="SA N 2-spring"
122, 163, 161
*Spring, elset="SA N 2-spring"
2, 2
1.02e+10
*Element, type=Spring2, elset="SA N 3-spring"
123, 163, 161
*Spring, elset="SA N 3-spring"
3, 3
5.89e+09
*Element, type=Spring2, elset="SA N 4-spring"
124, 163, 161
*Spring, elset="SA N 4-spring"
4, 4
4.9e+10
*Element, type=Spring2, elset="SA N 5-spring"
125, 163, 161
*Spring, elset="SA N 5-spring"
5, 5
1.27e+11
*Element, type=Spring2, elset="SA N 6-spring"
126, 163, 161
*Spring, elset="SA N 6-spring"
6, 6
1.51e+11
*Element, type=Spring2, elset="SA S 1-spring"
127, 162, 160
*Spring, elset="SA S 1-spring"

1, 1
 6.45e+09
 *Element, type=Spring2, elset="SA S 2-spring"
 128, 162, 160
 *Spring, elset="SA S 2-spring"
 2, 2
 6.98e+09
 *Element, type=Spring2, elset="SA S 3-spring"
 129, 162, 160
 *Spring, elset="SA S 3-spring"
 3, 3
 5.57e+09
 *Element, type=Spring2, elset="SA S 4-spring"
 130, 162, 160
 *Spring, elset="SA S 4-spring"
 4, 4
 3.35e+10
 *Element, type=Spring2, elset="SA S 5-spring"
 131, 162, 160
 *Spring, elset="SA S 5-spring"
 5, 5
 1.08e+11
 *Element, type=Spring2, elset="SA S 6-spring"
 132, 162, 160
 *Spring, elset="SA S 6-spring"
 6, 6
 1.3e+11
 *Element, type=Spring2, elset="SF1 N11-spring"
 133, 164, 63
 *Spring, elset="SF1 N11-spring", nonlinear
 1, 1
 -0.192,-803663.651315909
 -0.048,-568276.106627273
 0,0
 0.048,568276.106627273
 0.192,803663.651315909
 *Element, type=Spring2, elset="SF1 N12-spring"
 134, 164, 63
 *Spring, elset="SF1 N12-spring", nonlinear
 2, 2
 -0.096,-401943.302002273
 -0.024,-284217.290854545
 0,0
 0.024,284217.290854545
 0.096,401943.302002273
 *Element, type=Spring2, elset="SF1 N21-spring"
 135, 165, 64

```

*Spring, elset="SF1 N21-spring", nonlinear
1, 1
-0.192,-2012411.36324091
-0.048,-1422989.70893182
0,0
0.048,1422989.70893182
0.192,2012411.36324091
*Element, type=Spring2, elset="SF1 N22-spring"
136, 165, 64
*Spring, elset="SF1 N22-spring", nonlinear
2, 2
-0.096,-1186415.93164545
-0.024,-838922.026504545
0,0
0.024,838922.026504545
0.096,1186415.93164545
*Element, type=Spring2, elset="SF1 N31-spring"
137, 166, 65
*Spring, elset="SF1 N31-spring", nonlinear
1, 1
-0.192,-2417995.70793182
-0.048,-1709781.44302727
0,0
0.048,1709781.44302727
0.192,2417995.70793182
*Element, type=Spring2, elset="SF1 N32-spring"
138, 166, 65
*Spring, elset="SF1 N32-spring", nonlinear
2, 2
-0.096,-1569417.57717727
-0.024,-1109746.61926818
0,0
0.024,1109746.61926818
0.096,1569417.57717727
*Element, type=Spring2, elset="SF1 N41-spring"
139, 167, 66
*Spring, elset="SF1 N41-spring", nonlinear
1, 1
-0.192,-4235372.40945
-0.048,-2994859.76568409
0,0
0.048,2994859.76568409
0.192,4235372.40945
*Element, type=Spring2, elset="SF1 N42-spring"
140, 167, 66
*Spring, elset="SF1 N42-spring", nonlinear
2, 2

```



```

-0.096,-2928631.16457955
-0.024,-2070854.48753182
0,0
0.024,2070854.48753182
0.096,2928631.16457955
*Element, type=Spring2, elset="SF1 N51-spring"
141, 169, 68
*Spring, elset="SF1 N51-spring", nonlinear
1, 1
-0.192,-7269503.69871818
-0.048,-5140316.39798182
0,0
0.048,5140316.39798182
0.192,7269503.69871818
*Element, type=Spring2, elset="SF1 N52-spring"
142, 169, 68
*Spring, elset="SF1 N52-spring", nonlinear
2, 2
-0.096,-4820476.39461818
-0.024,-3408590.81715454
0,0
0.024,3408590.81715454
0.096,4820476.39461818
*Element, type=Spring2, elset="SF1 N61-spring"
143, 171, 70
*Spring, elset="SF1 N61-spring", nonlinear
1, 1
-0.192,-8891844.18483636
-0.048,-6287483.33436364
0,0
0.048,6287483.33436364
0.192,8891844.18483636
*Element, type=Spring2, elset="SF1 N62-spring"
144, 171, 70
*Spring, elset="SF1 N62-spring", nonlinear
2, 2
-0.096,-4820476.39461818
-0.024,-3408590.81715454
0,0
0.024,3408590.81715454
0.096,4820476.39461818
*Element, type=Spring2, elset="SF2 N11-spring"
145, 174, 96
*Spring, elset="SF2 N11-spring", nonlinear
1, 1
-0.192,-803663.651315909
-0.048,-568276.106627273

```

0,0
0.048,568276.106627273
0.192,803663.651315909
*Element, type=Spring2, elset="SF2 N12-spring"
146, 174, 96
*Spring, elset="SF2 N12-spring", nonlinear
2, 2
-0.096,-401943.302002273
-0.024,-284217.290854545
0,0
0.024,284217.290854545
0.096,401943.302002273
*Element, type=Spring2, elset="SF2 N21-spring"
147, 175, 97
*Spring, elset="SF2 N21-spring", nonlinear
1, 1
-0.192,-2012411.36324091
-0.048,-1422989.70893182
0,0
0.048,1422989.70893182
0.192,2012411.36324091
*Element, type=Spring2, elset="SF2 N22-spring"
148, 175, 97
*Spring, elset="SF2 N22-spring", nonlinear
2, 2
-0.096,-1186415.93164545
-0.024,-838922.026504545
0,0
0.024,838922.026504545
0.096,1186415.93164545
*Element, type=Spring2, elset="SF2 N31-spring"
149, 176, 98
*Spring, elset="SF2 N31-spring", nonlinear
1, 1
-0.192,-2417995.70793182
-0.048,-1709781.44302727
0,0
0.048,1709781.44302727
0.192,2417995.70793182
*Element, type=Spring2, elset="SF2 N32-spring"
150, 176, 98
*Spring, elset="SF2 N32-spring", nonlinear
2, 2
-0.096,-1569417.57717727
-0.024,-1109746.61926818
0,0
0.024,1109746.61926818

0.096,1569417.57717727
 *Element, type=Spring2, elset="SF2 N41-spring"
 151, 177, 99
 *Spring, elset="SF2 N41-spring", nonlinear
 1, 1
 -0.192,-4235372.40945
 -0.048,-2994859.76568409
 0,0
 0.048,2994859.76568409
 0.192,4235372.40945
 *Element, type=Spring2, elset="SF2 N42-spring"
 152, 177, 99
 *Spring, elset="SF2 N42-spring", nonlinear
 2, 2
 -0.096,-2928631.16457955
 -0.024,-2070854.48753182
 0,0
 0.024,2070854.48753182
 0.096,2928631.16457955
 *Element, type=Spring2, elset="SF2 N51-spring"
 153, 179, 101
 *Spring, elset="SF2 N51-spring", nonlinear
 1, 1
 -0.192,-7269503.69871818
 -0.048,-5140316.39798182
 0,0
 0.048,5140316.39798182
 0.192,7269503.69871818
 *Element, type=Spring2, elset="SF2 N52-spring"
 154, 179, 101
 *Spring, elset="SF2 N52-spring", nonlinear
 2, 2
 -0.096,-4820476.39461818
 -0.024,-3408590.81715454
 0,0
 0.024,3408590.81715454
 0.096,4820476.39461818
 *Element, type=Spring2, elset="SF2 N61-spring"
 155, 181, 103
 *Spring, elset="SF2 N61-spring", nonlinear
 1, 1
 -0.192,-8891844.18483636
 -0.048,-6287483.33436364
 0,0
 0.048,6287483.33436364
 0.192,8891844.18483636
 *Element, type=Spring2, elset="SF2 N62-spring"

156, 181, 103
 *Spring, elset="SF2 N62-spring", nonlinear
 2, 2
 -0.096,-4820476.39461818
 -0.024,-3408590.81715454
 0,0
 0.024,3408590.81715454
 0.096,4820476.39461818
 *Element, type=Spring2, elset="SF3 N11-spring"
 157, 184, 125
 *Spring, elset="SF3 N11-spring", nonlinear
 1, 1
 -0.192,-803663.651315909
 -0.048,-568276.106627273
 0,0
 0.048,568276.106627273
 0.192,803663.651315909
 *Element, type=Spring2, elset="SF3 N12-spring"
 158, 184, 125
 *Spring, elset="SF3 N12-spring", nonlinear
 2, 2
 -0.096,-401943.302002273
 -0.024,-284217.290854545
 0,0
 0.024,284217.290854545
 0.096,401943.302002273
 *Element, type=Spring2, elset="SF3 N21-spring"
 159, 185, 126
 *Spring, elset="SF3 N21-spring", nonlinear
 1, 1
 -0.192,-2012411.36324091
 -0.048,-1422989.70893182
 0,0
 0.048,1422989.70893182
 0.192,2012411.36324091
 *Element, type=Spring2, elset="SF3 N22-spring"
 160, 185, 126
 *Spring, elset="SF3 N22-spring", nonlinear
 2, 2
 -0.096,-1186415.93164545
 -0.024,-838922.026504545
 0,0
 0.024,838922.026504545
 0.096,1186415.93164545
 *Element, type=Spring2, elset="SF3 N31-spring"
 161, 186, 127
 *Spring, elset="SF3 N31-spring", nonlinear

```

1, 1
-0.192,-2417995.70793182
-0.048,-1709781.44302727
0,0
0.048,1709781.44302727
0.192,2417995.70793182
*Element, type=Spring2, elset="SF3 N32-spring"
162, 186, 127
*Spring, elset="SF3 N32-spring", nonlinear
2, 2
-0.096,-1569417.57717727
-0.024,-1109746.61926818
0,0
0.024,1109746.61926818
0.096,1569417.57717727
*Element, type=Spring2, elset="SF3 N41-spring"
163, 187, 128
*Spring, elset="SF3 N41-spring", nonlinear
1, 1
-0.192,-4235372.40945
-0.048,-2994859.76568409
0,0
0.048,2994859.76568409
0.192,4235372.40945
*Element, type=Spring2, elset="SF3 N42-spring"
164, 187, 128
*Spring, elset="SF3 N42-spring", nonlinear
2, 2
-0.096,-2928631.16457955
-0.024,-2070854.48753182
0,0
0.024,2070854.48753182
0.096,2928631.16457955
*Element, type=Spring2, elset="SF3 N51-spring"
165, 189, 130
*Spring, elset="SF3 N51-spring", nonlinear
1, 1
-0.192,-7269503.69871818
-0.048,-5140316.39798182
0,0
0.048,5140316.39798182
0.192,7269503.69871818
*Element, type=Spring2, elset="SF3 N52-spring"
166, 189, 130
*Spring, elset="SF3 N52-spring", nonlinear
2, 2
-0.096,-4820476.39461818

```

```

-0.024,-3408590.81715454
0,0
0.024,3408590.81715454
0.096,4820476.39461818
*Element, type=Spring2, elset="SF3 N61-spring"
167, 191, 132
*Spring, elset="SF3 N61-spring", nonlinear
1, 1
-0.192,-8891844.18483636
-0.048,-6287483.33436364
0,0
0.048,6287483.33436364
0.192,8891844.18483636
*Element, type=Spring2, elset="SF3 N62-spring"
168, 191, 132
*Spring, elset="SF3 N62-spring", nonlinear
2, 2
-0.096,-4820476.39461818
-0.024,-3408590.81715454
0,0
0.024,3408590.81715454
0.096,4820476.39461818
*Element, type=Spring2, elset="SF4 N11-spring"
169, 194, 150
*Spring, elset="SF4 N11-spring", nonlinear
1, 1
-0.192,-803663.651315909
-0.048,-568276.106627273
0,0
0.048,568276.106627273
0.192,803663.651315909
*Element, type=Spring2, elset="SF4 N12-spring"
170, 194, 150
*Spring, elset="SF4 N12-spring", nonlinear
2, 2
-0.096,-401943.302002273
-0.024,-284217.290854545
0,0
0.024,284217.290854545
0.096,401943.302002273
*Element, type=Spring2, elset="SF4 N21-spring"
171, 195, 151
*Spring, elset="SF4 N21-spring", nonlinear
1, 1
-0.192,-2012411.36324091
-0.048,-1422989.70893182
0,0

```

0.048,1422989.70893182
 0.192,2012411.36324091
 *Element, type=Spring2, elset="SF4 N22-spring"
 172, 195, 151
 *Spring, elset="SF4 N22-spring", nonlinear
 2, 2
 -0.096,-1186415.93164545
 -0.024,-838922.026504545
 0,0
 0.024,838922.026504545
 0.096,1186415.93164545
 *Element, type=Spring2, elset="SF4 N31-spring"
 173, 196, 152
 *Spring, elset="SF4 N31-spring", nonlinear
 1, 1
 -0.192,-2417995.70793182
 -0.048,-1709781.44302727
 0,0
 0.048,1709781.44302727
 0.192,2417995.70793182
 *Element, type=Spring2, elset="SF4 N32-spring"
 174, 196, 152
 *Spring, elset="SF4 N32-spring", nonlinear
 2, 2
 -0.096,-1569417.57717727
 -0.024,-1109746.61926818
 0,0
 0.024,1109746.61926818
 0.096,1569417.57717727
 *Element, type=Spring2, elset="SF4 N41-spring"
 175, 197, 153
 *Spring, elset="SF4 N41-spring", nonlinear
 1, 1
 -0.192,-4235372.40945
 -0.048,-2994859.76568409
 0,0
 0.048,2994859.76568409
 0.192,4235372.40945
 *Element, type=Spring2, elset="SF4 N42-spring"
 176, 197, 153
 *Spring, elset="SF4 N42-spring", nonlinear
 2, 2
 -0.096,-2928631.16457955
 -0.024,-2070854.48753182
 0,0
 0.024,2070854.48753182
 0.096,2928631.16457955

```

*Element, type=Spring2, elset="SF4 N51-spring"
177, 199, 155
*Spring, elset="SF4 N51-spring", nonlinear
1, 1
-0.192,-7269503.69871818
-0.048,-5140316.39798182
0,0
0.048,5140316.39798182
0.192,7269503.69871818
*Element, type=Spring2, elset="SF4 N52-spring"
178, 199, 155
*Spring, elset="SF4 N52-spring", nonlinear
2, 2
-0.096,-4820476.39461818
-0.024,-3408590.81715454
0,0
0.024,3408590.81715454
0.096,4820476.39461818
*Element, type=Spring2, elset="SF4 N61-spring"
179, 201, 157
*Spring, elset="SF4 N61-spring", nonlinear
1, 1
-0.192,-8891844.18483636
-0.048,-6287483.33436364
0,0
0.048,6287483.33436364
0.192,8891844.18483636
*Element, type=Spring2, elset="SF4 N62-spring"
180, 201, 157
*Spring, elset="SF4 N62-spring", nonlinear
2, 2
-0.096,-4820476.39461818
-0.024,-3408590.81715454
0,0
0.024,3408590.81715454
0.096,4820476.39461818
*End Part
**
**
** ASSEMBLY
**
*Assembly, name=Assembly
**
*Instance, name=BRIDGE-1, part=BRIDGE
** REBAR FOR WHOLE COLUMNS
**
*REBAR,ELEMENT=BEAM,MATERIAL="Steel Rebar",NAME=RB1

```


COLUMNSANDPILES,0.001007385,-0.5588,-0.254
 *REBAR,ELEMENT=BEAM,MATERIAL="Steel Rebar",NAME=RB2
 COLUMNSANDPILES,0.001007385,-0.4064,-0.254
 *REBAR,ELEMENT=BEAM,MATERIAL="Steel Rebar",NAME=RB3
 COLUMNSANDPILES,0.001007385,-0.2032,-0.254
 *REBAR,ELEMENT=BEAM,MATERIAL="Steel Rebar",NAME=RB4
 COLUMNSANDPILES,0.001007385,0,-0.254
 *REBAR,ELEMENT=BEAM,MATERIAL="Steel Rebar",NAME=RB5
 COLUMNSANDPILES,0.001007385,0.2032,-0.254
 *REBAR,ELEMENT=BEAM,MATERIAL="Steel Rebar",NAME=RB6
 COLUMNSANDPILES,0.001007385,0.4064,-0.254
 *REBAR,ELEMENT=BEAM,MATERIAL="Steel Rebar",NAME=RB7
 COLUMNSANDPILES,0.001007385,0.5588,-0.254
 *REBAR,ELEMENT=BEAM,MATERIAL="Steel Rebar",NAME=RB8
 COLUMNSANDPILES,0.001007385,0.5588,-0.127
 *REBAR,ELEMENT=BEAM,MATERIAL="Steel Rebar",NAME=RB9
 COLUMNSANDPILES,0.001007385,0.5588,0
 *REBAR,ELEMENT=BEAM,MATERIAL="Steel Rebar",NAME=RB10
 COLUMNSANDPILES,0.001007385,0.5588,0.127
 *REBAR,ELEMENT=BEAM,MATERIAL="Steel Rebar",NAME=RB11
 COLUMNSANDPILES,0.001007385,0.5588,0.254
 *REBAR,ELEMENT=BEAM,MATERIAL="Steel Rebar",NAME=RB12
 COLUMNSANDPILES,0.001007385,0.4064,0.254
 *REBAR,ELEMENT=BEAM,MATERIAL="Steel Rebar",NAME=RB13
 COLUMNSANDPILES,0.001007385,0.2032,0.254
 *REBAR,ELEMENT=BEAM,MATERIAL="Steel Rebar",NAME=RB14
 COLUMNSANDPILES,0.001007385,0,0.254
 *REBAR,ELEMENT=BEAM,MATERIAL="Steel Rebar",NAME=RB15
 COLUMNSANDPILES,0.001007385,-0.2032,0.254
 *REBAR,ELEMENT=BEAM,MATERIAL="Steel Rebar",NAME=RB16
 COLUMNSANDPILES,0.001007385,-0.4064,0.254
 *REBAR,ELEMENT=BEAM,MATERIAL="Steel Rebar",NAME=RB17
 COLUMNSANDPILES,0.001007385,-0.5588,0.254
 *REBAR,ELEMENT=BEAM,MATERIAL="Steel Rebar",NAME=RB18
 COLUMNSANDPILES,0.001007385,-0.5588,0.127
 *REBAR,ELEMENT=BEAM,MATERIAL="Steel Rebar",NAME=RB19
 COLUMNSANDPILES,0.001007385,-0.5588,0
 *REBAR,ELEMENT=BEAM,MATERIAL="Steel Rebar",NAME=RB20
 COLUMNSANDPILES,0.001007385,-0.5588,-0.127
 *REBAR,ELEMENT=BEAM,MATERIAL="Steel Rebar",NAME=RB21
 COLUMNSANDPILES,0.001007385,-0.4064,0
 *REBAR,ELEMENT=BEAM,MATERIAL="Steel Rebar",NAME=RB22
 COLUMNSANDPILES,0.001007385,0.4064,0
 *End Instance
 **
 *Orientation, name="DATUM CSYS-1"
 1., 0., 0., 0., 1., 0.

```

1, 0.
**
** CONNECTORS
**
*Element, type=CONN3D2, elset=_Conn-1_CnSet_
1, BRIDGE-1.42, BRIDGE-1.9
*Connector Section, elset=_Conn-1_CnSet_
Beam,
"DATUM CSYS-1",
*Element, type=CONN3D2, elset=_Conn-2_CnSet_
2, BRIDGE-1.73, BRIDGE-1.17
*Connector Section, elset=_Conn-2_CnSet_
Beam,
"DATUM CSYS-1",
*Element, type=CONN3D2, elset=_Conn-3_CnSet_
3, BRIDGE-1.106, BRIDGE-1.25
*Connector Section, elset=_Conn-3_CnSet_
Beam,
"DATUM CSYS-1",
*Element, type=CONN3D2, elset=_Conn-4_CnSet_
4, BRIDGE-1.135, BRIDGE-1.33
*Connector Section, elset=_Conn-4_CnSet_
Beam,
"DATUM CSYS-1",
*End Assembly
**
** MATERIALS
**
*Material, name=CONCRETE
*Concrete
5.17e+07, 0.
4.4e+07, 0.0047
0., 0.007
*Tension Stiffening
1., 0.
0.5, 0.00078
0.15, 0.00282
0., 0.004
*Damping, alpha=0.2, beta=0.007
*Density
2400.,
*Elastic
1.72e+10, 0.18
*Material, name=CONCRETELIN
*Damping, alpha=0.2, beta=0.007
*Density
2400.,

```

```

*Elastic
1.72e+10, 0.18
*Material, name=CONCRETE_HINGE
*Concrete
5.17e+07, 0.
8.53e+07, 0.0098
7.25e+07, 0.0236
0., 0.04
*Tension Stiffening
1., 0.
0.5, 0.00101
0.15, 0.00363
0., 0.005
*Damping, alpha=0.2, beta=0.007
*Density
2400.,
*Elastic
1.72e+10, 0.18
*Material, name="STEEL REBAR"
*Damping, alpha=0.2, beta=0.005
*Elastic
2e+11, 0.3
*Plastic, hardening=COMBINED
2.76e+08, 0.
4.14e+08, 0.00862069
6.21e+08, 0.0586207
6.21e+08, 0.0886207
4.96e+08, 0.138621
0., 0.15
**
** BOUNDARY CONDITIONS
**
** Name: BC-FixBase Type: Displacement/Rotation
*Boundary
BRIDGE-1.NSOILSPRINGS, 1, 1
BRIDGE-1.NSOILSPRINGS, 2, 2
BRIDGE-1.NSOILSPRINGS, 3, 3
BRIDGE-1.NSOILSPRINGS, 4, 4
BRIDGE-1.NSOILSPRINGS, 5, 5
BRIDGE-1.NSOILSPRINGS, 6, 6
** -----
**
** STEP: Step-1
**
*Step, name=Step-1, nlgeom=YES
*Static
1., 1., 1e-05, 1.

```

```

**
** LOADS
**
** Name: Load-1 Type: Gravity
*Dload
, GRAV, 9.81, 0., 0., -1.
**
** OUTPUT REQUESTS
**
*Restart, write, frequency=0
**
** FIELD OUTPUT: F-Output-1
**
*Output, field
*Node Output
RF, U
*Element Output, directions=YES
SE, SF
**
** HISTORY OUTPUT: H-Output-1
**
*Output, history
*Element Output, elset=BRIDGE-1.COLUMN SANDPILES
ELKE, ELPD, ELSE
*End Step
** -----
**
** STEP: Step-2
**
*Step, name=Step-2, nlgeom=YES, amplitude=RAMP, inc=200000
*Dynamic, alpha=-0.05, haftol=1e+08
0.01, 22., 0.00022, 0.02
**
** BOUNDARY CONDITIONS
**
** Name: BC-FN Type: Acceleration/Angular acceleration
*Boundary, op=NEW, amplitude=F14FN, type=ACCELERATION
BRIDGE-1.NSOILSPRINGS, 2, 2, 9.81
** Name: BC-FP Type: Acceleration/Angular acceleration
*Boundary, op=NEW, amplitude=F14FP, type=ACCELERATION
BRIDGE-1.NSOILSPRINGS, 1, 1, 9.81
** Name: BC-Fix Type: Displacement/Rotation
*Boundary, op=NEW
BRIDGE-1.NSOILSPRINGS, 4, 4
BRIDGE-1.NSOILSPRINGS, 5, 5
BRIDGE-1.NSOILSPRINGS, 6, 6
** Name: BC-FixBase Type: Displacement/Rotation

```

```

*Boundary, op=NEW
** Name: BC-Vert1 Type: Acceleration/Angular acceleration
*Boundary, op=NEW, amplitude=F14FN, type=ACCELERATION
BRIDGE-1.NSOILABUTANDFOOT, 3, 3, 6.54
**
** CONTROLS
**
*Controls, reset
*Controls, analysis=discontinuous
*Controls, parameters=line search
4, , , 0.15
**
** OUTPUT REQUESTS
**
*Restart, write, frequency=0
**
** FIELD OUTPUT: F-Output-1
**
*Output, field, frequency=1
*Node Output
RF, U
*Element Output, directions=YES
SE, SF
**
** HISTORY OUTPUT: H-Output-1
**
*Output, history, frequency=1
*Element Output, elset=BRIDGE-1.COLUMNSANDPILES
ELKE, ELPD, ELSE
*End Step

```